Development of the Glioblastoma HiSpot®: A novel 3D culture model for the culture of primary human glioblastoma cells and microglia

A thesis submitted for the award of

Doctor of Philosophy

Cardiff University

December 2019

Joanna Brown

Summary

Glioblastoma (GBM) is a common and aggressive grade IV brain tumour with a prognosis of ~18 months. It is highly heterogeneic between and within patients. Treatment options are limited and pharmaceutical interventions often fail at late stages of development, considered to result from poorly translatable models. GBM research has historically been performed using 2D, serum-cultured, established cell lines. These factors have been demonstrated to reduce the stem-like capacity and representativeness of the cancer cells. Animal and 3D models also lack the influence of microglia, which form a large bulk of the tumour mass and interact closely with GBM cells.

The aim of this study was to demonstrate whether the 3D, air-liquid interface, primary human tissue reaggregation model known as the HiSpot® can be adapted for GBM. It established the ability of the HiSpot® to support tumour cells and microglia and determined how well the resulting cultures represent the general and patient-specific features of GBM.

The HiSpot® culture technique was optimised for the support of GBM tissue. HiSpots® were compared to patient and pathological data. Their response to chemotherapeutic treatment was recorded, and multiple biopsies were used from certain patients to investigate intra-tumour heterogeneity.

HiSpots® can be cultured from primary GBM, in serum free, high density conditions, supporting tumour cells and microglia from each patient. The HiSpots® recapitulate patient-specific pathological features, and pharmacological sensitivity, and demonstrate variations in these features between different biopsy sites within each tumour.

The HiSpot® is a suitable model for the culture of primary human GBM cells, which maintains the key relationship between tumour cells and microglia. HiSpots® are representative of patient-matched tumours and demonstrate the inter- and intra-tumour heterogeneity of GBM. The HiSpot® model can be used to improve the understanding of GBM and can be adapted for a number of potential research avenues.

Contents

List of Figures

List of Tables

Glossary of abbreviations

- 5-ALA: 5-aminolevulinic acid
- ABT-414: depatuximab mafodotin
- ATCC: American Type Culture Collection
- ATRX: transcriptional regulator ATRX
- BBB: blood brain barrier
- BRAF: proto-oncogene B-Raf
- BrdU: 5-bromo-2'-deoxyuridine
- BSA: bovine serum albumin
- β-IIIT: β-III tubulin
- CAR: chimeric antigen receptor
- CDK4: cyclin-dependent kinase 4
- CSC: cancer stem cell
- CT: computerised tomography
- CTLA-4: cytotoxic T-lymphocyte-associated protein 4
- DAPI: 4'6-diamidino-2-phenylindole
- DIV: days in vitro
- DMEM: dulbecco's modified eagle's medium
- DMSO: dimethylsulfoxide
- ECM: extracellular matrix
- EdU: 5-ethynyl-2'-deoxyuridine
- EGF: epidermal growth factor
- EGFR: epidermal growth factor receptor
- FBS: foetal bovine serum
- FDA: Food and Drug Administration
- FGF: fibroblast growth factor
- GBM: glioblastoma
- GDNF: glial derived neurotrophic factor
- GEMM: genetically engineered mouse model
- GFAP: glial fibrillary acidic protein
- GFP: green fluorescent protein
- GSC: glioma/glioblastoma stem cell

- GSM: gliosarcoma
- HA: hyaluronic acid
- hESC: human embryonic stem cell
- HGCC: human glioblastoma cell culture
- HGG: high grade glioma
- HIF: hypoxia inducible factor
- HS: horse serum
- HSM: high serum media
- HTA: Human Tissue Act
- HUVECs: human umbilical vein endothelial cells
- IBA1: ionized calcium-binding adapter molecule 1
- IDH: isocitrate dehydrogenase
- IDO: indoleamine 2,3-dioxygenase
- IL-1β: interleukin 1 beta
- IL-8: interleukin 8
- iPSC: induced pluripotent stem cell
- LDH: lactate dehydrogenase
- LGG: low grade glioma
- M-CSF: monocyte colony stimulating factor
- MADM: mosaic analysis with double markers
- MCP-1: monocyte chemoattractant protein 1
- MGMT: O^6-methylguanine-DNA methyltransferase
- MRI: magnetic resonance imaging
- MTIC: 5-(3-methyltriazen-1-yl)-imidazole-4-carboxamide
- MUT: mutant
- NF-κB: nuclear factor kappa-light-chain-enhancer of activated B cells
- NF1: neurofibromatosis type 1 gene
- NG2: neural/glial antigen 2
- NICE: National Institute for Health and Care Excellence
- NOS: not otherwise specified
- NSC: neural stem cell

- O4: oligodendrocyte marker 4
- Olig2: oligodendrocyte transcription factor
- OPC: oligodendrocyte precursor cell
- PARP: poly-ADP-ribose polymerase
- PBS-T: phosphate buffered saline containing triton X
- PBS: phosphate buffered saline
- PCV: procarbazine, lomustine, vincristine
- PD-1: programmed cell death protein 1
- PD-L1: programmed death ligand 1
- PDGFRA: platelet-derived growth factor alpha
- PDOX: patient derived orthotopic xenograft
- PDX: patient derived xenograft
- PEG: polyethylene glycol
- PFA: paraformaldehyde
- PTEN: phosphatase and tensin homolog
- PVSRIPO: recombinant non-pathogenic polio-virus chimera
- RAGE: receptor for advanced glycation end product
- RT: radiotherapy
- S1P: sphingosine-1-phosphate
- SCID: severe combined immunodeficient
- SFM: serum-free media
- SGZ: subgranular zone
- SOX2: sex-determining region Y box 2
- STAT3: signal transducer and activator of transcription 3
- STI-1: stress-inducible protein 1
- SVZ: subventricular zone
- TAM/GAM: tumour/glioma associated microglia/macrophages
- TCGA: The Cancer Genome Atlas
- TERT: telomerase reverse transcriptase
- TGF-β: transforming growth factor beta
- TMZ: temzolomide

- TTFs: tumour treating fields
- VEGF: vascular endothelial growth factor
- WHO: World Health Organisation
- WNRTB: Welsh Neuroscience Research Tissue Bank
- Wnt5a: wnt family member 5a
- WT: wild type
- ZEB1: zinc finger E-box-binding homeobox 1

Acknowledgements

Firstly, I would like to thank my supervisors William Gray, Florian Siebzehnrubl and Malik Zaben for the opportunity to pursue this work, and for all their guidance during my PhD. Thank you to the NC3Rs for funding my research, and for providing so many opportunities to meet and learn from other 3Rs researchers.

Chen, thank you for making me feel so welcome from my first day, and for introducing me to the wonders of the HEB bake off. Niels, thank you for your incredible support throughout, whether in the form of scientific advice or a slice of chocolate orange tart. Rae and Prags, thank you for being there for me in both celebration and crisis. Thank you to the NMHRI staff and students, past and present, for providing such a friendly and encouraging community. Thank you to the ever-changing membership of the Gray Lab, for keeping me company throughout this process.

To my family, thank you for encouraging my interest in science from my first bicarbonate of soda volcano experiment onwards. Emma, thank you for your unwavering support as everything else around me seems to change. Manchester friends, thank you for making me feel at home, no matter where we find ourselves.

To all the nurses, doctors, and staff of the University Hospital of Wales, thank you for your enthusiastic help and support. My appreciation for the NHS has grown even stronger over these last few years.

Finally, I would like to thank all the patients who agreed to donate their tissue for this project. Without your generosity this work would have been truly impossible.

1 Introduction

1.1 Glioblastoma

1.1.1 Disease background

1.1.1.1 Basic details

Glioblastoma (GBM) is the most common and aggressive form of primary brain tumour in adults. It is a grade IV glioma according to the World Health Organisation (WHO). It predominantly occurs in elderly patients, but can occur at any age. The median age at diagnosis is ~62 years for primary GBM and ~44 for secondary GBM. The overall incidence of GBM is 5.02 per 100,000 people, although it is higher in men than women (6.26 vs 3.91), and increases with age (<30: 0.32, 30-54: 2.83, 55+: 12.28). The incidence of GBM has risen over the last 20 years, and although there are many theories, no specific cause has been identified for this increase (Philips *et al.* 2018). There are some hereditary conditions such as neurofibromatosis type 1 and 2, Cowden syndrome, Turcot syndrome and tuberous sclerosis which increase the risk of glioma development. Some risk loci for glioma development such as 20q13.33, 7p11.2 and 5p15.33 have been identified by GWAS studies (Shete *et al.* 2009). The only established environmental risk factor for GBM is ionising radiation. Retroactive studies have shown some increased risk for children who have undergone computed tomography scans, and in patients exposed to atomic bombs or nuclear weapons testing (Omuro and DeAngelis 2013).

The median overall survival for GBM is only 15 - 17 months, but without treatment this is much lower, and patients over 65 have a less favourable outcome, with overall survival ranging from 3.9 - 9.3 months depending on the care regimen used (Reitman *et al.* 2018). A 2017 trial using tumour treating fields (TTFs) showed an increase to 20.9 months, but this treatment is not currently available through the NHS due to high cost. Research is ongoing to find a more financially feasible alternative (National Institute of

Health and Care Excellence (NICE) 2018; Reitman *et al.* 2018). At 5 years post diagnosis, only 4.7% of patients still survive (Omuro and DeAngelis 2013).

The 2016 WHO guidelines replace the previous 2007 guidelines with definitions guided predominantly by the mutation status of the tumour, rather than purely histological diagnosis. This should hopefully reduce the variation between different collection sites for large research and clinical trials, and provide clearer diagnoses based on genetic assessment (Louis *et al.* 2007; Louis *et al.* 2016). One area that has been altered in this update is the definition of secondary GBM. GBM can also arise as a secondary tumour from a low grade glioma (LGG). Secondary GBMs were previously difficult to identify if the LGG was not previously diagnosed. However, recent advances in genetic characterisation of GBMs have provided diagnostic tests to distinguish primary and secondary GBMs. The WHO now define any GBMs with isocitrate dehydrogenase (*IDH*) mutations as secondary GBMs, and those without as primary GBMs (Louis *et al.* 2016). Mutations can be found in *IDH-1* and *IDH-2*, the most common being the *IDH-1* R132H mutation, but other mutations such as those in *IDH-2* at R172 are also found at lower frequency (Huang *et al.* 2019). It is important to note that research predating these definitions may have used criteria such as previously treated LGG or a mix of low and high grade histological features to define secondary GBMs. Secondary GBMs (*IDH* mutant) have a longer median overall survival compared to primary (*IDH* wildtype) GBMs (31 months with surgery, radiotherapy and chemotherapy vs 15 months (Louis *et al.* 2016).

Paediatric GBMs share many similarities with adult those in adults, but there are key differences which mean care must be taken in extrapolating treatments and understanding from adult GBMs. Although there are correlations between paediatric and adult GBM subtypes, the defining mutations may be different (Jones *et al.* 2012). Mutations in genes such as *H3F3A*, which encodes histone 3.3, are only found in paediatric or young adult high grade gliomas. There is evidence that the K27M gain of function mutation may be a main oncogenic driver in some cases (Sturm *et al.* 2014).

Alterations which are common in adult GBM are often more rare in paediatric GBM, such as *EGFR* amplifications, chromosome 7 gain, and chromosome 10q loss. Gliomas are predominantly low grade in paediatric cases, and high grade in adult cases, with the risk of high grade glioma (HGG, grade III or IV) increasing with age. Secondary tumours are extremely rare in paediatric cases, but more common within adult GBMs. It is becoming clearer that GBMs must be treated differently depending on the age of the patient and the tumour subtype.

1.1.2 Diagnosis and current treatment

Patients with GBMs often present with symptoms such as headaches, changes in cognition/personality, nausea or seizures (Omuro and DeAngelis 2013). They will often have a magnetic resonance imaging (MRI) or computerised tomography (CT) scan to determine the cause. If a tumour is suspected, they may have gadolinium with the scan, as GBMs will present a specific pattern of gadolinium enhancement, with an enhancing ring around a non-enhancing necrotic mass, which can be used to confirm diagnosis. The scan is analysed by a radiologist, and then often discussed with a multidisciplinary team including neurosurgical consultants in order to determine the diagnosis and treatment plan. Treatment regimens vary between countries and medical providers. The standard of care used by the NHS is described below. The National Institute for Health and Care Excellence (NICE) guidelines for brain tumours were most recently updated in 2018 (NICE 2018). They provide an investigative and diagnostic pathway for suspected GBMs. GBMs are diagnosed by a combination of histopathological features and molecular markers. The markers recommended are: *IDH1* and *IDH2* mutations, transcriptional regulator ATRX (*ATRX*) mutations, *1p19q* codeletion, histone *H3.3* K27M mutations, proto-oncogene B-Raf (*BRAF*) fusion/mutations, O^6-methylguanine-DNA methyltransferase *(MGMT)* promoter methylation, and telomerase reverse transcriptase (*TERT*) promoter mutations (NICE 2018).

1.1.2.1 Surgery

GBM treatment usually begins with surgery. If possible without causing neurological impairment, the consultant will attempt to debulk (remove) as much of the tumour as possible. This is sometimes referred to as a maximal safe resection. If a debulk is not possible, a small biopsy of the tumour will be taken for histopathological and molecular analysis to confirm the diagnosis of GBM, or provide an alternative diagnosis.

The invasive nature of GBM adds to the complexity of resection. 5-aminolevulinic acid (5-ALA) has been recently introduced to GBM surgery.

5-ALA is a prodrug which causes tumour cells to accumulate fluorescent porphyrins. These, when exposed to UV light, cause the tumour cells to appear pink. This can be used to assist the surgeon in deciding what and how much tissue to remove. 5-ALA is taken as a drink 2-4 hours before surgery, before the patient undergoes anaesthesia. A randomised controlled multicentre trial has shown 5-ALA to improve the percentage of tumour which can be removed, and the patients who underwent surgery with 5-ALA had improved progression free survival (Stummer *et al.* 2006). Although certain centres have been using 5-ALA for longer, it is now recommended by NICE as the standard of care for GBM.

1.1.2.2 Radiotherapy and Chemotherapy

After surgery, patients undergo radiotherapy treatment to any remaining tumour and the borders of the surgical cavity. If surgery was not possible, patients may still have radiotherapy to the entire tumour area. Specific recommendations vary according to the patient's age and performance status, but the standard treatment is with 60 Gy in 30 fractions with concomitant (during radiotherapy) temozolomide (TMZ). The patient will then have 6 cycles of adjuvant (post radiotherapy) TMZ. TMZ is still recommended for some patients even with unmethylated *MGMT*, or if it was not possible to obtain *MGMT* methylation status.

TMZ was introduced into the GBM treatment protocol after the randomised phase 3 clinical trial by Stupp *et al.* (2005). The trial compared the use of radiotherapy alone (60 Gy, RT) to radiotherapy with concomitant and adjuvant TMZ (RT + TMZ). The trial recruited 573 patients, 84% of whom had debulk surgery prior to starting treatment in either group. At a 28 month follow up, the median survival was 14.6 (RT + TMZ) vs 12.1 (RT). At this time point, the RT + TMZ group had a 37% relative reduction in risk of death compared to the RT group. The survival rate at 2 years was 26.5% (RT + TMZ) vs 10.4% (RT). A follow up study was also performed 5 years after the original trial, which found that patient survival was 9.8% (RT + TMZ) vs 1.9% (RT) (Stupp *et al.* 2009). Overall, the introduction of TMZ has made a dramatic

improvement in the survival time from GBM diagnosis, with a 5 year survival of less than 10%, there is still a long way to go.

1.1.2.3 Tumour Recurrence

Unfortunately, GBMs almost always recur. The majority of tumours recur after 7-10 months (Omuro and DeAngelis 2013). Treatment post recurrence depends on multiple factors such as volume of recurrence, previous treatment and performance status. Treatment options include repeated surgery, repeated radiotherapy, and other chemotherapeutic options. As TMZ is usually given as part of first line treatment, it is highly likely that the recurrent tumour will be resistant to it. It is therefore recommended to consider other options such as lomustine or PCV (a combination of procarbazine, lomustine and vincristine). Bevacizumab is not currently recommended for first or second line therapy for GBM through the NHS, but is available through private healthcare providers. It has shown some benefit with regards to progression free survival for primary and recurrent tumours, but no benefit in overall survival for initial tumours (Norden *et al.* 2008; Gilbert *et al.* 2014; Gramatzki *et al.* 2018).

1.1.3 Heterogeneity

1.1.3.1 Subtypes of GBM

The complex heterogeneity of GBM has led to many research groups aiming to subcategorise the disease, in order to improve understanding, predictability, and identify any potential treatment sensitivities. There have therefore been a number of characterisation systems developed by different groups and/or using different techniques to characterise GBM heterogeneity. Although other characterisation systems will be mentioned, summaries will be given of the systems developed by Verhaak *et al.* (2010) and expanded by Wang *et al.* (2017), and the recent study by Neftel *et al.* (2019).

The Cancer Genome Atlas (TCGA) collated 206 GBM samples, allowing for the genetic investigations into GBM on a large scale (McLendon *et al.* 2008). Using bulk sequencing for each tissue sample, Verhaak *et al.* (2010) divided GBM into four subtypes: proneural, neural, classical and mesenchymal, based on genetic mutations and expression patterns. TCGA continued collecting samples and the cohort grew to approximately 600 GBM samples a few years later (Verhaak 2016). Further work by Wang *et al.* (2017) used single cell RNA sequencing to clarify these subtypes, and identified the neural subtype as possible contamination by normal tissue. It is possible that the neural subtype arose as a result of samples from the tumour margin, which would have a high percentage of normal cells. These subtypes and their precursors have been used for characterisation of GBM samples in recent years and are often described as the TCGA subtypes. These subtypes correlated well with earlier work by Phillips *et al.* (2006), who categorised 76 high grade glioma samples into three subtypes; mesenchymal, proliferative (classical), and proneural. The authors noted the subtypes' correlation with stages of adult forebrain neurogenesis.

The TCGA proneural subtype is characterised by platelet-derived growth factor alpha (*PDGFRA*) amplification, *TP53* mutations and *IDH-1* point

mutations, such as *IDH-1* R132H, which is now used to distinguish secondary GBMs from primary GBMs. All secondary GBMs analysed were sorted into the proneural subtype. Amplifications in *MYC*, sex-determining region Y box 2 (*SOX2*) and cyclin-dependent kinase 4 (*CDK4*) were also found to indicate proneural GBM (Verhaak *et al.* 2010; Wang *et al.* 2017). A retrospective study demonstrated that patients with tumours of the proneural subtype may have an overall survival benefit (Sandmann *et al.* 2015).

The TCGA classical subtype of GBM is characterised by amplifications in chromosome 7, deletions in chromosome 10, and alterations in epidermal growth factor receptor (*EGFR*). These include amplifications, increased expression, and the vIII mutation. There is a distinct lack of *TP53* mutations in the classical subtype, especially given that *TP53* has been noted as a commonly mutated gene in GBM. Deletion of *CDKN2A*, which commonly co-occurs with *EGFR* amplification is also a feature of classical GBMs (Verhaak *et al.* 2010; Wang *et al.* 2017).

The key features of TCGA mesenchymal GBM are abnormalities in neurofibromatosis type 1 gene (*NF1*), such as deletion, mutation, or low expression. *NF1* is commonly found co-mutated with phosphatase and tensin homolog *(PTEN*). NF1 deficiency has been demonstrated to promote tumour associated macrophage/microglia (TAM) infiltration into GBMs. High expression of genes from the tumour necrosis factor super family and nuclear factor kappa-light-chain-enhancer of activated B cells (NF-κB) pathway have been noted in mesenchymal GBM, potentially because of the increased TAM infiltration. TAM factors IBA1 and CD11B were particularly highly expressed in mesenchymal GBMs. Markers indicative of an M2-like tumour promoting TAM phenotype were more highly associated with the mesenchymal subtype than either of the others. This indicates that the mesenchymal subtype may be particularly sensitive to treatments targeting TAMs (Verhaak *et al.* 2010; Wang *et al.* 2017).

Wang *et al.* (2017) found that the mesenchymal subtype had the worst prognosis of the three, (11.5 months median survival), which was

significantly lower than the classical (14.7) or proneural (17.0) subtypes. This, in addition to the potential differences in drug susceptibility illustrates the importance in taking subtypes into account when designing and administering treatments for GBM.

Other methods such as DNA methylation profiling have also been used to sort GBMs and other gliomas into subtypes. Ceccarelli *et al.* (2016a) categorised 1122 gliomas from the TCGA database including grades II, III and IV using sequencing and molecular profiling. They sorted all gliomas into IDH-mutant and IDH-wildtype first, and subcategories within these. IDH-mutant patients were subcategorised as codeleted (LGGs), G-CIMP-high, and G-CIMP low. IDH-wildtype patients were sorted into classic-like and mesenchymal-like, correlating with the TCGA GBM classifications, and LGm6-GBM and PA-like categories, which were predominantly low grade tumours.

Capper *et al.* (2018) used genome-wide DNA methylation profiling to sort 82 CNS tumour samples of many diagnoses into groups. Although there was a high level of correlation with histological diagnosis (76%), a proportion of samples were re-diagnosed after further investigation to match the DNA methylation-based diagnosis instead. Glioma grouping correlated well with previous work (Ceccarelli *et al.* 2016). Gliomas were correlated into two main clusters, distinguished predominantly by IDH mutations. The non-IDH mutation gliomas formed 8 subclasses, with a high correlation with TCGA work.

In a landmark study, Neftel *et al.* (2019) developed a new categorisation system for GBM. Although their work builds on previous characterisations, they also describe a more fluid system for subtype characterisation. They performed single cell RNA sequencing on tissue samples from 20 adult and 8 paediatric GBM patients. This is a much smaller group of patients than the previously described TCGA analysis. They describe a highly plastic system of four cellular states, between which cells can transition depending on their environment and genetic signals. The states correlate to key developmental

cell types: oligodendrocytes (OPC-like), neural progenitor cells (NPC-like), astrocytes (AC-like), and mesenchymal cells (MES-like). The four different cell types can all exist within one tumour, but a particular subtype or types tends to predominate, especially if certain mutations or alterations are present. *EGFR* mutations bias a population towards the AC-like state, *PDGFRA* mutations towards the OPC-like state, *CDK4* alterations towards the NPC-like state, and *NF1* mutations towards the MES-like state. The authors propose that these predominant states are responsible for the bulk-tumour subtypes described by Wang *et al.* (2017). The AC-like state correlates with the classical subtype, and the MES-like state with the mesenchymal subtype. The proneural subtype is a combination of OPC-like and NPC-like states. This pair of states are often found clustered together, as are the AC-like and MES-like states. All samples contained a combination of different cell states, but the frequency of each group differed significantly. The authors used cell barcoding to demonstrate that cells can transition between the states, providing a heterogenous population from a single original cell. They also note that 15% of the cells analysed were a hybrid of two states, and although transitions were only noted between certain states, these connect to allow transition between all cell states, but only along the arrows shown (**Figure 1-1**). Interestingly, the MES-like subtype was shown to be promoted by hypoxia and immune cells, which correlates with high microglial infiltration in the TCGA mesenchymal subtype.

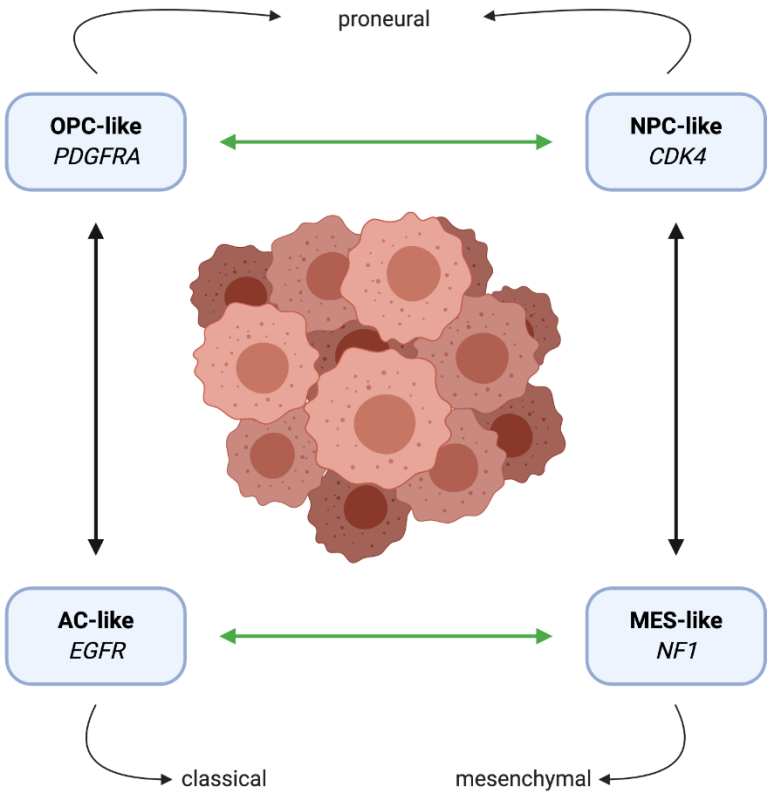

Figure 1-1: A summary of GBM subtypes

Subtypes are shown according to Neftel et al. (2019). The arrows represent plasticity between the groups, with the green arrows representing groups that are found more commonly clustered together. For each group, the subtype name is shown in bold, indicating the cell type or status they correlate with: OPC = oligodendrocyte, NPC = neural progenitor, AC = astrocyte, MES = mesenchymal. Commonly mutated or affected genes are shown in italics. The small arrows and text indicate the Wang et al. subtype with which that group best correlates.

1.1.3.2 Diagnostic variants of GBM

For clinical purposes, the WHO 2016 classification classifies GBM into three subtypes: GBM, IDH-wildtype; GBM, *IDH*-mutant; and GBM, not otherwise specified (NOS). NOS indicates that is was not possible to sort the tumour into one of the previous categories, when it is not possible to test for *IDH* status. Approximately 90% of GBMs are IDH-wildtype, leaving ~10% as *IDH*-mutant. *IDH*-mutant GBMs were previously categorised within the proneural subtype, but are now excluded from overall analysis and investigated separately to the *IDH*-wildtype GBMs (Wang *et al.* 2017). The GBM, *IDH*-wildtype category also contains variants, based on histological features of the tumour. Giant cell GBM and gliosarcoma (GSM) are well-known variants of GBM. They are still categorised within the GBM *IDH*-wildtype diagnosis. Epithelioid GBM has been included as a provisional entry, noted by pathologists but not yet well defined as a GBM variant. Giant cell GBMs are rare but distinctive. They are defined by *"bizarre, multinucleated giant cells and an occasionally abundant reticulin network"* according to the WHO 2016 classification. They are almost entirely primary GBMs, although it is possible for secondary GBMs to have giant cells. Giant cell GBMs also tend to present earlier than other GBMs, and are associated with better overall survival. Patients with giant cell GBMs are also more likely to survive beyond 5 years (Kozak and Moody 2009; Louis *et al.* 2016; Oh *et al.* 2016).

GSMs are glioblastomas which show both the standard glial tumour and a sarcomatoid pattern histologically. The two areas are thought to develop from the same original tumour, as they have common genetic alterations. GSMs commonly have mutations in *PTEN*, but rarely *EGFR* mutations, which may indicate that they would be categorised within the mesenchymal subtype of GBM. Much like GBMs, GSMs can arise either as primary tumours, with no precursor, or can develop from either primary or secondary GBMs. Oh *et al.* (2016) found the loss of heterogeneity in chromosome 10q was very common in GSMs (88%) and relatively common

in giant cell GBMs (50%). Mutations in *TP53* have also been demonstrated as common in GSMs. One retrospective study showed that primary GSMs have a better overall survival than secondary GSMs (24.7 months vs 8.95 months), but this was a small study with only 34 patients (Cachia *et al.* 2015). The sarcomatoid phenotype of GSM has also been demonstrated to metastasise, which is very rare for GBM (Beaumont *et al.* 2007). Epithelioid GBMs are not well defined as of the 2016 WHO classification, but have been noted to preferentially arise in young patients, mostly under 30, and approximately 16.7 - 50% of these tumours have a *BRAF* V600E mutation. The V600E mutation was not found in giant cell GBMs, but has been demonstrated in a case of GSM. It has been noted that immunohistochemical staining alone can provide false positive results, so it is important to confirm *BRAF* mutation status through genetic testing, especially in younger GBM patients (Kleinschmidt-DeMasters *et al.* 2013; Behling *et al.* 2016; Tosuner *et al.* 2018). As BRAF is commonly mutated in other tumour types such as colorectal cancer and melanoma, it is possible that chemotherapeutic treatments could be repurposed for epithelioid GBMs with the *BRAF* V600E mutation.

1.1.3.3 MGMT methylation

MGMT is a gene involved in DNA repair. Methylation of the *MGMT* gene promoter silences the gene, significantly reducing the amount of the MGMT enzyme present in the cell. This sensitises the cells to DNA damage, as they cannot effectively repair the damage caused. Alkylating agents such as temozolomide (TMZ) damage DNA, leading to apoptosis (Zhang *et al.* 2012). In tumours with unmethylated *MGMT*, this DNA damage is swiftly repaired by MGMT, allowing the tumour to continue proliferating. However, if the *MGMT* promoter is methylated, the tumour cells do not have sufficient levels of MGMT to repair the damage caused, and so repeated exposure to TMZ can kill the tumour cells, by blocking their ability to proliferate. Approximately 50% of GBMs are *MGMT* methylated.

Hegi *et al.* (2005) demonstrated the importance of *MGMT* methylation for GBM as a post-hoc study following on from the successful phase 3 trial of TMZ (Stupp *et al.* 2005). They demonstrated that patients with a methylated *MGMT* promoter benefitted from treatment with TMZ alongside the standard radiotherapy, but patients with an unmethylated *MGMT* promoter did not. This translated to an increase in median overall survival for patients with methylated *MGMT* from 15.3 months (radiotherapy alone) to 21.7 months (TMZ and radiotherapy). In comparison, patients with unmethylated *MGMT* showed a small but not significant increase (11.8 months vs 12.7 months). The authors recommended the use of TMZ for patients with *MGMT* methylation, and that methylation status should be analysed for patients going forward. *MGMT* methylation also provides an advantage for patients treated with radiotherapy alone compared with *MGMT* unmethylated patients (15.3 months vs 11.8 months).

1.1.3.4 Intra-tumour heterogeneity

In addition to the variants, subtypes, and methylation statuses of GBMs, there is also variability within tumours. Heterogeneity has been demonstrated in GBM in multiple spatial arrangements. There are differences between the different layers of the tumour, from the necrotic core in the centre of the tumour, to the far edge where the tumour cells invade into healthy brain. There are also differences between areas due to the tumour development, meaning biopsies from the top and bottom of the tumour may also have important differences in genetic abnormalities and potentially drug sensitivity.

The structure of a GBM tumour visible on a CT scan is shown in **Figure 1-2A**. A ring of brightness is visible within the image, with a darker area within. Example biopsy areas are shown to represent the core (purple), contrast-enhancing (blue) and peripheral (orange) areas of the tumour. This appearance is how GBM tumours commonly appear with gadolinium enhancement. The peripheral area is mostly healthy brain, with invading tumour cells within. Cancer stem cells (CSCs) cells beyond the visible border

of the tumour are thought to be responsible for tumour recurrence as it is not possible to remove them all without damaging healthy brain (Chen *et al.* 2012). The enhancing area is highly vascularised with leaky vessels. These allow the release of gadolinium, causing the enhancement. This is a highly invasive tumour area. In comparison the core is more proliferative, producing new tumour cells to add to the bulk of the tumour. This area is hypoxic, and certain areas can become necrotic (Pistollato *et al.* 2010; Persano *et al.* 2011).

GBMs are thought to develop from one initial population of CSCs, which produce a heterogeneic population of cells. In addition, as these populations grow larger they accumulate further mutations, developing into multiple subclones within the one tumour. A visualisation of this is shown in **Figure 1-2B,** with the four circles representing biopsies which could theoretically represent four difference subclones within the tumour. These subclones were categorised as different subtypes by Sottoriva *et al.* (2013). However since the recent developments in single cell RNA sequencing of GBM, this may indicate that different regions affect the frequency of different states instead of specific subtypes (Neftel *et al.* 2019). This intra-tumour variation means that certain areas may vary in resistance to treatment, and therefore survive to cause recurrence, in addition to any CSCs that have invaded into the healthy brain and survive to repopulate the tumour. It also means that biopsies used for diagnosis or molecular analysis may only represent a certain area of the tumour and may not provide a result which can be extrapolated to the rest of the tumour. This could be a particular problem in cases where the patient does not undergo a debulk but only has a very small biopsy taken as a less invasive procedure. Given that different subtypes or states have been demonstrated to have specific or higher sensitivities to certain treatments, this is of obvious concern when making a diagnostic decision which will affect therapeutic options (Perrin *et al.* 2019).

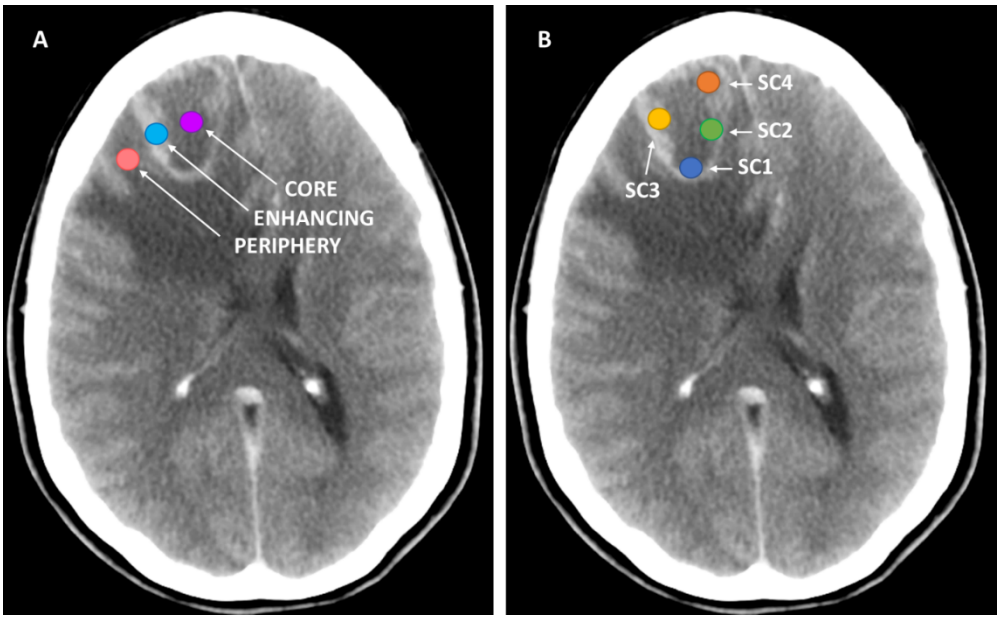

Figure 1-2: Intratumour heterogeneity in GBM.

Images shown are from an axial CTI scan with gadolinium contrast. A: Purple, blue and pink circles represent example biopsy areas from the core, enhancing area, and periphery of the tumour respectively. B: The four circles represent four biopsy locations that could potentially represent four different subclones/populations of the tumour with different phenotypes.

1.1.3.5 GBM cell of origin

The GBM cell of origin has been highly debated, although the most prominent theories have been that either the neural stem cell (NSC) population of the subventricular zone (SVZ), or oligodendrocyte precursor cells (OPCs) are the starting point for GBM development. Importantly, cell of origin refers to the cell type which acquires the initial oncogenic mutations, and not later-developed tumour cells which are capable of tumour formation *in vitro* or *in vivo.* GBM cells share expression patterns with both NSCs (Nestin, GFAP, SOX2) and OPCs (Olig2, NG2, O4).

Lee *et al.* (2018) have recently provided some further evidence supporting the NSC theory. They sequenced matched human brain samples from tumours, SVZ and normal cortex or blood from 30 patients, 19 of which were then diagnosed as GBM. Non-GBM samples were used for comparison. Using deep whole exome sequencing, the authors found that the cortex or control blood samples had an average of 4.3 somatic mutations, the tumour itself had 80.7, and the SVZ tissue had 23.0. 42.3% of patients had at least one mutation in *TERT* which was shared between the tumour and the SVZ. 81.8% of these patients also had low level driver mutations in *EGFR, PTEN* or *TP53* in the SVZ tissue. An average of 15.6 mutations were shared between the tumour and matched SVZ tissue. This was demonstrated to not be in the case in other tumour types. Mutations in the *TERT* promoter were noted as a likely early driver for GBM, as 56.3% of the GBM patients had *TERT* promoter mutations in the SVZ, compared to only 6.1% of normal brain samples. The authors suggested that low level driver mutations accumulate in the SVZ, potentially triggered by alterations in *TERT* which allow the NSCs to avoid senescence. To confirm this, they used CRISPR Cas9 technology to introduce mutations in *p53*, *PTEN* and *EGFR* into tdTomato labelled NSCs in the SVZ of mice. 90% of these mice developed tumours. The migration of the tdTomato cells was tracked, and showed that the NSCs either migrated to the dorsolateral-caudal cortex, where they developed into tumours, or the olfactory bulb, where they differentiated into neurons.

Immunohistochemistry also showed that the tdTomato cells were also positive for markers of oligodendrocyte precursors, which develop from NSCs. Tumours were confirmed by immunohistochemistry to resemble gliomas. 67% of these gliomas developed away from the SVZ, as is seen in GBMs. Together these data support the theory that GBMs develop from the NSC population in the SVZ, and potentially acquire characteristics of OPCs later on in the process.

Alcantara Llaguno *et al.* (2015) have proposed that both OPCs and NPCs are the cell of origin for GBM, but that the cell of origin differs between GBM subtypes. Targeting each cell type separately and in combination with the same mutations using their Ascl1-creER^{T2} model crossbred with animals with mutations in *NF1, Trp53,* or *PTEN* to produce a variety of genotypes, the authors showed that GBM-like tumours were produced from both cell types but that they harboured distinct features of separate GBM subtypes. The Type 1 subtype was designated NSC-specific, and the Type 2 subtype as derived from OPCs, and more reminiscent of the proneural subtype of GBM (Verhaak *et al.* 2010). *PDGFRA* is a key gene in OPCs, and is commonly amplified in TCGA proneural GBM. Mouse models with targeted deleted of *NF1* form tumours in SVZ related areas, and abnormalities in *NF1* are a marker of TCGA mesenchymal GBM (Verhaak *et al.* 2010; Fan *et al.* 2019). The Parada group then further established their theory by confirming with tumour suppressor conditional knockout models that differentiated neurons could not be used to initiate GBM tumour formation. They used targets commonly mutated in GBM: *NF1*, *Trp53*, and *PTEN*. Although damage was seen in histological examination, this did not show any evidence of tumour formation. This further supports their theory that NSCs and OPCs are the cell/s of origin for GBM (Alcantara Llaguno *et al.* 2019).

However, not all evidence supports NSCs as cell of origin for GBM. Liu *et al.* (2011) used the mosaic analysis with double markers (MADM) lineage tracing technique to identify the cell-of-origin for GBM. Using mouse models with concurrent *p53* and *NF1* mutations, they tracked aberrant growth in

the cell populations of interest. They found that although NPCs may be subject to initial mutation, the cancerous growth was only recorded in OPCs, forming glioma-like tumours with OPC-like expression patterns. They also found that oncogenesis could be directly triggered in OPCs, with the tumours formed showing no significant differences from those with initial NPC mutations.

Fan *et al.* (2019) discuss the previous and many other papers in their review, as well as evidence for OPCs being the cell of origin. They propose that the current evidence can be collated into a unified theory of GBM origins. The authors suggest that the NSCs may be the cells which first undergo mutation, leading to an uncontrolled cycling NSC population which then accumulate further tumourigenic mutations. This population then develops into OPCs, and then spread beyond the SVZ. These OPCs then undergo further transformations and develop into GBMs, at their current location. This is supported by fact that GBMs do not arise solely in the SVZ, but around the brain. Therefore the tumour cells must translocate either during or after the acquisition of mutations, and the work by Lee *et al.* (2018) suggests that not all of the mutational load is acquired in the SVZ.

If as this work suggests, GBMs are derived from both NSCs and OPCs, it would clearly explain the strength of evidence for each cell type as the cell of origin previously. Although not a complete subtype-to-cell type match, it has previously been suggested that different GBM subtypes represent different stages in the neurogenic pathway (Phillips *et al.* 2006). However the recent classification of GBM into fluid states with varying frequencies may reveal more about the GBM cell of origin in the next few years (Neftel *et al.* 2019).

1.1.4 Cell types and the microenvironment in GBM

Not only is there variability in the tumour cells themselves, but GBM cells are also in constant interaction with their surrounding microenvironment. This includes the tumour extracellular matrix (ECM) and surrounding cells. The specifics of these complex interactions are still poorly understood. Simple two-dimensional monolayer cultures have not been able to model these interactions. It is important that new models are developed to help further the understanding of these interactions.

1.1.4.1 Cancer cells

Tumour development has historically been a key subject of debate (Rahman *et al.* 2011). There are two main models of tumour development, the clonal evolution model and the hierarchical model (Shackleton *et al.* 2009). The clonal evolution model starts with a tumour in which cells accumulate mutations and produce subpopulations with different mutational landscapes. Under treatment, one subpopulation may have gained a mutation which makes it resistant, and therefore survives to recur later on. This model designates every tumour cell as having the potential to repopulate the tumour after treatment or transplantation. This was previously the accepted model for tumour development.

However, in the hierarchical model, it is a specific population only within the tumour which survives treatment or is capable of tumour formation after transplant, the cancer stem cells. These cells survive by nature of their stem-like state, whereas the daughter subpopulations are destroyed. They then divide again to repopulate the tumour. Either of these models can be used to explain the heterogeneity of tumours. Unfortunately, the two models require different approaches with treatment. In the clonal evolution model, it is sufficient to kill off the populations of tumour cells, whereas in the hierarchical model it is necessary to kill of the cancer stem cell population specifically. CSCs have now been demonstrated and are now a focus for treatment in many cancers (Dick and Bonnet 1997; Bousquet *et al.* 2017; Huang and Rofstad 2017), including adult and paediatric GBM (Ignatova *et*

al. 2002; Hemmati *et al.* 2003; Singh *et al.* 2003; Galli *et al.* 2004), for which the hierarchical model is now generally accepted as the method of tumour development (Lathia *et al.* 2015).

CSCs are regulated by many factors including their local microenvironment, tumour niche, and immune surroundings. They also differ depending on their particular genetic or epigenetic landscape, and metabolic state (Lathia *et al.* 2015; Hoang-Minh *et al.* 2018). They have also been demonstrated to be more slowly cycling than their progeny, and more resistant to TMZ treatment (Hoang-Minh *et al.* 2018). They are responsible for the regrowth of tumours after treatment as they are resistant to both chemotherapy and radiotherapy (Bao *et al.* 2006; Chen *et al.* 2012). The therapeutic resistance of CSCs is mediated by multiple molecular mechanisms, through mediators such as poly-ADP-ribose polymerase (PARP), NF-κB, and the DNA damage response (Bao *et al.* 2006; Bhat *et al.* 2013; Venere *et al.* 2014).

One difficulty of studying CSCs is the range of nomenclature used. They have been referred to as various combinations of cancer/tumour/brain tumour/glioma stem/stem-like/initiating cells. Although these descriptions have been used interchangeably in some places, it is important to note that a cell capable of forming spheroids is not necessarily a stem cell, and that these cells are not necessarily the same as the cell of origin **(1.1.3.5**). CSCs must be self-renewing, persistently proliferative, and capable of initiating a tumour with the original heterogeneity in a new environment. They usually but do not always express stem cell markers and are capable of producing multiple lineages of cells (Lathia *et al.* 2015). CSC research has also been limited by the lack of a clearly defined marker for these cells. CD133 is often used as this is a marker for stemness in non-tumour cells. However CD133 negative cells have also been shown to be capable of recreating the tumour, so this is not an ideal marker (Beier *et al.* 2007). Similarly, SOX2 and nestin have been used to identify CSC populations (Hemmati *et al.* 2003; Tunici *et al.* 2004). However, concerns have been voiced that these markers may not necessarily be marking all CSCs, potentially missing the quiescent cells. In

addition, the inherent variability in CSCs may make it difficult to ever determine a truly specific marker for this population (Lathia *et al.* 2015). Overall, CSCs are an essential part of the tumour to model, but are difficult to reliably isolate.

It is important however to remember that the bulk of the tumour is formed from non-stem cancer cells which develop from the CSCs. The non-stem cancer cells are more differentiated than CSCs, and they are highly diverse, as demonstrated by both bulk and single cell RNA sequencing (Sottoriva *et al.* 2013; Neftel *et al.* 2019). Fate mapping of GBM cells has led to a model of slow cycling stem cells, which produce faster cycling progenitor cells, which in turn produce differentiating cells, which no longer divide. The faster cycling and differentiating cells form the bulk of the tumour population, and the slow cycling cells resist treatment and repopulate the tumour (Lan *et al.* 2017; Hoang-Minh *et al.* 2018).

1.1.4.2 The role of microglia in the GBM microenvironment

The GBM microenvironment is made up of many cell types, the majority of which are microglia. In the healthy brain, microglia have important roles in pathological response and neuronal maintenance, and comprise up to 10% of the total cells. In GBM, 30-45% of the total cells are microglia, highlighting their importance in this disease (Morantz *et al.* 1979; Graeber *et al.* 1988; Glass and Synowitz 2014). It has been demonstrated that as the grade of glioma increases, so does the level of macrophage infiltration in the tumour tissue (Komohara et al. 2008). It was previously assumed that microglia and macrophages both arose from bone marrow haematopoietic stem cells. However, it is now understood that microglia arise separately from the haematopoietic precursor cells of the yolk sac (Ginhoux *et al.* 2010). Microglia and macrophages express common markers such as CD11b, CD68 and IBA1 (Roesch *et al.* 2018). Osteopontin is a chemokine produced in the GBM microenvironment which has been demonstrated to attract macrophages into the tumour area. It is upregulated in tumours which are categorised as the TCGA mesenchymal subtype, which has been

demonstrated to have higher microglia/macrophage infiltration than the proneural or classical subtypes (Kaffes *et al.* 2019; Wei *et al.* 2019).

This means that GBM tumours contain both microglia and infiltrative macrophages. These are often grouped together as glioma/tumour associated microglia/macrophages (GAMs/TAMs). Previously, CD45 staining has been used to distinguish infiltrating macrophages ($CD45^{high}$) from microglia ($CD45^{low}$) using flow cytometry, and this has been used to demonstrate that the majority of the immune cell population infiltrating GBMs are macrophages rather than microglia (Parney *et al.* 2009). However, Müller *et al.* (2015) challenged this, by demonstrating that microglia recruited to the tumour can upregulate their CD45 expression to the levels seen in macrophages and represent up to 40% of the $CD45^{high}$ population. Therefore, it can be difficult to reliably distinguish these two cell types in the GBM disease state, especially without the use of flow cytometry (Roesch *et al.* 2018).

Gliomas have been shown to attract both microglia and macrophages to the tumour site by releasing signals such as MCP-1 (monocyte chemoattractant protein 1), M-CSF (monocyte colony stimulating factor), EGF (epidermal growth factor) and GDNF (glial cell-derived neurotrophic factor) (Platten et al. 2003; Ku et al. 2013). Pyonteck et al. (2013) demonstrated that blockade of M-CSF mediated communication between glioma cells and microglia slowed tumour progression in mice models and human tumour spheroids (Roesch et al. 2018). M-CSF and other factors cause the GAMs to transition to a more traditionally defined M2-like, anti-inflammatory phenotype, causing the expression of markers such as CD163 and CD204. This M2-like phenotype also supports tumour growth (Pyonteck et al. 2013).

Once the GAMs have been recruited to the tumour, they support the growth, motility and invasion of the tumour cells. Among other factors, release of stress-inducible protein 1 (STI-1) from GAMs increases GBM proliferation and migration (Carvalho da Fonseca *et al.* 2014). GAMs also release EGF, which increases invasion. This EGF release is triggered by the

release of M-CSF from tumour cells (Coniglio *et al.* 2012). TGF-β release from GAMs also promotes growth and triggers ECM breakdown, facilitating GBM invasion into the healthy brain (Wesolowska *et al.* 2008). Finally, GAMs have also been shown to promote angiogenesis through receptor for advanced glycation end product (RAGE) signalling, although there is some evidence that this may be specifically mediated by microglia and not macrophages (Chen *et al.* 2014; Brandenburg *et al.* 2016).

This results in a cycle of GBM cells recruiting and converting GAMs, and GAMs supporting the invasion and proliferation of GBM cells (represented in **Figure 1-3**, Komohara et al. 2008). Unfortunately targeting the M2-like phenotype of GAMs may not provide a simple solution, as M1-like expression of IL-1β has been demonstrated to promote tumour growth in GBM, and higher levels of IL-1β expression in proneural GBM correlated with worse survival (Feng *et al.* 2015). Therefore, there may not be a simple correlation between GAM phenotype and tumour support. Instead, specific pathways will have to be determined and potentially tackled simultaneously in order to target GAMs as a treatment for GBM (Hambardzumyan *et al.* 2016). Tumour heterogeneity also affects GAMs, as Kaffes *et al.* (2019) demonstrated that the number and phenotype of GAMs changed between the core of the tumour and the surrounding healthy brain.

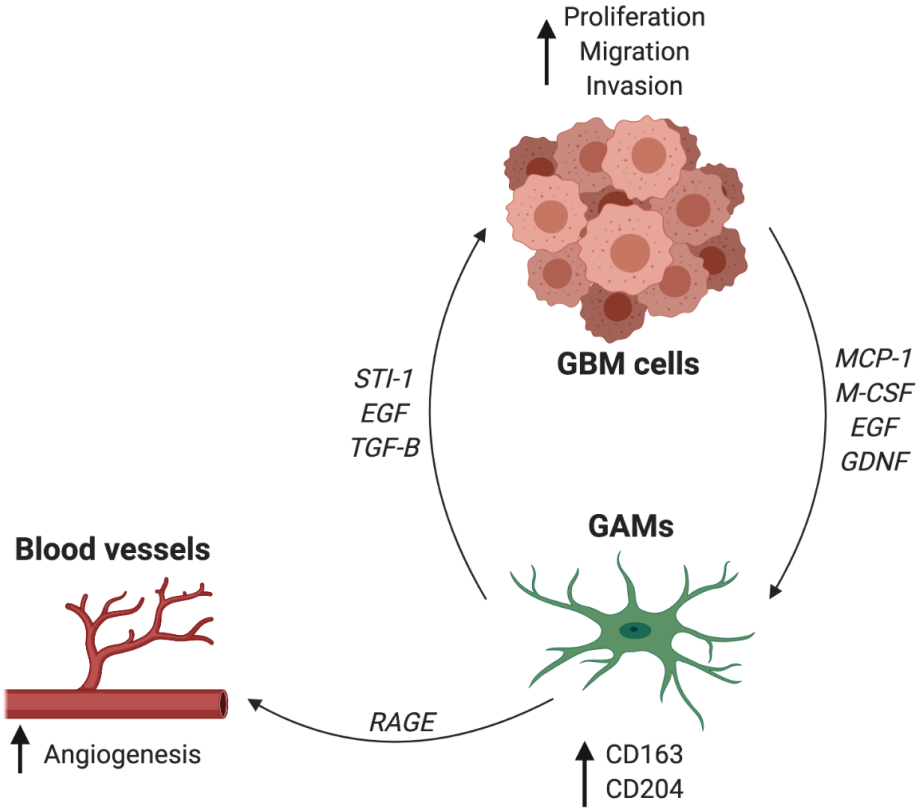

Figure 1-3: A simplified representation of the GBM-GAM cycle.

A summary of the text is shown. GBM cells release factors which affect the function of GAMs and upregulate anti-inflammatory markers. GAMs in turn release factors which promote the proliferation, migration and invasion of GBM cells, and promote angiogenesis. Figure created using www.biorender.com

1.1.4.3 Other cells of the tumour microenvironment

In addition to the reciprocal communication with microglia, GBM cells are in constant interaction with other cells of the tumour microenvironment. These include endothelial cells, fibroblasts, pericytes, and reactive astrocytes, although any cell present within the tumour could be categorised as part of the microenvironment. As with microglia, many of these cells are reported to support tumour growth and invasion.

GBMs are known to be highly vascularised tumours and this vascularisation has been investigated as a treatment target through anti-angiogenic therapies such as bevacizumab (Charalambous *et al.* 2006; Gilbert *et al.* 2014; Scholz *et al.* 2016). Endothelial cells are therefore a very important part of the GBM microenvironment, and their interaction with CSCs is an important contributor to tumour behaviour. It is becoming clear that at least some endothelial cells are in fact derived from the tumour and not the healthy brain, which may contribute to their pro-tumour behaviour (Wang *et al.* 2010). GBM tumour cells promote endothelial cell proliferation and therefore angiogenesis via signals such as VEGF and sphingosine-1-phosphate (S1P). Endothelial cells in turn promote tumour invasion and support CSC maintenance via release of factors such as TGF-β, fibroblast growth factor 2 (FGF2), S1P and interleukin-8 (IL-8), and Notch activation in a pro-tumour feedback loop (Abdel Hadi *et al.* 2018; Brandao *et al.* 2019; Mccoy *et al.* 2019; Schiffer *et al.* 2019). Endothelial cells present in GBM have different morphological features and altered expression patterns compared to healthy brain endothelial cells (Charalambous *et al.* 2006).

Pericytes are cells which cluster around and support the vasculature of the brain. They are also an important part of the blood-brain barrier (BBB) and are in constant communication with endothelial cells. As with endothelial cells, there is evidence that CSCs produce their own pericytes for further tumour support via TGF-β. In fact tumours with fewer pericytes are more susceptible to treatment, so they may provide a useful therapeutic target (Cheng *et al.* 2013).

Fibroblasts form a key part of the microenvironment of many solid tumours such as melanoma and colon cancers, and have been demonstrated to promote tumour progression (De Wever *et al.* 2004; Gallagher *et al.* 2005; Kalluri and Zeisberg 2006). Their role is not as significant or well-understood in GBM. However, they have been demonstrated to promote the invasion of tumour cells through the action of membrane-type 1 matrix metalloprotease (Beliën *et al.* 1999).

Reactive astrocytes are becoming more well-recognised as an important feature of the GBM microenvironment. They are found surrounding the tumour in humans and in animal models, and have been demonstrated to support invasion, proliferation, and GBM cell survival (O'Brien *et al.* 2013; Shabtay-Orbach *et al.* 2015; Ferrer *et al.* 2018; Jin *et al.* 2018; Brandao *et al.* 2019). There is evidence that they have multiple roles within the microenvironment, including protecting the tumour from chemotherapy and the immune system (Huang *et al.* 2010; Kim *et al.* 2014; Brandao *et al.* 2019). Astrocytes are attracted to the tumour microenvironment and secrete GDNF which promotes GBM invasion into the brain (Shabtay-Orbach *et al.* 2015). Reactive astrocytes also contribute to the disruption of the BBB in GBM (Schiffer *et al.* 2019).

Overall, the cellular microenvironment of GBM is complex and highly interlinked. Targeting these tumour-supportive cells along with CSCs may provide the best chance of preventing GBM recurrence.

1.1.4.4 The non-cellular microenvironment

Hypoxia is a low partial pressure and therefore availability of oxygen. It is a hallmark of the GBM microenvironment which itself triggers angiogenesis, maintenance of CSCs in a stem state, and invasion, via hypoxia inducible factors (HIFs), particularly HIF-1α (Yang *et al.* 2012). The hypoxic state of the GBM microenvironment also contributes to both chemotherapy and radiotherapy resistance, partly by triggering the process of autophagy. Autophagy is a response to stress (such as hypoxia) in which inessential

cellular components are recycled into essential fatty acids, amino acids and ATP. This allows the cells to survive for longer. TMZ has been demonstrated to trigger autophagy in GBM cell lines, which may allow the cells to avoid DNA damage. It is hoped that combining anti-autophagy treatments with TMZ may increase treatment response (Kanzawa *et al.* 2004; Jawhari *et al.* 2016). HIFs are being investigated as potential targets for treatment, with some such as the HIF-2α inhibitor PT2385 already in clinical trials (Renfrow *et al.* 2018).

The various cell types of the microenvironment are connected via the ECM. The ECM is a highly complex and dynamic part of the healthy brain, which is further complicated in the GBM disease state. Importantly, the ECM of the brain is different than that of other organs, so this must be taken into account when investigating how it differs in disease (Barros *et al.* 2011; Schiffer *et al.* 2019). GBM has been shown to affect the levels of different ECM components such as agrin, tenascin, and hyaluronic acid (HA). HA is the most abundant of these and plays an important role in tissue mechanics, as well as cell signalling. It can have pro- and anti-invasive roles depending on its molecular weight (Wolf *et al.* 2019). Although important for tissue homeostasis in healthy brain, HA has been demonstrated to support and promote tumour invasion. It is often upregulated in the tumour environment (Ferrer *et al.* 2018). Physical factors are also important as the rigidity of the ECM has been demonstrated to affect the proliferation and invasion of GBM cell lines, with a more rigid ECM supporting tumour cell invasion. Interestingly, collagen and fibronectin, which are important components of the ECM in many organs, are far less frequent in the brain (Bonneh-Barkay and Wiley 2009).

GBM also has the ability to alter its local ECM microenvironment to facilitate its own invasion through the secretion of enzymes such as matrix metalloproteinases and hyaluronan synthase (Rascher *et al.* 2002; Koh *et al.* 2018; Perrin *et al.* 2019). The GBM microenvironment is also more acidic than in a healthy brain, due to increased local lactate production as a result

of the tumour undergoing aerobic glycolysis for ATP production. There is also variability within the tumour microenvironment, as factors such as the necrotic core, and interaction with non-tumour cell types, can affect microenvironmental factors such as the elastic modulus, interstitial fluid flow, and oxygen availability (Wolf *et al.* 2019).

The BBB is a barrier which maintains the central nervous system as an isolated compartment from the rest of the body, allowing it to maintain its specialised functions. It is well-known to be disrupted in GBM, but is still capable of preventing potential therapeutic molecules from entering the brain. It is formed of endothelial cells, pericytes, and astrocytic end feet. As described above, these three cell types are all affected by the presence of a GBM, so it stands to reason that the functionality of the BBB would be affected in some way. Tumours have a number of effects on the BBB, including but not limited to: a loss of astrocytic connections, heterogenous permeability, reduced integrity but maintaining limited drug permeability, and interactions with tumour cells (Arvanitis *et al.* 2019). These factors add extra complexity to the determination of drug delivery methods and dosing, and techniques such as convection enhanced delivery and surgical site drug delivery (e.g. via wafers or gels) are being trialled to try and circumvent these issues, but still require optimisation (Vellimana *et al.* 2013; Chowdhary *et al.* 2015; Arvanitis *et al.* 2019).

1.1.5 Treatments in development

1.1.5.1 Tumour Treating Fields

Tumour treating fields (TTFs) are a low intensity alternating 200 kHz electrical fields, delivered to the tumour via a device worn on the patients' shaved scalp for ideally >18 hours per day. They act by blocking cell division by disrupting microtubule assembly. Dividing cells eventually die via apoptosis (Hottinger *et al.* 2016). TTFs have been investigated in phase III trials for both newly diagnosed and recurrent GBM. In the recurrent trial, TTFs did not show a significant improvement over the control group, with a median overall survival of 6.6 months vs 6.0 months. However, TTFs were still approved by the Food and Drug Administration (FDA) for use in the USA, and data from clinical use then showed a median overall survival of 9.6 months, with use being initiated earlier, rather than as a last resort. These data are uncontrolled, but seem to indicate an improvement in overall survival for patients with recurrent GBM. The phase III trial for newly diagnosed GBM showed a successful improvement compared with control with median overall survival reaching 19.6 months vs 16.6 months. There were some side effects associated with TTFs, including local skin irritation and headaches, but no increase in seizures. TTFs were also approved by the FDA for use in newly diagnosed GBM. However, TTFs are still a very expensive treatment and because of this are not currently available on the NHS (NICE 2018; Guzauskas *et al.* 2019).

1.1.5.2 Immunotherapy

Over recent years, immunotherapy has risen in popularity for treatment of GBM. Although not yet at the point of being universally implemented, immunotherapeutic treatments have shown promise in clinical trials so far and include vaccination therapy, T cell therapy, immune-checkpoint blockade and oncolytic viral therapy. GBM creates an immunosuppressive microenvironment through increased levels of programmed death-ligand 1 (PD-L1), expression of indoleamine 2,3-dioxygenase (IDO) enzymes, signal transducer and activator of transcription 3 (STAT3) signalling, and induction

of apoptosis in immune cells. In comparison to other tumour types, infiltrating T cells are far outnumbered by resident TAMS in GBM, which indicates that different immunotherapy treatments are likely to be required in GBMs compared to other solid tumours.

A significant obstacle however, is that the standard of care for GBM currently has immunosuppressive properties due to radiation, chemotherapy and steroid use. It is therefore important to take this into account in trial design and implementation of immunotherapies into care regimes. It has also been suggested that immunotherapy treatments may be more effective when a larger tumour mass remains, able to trigger a significant immune response (Lim *et al.* 2018).

Chimeric antigen receptors (CAR) are synthetic receptors that can be used to direct T cells to selectively target GBM cells over healthy cells for destruction. The technology is being developed for a number of cancers (Priceman *et al.* 2015; Akhavan *et al.* 2019). Although promising, their use in GBM is limited by tumour heterogeneity, the immune suppressive microenvironment, and difficulties with delivering the cells to the tumour site. CAR T cells are developed from the patient's own T cells, which are cultured *ex vitro*, stimulated to become active, and genetically modified to express the CAR through viral transduction. The CAR T cell population is then cultured in a selection of cytokines, although the specific ones used vary between manufacturers. CAR T cells can then be delivered in large volumes directly to the tumour site, via a device inserted during surgery. The cells can be engineered to target tumour specific antigens or mutations such as CD133, *EGFRvIII*, IL13Rα2, *HER2*, *CSPG4* and *EphA2* (Lim *et al.* 2018; Akhavan *et al.* 2019). The availability of EGFRvIII has particular relevance for patients with the classical subtype of GBM, as this is typically the subtype where EGFR mutations are found (Verhaak *et al.* 2010). It is possible that future treatments for GBM will require testing patients for subtype as well as methylation and *IDH-1* status in order to guide decision making. Although CAR T cells have shown tumour infiltration and eradication of tumour mass,

trials so far have still shown recurrence, with tumours seeming to adapt and lose the original target expression (Lim *et al.* 2018).

Peptide vaccines which target specific mutations or antigens have reached phase III clinical trials. Rindopepimut, which targets the *EGFRvIII* mutation showed promise in early trials, but the phase III trial was terminated early due to a lack of patient response. However, a phase II trial using rindopepimut in combination with bevacizumab was more positive, which demonstrates that combination therapy may be key to using immunotherapeutic options to treat GBM. Peptide vaccines for the secondary GBM marker *IDH-1* R132H mutation are currently in phase I trials.

Dendritic cell vaccines have also reached phase III clinical trials for GBM with DCVax-L (dendritic cell vaccine, Northwest Biotherapeutics). Dendritic cells are cultured from patient blood samples and treated with tumour lysate from surgically resected tissue. This primes the cells to attack the patient's tumour. The patients are then repeatedly treated with the primed dendritic cells over the course of treatment by intradermal injection. This process starts with injections every ten days and is eventually reduced to six month intervals (Liau *et al.* 2005). Although the trial is still ongoing, early results have been released, which indicate an improvement in median overall survival of 23.1 months for still-blinded patients compared with the usual 15-17 (Liau *et al.* 2018). The median overall survival also seemed to be more favourable for patients with a methylated *MGMT* promoter (34.7 months). TMZ was used in both treatment and control groups.

Although previously considered separate strategies, the immune response triggered by oncolytic viral therapies has inexplicably linked them to immunotherapy. Viruses such as retroviruses, adenoviruses and polio virus can enter tumour cells and activate macrophages. A phase 1 clinical trial for the polio virus-derived therapy recombinant non-pathogenic polio-virus chimera (PVSRIPO), which recognises the CD155 receptor commonly expressed on GBM cells, showed promising results in patients with recurrent

GBM (Desjardins *et al.* 2018). The treatment is delivered via catheter directly into the tumour site.

Immune checkpoint inhibitors are antibodies which counteract the T cell suppressive behaviour of tumours. They have been developed to block immune checkpoint proteins such as cytotoxic T-lymphocyte-associated protein 4 (CTLA-4) and programmed cell death protein 1 (PD-1). Preclinical studies for GBM have been positive but a phase III clinical trial for nivolumab, which has had success in other cancers, failed to meet its overall survival target for patients with an unmethylated *MGMT* promoter. A parallel study is still ongoing for patients with *MGMT* methylation (Weller *et al.* 2016; Bristol-Myers Squibb Company 2019).

It is becoming clear that combination therapies will likely hold the key to immunotherapy for GBM, in order to simultaneously challenge any compensatory mechanisms with other immunotherapies or treatments such as stereotactic radiosurgery, which does not have the same immunosuppressive effect as standard radiotherapy (Lim *et al.* 2018).

1.1.5.3 Nanoparticles

Nanoparticles encompass a number of technologies, including liposomes, nanoemulsions, polymeric micelles and iron oxide nanoparticles. These can contain or be conjugated to various anti-tumour substances such as chemotherapeutic drugs or siRNA. Their main advantage is that they are easily delivered to GBM cells, as a result of the increased BBB permeability and damaged lymphatic system which are found in GBM. However, the heterogeneity of GBM can mean that nanoparticles are not delivered evenly, and so work is undergoing to improve targeting to deliver nanoparticles directly to tumour cells (Huynh and Zheng 2015; Michael *et al.* 2018).

1.1.5.4 Other ongoing trials

There are many phases of trials currently active, including ones for repurposed or combination therapies. A few trials of particular interest in the UK are described below, but do not constitute a comprehensive list.

Depatuximab mafodotin, known as ABT-414, is an antibody drug conjugate currently in phase II trials for GBM (NCT02573324). It targets tumours with overexpression of EGFR by binding to cells with an amplification, mutation, or overexpression of the receptor, and then delivers a cytotoxin into the cell. It successfully crosses the BBB. ABT-414 is relatively well tolerated, and the most common side effects are ocular in nature, but recoverable (Reardon *et al.* 2016; Gan *et al.* 2018).

Olaparib is a PARP inhibitor commonly used in the treatment of ovarian and breast cancer, with a particular benefit in patients with *BRCA* gene mutations (Munroe and Kolesar 2016; Robson *et al.* 2017). It acts as a radiosensitiser, making cancer cells more sensitive to treatment with radiotherapy. The PARADIGM trials are parallel phase I clinical trials testing dose escalation for olaparib treatment in GBM, with or without *MGMT* promoter methylation. If well-tolerated, the trial will then move into a phase II regimen (Fulton *et al.* 2018).

Ipilimumab is an immune checkpoint inhibitor which has been used in multiple cancers (Mason *et al.* 2019; Ready *et al.* 2019). There is also an ongoing phase II trial for ipilimumab in GBM (Mulholland 2018). A small non-randomised trial has shown a potential benefit to combining ipilimumab with bevacizumab (Carter *et al.* 2016).

1.2 Models of GBM

1.2.1 *In vitro* models of GBM

The problem with modelling a disease is that simpler models have simple, easy readouts, and are more applicable to large scale experimentation, but are poorly representative of overall disease, whereas complex models have much more difficult readouts with more confounding factors, and lower throughput, but are usually more representative of the disease conditions and microenvironment. It is important to have models at various different levels of complexity, for answering a range of questions. Individual cellular models may be the best for answering questions about specific molecules or pathways, whereas *in vivo* models are often required for pharmaceutical testing. Therefore, a range of models are needed which are as physiologically relevant as possible for their level of complexity, which can be used together to provide answers to research questions.

Existing *in vitro* models of GBM can be roughly sorted into five categories: 2D established cell lines, 2D patient derived cell lines, simple 3D cell models, complex 3D cell models, and organ-slice models. There are subtypes of each of these models, but they reflect the relative levels of complexity found in GBM modelling and are summarised in **Figure 1-4**.

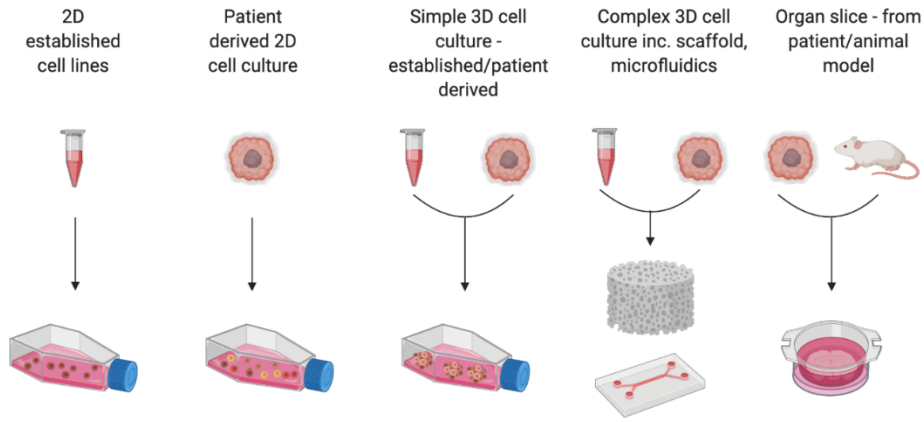

Figure 1-4:* In vitro *model types of GBM.

A summary of the text is shown. In vitro *model types can be categorised as 2D established cell lines, patient derived 2D cultures, simple 3D cultures, complex 3D cultures, and organ slice models. Difference sources of cells or tissue can be used for most models. Figure created using biorender.com.*

1.2.1.1 2D and cell line models of GBM

The most basic available models of GBM are the established cell lines present throughout the literature. These were originally developed from primary human GBMs, but have been through decades of culture and passaging. The cell line U87 (also reported as U87MG) has been in use for over 50 years, but it was recently discredited by the group from Uppsala University who originally developed the cell line (Allen *et al.* 2016). They used short tandem repeat DNA profiling to compare their stocks of the original U87 cell line with the U87 cell line available publicly from the American Type Culture Collection (ATCC). They found that the Uppsala U87 and ATCC U87 cell lines were from different original sources. Previous short tandem repeat profiling of the U87 line by Bady *et al.* (2012) matched the ATCC line but not the Uppsala sample. The authors believe that the sample was contaminated or replaced at some point between providers, and recommend the use of more recent cell lines, established and maintained in serum-free media, with short tandem repeat genotypes available for comparison. However, despite this advice and available alternatives, U87 is still being used in many labs. With a search limited to after the publication of the U87 profiling, over 800 PubMed references still appear for "U87 glioma". Other established cell lines also include U251 and U373, which even without contamination, have still undergone long term culture in serum, known to diminish the population of stem cells by triggering differentiation (Lee *et al.* 2006). The research community is moving away from these established cell lines, towards recently developed and better characterised patient derived lines.

To replace the established cell lines, multiple groups have developed or used GBM patient-derived cell lines. There are now banks available of patient-derived cell lines which are of a low passage and cultured entirely serum-free to reduce the possibility of genetic and epigenetic drift, and maintain a stem-like state. The human glioblastoma cell culture (HGCC) resource, developed by Uppsala University, has a bank of 48 cell lines covering the

four subtypes established by Verhaak *et al.* (2010), although this does include the now no longer used neural subtype category. The HGCC has clinical and genetic profiles for all the lines available, and has characterised their proliferation level, tumorigenicity in mice, and transcriptional stability. Stringer *et al.* (2019) have also developed a collection of 12 low passage, serum-free, patient-derived cell lines. Clinical, subtype, and subtype stability information is available for all lines, in addition to genetic characterisation.

Patient-derived cell lines represent a significant improvement in the representativeness of 2D GBM models. They are still a very simple model of a complex disease, but are essential for high-throughput and basic research. With the banks of patient-derived cell lines available, hopefully the field can move on from the previous, poorly categorised established cell lines to a more relevant model. Cell lines in 2D can be easier to maintain and expand (Pollard *et al.* 2009; Xie *et al.* 2015). There are limits to 2D models however, as growing cells as a monolayer has been shown to affect patient translatability, particularly the cells' response to chemotherapy or radiotherapy in a number of disease models (Zschenker *et al.* 2012; Luca *et al.* 2013). Differences have been demonstrated between 2D and 3D GBM models, although with ATCC-purchased U87 cells only, so this can not necessarily be extrapolated to GBM in general (Ma *et al.* 2018). Yu *et al.* (2018) demonstrated that both 2D and 3D cultures of primary GBM cells can be used in a high throughput platform, although they did note some drug-specific differences between 2D and 3D responses in their system. The discovery of key mutations in *p53* and receptor tyrosine kinase dysregulation led Sancho-Martinez *et al.* (2016) to develop a human induced pluripotent stem cell (iPSC) line to investigate these driver mutations as a model for GBM.

1.2.1.2 Simple 3D GBM models

Patient-derived cell lines can also be adapted into simple 3D models such as spheroids. 3D models can also be developed from established cell lines, iPSCs, or primary cells directly from patients. For adherent primary cells,

culture flasks are coated with laminin. Without this, the primary GBM cells will usually form spheroids suspended in the culture media (Pollard *et al.* 2009). Cells that have been grown as adherent cultures can be triggered to form spheroids by a change of media conditions, therefore providing simple 3D structures for experimentation (Yu *et al.* 2018). Spheroid models are becoming increasingly popular, as they provide an extra level of complexity and representation beyond that of 2D models, but are also still relatively high throughput, depending on the cells used. Systems such as the hanging drop method, rotary cell culture and non-adherent flasks can be used to encourage spheroid formation. Self-aggregating models can however lead to inconsistently sized spheroids, which can make high throughput systems difficult to use, especially if manual selection of the spheroids is required. Adaptations have been made to some models to improve their throughput and consistency. There are also concerns about the specificity and reproducibility of spheroid formation models, including the effects of growth factors and a wide variety of protocols between groups (Pastrana *et al.* 2011). Tung *et al.* (2011) have developed a hanging drop system which works within a 384-well plate high throughput system, and which demonstrates marked differences in chemotherapeutic response between 2D cultures and their 3D system. However, it is important to consider that the cells may have undergone genetic or epigenetic drift while in 2D culture that may not be resolved by returning them to a 3D environment. Therefore some models form and maintain cultures in 3D. Zhang *et al.* (2018) cultured primary human GBM cells directly as neurospheres in order to test their drug candidates against the standard TMZ. They used these alongside an established cell line, cultured in serum, U251N, but acknowledged that this represented a more differentiated population of tumour cells.

1.2.1.3 Complex 3D GBM models

To increase the physiological relevance of 3D models, many hydrogel and scaffold systems have been developed. The most well-known of these is Matrigel, but other methods include polystyrene scaffolds, nanofibre

scaffolds, and alginate gels (Hubert *et al.* 2016; Gomez-Roman *et al.* 2017; Hermida *et al.* 2019; Saleh *et al.* 2019). They aim to recapitulate the microenvironment of GBM, as this has been demonstrated to have a significant effect on tumour cell behaviour and drug response. There are many features to consider when selecting or designing support structures for GBM. Importantly, the structure and constituents of the brain's ECM differs in composition from other organs, and local differences are present as a result of the tumour (**1.1.4.4,** Bellail *et al.* 2004). The amount of pressure imposed by the scaffold is also important, especially for the study of GBM cell invasion.

Scaffold systems allow large, 3D cultures of GBM to be grown and monitored over time. This means that the growth, invasive, or survival of individual cultures can be tracked, and their responses to stimuli measured directly. These more complex 3D culture systems can also allow for co-culture of multiple cell types or lines (Hermida *et al.* 2019). 3D scaffolds also allow for the introduction of an oxygen gradient, and cell invasion through a substrate which mimics the healthy brain.

Matrigel is a simple to use reconstituted basement membrane which can be used to encase tumour cells. It is however poorly defined, and derived from a mouse sarcoma, so there are concerns about cross-species differences. It is also rich in collagen, which is far more rare in the brain ECM. This is also a concern with collagen-based matrices, which provide poor models for invasion especially. Alternatives include alginate-chitosan (Wang *et al.* 2016), polyethylene glycol (PEG, Xiao *et al.* 2018), and brain-derived ECM (Yi *et al.* 2019).

One feature that is not represented in static 2D, 3D, or scaffold models is the flow of interstitial fluid around the tumour microenvironment. This is yet another complex aspect of the tumour microenvironment which groups are aiming to model, through the use of microfluidic platforms (Akay *et al.* 2018). These '-on-a-chip' models enable wells and channels to be printed or etched into a material such as glass, silicone, or hydrogels. The chips can be

designed specifically to allow or prevent molecule and/or cell transfer between the wells and channels. This allows features such as cell-cell communication and drug interactions to be measured. Some 3D models combine these techniques, such as in the bioprinted 'human-glioblastoma-on-a-chip' model developed by Yi *et al.* (2019), which uses decellularised porcine brain to provide an ECM as close as possible to the human brain. They also designed the chip to have an oxygen gradient representative of that in a GBM tumour, with oxygen access at the edges of the structure only causing the development of a necrotic core in the cultured GBM cells.

Bio-printing technology has also been used by Hermida *et al.* (2019) to create a 3D modified alginate model of GBM, combining multiple cell types into one model. They combined mCherry-expressing GBM stem cells, green fluorescent protein (GFP)-expressing microglia, and cerulean-expressing glioma-associated stromal cells in one 3D printed matrix model.

Co-culture systems allow GBM cells to be cultured alongside microenvironmental cells to further understand their roles in tumour development. Cell lines used can be from the same or different species, although the potential cross-species effects of the latter must be taken into account. Often, the cell lines used are established lines, which limits the translatability of the model from the start. The use of lentiviral transfection to produce fluorescently tagged cell lines is particularly common in co-culture systems and allows simple tracking of the different cell types without fixation and/or antibody staining. Although many studies are somewhat limited by their reliance on U87 cells, systems have been demonstrated for the investigation of angiogenesis by co-culturing GBM tumour cells with human umbilical vein endothelial cells (HUVECs, Chen *et al.* 2009; Nguyen *et al.* 2016). The supportive/protective role of non-tumour astrocytes has also been demonstrated in co-culture systems with established and patient derived GBM cell lines (Yang *et al.* 2014; Mega *et al.* 2019). Oppermann *et al.* (2018) demonstrated how a fibroblast co-culture model could be used with patient derived primary GBM cell lines to investigate cell migration and

drug response. Importantly, co-culture models have been developed to investigate the complex interactions between GBM tumour cells and microglia (Coniglio *et al.* 2012; Hermida *et al.* 2019). Multiple groups have developed different models which combine human embryonic stem cell (hESC)-derived organoids to represent the healthy brain, and primary patient-derived glioblastoma cells, to monitor tumour cell proliferation and invasion (Cosset *et al.* 2019; Linkous *et al.* 2019).

Predominantly, *in vitro* models of GBM rely on pre-established populations of tumour cells. These are useful for investigating invasion, proliferation, and drug response. However, they do not give an insight into the initial development of the tumour itself. This is where genetically modified cell lines play a role. Bian *et al.* (2018) developed a model using transposon and CRISPR-Cas9 technology to trigger the formation of GBM-like tumours in cerebral organoids, allowing them to investigate the early stages of tumour formation. A similar technique has been established by Ogawa *et al.* (2018) who have also demonstrated that both their tumour-organoid cells and primary patient-derived GBM cells can be implanted into other cerebral organoids to initiate tumour formation. With the growing popularity of CRISPR-Cas9 technology, further groups and models are likely to join them.

3D models are typically more physiologically relevant than 2D models, and the range of techniques available allows for more complex hypotheses to be tested. Co-culture and bio-printing models demonstrate the increasing complexity of these systems. However, they are usually more expensive than 2D models, and many are still reliant on, or developed using, U87 or other established cell lines which are not sufficiently representative of primary tumour cells. The use of synthetic gels and scaffolds has unknown effects on cell behaviour and treatment response, and it is important to establish how these may differ in models of the brain and tumour microenvironment when compared with other organs.

1.2.1.4 Organ slice models

Organ slice models have frequently been used in neurological research, and more recently for GBM (Stoppini *et al.* 1991). They can be created from primary human GBM samples or mouse brains (Merz *et al.* 2013; Marques-Torrejon *et al.* 2018). Merz *et al.* (2013) used primary human samples which were sliced to a thickness of 350 µm and placed on a membrane insert in a 6 well plate containing serum-free media. The slices retained histopathological features of GBM over a minimum of 16 days. The slices were then treated with TMZ or irradiated to mimic patient treatment, and the responses measured in proliferation levels, DNA damage, necrosis and apoptosis levels. Marques-Torrejon *et al.* (2018) used 200 µm slices of young adult mice in a similar model, also with serum-free media to avoid triggering differentiation of any NSCs. They then engrafted patient-derived GSCs into the slices, allowing them to investigate host-graft interactions without having to sacrifice animals post-graft. They were also able to use the organ slice model to monitor responses in proliferation and DNA damage to TMZ and cytosine arabinoside (another anti-mitotic drug) specifically in the GFP-labelled GSCs.

These examples demonstrate the potential applications of organ slice models in GBM research. However, there are limitations to organ slice models. Culture length can be a limitation, as slices can often lose integrity and degrade after 2-3 weeks. Organ slice models are not applicable for high-throughput systems, due to the requirement of whole organs or tissue samples, but they do provide a level of complexity beyond that of the simple 3D culture models, as they maintain the architecture and cell types of the brain or tumour.

1.2.2 *In vivo* models of GBM

Although there are many similarities between mouse and human brains, there are also many species-specific differences, particularly in the proportions and transcriptional profiles of the different cell types. Single nucleus RNA sequencing analysis of frozen human cortex samples compared to single cell RNA sequencing of mouse cortex revealed that the most differences were found in non-neuronal cells, and that the most commonly altered structures included neurotransmitter receptors, ion channels, cell adhesion molecules and extracellular matrix components (Hodge *et al.* 2019). *In vivo* models of GBM are predominantly performed in mice, although rats are sometimes used (Miyai *et al.* 2017; Giakoumettis *et al.* 2018; De Meulenaere *et al.* 2019). However, some experiments have used canine models, as dogs develop spontaneous GBM tumours (Chen *et al.* 2013; Hubbard *et al.* 2018). Porcine xenograft models have also been used (Selek *et al.* 2014; Khoshnevis *et al.* 2017). Smaller animal models such as drosophila and zebrafish have also been used (Feitsma *et al.* 2008; Witte *et al.* 2009). There are three main types of mouse model for GBM, although these techniques are not limited to mice. Graft models, viral-mediated models and genetically engineered models will be discussed briefly below. Chemically induced mutations were previously common but have become somewhat replaced by the more targeted approaches (Schiffer *et al.* 1978; Robertson *et al.* 2019). A visual summary of the models is shown in **Figure 1-5**.

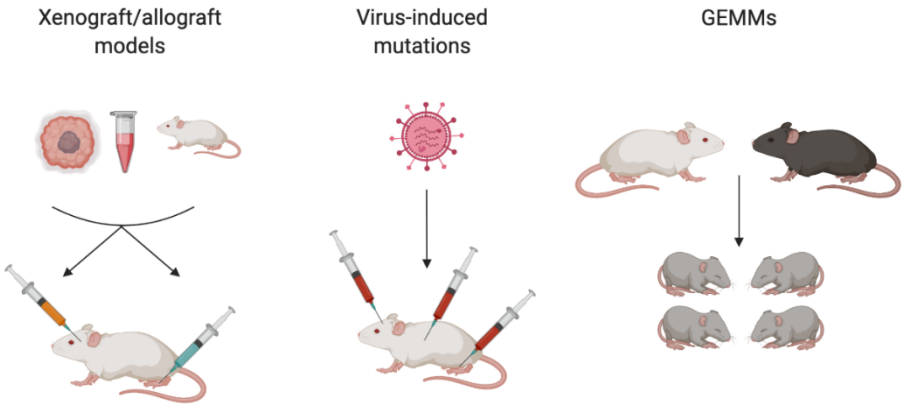

Figure 1-5: **In vivo *mouse models of GBM.***

A summary of the text is shown. Commonly used mouse models can be categorised as xeno/allograft models, virally-induced models, and genetically engineered mouse models. Different cellular sources and/or injection routes are shown. Figure created using www.biorender.com

1.2.2.1 Xenografts/allografts

Graft models can be subcategorised in two ways. The models can either use cells or tissue from a different species (xenograft) or the same species (allograft). Either graft type can then be injected in the disease relevant location (i.e. intracranially for GBM, orthotopic) or in a different location (e.g. flank, heterotopic). Xenograft systems are often used to maintain primary human xenograft cultures (Lee *et al.* 2019). These cultures are then known as patient derived xenografts (PDX) and initially to maintain some of the original tumour heterogeneity (Soeda *et al.* 2015). They are however subject to genetic selection and drift over multiple passages (Ben-David *et al.* 2017; Zhao *et al.* 2019). Tumours can also be implanted into mice without undergoing *in* vitro culture in between. These are known as patient-derived orthotopic xenografts (PDOX) but do not provide a significant advantage over PDX models (deCarvalho *et al.* 2018). However, grafts have often been established from established cell lines such as U87 (Miyai *et al.* 2017; Ovcharenko *et al.* 2019). This is a key limitation of such models, as if the cell line used is not physiologically relevant, then implanting it into a more appropriate microenvironment does not make it a more appropriate model. The best xenograft model needs to start with an appropriate population of cells for implantation, or their relevance is limited before the experiment begins. Some techniques will use cells cultured for a short time as spheroids, so that they are maintained in a somewhat 3D environment, and/or cells which have been engineered to carry oncogenic mutations through techniques such as CRISPR-Cas9 (Stringer *et al.* 2019).

The primary limitation of xenograft models is that the mice cannot have an intact immune system, as it would attack the graft cells. Various immune-incompetent models such as SCID or NOG mice are therefore used. This means that the actions of microglia, a key cell type in the GBM microenvironment, are lacking in these models. This is in addition to the species difference problem, which can significantly affect the translatability of any results from animal models. Despite the lack of microglia, the other

constituents of the microenvironment are still present. However, the difference in species means that this microenvironment may not be representative of the tumour microenvironment in humans. Research is ongoing to produce mice with humanised immune systems, but the focus of this research has been on T-cells as opposed to microglia (Billerbeck *et al.* 2011; Lathia *et al.* 2015; Mahne *et al.* 2017). In comparison however to other mouse models, graft models are fast and cheap to use. Graft models, much like many 3D *in vitro* models, are often used to look at later stages of tumour development.

1.2.2.2 Genetically engineered mouse models

Genetically engineered mouse models (GEMMs) are used, much like genetically engineered organoids, to look at initial tumour formation and the roles of specific genes and pathways in GBM. They are however much slower and more expensive than the simpler graft models, but can be developed in immunocompetent animals, meaning that the important impact of the immune system can be studied. GEMMs are developed by breeding animals with mutations in oncogenes and tumour suppressors together to produce offspring with a combination of mutations that lead to tumour development. Using conditional knockout or alteration models such as Cre-*lox*P can allow the use of mutations which would be lethal if present from early development. Key oncogenes and functions such as *EGFR, NF1, Trp53*, and *PTEN* are used as targets. Mouse offspring can then be produced with multiple key oncogenic mutations. The development and progression of tumours in these mice can then be monitored, and any further accumulated mutations analysed. These models have been of particular importance in research into the GBM cell of origin (Alcantara Llaguno *et al.* 2015; Robertson *et al.* 2019). GEMMs do require large breeding programs, which is of significant concern when trying to reduce the number of animals required for GBM modelling.

1.2.2.3 Viral-mediated

Another method of triggering tumour formation in mice is with viral-induced genetic alteration. Lentiviruses, adenoviruses and retroviruses have all been used for this purpose. The virus is used as a system to delivery GBM-specific oncogenes into mouse models. Similarly, to GEMMs, these models can then provide insight into initial tumour formation and cell of origin. The route of injection is particularly important in this system, as the amount of virus required increases dramatically as the specificity and invasiveness of the location decreases. An intracerebral injection requires the least virus, is the most specific, but also the most invasive route. Intravascular infusions require the most virus, are the least specific, but also the least invasive. Intrathecal and intraventricular injections lie in between.

1.2.3 Discussion of GBM models

Despite the plethora of GBM models available and significant discoveries in GBM origins and genetic characterisation, little progress has been made in drug development or prognosis for these patients. Many areas of research have shown promise early on, only to fail in clinical trials. In the cohort of trials studied by Vanderbeek *et al.* (2018), only one of eight phase III trials was successful, this being the 'NovoTTF' trial for TTFs. Even when treatments such as this have shown effectiveness, this does not necessarily mean that they are accessible to patients due to financial limitations and small survival advantages. Vanderbeek *et al.* (2018) also reported low patient participation in trials, which given the heterogeneity of the disease, reduces the possibility of determining subtype or status-specific treatment efficacy for GBM. This is especially important as targeted treatments are being developed for patients with certain specific mutations such as *EGFRvIII* or *PDGFRA* mutations (Chuang and Lin 2019). As GBM mutations and subtypes become better characterised, it is possible that treatments would become more personalised and effective, but to achieve this, highly predictive models are needed which represent the inter- and intra-tumour heterogeneity of GBM. To some level, this is already seen in the stratification of patients with or without *MGMT* promoter methylation, due to their different sensitivities to TMZ treatment.

The late-stage failure seen in GBM clinical trials implies that the current models being used for treatment response are failing to predict efficacy in GBM. Not only does this lead to false positive errors, where ineffective treatments are being taken through to late stage clinical trials, it also implies that potentially effective drugs are being miscategorised as ineffective and discarded earlier in the pipeline. In order to develop effective treatments for GBM, it is essential to improve the physiological relevance and predictiveness of the models being used at each stage of complexity. Furthermore, if the treatments being taken forward from *in vitro* models are potentially ineffective, it is a waste of animals and resources to assess their

effectiveness *in vivo*. This is compounded by the limits of certain *in vivo* models, particularly regarding the common lack of immune system integration. Although there is a broad overlap, there are still differences in gene expression profiles between human and mouse microglia, and expression profiles are significantly affected by disease (Masuda *et al.* 2019). Therefore, even in immuno-competent models, there may still be species-specific differences in the interaction between tumour cells and microglia.

Overall, there are many *in vitro* and *in vivo* models which aim to represent different stages of GBM development and behaviour. However recent characterisation of established cell lines and increasing understanding of GBM stem cells and origins have revealed many of these models to be insufficiently representative of the human disease. Therefore it is important to adapt old or develop new models to be more physiologically relevant, in order to discover efficacious treatments for this disease.

1.3 The HiSpot® model

1.3.1 Previous research and development of the HiSpot® model system

The HiSpot® is an *in* vitro air-liquid interface model in which dissociated cells from primary tissue or stem cell-derived spheroids are seeded at a high density, allowing them to re-aggregate and develop into a 3D structure (Sundstrom *et al.* 2012). It is adapted from the organ slice model developed by Stoppini *et al.* (1991) and initially developed for the culture and expansion of human embryonic stem cell derived NPCs, although the technology has now been adapted to a wide range of uses (Preynat-Seauve *et al.* 2009; Sundstrom *et al.* 2012). The model was previously successfully used for the culture of human glioblastoma cells, although these had undergone culture to produce spheroids prior to seeding onto the PFTE membranes, so would represent tumour stem cells only. The model is formed of a 6 well plate, containing ~1 ml media per well. A semipermeable membrane insert is placed in each well on top of the media. Three small 'confetti' disks are then placed on top of the insert membrane. Cells are added on top of each confetti disk (***Figure* 1-6**). Cells are prevented from drying out by a nanofilm of medium which coats the culture. The air-liquid interface system allows for thick 3D cultures to grow without reaching high levels of hypoxia. Further details of the HiSpot® culture set up are described in sections **2.2** and **2.3.**

The model was then further developed for the culture of postnatal rodent CNS tissue (Bailey *et al.* 2011), and more importantly for the current topic of discussion, the study of glioblastoma (Biggs *et al.* 2011). This study combined GBM cell lines (LN18, GL15, U87, A172) with rat brain cells at a ratio of 5%:95% to create HiSpot® cultures containing small numbers of GBM cells. The authors transfected the GBM cells with GFP to allow the cells to be easily identified within the mass of healthy brain cells. The GBM cells developed into aggregates within the brain HiSpots® and recapitulated features of GBM, i.e. 5-ALA conversion to its fluorescent substrate, and lactate production. Biggs *et al.* (2011) also confirmed the response of their

GBM/brain HiSpots® to TMZ treatment, demonstrating a reduction in the fluorescence levels of GFP within the cultures over six days of TMZ treatment. They also showed that a similar TMZ regimen had little effect on 2D cultures of the same GBM cells, and that cytosine arabinoside and taxol, which show effectiveness in 2D but not clinically, were ineffective or significantly less effective within a clinically appropriate range on GBM/brain HiSpots®.

The HiSpot® model has also been successfully used for the culture of cardiac cells (Zhao *et al.* 2016), as well as primary human hippocampal and cortical tissue from patients with epilepsy (Zhu 2018). BioIVT, who currently hold the intellectual property licence for the technology**,** offer their disease modelling services using the HiSpot® (as OrganDot™) model for lung cancer, lung fibrosis, and pancreatic islet modelling. As the HiSpot® model has been demonstrated to successfully and three-dimensionally culture many different cell types, including GBM lines, it was chosen for this project to be developed into a further tool for tackling GBM.

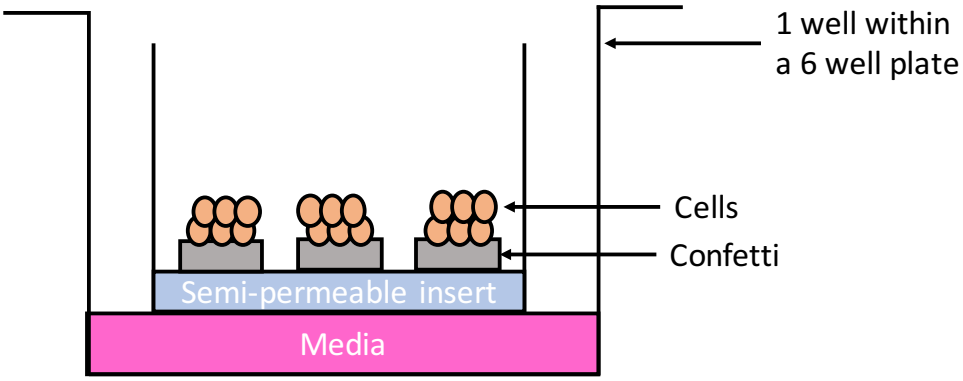

Figure 1-6: A cross-section representation of the HiSpot® model.

A cross section of the structure of the HiSpot® model. Media is placed in each well of a 6 well plate. A semi-permeable membrane insert is placed on top of the media. Three confetti disks per well are placed on top of the membrane. Cells are pipetted gently on top of the confetti disks. This structure keeps the cells out of the media but allows them to access the media. A nanofilm of media is drawn up and over the cells which prevents them from drying out.

1.4 Summary and thesis aims

Glioblastoma is an aggressive, incurable, heterogeneic disease that is extremely complex to represent in models either *in vitro* or *in vivo.* Many previous models have been based on or developed using established cell lines now known to be flawed due to their lack of representation of the stem cells or diversity of the original tumours. Few models are able to recapitulate the interaction of the tumour with its local immune microenvironment, which is key to determining the tumour's sensitivity to treatment. The organ slice model is capable of supporting the function of brain tissue for studies, and this functionality is developed further in the HiSpot® model for tissue reaggregation. It has been previously been shown that the HiSpot® model is capable of supporting human GBM-derived cells, and can be used to monitor treatment response. Xenograft models are commonly used to culture primary human brain tissue, but lack the immune microenvironment of the original tumour and subject the cells to non-human factors. In this study the HiSpot® model will be optimised to best culture primary human GBM cells, with the inclusion of microglial cells if possible, to provide a simple, 3D, human-only model for GBM which represents the heterogeneity and reactivity of the original tumour. This will then be used for mechanistic and pharmacological studies into GBM. Primary cells were obtained from patients undergoing neurosurgery for the removal of potential GBM tumours at the University Hospital of Wales through the Welsh Neuroscience Research Tissue Bank (WNRTB).

Aims:

1. Optimise the pre-existing HiSpot® protocol to stably culture primary human GBM cells, prioritising tumour cells and microglia
2. Confirm that the optimised protocol produces a culture model which represents key pathological features and pharmacological response of GBM in human patients
3. Determine whether the HiSpot® model can recapitulate the variation of cellular and structural features, and pharmacological responses, between biopsy locations

2 General Materials and Methods

2.1 Patient identification and consent

Suitable patients were identified by clinical staff while attending the Neurosciences Department at the University Hospital of Wales. Informed consent was obtained via the WNRTB (Ethics Rec Ref: 14/WA/0073 and 19/WA/0058) using the relevant patient information sheets and consent forms (**Appendices 8.1-4**). Consent was obtained by clinicians or research tissue bank team members trained in obtaining informed consent and with full Cardiff University Human Tissue Act (HTA) governance training. All patient tissues were link anonymised by WNRTB. An application was made to the WNRTB to obtain fresh brain tissue, acutely from neurosurgery and approval was granted. Clinical and pathological data were collected by a member of the neurosurgical clinical team, anonymised, and matched to WNRTB patient sample codes. No identifiable information was shared. All cell culture and post-fixation analysis was performed under HTA approved conditions in HTA approved laboratories. Pathology report data and images were anonymised and linked to coded patient sample numbers by NHS clinical staff. Not all data were available for every patient, but these absences are noted in the data set provided.

2.2 Tissue Processing

The steps of tissue collection and processing are detailed in **Figure 2-1** and are described below. Unless otherwise specified, cell culture consumables used were obtained from Gibco (Life Technologies). Upon collection tissue was immediately placed in 30 ml Gey's solution (Sigma Aldrich Company Ltd, G9779) with 10µM (+) MK-801 maleate (MK-801, Abcam ab120027), on ice (**A**). This was transported to the laboratory within 5 mins. Using a McIlwain tissue chopper, the tissue was chopped to produce approximately 1mm cubes (**B**). These were transferred to a petri dish and dissociated in 30 ml DMEM (Life Technologies, 41965062), with 1 µl/ml MK-801 and 2mg/ml

papain (Sigma, P4762-1G) at 37°C and 5% CO_2 for 45 mins (**C**). The solution was filtered using a 50ml syringe (Greiner Bio-one, SYR50) and a 0.22 µm filter (Millex GV, Merck, F7648) before use.

> *Optimisation: For the creation of HiSpots® from GBM23 onwards, two additional enzymes were used for tissue digestion. These were 1mg/ml dispase II (Roche, 4942078001) and 0.1mg/ml DNase I (Roche, 10104159001), in accordance with Siebzehnrubl and Steindler (2013). The papain, dispase II, DNase I and MK-801 were dissolved in fresh DMEM and then filtered as above. 25 ml aliquots of this filtered enzyme solution were then stored at -20°C, and only defrosted on the day of tissue collection. Once or twice during the digestion period, the tissue was also triturated using a Pasteur pipette to encourage the breakdown of large pieces of tissue.*

The remaining tissue was triturated using a Pasteur pipette. Cells were strained through 100 µm (VWR International Ltd, 734-0004) then 40 µm cell strainers (**D**, VWR International Ltd, 734-0002) and centrifuged at 244g (1100 rpm) for 5 minutes (**E**, Eppendorf centrifuge 5810, A-4-81). The supernatant containing the digestive enzymes was removed (**F**), and the pellet made up to 10 ml with fresh media (**G**). A 20 µl sample of the cell solution was diluted in 180 µl trypan blue solution (Life Technologies, 15250061) and mixed thoroughly (**H1**). 10 µl of this was added to a haemocytometer (Reichert Bright-Line® Improved Neubauer 0.1mm deep) for cell counting (**I1**). A mean count from 3-4 squares was used to calculate the total cell count in the 10 ml cell suspension. The cell suspension was then centrifuged again as above (**H2**). The supernatant was removed (**I2**) and the resuspended at the required density (**J**, see **2.4**).

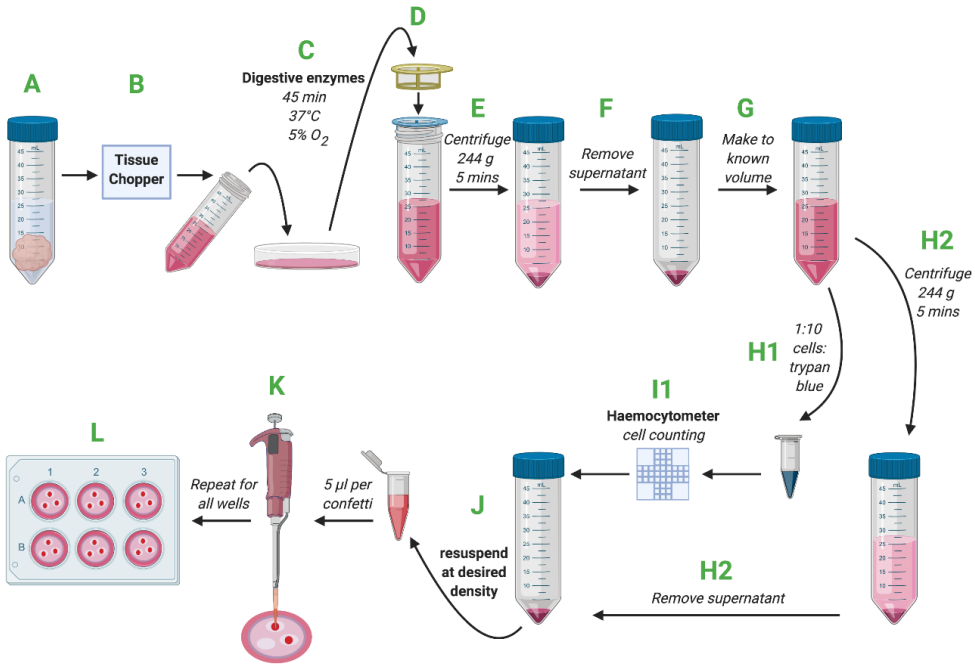

Figure 2-1: Tissue preparation for HiSpot® production.

The steps of tissue processing are demonstrated. A: Tissue is received in Gey's solution with MK-801. B: Tissue is dissected into 1mm cubes using a tissue chopper. C: Chopped tissue is mixed with digestive enzymes and incubated for 45 minutes. D: The tissue solution is passed through 100 µm and 40 µm strainers to produce a single cell suspension. E: The cells are centrifuged for 5 mins. F: The supernatant is removed. G: The pellet is made up to 10 ml with fresh media. H1: A sample of the cell suspension is taken for mixing 1:10 with trypan blue. I1: The cell/trypan blue mix is counted using a haemocytometer. H2: At the same time the cell suspension is centrifuged again. I2: The supernatant is removed. J: The cell pellet is resuspended at the required experimental density. K: 5 µl of the cell solution is pipetted as a droplet in the centre of each confetti. L: Three HiSpots® are created per well in a 6 well plate. Figure created using biorender.com.

2.3 Culture Set-up

The standard high serum HiSpot® media (HSM) contains 62% Dulbecco's modified eagle's medium (DMEM), 20% foetal bovine serum (FBS, Life Technologies, 11573397), 10% Ham's F12 nutrient mix (Life Technologies, 21765029), 5% horse serum (HS, Thermo Fisher, 16050122), 1% glutaMAX (Life Technologies, 35050061), 1% HEPES buffer (Sigma Life Science, H3537) and 1% penicillin/streptomycin (Life Technologies, 15130122). The serum-free media (SFM) contains 96% neurobasal A (Life Technologies, 10888022), 2% B27 (Life Technologies, 17504044), 1% glutaMAX and 1% penicillin/streptomycin. Media was disposed of two weeks after assembly.

Cultures were grown in 6 well plates, containing 1200 µl media (HSM or SFM) and one Millicell insert (Millipore PCF 30mm 0.4 µm, polycarbonate, PIHP03050) per well, and three PTFE membrane 'confetti' discs (Hepia Biosciences, Art 001, SA, 0.4 µm pores, 30µm thickness) were added to each insert using forceps (***Figure* 1-6**). Care was taken to remove any bubbles from the media. 700 µl media was refreshed every 3-4 days. Sterile DPBS (Life Technologies, 14190-094) was used for sterile wash steps during fixation. For post-fixation purposes, non-sterile PBS was used, made up from tablets (1 tablet per 200 ml distilled water, Sigma Life Science, P4417).

2.3.1 Culture media optimisation

GBM cultures can be negatively affected by the presence of serum in the media. Therefore, it was decided to compare different media conditions to determine if GBM HiSpots® could survive without serum, and whether if so they required supplementation with growth factors.

A variety of different cell culture protocols were used to find the optimum protocol. These are detailed in **Figure 2-2**. Condition A kept HiSpots® in HSM for the entire culture time. For condition B, at 7 days in vitro (DIV) the media was removed and replaced with a 50:50 mixture of HSM and SFM (12.5%). This media was then used for the remaining culture time. For condition C, The media was removed again at 7 days in vitro (DIV) and replaced with SFM.

This was then used for the remaining culture time. Condition D had HiSpots® cultured in SFM for the entire culture time. Condition E was SFM for the entire time as for condition D, but with the addition of EGF (20ng/ml, RnD Systems), FGF2 (20ng/ml, RnD Systems), and heparin (2ng/ml, Sigma), as a 'feeding solution' added with each media change. HiSpots® were usually fixed at 14DIV, although some cultures were fixed at earlier or later timepoints for comparison.

Conditions F, G, H and I were initially cultured in HSM for 4 DIV, then moved to SFM for a further 7 DIV. After this point, condition F was kept in SFM, condition G was cultured in HSM without FBS (5%), condition H in HSM without HS (20%), and condition I had complete HSM. These were all fixed at 14 DIV.

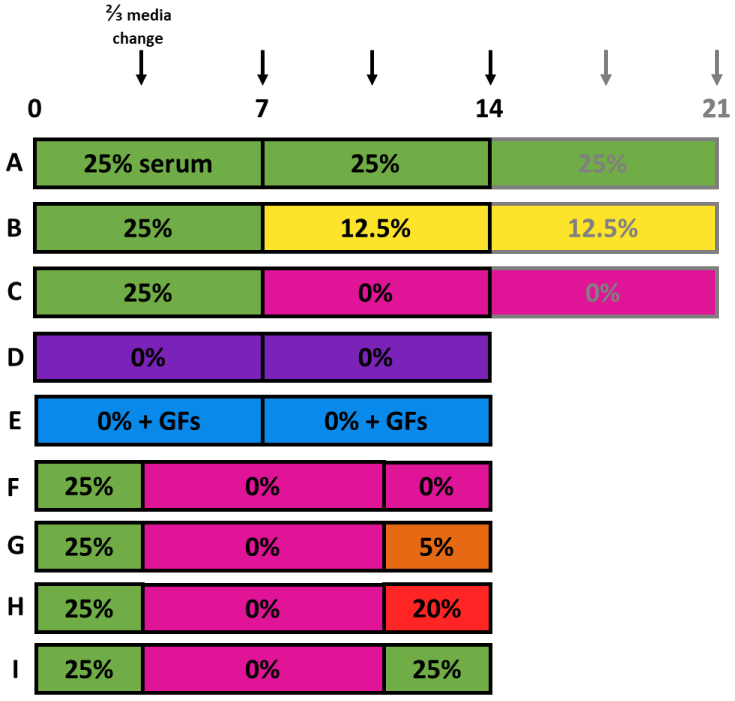

Figure 2-2: Culture media optimisation protocols

Different timelines for HiSpot® culture are shown. The percentages refer to the level of serum in the media. Media changes were performed every 3-4 days, indicated by the arrows, and HiSpots® were fixed at the end of the timeline. The number of DIV is shown along the top. For conditions A-C, some HiSpots® were fixed at 14 DIV (black lines) and some at 21 DIV (grey lines).

2.4 Hi-Spot Generation and Culture

For initial experiments, cells were resuspended at $5x10^7$ cells/ml, in accordance with previous HiSpot® experiments (Zhu 2018). $2.5x10^5$ cells in 5 µl were used for each Hi-Spot. These were gently pipetted onto each confetti, creating a droplet in the centre of the disk (**Figure 2-1 J-L**). HiSpots® were cultured at 37°C and 5% CO_2 in a HERAcell Heraeus incubator. Cell culture was performed in a sterile tissue culture hood (HERAsafe).

From sample GBM25 onwards, some HiSpots® were seeded at higher densities. The initial density ($5x10^7$ cells/ml) was compared with $2.5x10^8$ cells/ml and $5x10^8$ density HiSpots®.

> *Optimisation: Higher density HiSpots® were found to grow far more successfully than $5x10^7$ cells/ml HiSpots®, so from GBM28 onwards, HiSpots® were seeded at a minimum density of $2.5x10^8$ cells/ml. A seeding density of $5x10^8$ cells/ml produced even higher density HiSpots® but further reduced the total number which could be created per patient sample, so $2.5x10^8$ cells/ml was taken forward as a compromise.*

2.4.2 Multiple biopsy sampling

For certain patients, multiple biopsies were collected from one tumour. Biopsy collection was coordinated with the operating surgeon to obtain the following biopsies wherever possible, with a focus on collecting core and enhancing tumour biopsies.

- Tumour core (C) - from the central, often necrotic area of the tumour (**Figure 2-3A**)
- Enhancing tumour (E) - from the outer rim of the tumour, enhanced with gadolinium on CT **(Figure 2-3B**)
- Peripheral tissue (P) - from beyond the enhancing area of the tumour

Biopsy areas were selected and recorded using a neuronavigation platform and neuronavigation probe (StealthStation™ S7, Medtronic). Snapshot CT images were taken with the probe pinpointing the area from where a biopsy would be taken, during surgeries where this platform was in use (**Figure 2-3).** Not all biopsies were available from all patients, and depended on the location of the tumour, and surgical factors such as cystic areas or bleeding. Biopsies were collected in separately labelled collection tubes and kept on ice. As soon as all biopsies were collected, they were dissociated and processed in parallel using the same methodology as for single biopsies.

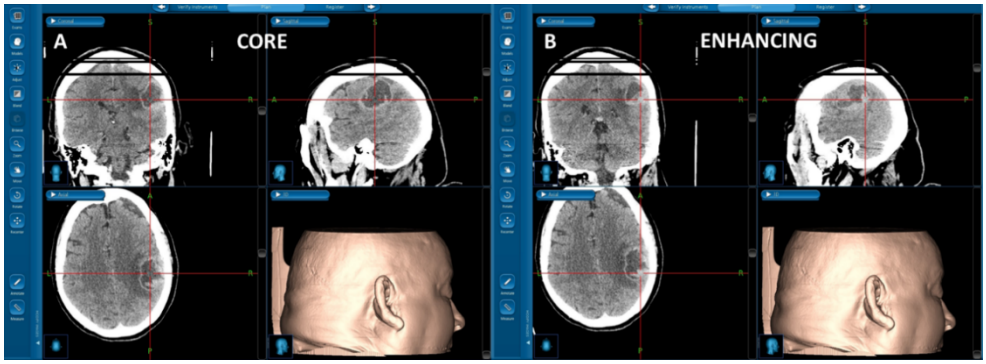

Figure 2-3: Snapshot images from neuronavigation software.

Screenshots are shown from the neuronavigation software used during surgery. The probe pinpoints (with red lines) where biopsies were taken from the core (A) and enhancing (B) areas of the tumour on multiple views from a CT scan.

2.4.1.1 Combined biopsy HiSpots®

As well as HiSpots® from individual biopsies, some HiSpots® were created with a combination of multiple biopsies. The cells from each biopsy were resuspended at $2.5x10^8$ cells/ml, to produce an isolated population of single cells from each biopsy. To produce combined HiSpots®, equal volumes from each constituent biopsy were combined in a separate Eppendorf tube and mixed thoroughly. This cell population was then used to create combined HiSpots®. Biopsies from patient GBM46 were not able to be defined by location due a large cyst within the tumour compromising the accuracy of the neuronavigation platform. The two biopsies collected are therefore labelled A and B. Biopsies from GBM46 were only used for initial analysis and excluded from further data sets. All other biopsies were collected in accordance with the descriptions of core, enhancing, and peripheral locations above. The biopsies collected and analyses performed are summarised in **Table 2-1**.

Table 2-1: Details of multiple biopsy collection.

Details are shown for each GBM patient where multiple biopsies were collected from one patient. The patient number and biopsies collected are shown. Any combined HiSpots® created are detailed with the biopsies used. The final column details which biopsies or combined biopsies were used for either β-IIIT, GFAP and IBA1 staining (1), and/or TMZ treatment and analysis (2).

Patient number	*Biopsies collected*	*Combined HiSpots®* *created*	*Analyses performed*
GBM39	Core[1, 2] Enhancing[1, 2] Peripheral[2]	C + E + P[1]	[1] B-IIIT, GFAP, IBA1 staining [2] TMZ treatment
GBM40	Core Enhancing	None	B-IIIT, GFAP, IBA1 staining
GBM41	Core Enhancing	None	B-IIIT, GFAP, IBA1 staining
GBM46	Biopsy A Biopsy B	A + B	Total area fluorescence intensity
GBM47	Core[1, 2] Enhancing[1, 2]	C + E [1, 2]	[1] B-IIIT, GFAP, IBA1 staining [2] TMZ treatment

2.5 LDH assay

Lactate dehydrogenase is an enzyme which is released from cells during necrotic cell death. Levels of LDH can be detected in media using a colorimetric assay. This provides a measurable readout of necrotic cell death in the culture system.

During media changes, an aliquot of each media type was saved and stored at -20°C. These were defrosted and analysed using the Pierce LDH cytotoxicity assay kit (Thermo Fisher Scientific, 88954) according to the kit protocol. 50 µl of each aliquot was added to triplicate wells in a 96 well plate, along with the kit positive control and aliquots of media which had not been exposed to cells. 50 µl of the kit reaction mix was added to each well and the plate was incubated at room temperature, protected from light, for 30 minutes. 50 µl of stop solution was then added to each well. Using a plate reader and associated software (BMG Labtech, CLARIOstar) the absorbance for each well was measured at 490nm and 680nm. The absorbance at 680nm was subtracted from the absorbance at 490nm for each well. This was then normalised to the mean measurement from the appropriate blank media, and then the mean value was calculated for the triplicate wells. Data were plotted using GraphPad Prism.

For one experiment, one well per timepoint was treated with 20 µl lysis buffer (from Thermo Fisher Scientific kit 88954) for 45 minutes, then media was collected and stored as above. The cells were then considered no longer viable and disposed of. This media was analysed along with untreated media from HiSpots® from the same patient. The data were tested for normality using a Shapiro-Wilk test and compared using a two way ANOVA test with Bonferroni's multiple comparisons.

2.6 Fixation

Fixation of cells using formaldehyde preserves cellular structure and arrangement which allows them to be imaged and analysed in detail. Each confetti was gently removed with curved forceps, taking care to avoid

touching the cells, and placed in one well of a 48 well plate. 20 µl of 4% paraformaldehyde (PFA, Santa Cruz Biotechnology Inc., sc-281692) was added on top of each Hi-Spot. They were then kept at 4°C for 30 minutes. 50 µl PBS was then added to dilute the PFA. This was removed and replaced with fresh PBS. Plates of fixed HiSpots® were sealed with parafilm to reduce evaporation and stored at 4°C until required for immunocytochemistry. HiSpots® were fixed at different timepoints for certain experiments, but where not otherwise specified, all HiSpots® were fixed at 14 DIV.

Optimisation: Confetti were originally fixed in a 24 well plate and transferred to a 48 well plate for staining. By fixing the confetti directly in the 48 well plate, the confetti did not need to be moved again before mounting and potential damage at this stage was avoided.

2.7 EdU treatment

EdU is a thymidine analog used to measure proliferation levels in cells. Many older studies used BrdU, another thymidine analog, for which the detection process required strong acids and heat. EdU detection is considered safer as it does not require these factors, so it has become a replacement for BrdU.

EdU is integrated into DNA during the S-phase of the cell cycle. It will be taken up into any cells that enter the S-phase during the exposure time. The percentage of the total cycling cells which incorporate EdU will therefore be proportional to the exposure time. For example, a 1 hour exposure may detect 20% of cycling cells, whereas a 4 hour exposure may detect 80% of cycling cells. EdU levels can therefore be used as an indicator of proliferation in a cell population as long as exposure time is kept consistent. EdU can also be used in combination with a stain such as Ki-67 which detects all cycling cells, in order to indicate the speed at which those cells are proliferating.

EdU treatment and detection was performed using the Click-iT EdU imaging kit (Invitrogen, C10340) When required, HiSpots® were treated with 10 µM EdU added to the culture medium for 45 minutes, according to the Invitrogen Click-iT EdU imaging kit protocol. HiSpots® were then fixed as described above.

> *Optimisation: From patient 29 onwards (all TMZ experiments), the EdU exposure time was increased to 4 hours to improve the yield of EdU+ cells, and to better match similar experiments* (Weil *et al.* 2001)*. EdU will only detect cells entering the S-phase of the cell cycle, so will only detect a proportion of the total cycling cells. Increasing the exposure time increases the proportion of cycling cells which are detected.*

EdU uptake was detected using the kit protocol. HiSpots® were washed twice using 3% bovine serum albumin (BSA, PAA The cell culture company, K45-001) in PBS. The reaction mix (including AlexaFluor azide 647 nm) was then added at 100 µl per well in a 48 well plate for 30 minutes at room temperature, protected from light. HiSpots® were washed again using the 3% BSA solution. Immunocytochemistry was then performed as standard, but with care to protect the HiSpots® from light during the entire process to avoid bleaching the 647 nm signal.

> *Optimisation: From patient 37 onwards, HiSpots® for EdU detection were permeabilised in 0.5% PBS-T for 20 mins before BSA washes. HiSpots® being used as controls were returned to PBS for the duration of the detection protocol.*

2.7.1 Temozolomide preparation and dosing

Temozolomide is a chemotherapeutic drug. It is the standard first line treatment for patients with GBM. It can also be applied to cells in culture to check their sensitivity to this drug. Temozolomide (TOCRIS bioscience 2706, molecular weight 194.15) was dissolved in 5.0569 ml dimethyl sulphoxide (DMSO) to make a 50 mM stock. 60 µl aliquots of different concentrations were then made from the stock according to **Table 2-2**. 10 µl of each aliquot

was added to each well (into 1 ml media) to reach final concentrations of 0, 5, 50, 100, and 500 µM.

Table 2-2: Temozolomide aliquots and doses.

Aliquot concentrations are shown, with their final concentration in media, and required volumes of TMZ and DMSO to create a 60 µl aliquot.

Aliquot concentration (mM)	*Final concentration in media (µM)*	*50 mM TMZ stock (µl)*	*DMSO (µl)*
0	0	0	60
0.5	5	0.6	59.4
5	50	6	54
10	100	12	48
50	500	60	0

For patients GBM30-36, HiSpots® were cultured in high serum media (HSM) for 7 DIV, after which they were transferred to serum free media (SFM). From patient GBM37 onwards, HiSpots® were cultured in SFM for the duration of the 14 DIV. TMZ was applied at a range of concentrations (**Figure 2-4**) at 9 DIV. Some HiSpots® were also left untreated and used for comparison with the vehicle control. Previous data had shown a peak in proliferation at 7-9 DIV, so the 9 DIV timepoint was selected to allow the HiSpots® enough time to mature and become actively proliferative.

At 14 DIV, HiSpots® were treated with EdU alone, or with EdU and 5µM Nucview® 488 Caspase-3 enzyme substrate for 4 hours. All HiSpots® were then fixed. This timeline meant that HiSpots® were incubated for 5 DIV after the addition of TMZ, noted by Zhang *et al.* (2012) to be the timepoint at which the peak response was seen. In addition to normal media changes, media was changed at 9 DIV before the addition of TMZ. The media change between 9 DIV and 14 DIV was not a concern as TMZ has a half-life of 2 hrs, so would have already had the relevant effect on the cells (Kim *et al.* 1997). Each concentration of TMZ was made up separately from the stock solution

(50 mM), in order to ensure the same volume of DMSO (10 µl) was added to each well.

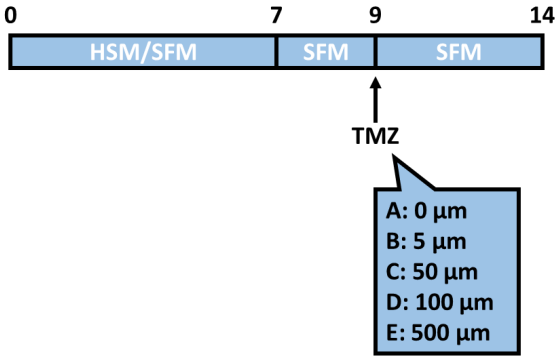

Figure 2-4: Treatment of HiSpots® with TMZ

A: The timeline of HiSpot® growth and treatment. For early samples, HiSpots® were grown in HSM until 7 DIV, then SFM until 14 DIV. For further samples HiSpots® were cultured in SFM for the whole duration. TMZ was added at 9 DIV at a range of concentrations. All HiSpots® were fixed at 14 DIV.

2.8 Immunocytochemistry

2.8.1 Immunofluorescence

Immunofluorescent staining is a useful method of visualising and identifying cells. Primary antibodies to specific target proteins can be used to distinguish between different cell types and areas of the cell. These antibodies can then be detected using secondary antibodies to the host species used for the primary antibody. Secondary antibodies have fluorescent tags at different wavelengths which can be detected using fluorescence microscopy. Up to four wavelengths can be detected at once, and these are often referred to as channels. In this project, one channel is used only for 4'6-diamidino-2-phenylindole (DAPI). DAPI is a nuclear stain which binds to DNA and can be detected using an excitation wavelength of 350 nm. DAPI is used to detect all cell nuclei and can therefore be used to calculate the total number of cells in an image.

HiSpots® were washed three times (5 mins each) with 0.1 % triton-X (Merck, 9036-19-5) in PBS (PBS-T) and incubated in PBS-T containing 3% donkey serum (Millipore (UK) Ltd, S30-100ml) for 30 mins at room temperature to block non-specific antibody binding. They were then incubated in the primary antibodies (detailed in **Table 2-3**) in 3% donkey serum in PBS-T overnight at 4°C.

> *Optimisation: From patient 25 onwards, 0.5% PBS-T was used for all stages instead of 0.1% in order to improve antibody penetration of the thicker HiSpots®.*

Table 2-3: Primary antibodies used for staining of HiSpots®.

All primary antibodies used or tested in this study are shown, with their species specificity and concentration used for immunofluorescent staining. Suppliers and catalogue numbers are also shown. Antibodies in bold were used as the standard triple-stain for Chapters 4-5.

Target	*Species*	*Concentration*	*Supplier and Catalogue Number*
Nestin	Rabbit	1:500	Abcam ab105389
Nestin	Mouse	1:500	R&D biosystems MAB1259
β-III tubulin	**Mouse**	**1:500**	**BioLegend 801202**
β-III tubulin	Rabbit	1:500	Abcam ab18207
IBA1	**Rabbit**	**1:2000**	**Wako 019-19741**
IBA1	Goat	1:500	Abcam ab5076
GFAP	**Rat**	**1:500**	**Invitrogen 2.2b10 13-0300**
Cleaved caspase-3	Rabbit	1:500	Cell signalling technology d175 9661s
Vimentin	Chicken	1:2000	EnCor Biotechnology Inc. CPCA-Vim
Ki-67	Rabbit	1:500	Abcam ab15580
CD68	Mouse	1:500	Biolegend 333801
CD31	Rabbit	1:500	Abcam ab28364
SOX2	Mouse	1:250	Abcam ab79351
SOX2	Rabbit	1:500	Abcam ab97959
IDH-1 R132H	Mouse	1:100	Dianova DIA-H09

The following day, the HiSpots® were washed three times (10 mins each) in PBS-T and incubated in the secondary antibodies (detailed in **Table 2-4**) in PBS-T for 1 hr at room temperature in the dark. Following further washing (1 time, 10 mins) in PBS-T, HiSpots® were counterstained with 0.5 µg/ml DAPI (Life Technologies, D1306) in PBS for 5 minutes, then washed (3 times, 5 mins). HiSpots® were then gently placed cell-side up on microscope slides. Mowiol mounting solution (Aldrich, 81381-25OG) was added and a glass cover slip was added on top. Slides were refrigerated at 4°C for a minimum of 30 mins to allow the mowiol to set.

Optimisation: From patient 36 onwards, secondary antibodies were also incubated overnight, at room temperature, to improve antibody penetration of the thicker HiSpots®.

Optimisation: For later HiSpots®, two smaller, round cover slips were affixed to each end of the slide using small droplets of clear nail varnish. HiSpots® were moved to the slide and mowiol added as normal, then the large cover slip was rested on top of these, in order to reduce any possible compression of large HiSpots®.

Table 2-4: Secondary antibodies used for fluorescent detection of primary antibodies.

All secondary antibodies used or tested in this study are shown, with their target species, origin species, concentration, and emittance wavelength. Suppliers and catalogue numbers are also shown.

Target species	*Species*	*Concentration*	*Wavelength*	*Supplier and Catalogue Number*
Mouse	Donkey	1:500	488	Invitrogen a21202
Mouse	Donkey	1:500	555	Invitrogen a31570
Mouse	Donkey	1:500	647	Life technologies a31571
Rabbit	Donkey	1:500	488	Invitrogen a21206
Rabbit	Donkey	1:500	555	Invitrogen a31572
Rabbit	Donkey	1:500	647	Life technologies a31573
Rat	Donkey	1:500	488	Invitrogen a21208
Rat	Goat	1:500	555	Invitrogen A21434
Rat	Donkey	1:500	594	Invitrogen a21209
Chicken	Goat	1:500	647	Abcam ab150171
Goat	Donkey	1:500	488	Life technologies a11055

2.8.2 Replacement of caspase-3 antibody with nucview substrate

Caspase-3 is an enzyme involved in cell death via apoptosis. The cleaved (activated) form can be detected using an antibody. This method is used in some initial experiments in this project. Caspase-3 activity can also be detected using a substrate for the enzyme itself. This substrate (nucview caspase-3 substrate) is broken down by caspase-3 to produce a fluorescent byproduct. This accumulates in the nucleus and can be detected using fluorescence microscopy (488 nm).

For TMZ-treated experiments, the addition of the nucview caspase-3 substrate along with EdU in the standard protocol allows a much longer exposure time for the eventual caspase-3 readout, in comparison with a single treatment with a cleaved caspase-3 antibody. As with EdU, in order to use caspase-3 as a measurement of treatment response, it is important to have a suitable exposure time which allows enough positive cells to be picked up in order to be able to track changes. With only one or two positive cells in a HiSpot®, it would be very difficult to track whether these levels changed significantly, however if the baseline level is higher (such as 20-50 positive cells) this allows a more reliable comparison and analysis of variability within the HiSpots®.

The cleaved caspase-3 antibody used in the early parts of this research (**3.2.1.1**) only captures a snapshot of time for the cells in the HiSpots® which results in a smaller readout of the total number of apoptotic cells. As visible in **Figure 2-5**, only one cell (double circled) is positive for both the antibody and substrate, whereas there are four other cells positive for the substrate only. Panels **D-F** show a higher magnification of the lower centre-right of the same area. The area magnified is shown with the white box on panel **C.** Panels **D-F** show the cell positive for the antibody, and two positive for the nucview substrate. Panel **G** shows an overlay image of the three channels to demonstrate the overlap of the staining with DAPI.

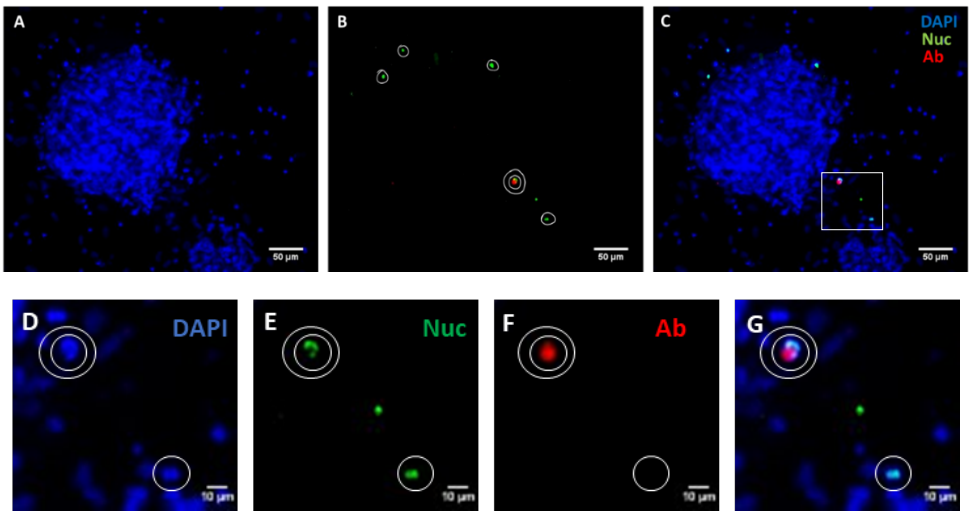

Figure 2-5: Comparison of caspase-3 substrate and cleaved caspase-3 antibody.

Immunofluorescence images are shown in panels A-C. Panel A shows nuclei (DAPI, blue) only. Panel B shows staining with the nucview caspase-3 substrate (green) and the cleaved caspase-3 antibody (red). Nuclei positive for the nucview caspase substrate are circled once, and nuclei positive for both the nucview caspase-3 substrate and the cleaved casapase-3 antibody are circled twice. Panel C shows a composite image of all stains. Scale bars are shown for reference.

Panels D-G are a higher magnification of the same image, showing DAPI (D), nucview substrate (E), cleaved caspase-3 antibody (F) and an overlay of all channels (G). They show the overlap of the DAPI nuclear stain with the other channels. Scale bars are shown for reference.

2.8.3 Test of *IDH-1* R132H antibody

IDH-1 R132H is a mutation which is used to diagnose secondary GBMs. It is detected using an antibody in histological samples, but there are few instances of an *IDH-1* R132H antibody being used for immunofluorescence. Therefore it was important to test the antibody and determine the appropriate dilution for immunofluorescent staining. HiSpots® were tested with *IDH-1* R132H antibody at 1:20, 1:100 and 1:200. These are shown in **Figure 2-6 B-D** compared to a negative control **Figure 2-6 A**. In all stained HiSpots®, *IDH-1* R132H is visible in the cytoplasm of a number of cells in the image. The dilution of 1:100 was selected for future analysis. The HiSpots® used for *IDH-1* R132H staining were created at a density of $2.5x10^8$ cells/ml.

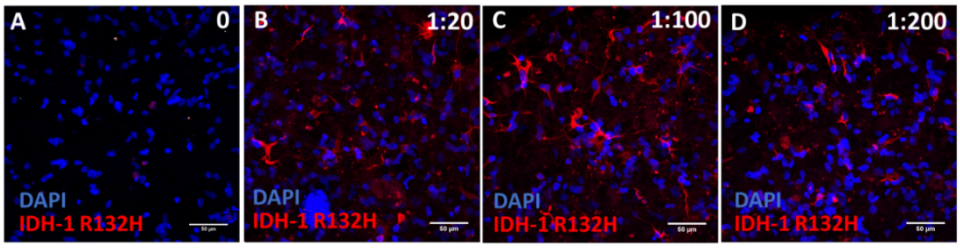

Figure 2-6: IDH-1 R132H antibody testing.

Immunofluorescence images of IDH-1 R132H antibody testing at a range of concentrations. All images are stained for nuclei (DAPI, blue) and IDH-1 R132H (red). Scale bars are shown for reference. Panel A shows a negative control, with no primary antibody applied. Panel B shows a 1:20 dilution, panel C 1:100 and panel D 1:200.

2.9 Imaging

2.9.1 Upright fluorescence microscopy

2.9.1.1 Imaging

Images for this project were taken in a number of ways depending on the experiment, antibodies used and the HiSpot® structure. Basic images of cells within HiSpots® were taken using an upright fluorescence microscope, using a 20x objective lens unless otherwise specified (Leica DM6000B, with Leica Application Suite software). This microscope takes a top-down style 2D image of the cells. A separate image is taken for each channel, and these are combined into a composite image of all channels. These images do not allow separate cell layers to be distinguished. The same microscope was also used to take tile scan images, using a 5x objective lens unless otherwise specified.

Tile scan images were taken of HiSpots® using the Leica software tile scan function, which allows an entire HiSpot® to be imaged at the set magnification by taking many individual images, referred to as tiles. These tiles are then automatically stitched together to form the final tile scan image. Tile scan images allow the entire HiSpot® structure to be visualised at once. The HiSpots® are too large to fit in a single image using the lowest magnification available without using the tile scan function.

Tile scans for quantification were taken at identical exposure, gain, and intensity settings for each channel within the HiSpots® from each patient, to allow for direct comparison of fluorescence intensity.

All images were analysed using the software package ImageJ with the FIJI plugin package. Relative focus correction was applied to ensure that all wavelengths were in adequate focus. All scale bars were added using ImageJ.

2.9.1.2 Single image quantification

For each image, the fluorescent channel showing DAPI staining was duplicated (**Figure 2-7B-C**), and a threshold filter applied to cover the visible nuclei (**Figure 2-7D**). The watershed function was applied to separate overlapping nuclei (**Figure 2-7E**). The analyse particles function was applied to the threshold image, excluding particles smaller than 50 pixels (approximately 23 μm^2), in order to eliminate debris and picnotic nuclei. This then provides a count of the total number of DAPI in the image (**Figure 2-7F**). Individual antibody stains were then counted manually, either as separate channels or specifically when overlapping (**Figure 2-7G-H**).

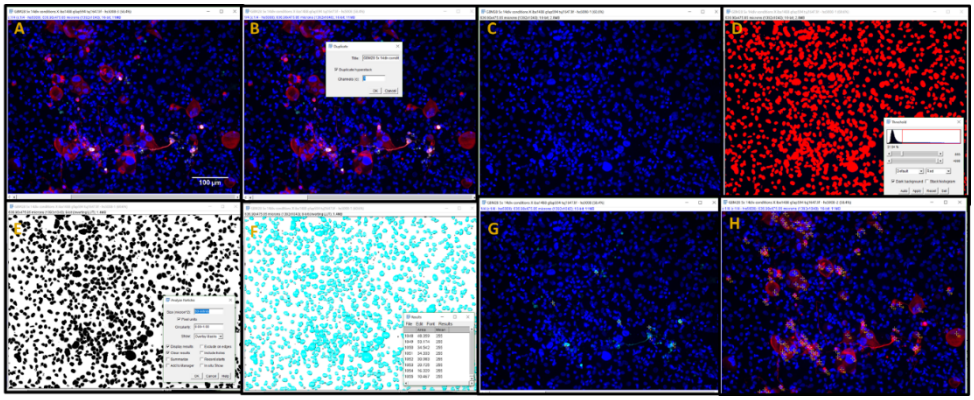

Figure 2-7: Quantification of immunocytochemistry images using ImageJ.

Panels A-H show screenshots of the process of image analysis and quantification using ImageJ. A scale bar is shown in panel A for reference. An image is opened in ImageJ as a composite image showing all channels (A). The DAPI channel is duplicated from the original image (B) producing a single channel image (C). A threshold filter is applied to overlap the individual DAPI stained nuclei (D). The watershed function is then applied (E) to separate overlapping nuclei. The analyse particles function is then applied to the image, excluding particles <50 pixels (F). Individual cytoplasmic or nuclear antibody stains are then counted by hand (G-H).

2.9.1.3 Tile scan analysis

Once the HiSpot® density had been increased, it became difficult to measure DAPI levels using the previous automated counting method due to high overlap of cells. Instead, a measurement of HiSpot® total area fluorescence intensity was used for these experiments. HiSpots® were selected and the mean fluorescence intensity per pixel was measured across the HiSpot® area. The more cells present, the more pixels should be positive for fluorescence, and therefore the higher the mean intensity. This value was then multiplied by the total HiSpot® area in mm^2 to give a value for the total cellular content of the HiSpot®. This is not a direct count of total cell numbers, but gives a comparative indicator of cell numbers within the HiSpot®. This reasoning is portrayed in **Figure 2-8** below.

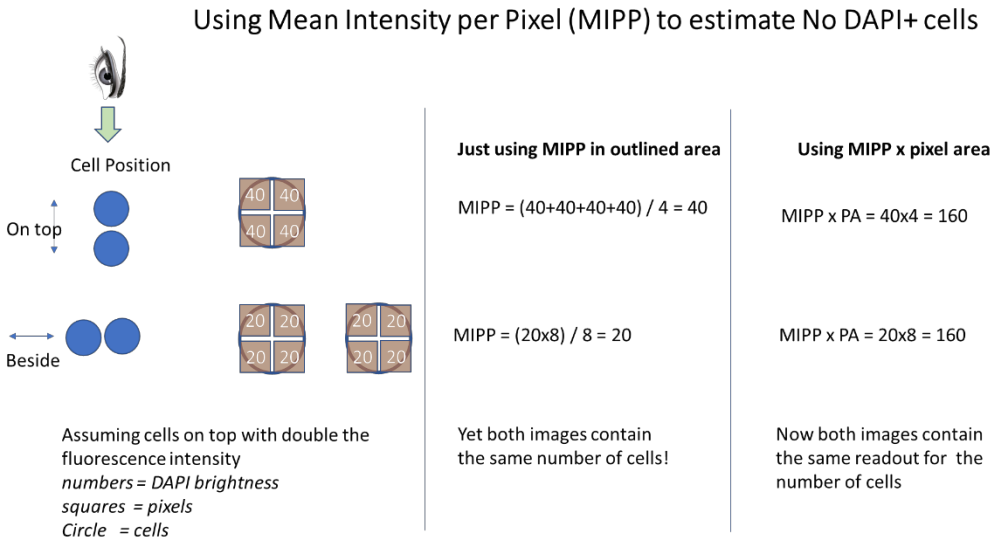

Figure 2-8: Mean intensity calculations for pixel intensity.

Two arrangements of eight cells are shown as examples. The calculations of mean intensity per pixel, and this value multiplied by pixel area, are shown to demonstrate why mean intensity multiplied by pixel area was chosen. This value provides a more representative value for the number of cells within the HiSpot®, as they are not of uniform size.

DAPI was measured as HiSpot® total area fluorescence intensity. HiSpots® were imaged at the same exposure for DAPI throughout individual experiments. This ensured that each HiSpot® tile scan images were directly comparable to others from the same patient. Tile scan images were taken

at using a 5x objective lens and stitched together automatically by the Leica software. The stitched images were analysed using ImageJ (**Figure 2-9A)**. A Lenovo ThinkPad laptop touchscreen pen was used to draw around the HiSpot® with the selection tool (**Figure 2-9B)**. This was chosen over the circular selection tool, as although some HiSpots® were uniform and round, others would have been impossible to select using the circle tool as they were less uniform shapes. Extra selections could be added or removed if an area of debris or a detached area of cells was affecting the readout.

The DAPI channel only was then duplicated and measured using the built in analysis function (**Figure 2-9C-D**). This provides a readout of the total selection area and mean fluorescence intensity for the selection. Other channels were then duplicated from the original image (**Figure 2-9E-F**). The EdU and caspase-3 channels were then set to thresholds which were kept consistent throughout the HiSpots® from each patient, wherever possible (**Figure 2-9G**). However, sometimes high levels of background noise made it impossible to have a consistent threshold. For the HiSpots® from these patients, the threshold was set manually to match the visible EdU or caspase-3 staining as accurately as possible. The threshold image was then quantified using the analyse particles function. Options were selected to eliminate single pixels, and provide an overlay image showing which particles had been counted. Only particles within the original border were counted. EdU and caspase-3 data were recorded as the number of particles within the selection area (**Figure 2-9H**). Each condition had up to 5 HiSpot® repeats.

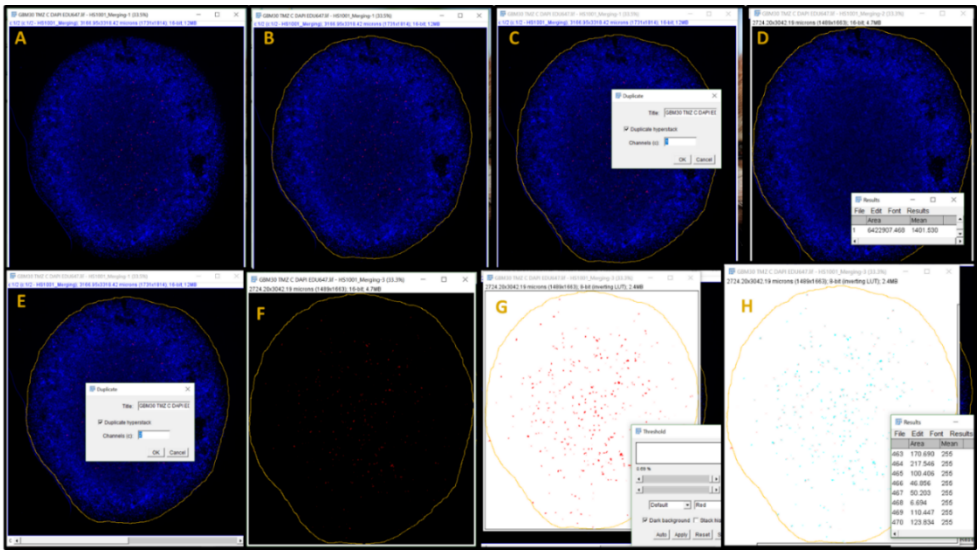

Figure 2-9: Quantification of tile scan HiSpot® images.

Panels A-H show screenshots of the method for the quantification of tile scan images by fluorescence intensity and threshold particle analysis. Combined tile scan images are opened in ImageJ (A). The HiSpot® outline is selected using the free drawing tool (B). The DAPI channel is duplicated (C), and the mean fluorescence intensity per pixel is measured (D). From the original image, the other channel (EdU) is duplicated (F) and a threshold filter applied (G). The selection is then reapplied, to exclude any debris outside the HiSpot® borders, and the analyse particles function used to count the number of EdU+ particles within the HiSpot® (H), excluding any particles only one pixel in size.

2.9.1.4 HiSpot® structure analysis

Tile scan images were used for analysis of whole HiSpot® structure. Many HiSpots® were found to be formed of concentric rings. The structure often consisted of a large, 3D central mass, extending from which was a ring of migratory cells, surrounded by a ring of monolayer cells. The cellular area did not reach the edge of the confetti. ImageJ software was used to draw around these rings and measure the area within. The area of each ring could then be calculated using the measurements as below, with regards to the selection areas shown in **Figure 2-10.** These measurements were then compared between HiSpots® from different biopsy areas from the same original tumour.

$$Area\ of\ invasive\ ring = Area\ up\ to\ edge\ of\ invasive\ cells\ (B) - area\ of\ central\ mass\ (A)$$

$$Area\ of\ outer\ ring = total\ cellular\ area\ (C) - area\ up\ to\ edge\ of\ invasive\ cells\ (B)$$

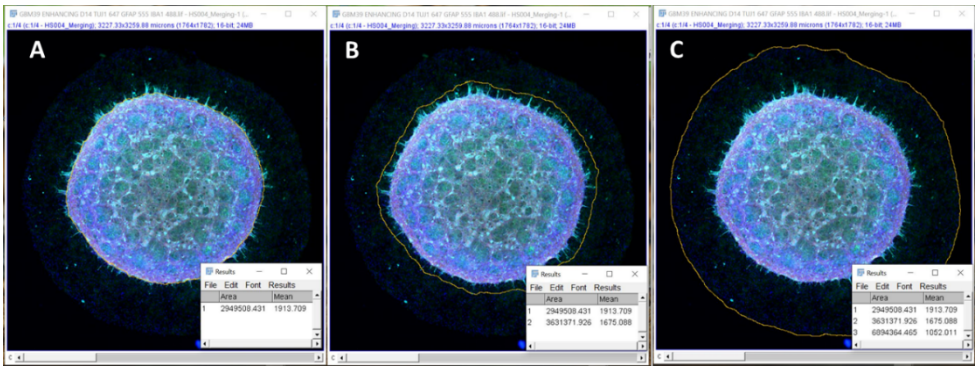

Figure 2-10: Analysis of HiSpot® rings as a structural feature.

Screenshots of ImageJ software showing the open immunofluorescence HiSpot® image with different selections and measurements. Selections were drawn around the borders of HiSpot® areas and were used to calculate the area of each concentric ring structure. A: The central mass. B: The invasive cells. C: The total HiSpot® area.

2.9.1.5 Microglial clusters and satellite areas

From certain patients, HiSpots® contained clusters of cells which stood out from the general HiSpot® structure. In patient GBM39, IBA1+ microglia were grouped together without tumour cells running between them. In GBM47, clusters of β-IIIT+GFAP+ tumour cells surrounded but were not connected to a central mass. Both types of clusters were counted and their sizes recorded so that their size and number could be compared between biopsies. The number and size of these clusters were measured using tile scan images of the HiSpots® in ImageJ. Freehand outlines were drawn around clusters of two or more microglia not divided by tumour cells using the Lenovo ThinkPad touchscreen pen. These were measured using the multiple regions of interest plugin, which allows multiple regions to be selected at once. Measurements of number and area for each selection can then be calculated. Total cluster counts per HiSpot®, and mean cluster size values per HiSpot® were analysed using GraphPad Prism. **Figure 2-11** below demonstrates how a region can be selected and added to the regions of interest collection (**A**), and how multiple regions of interest can be collated (**B**). Panel **C** includes the results panel, showing the areas calculated for each selection and the total number of selections. Panels **A-C** demonstrate how this was applied for quantification of IBA1+ microglial clusters in GBM39. Panels **D-F** show this application for β-IIIT+GFAP+ satellite clusters in GBM47. Firstly, the central mass was selected and measured **Figure 2-11D**). Satellite clusters were then selected using the regions of interest plugin and measured (**Figure 2-11E-F**). Mean measurements of multiple regions of interest were calculated for each HiSpot® and compared between biopsies from the same original tumour.

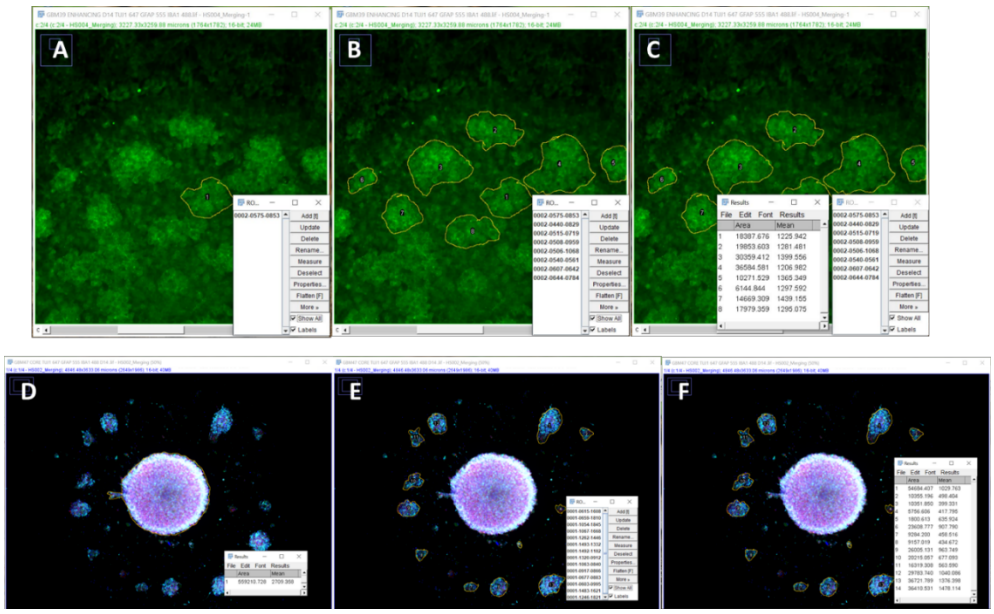

Figure 2-11: Analysis of multiple regions of interest within one HiSpot®.

Screenshots of immunofluorescence HiSpot® images open in ImageJ software during multiple region of interest analysis are shown. A-C: Measurement of microglial clusters. A: One region of interest is added to the panel. B: Further regions of interest are added to the panel. C: The regions of interest are measured, showing the area of each region and the total number of regions. D-F: Measurement of satellite clusters. D: The central mass is measured independently of the satellite clusters. E: Satellite clusters are selected and added as regions of interest. F: Satellite cluster regions of interest are measured, showing the area of each region and the total number of regions.

2.9.1.6 Analysis of cell protrusions

HiSpots® from some patients included cells which extended beyond the central mass, invading into the outer ring of the HiSpot®. These cells which extended beyond the main body of the HiSpot® were measured. The length of the protrusion was measured from the edge of the HiSpot® body to the end of the protrusion visible with either GFAP or β-IIIT expression. The total number of protrusions and mean protrusion length were collated for each HiSpot®. ImageJ was used to draw a line along the length of the protrusion (**Figure 2-12A)** and this was measured before moving onto the next protrusion (**Figure 2-12B, C**). Where multiple protrusions were clustered together, the longest was measured. Measurements began with a recognisable protrusion at the top centre of the HiSpot®, and measurements made clockwise around the HiSpot® until the same protrusion was reached.

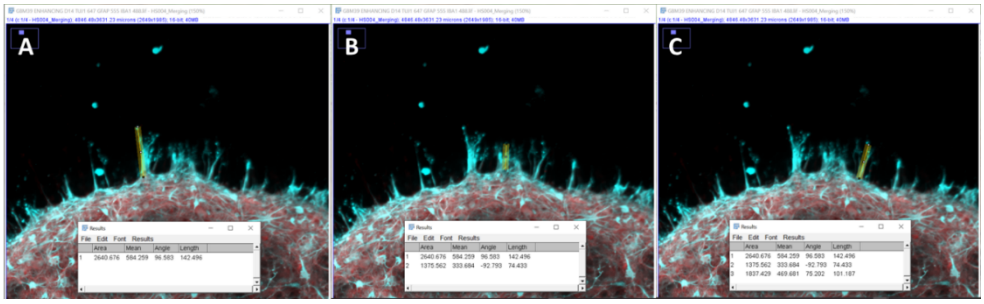

Figure 2-12: Analysis of invading cells.

A-C: Screenshots of immunofluorescence image analysis in ImageJ software. The length of protrusions were measured from where they connected with the main HiSpot® mass to the end of the cellular protrusion. Each protrusionl was measured (A), then the following invading cell clockwise was measured (B). This continued around the edge of the HiSpot® (C) until the entire circumference had been covered. The length measurements (A-C) and total number of protrusions per HiSpot® was recorded.

2.9.2 Confocal microscopy

Confocal microscopy allows the 3D structure of HiSpots® to be imaged in more detail. Rather than taking one 2D image of the cells, confocal microscopes take a number of images at different heights within the culture. These individual images are known as slices. These slices are layered above one another to provide a representation of the whole 3D structure of the HiSpot®. Confocal images were taken using a Zeiss LSM710 confocal microscope and the Zen Confocal software.

For quantification, images were taken using a 20x objective lens. Z-stacks were converted into single image maximum intensity projections or analysed as individual slices (**Figure 2-13**). Maximum intensity projections are produced by combining the brightest signals from each of the z slices (**Figure 2-13A-E**) into one image (**Figure 2-13G**). Images were processed and counted manually using ImageJ. Images were also taken using 40x or 63x oil immersion objective lenses for analysis of HiSpot® structure and cellular interactions. Scale bars were added using ImageJ.

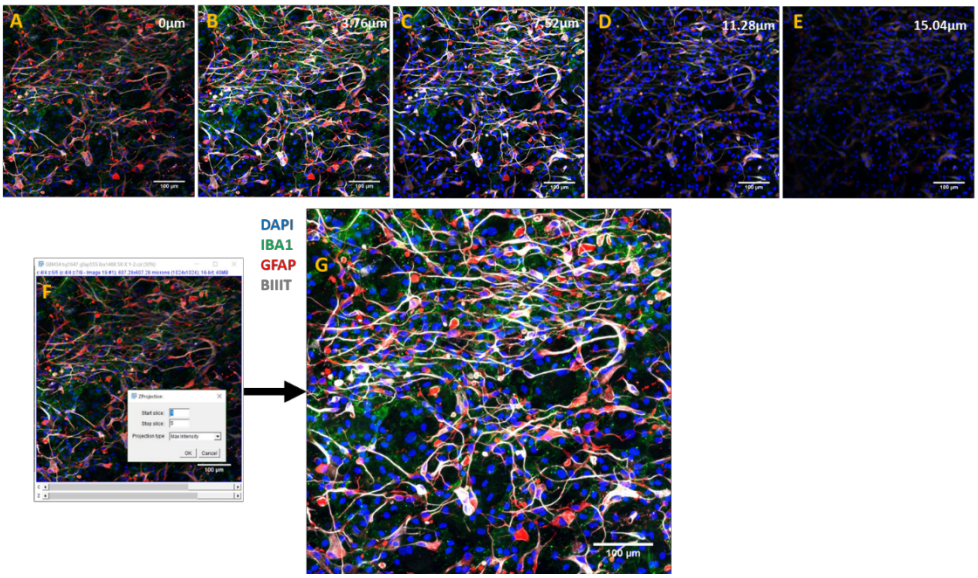

Figure 2-13: Combining a Z-stack into a maximum intensity projection.

Panels A-E show 5 slices of an immunofluorescence Z-stack image from the base of the HiSpot® (A) to the top (E). Scale bars and height from the base of the HiSpot® are shown in the bottom and top right respectively of each image for reference. F: A screenshot of the ImageJ maximum intensity function being applied to the Z-stack shown in A-E. G: The maximum intensity image produced in F. For all images, DAPI is shown in blue, IBA1 staining in green, GFAP in red and ß-IIIT in grey.

2.9.2.1 Centre and edge of HiSpot® images

Confocal images were taken of HiSpots® for quantification. To accommodate the variation visible between the centres and edges of HiSpots® from particular patients, a Z-stack image was taken at the centre and edge of each HiSpot® and the cell counts in the two areas quantified separately, using a 63x objective lens. The centre (C) and edge (E) image areas are shown as orange squares imposed over a HiSpot® tilescan in **Figure 2-14.** The squares are an approximate representation of the scale of the images taken (192.79 µm by 192.79 µm) in relation to the total HiSpot® area.

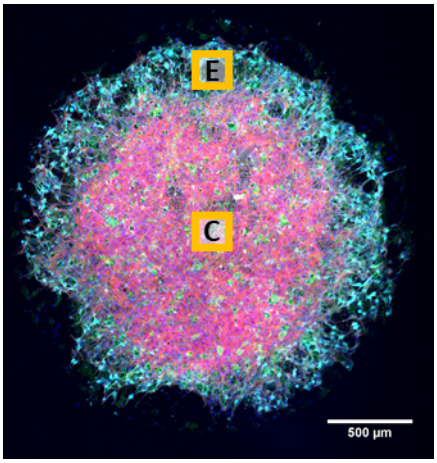

Figure 2-14: Multiple images from one HiSpot®.

The images show a representation of the relative locations of centre (C) and edge (E) confocal images within a whole HiSpot® diagram (A) and example tile scan immunofluorescence image (B). Squares showing C and E images are approximate representations of the relative image size. A scale bar is shown for reference.

2.10 Data Analysis

2.10.1 Cell count data

Raw cell count data were entered into Microsoft Excel, and mean values were calculated from 3 images per HiSpot®. Mean values were then analysed in GraphPad Prism. Where required, percentages of total cell counts were calculated for each raw image, before taking a mean value of the repeats per HiSpot® (example equation below). These data were then input into GraphPad Prism. Where there was only one value per HiSpot® (e.g. with tile scans), all data points were directly analysed in GraphPad Prism.

$$X = Mean\left(\frac{GFAP^{+}}{DAPI}\right)$$

Data were tested for normal distribution using a Shapiro-Wilk test, and then appropriate statistical tests (such as one-way ANOVA with Bonferroni's multiple corrections and unpaired t-tests) were performed using GraphPad Prism. Equivalent non-parametric tests were used if any data sets did not pass the normality test. Data are displayed as mean ± SEM throughout. N values represent technical replicates (n=1 is 1 HiSpot®) and the number of patient samples from which those HiSpots® were created are specified for each graph. HiSpots® from different patient samples were grouped together as replicates unless otherwise specified. $p \leq 0.05$, $p \leq 0.01$, $p \leq 0.001$ and $p \leq 0.0001$ are denoted as *, **, ***, and **** respectively. The statistical tests used are detailed below in **Table 2-5**.

Cell count data are shown throughout as cells per field. Conversion factors for cells per 1mm^2 (cells per field x conversion factor = cells/mm^2) are as follows: for images taken using the upright microscope and 20x objective lens, 3.2296; confocal microscope and 40x objective lens, 10.8463; confocal microscope and 63x objective lens, 26.9056.

Table 2-5: Statistical tests used for data analysis.

Parametric tests were applied to data found to be normally distributed. Non-parametric tests were applied to data found to not be normally distributed. Post-hoc tests were applied where appropriate.

No. groups	*No. variables*	*Statistical Test (parametric data)*	*Post-hoc test*	*Statistical Test (non-parametric data)*	*Post-hoc test*
2	1	Unpaired t-test	N/A	Mann-Whitney	
>2	1	One-way ANOVA	Bonferroni	Kruskal-Wallis	Dunn's
≥2	2	Two-way ANOVA	Bonferroni	N/A	N/A

2.10.2 Analysis of TMZ treated HiSpots®

Fluorescence intensity and EdU+/caspase-3+ cell counts were calculated per HiSpot® for each dose and input into GraphPad Prism. Data were grouped by patient number and compared using a two-way ANOVA with Bonferroni's multiple comparisons. TMZ doses were plotted as the log [TMZ dose] (M). For graphical presentation, the data for the DMSO control HiSpots® were input with a dose of -10 (log [TMZ] (M)) in order to show the data points on a logarithmic scale. X-axes are on a logarithmic scale, with a break shown to distinguish the DMSO control dose. The doses as shown on the logarithmic x-axis are therefore: 10^{-10} (0 µM), $10^{-5.3}$ (5 µM), $10^{-4.3}$ (50 µM), 10^{-4} (100 µM) and $10^{-3.3}$ (500 µM).

2.10.3 Chi-squared analysis

A chi-squared test was performed using GraphPad Prism to determine whether there was an association between *MGMT* promoter methylation status and HiSpot® response to TMZ treatment. Sensitivity and specificity values were calculated.

2.10.4 HiSpot® patient samples

Table 2-6 below lists the patient samples used to generate HiSpots® for each figure throughout this project. The patient numbers can be correlated with the pathological and diagnostic data available in **Table 4-1.**

Table 2-6: Patient samples used per figure.

The patient samples used to generate HiSpots® for each figure containing data are shown.

FIGURE	PATIENT SAMPLES USED
3-1	18
3-2	1, 2, 3, 4, 5, 7, 8, 9, 10
3-3	22, 23, 24
3-4	11, 16, 18
3-5	41
3-6	45, 49
3-7	36
3-8	5, 7, 8, 9
3-9	11, 14, 19
3-10	15, 16, 18
3-11	11, 16, 18
3-12	22, 24, 26
3-13	26, 27 (direct DAPI counts), 25, 28, 30
3-14	26, 27
3-15	28
3-16	28, 34
3-17	28, 34
3-18	28, 34
3-19	28, 34, 30
4-1	30, 37, 38, 39
4-2	28, 36, 40, 46
4-3	33, 36, 40
4-4	30, 33, 34, 37
4-5	30, 33, 34, 37, 44, 45, 46, 49

4-6	33, 34, 37, 44, 45
5-2	30, 33, 34, 37, 39, 40, 41, 44, 45, 46, 47, 49,
5-3	39, 40, 41, 47
5-4	39, 40, 41, 47
5-5	39, 40, 41, 47
5-6	39, 40
5-7	39, 40, 47
5-8	39, 40, 47
5-9	39
5-10	39, 40, 47
5-11	39, 47
5-12	39, 47

3 Initial characterisation and optimisation of the HiSpot® model for GBM

3.1 Introduction

3.1.1 Background

The HiSpot® model has been used for a number of applications (Preynat-Seauve *et al.* 2009; Bailey *et al.* 2011; Biggs *et al.* 2011; Sundstrom *et al.* 2012; Zhao *et al.* 2016; Zhu 2018). With adaptations for GBM cell culture, the HiSpot® model could provide a method for fast screening of chemotherapeutic options for individual patients, allowing feedback to the patient's clinical care team. HiSpots® have some advantages over other current models. HiSpots® are 3D, allowing the cells to form cell:cell interactions throughout multiple layers. They are formed by re-aggregation of cells at a high culture density, which allows them to form a complex 3D structure within 7 DIV. As they are created with human cells, they have no species differences to take into account, and their growth at the air liquid interface prevents unknown effects of synthetic scaffolds. HiSpots® include multiple cell types from the original tumour, rather than just the sphere-forming population.

The first step in this process is to establish whether the previously developed HiSpot® model will allow the culture of primary GBM cells. The model has previously been successfully used for the culture of primary brain tissue. However it is possible that some changes will be required to the protocol in order to successfully culture GBM cells. Therefore this section will focus on determining the optimum conditions for culture.

3.1.2 Characterisation

3.1.2.1 Identification of cycling cells

Measures of cell cycle and death can be used to monitor the health of a cell culture population. Caspase-3 is an enzyme involved in the apoptotic

pathway. It can be used to identify cells in the late stages of apoptosis, either by using an antibody for cleaved (activated) caspase-3, or with a fluorescent substrate for the enzyme itself (Hadjiloucas *et al.* 2001; Cheng *et al.* 2009). Lactate dehydrogenase (LDH) is an enzyme which is released into the culture media during necrotic cell death. Levels of LDH can be measured in the removed media at each media-change timepoint in order to analyse the amount of necrosis within the cultures.

Staining for Ki-67 identifies all actively cycling cells (those not in G0). EdU is a thymidine analog taken up by any cells in S-phase, so with an exposure time shorter than the S-phase it will identify only the S-phase cells. EdU should therefore be detectable in a set percentage of all cycling cells depending on the exposure time. A longer exposure can be used in much the same way as Ki-67 (to indicate total cycling cells), and uses in literature vary.

EdU can be detected in cells post-fixation. Either Ki-67 or EdU can be used to indicate the level of proliferation in a cell population, known as the growth fraction (Ki-67+ cells/DAPI). Although EdU will stain fewer cells in total, this measurement can still be used to compare between conditions. Used in combination, Ki-67 and EdU can allow an approximation of the cell cycle speed, known as the labelling index (EdU+ cells/Ki-67+ cells). These factors can be compared between variables in order to see the effects on the cycling cells.

In this project, cleaved caspase-3 staining and LDH assays were used to investigate the levels of cell death in the HiSpots®. Ki-67 and EdU analysis were used to monitor the cycling of the cells within the HiSpots® at various timepoints and confirm the optimum culture length for future studies.

3.1.2.2 Tumour cells

Different cell types are identified within the cultures using antibodies for a number of markers. The following markers were used to try and capture the main tumour cells: β-III tubulin (β-IIIT), a marker of early neurons; GFAP, a

marker of astrocytes; and nestin, a marker of progenitor cells. In healthy adult brain, these three markers would not be co-expressed on the same cells. GFAP and nestin are both intermediate filaments. GFAP is a type III intermediate filament expressed predominantly in astrocytes, although it has been shown to be expressed in other cell types (Middeldorp and Hol 2011). Nestin is the only type VI intermediate filament, found in CNS stem cells, and is often used as a marker for CSCs in various cancers including GBM (Cooper 2000; Neradil and Veselska 2015). GFAP and nestin are co-expressed in healthy cells during neurogenesis, in radial-glia like NSCs and astroglia progenitors (Zhang and Jiao 2015). β-IIIT is a microtubule used to identify neuronal progenitors (Katsetos *et al.* 2001). It is usually only found co-expressed with GFAP and nestin in foetal development (Dráberová *et al.* 2008). In gliomas, β-IIIT levels have been shown to correlate with tumour grade. It has been demonstrated that GFAP, nestin and β-IIIT can be co-expressed in tumour cells, and it is possible that this combination is indicative of an embryonal-like phenotype, with this being the only time in human development that otherwise healthy cells express this combination of markers (Ignatova *et al.* 2002; Rieske *et al.* 2007). For simplicity, cells stained with β-IIIT, GFAP and nestin will be referred to as 'triple-positive tumour cells' within this thesis. In later experiments, nestin was no longer used, to allow for co-staining with other antibodies, but the 'triple-positive tumour cell' label remains used throughout to avoid confusion. Vimentin is another type III intermediate filament found in a number of cell types including astrocytes and fibroblasts (Janeczko 1993; Cooper 2000).

In secondary GBMs, tumour cells will carry a mutation in *IDH-1/2*. The most common mutation is the *IDH-1* R132H mutation. This can be detected using an antibody commonly used in pathological testing. Any cells positive for this marker are tumour cells. However as this mutation is only present in secondary GBMs, it can not be used generally to identify tumour cell populations.

3.1.2.3 SOX2

SOX2 is a marker of neural stem cells, but it is also a key feature of GBM cancer stem cells (Hemmati *et al.* 2003; Tunici *et al.* 2004). It is a useful marker for the detection of stem-like cells, demonstrating that tumour cells in culture are retaining their undifferentiated state, and is a target of interest in pharmaceutical research for GBM treatment. This transcription factor is therefore a key feature of GBM, and so it is important to confirm its presence in the tumour cells of the HiSpot® GBM model (Garros-Regulez *et al.* 2016; Garnier *et al.* 2019). It has been used to identify cancer stem cell (CSC) populations (Hemmati *et al.* 2003), although as discussed previously, it is not a truly definitive marker of CSCs (Lathia *et al.* 2015).

3.1.2.4 Microglia in GBM

The importance of microglia in GBM cultures has previously been underestimated. A key advantage of the HiSpot® model is the inclusion of all cell types present in the initial tissue sample, so it was particularly important to identify whether microglia were present in the HiSpots®. Even when microglia are included in models, they are often rodent derived, and differences between rodent and human microglia could be a key factor in mistranslation of animal models to human patients (Lenz and Nelson 2018). For instance, the genes upregulated in GBMs when compared to healthy tissue vary between humans and mice (Szulzewsky *et al.* 2016).

There is an abundance of markers available for microglia, although not all will also stain tumour associated macrophages (**Table 3-1**, Roesch *et al.* 2018). CD11b and CD45 can be used together to distinguish microglia and macrophages, but require co-staining and sorting into low and high expression to identify cell types. Flow cytometry is often used to separate microglia from macrophages using these markers (Parney *et al.* 2009). CD68 is another common marker (De Groot *et al.* 2000). Hendrickx *et al.* (2017) directly compared CD68 and IBA1 and described that the different staining patterns made IBA1 a better choice for identifying cell protrusions and morphology of microglia. This is because IBA1 is a cytoplasmic stain, so is

not reliant on the lysosomes being evenly distributed within the cell as is the case with CD68. TMEM119 is a recently characterised marker, which identifies both ramified and amoeboid microglia, but does not stain macrophages, so can be used to distinguish these two cell types. However, it is still unclear whether these would be distinguishable in the case of high grade glioma due to the effect of the tumour on macrophage expression patterns (Haage *et al.* 2019).

Table 3-1: Markers of microglia and macrophages.

Markers commonly used for the identification of microglia and/or macrophages are shown, with their specificity for each cell type.

Marker	*Expressed by microglia*	*Expressed by macrophages*
IBA1	Y	Y
CD11b + CD45 (low)	Y	N
CD11b + CD45 (high)	N	Y
CD68	Y	Y
TMEM119	Y	N

IBA1 was selected for this project because it is a marker for both microglia and macrophages, and does not distinguish microglia by activation state, making it possible to identify the total immune cells population within the HiSpots®. Other members of the research group had also had success with IBA1, specifically the Wako antibody, which supported this decision.

3.1.3 Optimisation

3.1.3.1 Culture media

Media composition can have a significant influence on the survival or behaviour of cultured cells (Lee *et al.* 2006). The effects of serum in cell culture can be particularly relevant.

Some of the benefits of removing serum include less batch to batch variation, less reliance on animal-derived products, and defined supplements. These factors are not to be underestimated. Defined media conditions are more easily translatable to an industrial setting. Batch variation in ingredients such as foetal bovine serum can cause unnecessary problems in cell culture of many types, especially when it comes to replicating results in different research groups or translating methodology to an industrial setting.

However, there is no point to changing culture media if the cells will not grow. GBM HiSpots® were initially cultured according to previous HiSpot® research and compared to other conditions later on (Zhu 2018). Different culture conditions for comparison were adapted from the Siebzehnrubl group's standard protocols for GBM neurosphere culture and represent standard conditions for serum-free culture of primary GBM (Hemmati *et al.* 2003; Lee *et al.* 2006; Sarkisian *et al.* 2014; Hoang-Minh *et al.* 2016). The most important points to establish were whether serum could be removed from the culture media after 7 DIV without negatively impacting the HiSpots®, and whether the HiSpots® could be grown without serum from 0 DIV. EGF and FGF2 were added to some serum-free HiSpots® to determine whether these affected the growth or development of the cultures.

Specifically for GBM, there is a large body of evidence which shows that the presence of serum in cell culture media can drive the tumour cells to irreversibly differentiate, whereas cells cultured in serum free media with supplementary growth factors are much better matches to the histological and genotypic features of the original tumour, and were better at

maintaining a capacity for multilineage differentiation (Lee *et al.* 2006; Wakimoto *et al.* 2012; Lenting *et al.* 2017). This can lead to cells with different gene expression, and potentially treatment response, to the original tumour (Ernst *et al.* 2009). Stockhausen *et al.* (2014) demonstrated that the presence of serum in neurosphere cultures causes the cells to differentiate and decreases their tumorigenicity. The main aim of the HiSpot® model for GBM is not to establish long term cultures, but to create a predictive representation of the original patient tumour. Therefore it is especially important to avoid altering the tumour composition and behaviour as much as possible. It is key to avoid the use of serum for GBM cell culture if at all possible, so it was essential to establish whether GBM HiSpots® could survive the removal of serum.

3.1.3.2 Culture density

Three dimensional cultures often reach a maximum size or density, after which they become necrotic and die (Akkerman and Defize 2017; Qian *et al.* 2018). This must be taken into account when creating high density cultures such as the HiSpots®. However, GBM cells by nature do not behave in the same way as healthy cells, so may require different conditions. The core of a GBM is highly hypoxic with many areas of necrosis, and GBM organoids have been demonstrated to be less sensitive to the size limitations seen in normal brain organoids (Hubert *et al.* 2016).

The density of a culture system is also important for maintaining features of the original tumour. It has been noted that *EGFR* amplification found in GBMs is often lost when the cells are transferred to an *in vitro* system but is maintained in cells which have been xenotransplanted into mice (Pandita *et al.* 2004). Similarly, expression of Shc3 is lost after ~4 passages *in vitro* in 2D. Shc3 is a protein found in the neurons of healthy adult brains, but not in glia. It is very highly expressed in GBM cells (Magrassi *et al.* 2005). Azzalin *et al.* (2014) demonstrated with both established lines and primary GBM cells that Shc3 expression is retained much better in multicellular tumour spheroids than in 2D culture. They also showed that the expression of Shc3 increased

in 2D as the cell density increased, peaking when the cells reached confluence. The tyrosine kinase Fak is involved in the regulation of Shc3 expression, and the communication between cell:cell signals and cell growth and proliferation. These factors indicate that Shc3 expression is affected by cell density, and that the numerous connections between cells in high density cultures are required to maintain its expression.

The initial culture density of $5x10^7$ cells/ml was taken from previous work in the Gray lab, initially on cells from patients undergoing surgery for epilepsy, and some work on GBM (Rymer 2011). However, taking into account the importance of suitably high cell density in GBM cultures, it was considered that GBMs may require a higher cell density within the HiSpots® in order to thrive, so HiSpots® were created with a range of different densities to investigate the cell survival, growth and HiSpot® structure. Once the optimum density was determined, it was also key to determine whether these HiSpots® also responded to different media compositions in the same way.

3.1.3.3 Length of culture time

All of the factors described above are informative alone, but further information can be gleaned from comparison between different time points. It was important to clarify an appropriate timepoint for future investigations which allowed the HiSpots® sufficient time to develop into 3D cultures. Previous work looked at timepoints of 7 and 21 DIV so these were chosen for initial analysis (Rymer 2011). Later experiments were predominantly ended at 14 DIV as these cultures were deemed sufficiently developed for analysis.

3.1.4 Aims

The experiments described in this chapter aim to characterise HiSpots® created using primary human GBM cells, and to optimise the culture method for these cells.

3.2 Results

3.2.1 The HiSpot® model can support primary GBM cells

3.2.1.1 HiSpots® contain low levels of apoptosis

HiSpots® have been successfully cultured up to 7, 14 and 21 DIV. Although some cultures failed, this tended to happen early on and may have been a result of high levels of necrosis in the tumours received. The successful cultures had low numbers of apoptotic cells. Cleaved caspase-3 is an indicator of late stage apoptosis, which can be used to demonstrate the levels of apoptosis in a culture (**Figure 3-1A**). Vimentin is a marker of astrocytes which has been linked to the invasiveness of tumour cells (Noh *et al.* 2016). It helps visualise the cell morphology of the majority of the cell types in the HiSpot®.

The data were not normally distributed according to a Shapiro Wilk test, so were compared using a Mann Whitney test. The percentage of cells positive for cleaved caspase-3 was not significantly different between 7 and 14 DIV (1.648 ± 0.3668 vs 1.453 ± 0.3528, p=0.4206, n=4-5 from 1 patient, **Figure 3-1B, C**).

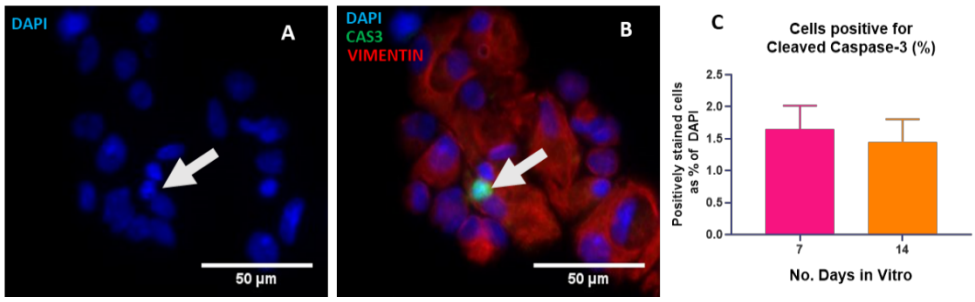

Figure 3-1: Cleaved caspase 3 staining.

A/B: Immunofluorescence images are shown. HiSpots® were stained with DAPI (blue), and antibodies for cleaved caspase-3 (green) and vimentin (red). The DAPI stained nuclei are shown in panel A. The arrow points out the cell which in panel B can be seen as positive for cleaved caspase 3. The cytoplasm of the cells are clearly visible when stained with vimentin (red). Scale bars are shown for reference.

C: Levels of cleaved caspase-3 staining were measured at 7 and 14 DIV, comparing HiSpots® kept in HSM (25%) with those transferred to SFM (0%). Data are shown as mean ± SEM. The groups were not significantly different according to a Mann Whitney test. N=4-5 from 1 patient. All HiSpots® were cultured in HSM (25%) until 14 DIV. Counts from HiSpots® fixed at each timepoint are shown.

3.2.1.2 LDH release is stable, but not a reliable assay of cell death in high serum media

The levels of LDH in culture media can be measured to indicate the amount of necrotic cell death in the culture. Over HiSpots® from 9 different patients, the release of LDH was stable from 4-21 DIV, compared to media controls (**Figure 3-2A, B**).

There was a large variation between HiSpots® from different patients. Some variation is to be expected due to the heterogeneity between patients with GBM. The LDH assay is affected by the levels of serum in the media. Media collected from growing cells was compared to media from cells which had been treated with a lysis buffer to kill all the cells available. There were significantly higher levels of LDH in the untreated cell media than in that treated with lysis buffer (**Figure 3-2C**). A two way ANOVA showed no significant differences over time ($F(5, 5) = 4.898$, $n=6$, $p=0.0530$) but significantly less relative LDH in the lysed group ($F(1, 5) = 60.39$, $n=6$, $p=0.0006$). Values used for two way ANOVA were the mean of three technical replicates. This difference was significant at each timepoint according to Bonferroni's multiple comparisons ($p=0.0034$, group means for lysed vs non-lysed, 0.2974 ± 0.03357 vs 0.5910 ± 0.05551, $n=6$ per treatment group).

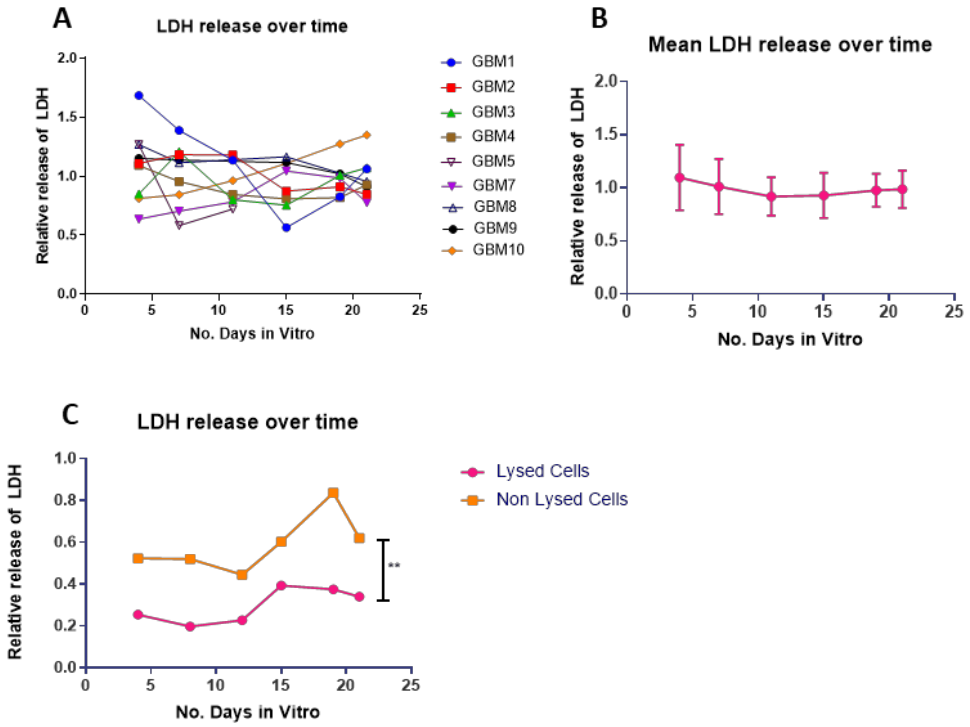

Figure 3-2: LDH release from HiSpots®.

*LDH levels were measured in media removed from cells at various time points. A. LDH levels measured at each media change up to 21 DIV, by individual patient source. B: The mean values of the data from A. C: A comparison of lysed and non lysed cells from HiSpots® from the same patient at the same timepoints. **p<0.01. Data shown in A are means of three well repeats from HiSpots® from one patient each. Data shown in B are means of HiSpots® from 9 patients. Data shown in C are means of three well repeats from HiSpots® from one patient.*

3.2.2 HiSpots® support key cell types in GBM

3.2.2.1 HiSpots® contain and support microglia

Microglia are a key cell type in GBM and so must be represented in HiSpot® cultures. HiSpots® fixed at 1, 3, 7 and 10DIV were stained for IBA1. Total cells (DAPI) and IBA1+ cells were counted per field (**Figure 3-3A**). The percentage of microglia (IBA1+ cells) in the HiSpots® did not vary significantly between the timepoints (p=0.3695, n=13-15 from 3 patients, Kruskal-Wallis test) and ranged from 12-29% of the total cells (**Figure 3-3B**).

Microglia mostly showed a large, round morphology, as visible in **Figure 3-3A** below. The green arrow shows a clearly stained microglial cell. The red arrow indicates a cell negative for IBA1 for comparison.

Co-staining with markers for other cell types demonstrated that the populations of tumour and microglial cells were interlinked, with the microglial cells taking up a large proportion of the space between other cells **Figure 3-3C, D**.

Optimisation: Originally tested the α-IBA1 antibody from Abcam but microglia were not reliably identifiable. An alternative α-IBA1 antibody was purchased from Wako which provided much clearer staining for microglia identification.

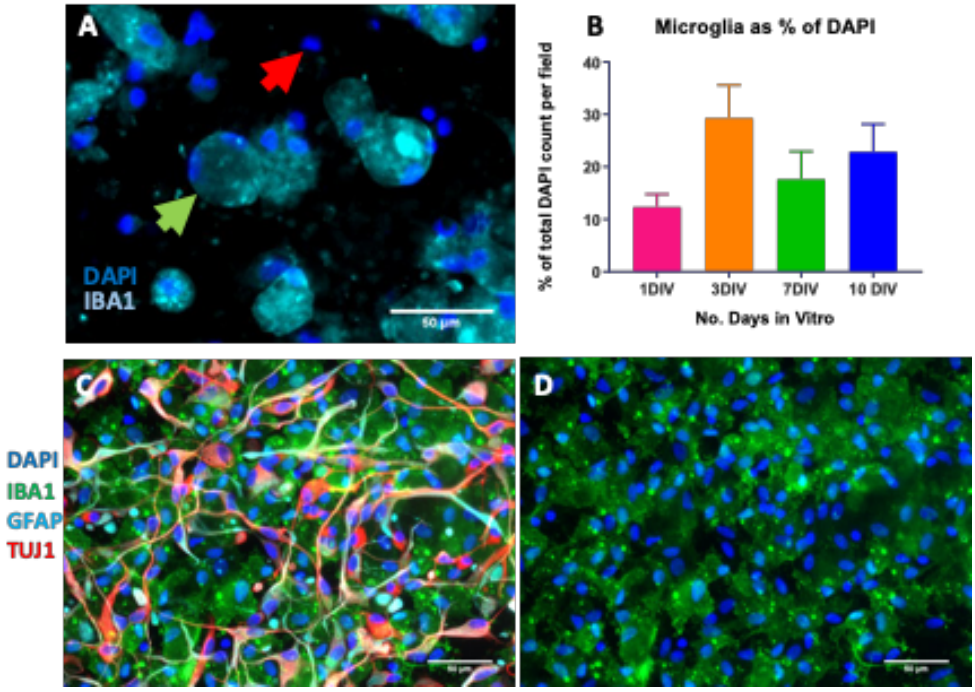

Figure 3-3: Microglia staining in HiSpots®.

A: A fluorescence microscope image of microglial cells in a HiSpot®. IBA1 staining is shown in turquoise, DAPI nuclear stain in dark blue. The red arrow (upper) shows a cell negative for IBA1, the green arrow (lower) shows a cell positive for IBA1. 50 µm scale bar is shown. B: Percentage of cells positive for IBA1 at 1, 3, 7 and 10 DIV. Data are shown as mean ± SEM. Groups were not significantly different according to a Kruskal-Wallis test. C/D: Immunofluorescence images of HiSpots® stained for DAPI (blue), IBA1 (green), GFAP (turquoise) and β-IIIT (red). All channels are shown in C, and only DAPI and IBA1 in D to more clearly demonstrate the morphology of the microglia. Scale bars are shown for reference. N=13-14 from 3 patients.

3.2.2.2 HiSpots® contain β-IIIT+, GFAP+, nestin+ and triple-positive tumour cells

β-IIIT is conventionally used as a marker of early neurons. GFAP is the typical astrocytic marker, and when co-stained with nestin commonly indicates progenitor cells. Cells positive for nestin but not for GFAP are usually identified as intermediate progenitors. Although GFAP and nestin are commonly co-expressed in cells such as astrocytes, β-IIIT is not seen co-expressed with GFAP in healthy adult human brain. Cells can be seen in **Figure 3-4E** (overlay image) which co-express β-IIIT, GFAP and nestin. The individual channels can be seen in panels **A-D.** These are referred to as triple positive cells.

HiSpots® were fixed at 7 DIV and stained for β-IIIT, GFAP and nestin. Total cells (DAPI) and numbers of cells positive for each stain and combination of β-IIIT, GFAP and nestin were counted. 1.642 ± 0.3631 % of the cells were positive for β-IIIT only. 2.799 ± 0.7578 % of the cells were positive for GFAP and nestin but negative for β-IIIT. 12.00 ± 3.665 % of the cells were positive for β-IIIT, GFAP and nestin (n=14 from 3 patients, **Figure 3-4F**).

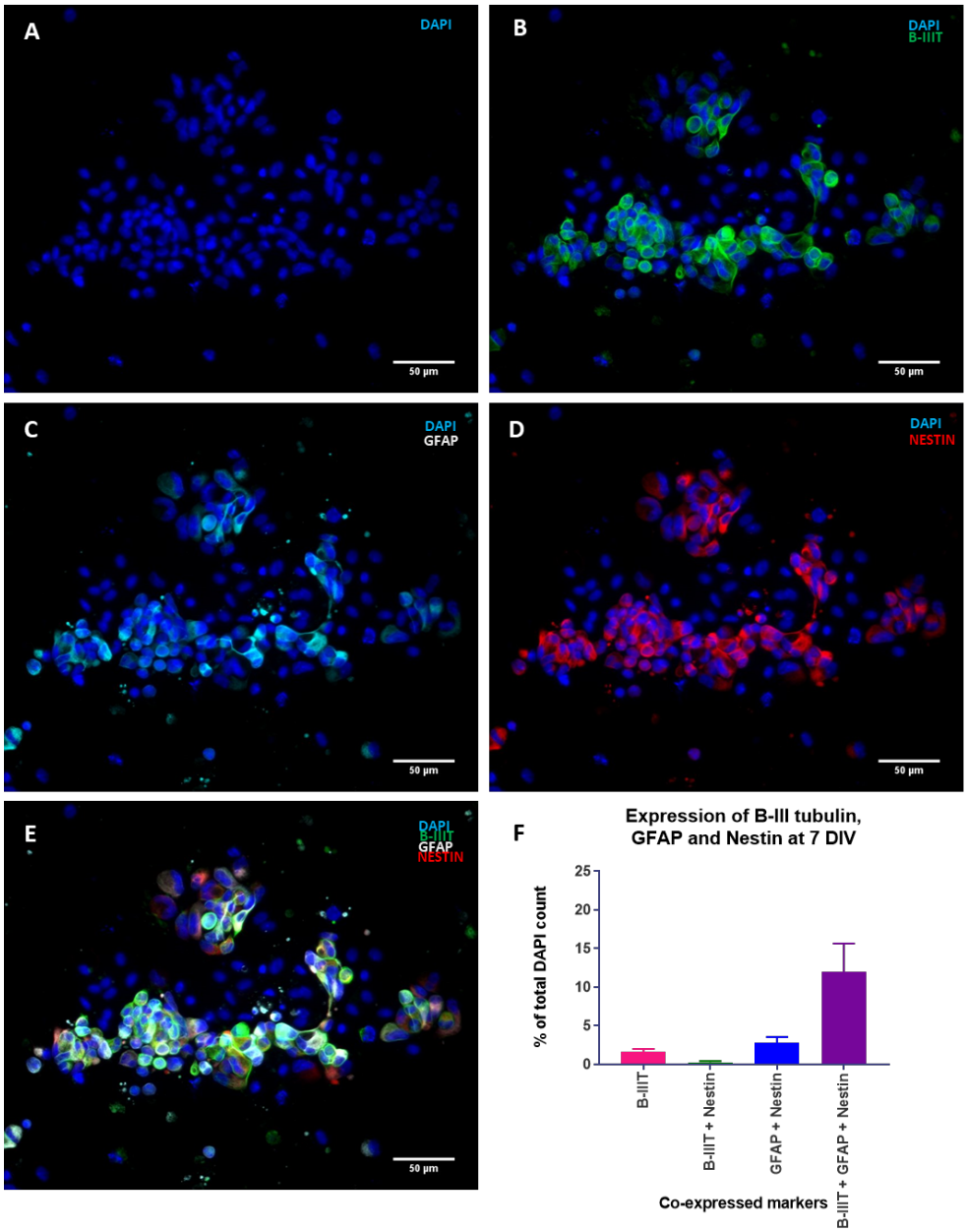

Figure 3-4: Cell types found in GBM HiSpots® with co-staining analysis

A-E: Immunofluorescence images of HiSpot® cells. Each panel shows DAPI nuclear staining in blue. Panel B also shows β-IIIT (green), panel; C shows GFAP (turquoise), panel D shows nestin (red), and panel E shows all channels as a composite image.

F: Quantification of immunofluorescent co-staining. The percentages of total cells with each combination of the antibodies used are shown. Combinations not shown had no positive cells present. Data shown are mean ± SEM. N=13-14 from 3 patients.

3.2.2.3 IDH-1 R132H+ cells are present in HiSpots® and co-stain with GFAP

Although there were three patients with mutant *IDH-1* R132H within the 50 collected, only one (GBM41) was able to be used for the detection of tumour cells using the *IDH-1* R132H antibody. This was the only patient diagnosed with a GBM to have mutant *IDH-1*. There were not sufficient HiSpots® remaining from one other patient, and another failed to show any positivity which may have been due to high calcification in the tissue.

HiSpots® from patient GBM41 were costained with antibodies for *IDH-1* R132H, GFAP and β-IIIT. *IDH-1* R132H positive cells can be seen in **Figure 3-5 B.** In order to determine whether these markers were co-expressed on the same cells, images were taken using a confocal microscope. The different channels are visible in **Figure 3-5 A-D** and overlay images in **E-F**.

Confocal images of GFAP and *IDH-1* R132H immunofluorescence were taken for quantification. Three non-consecutive slices were analysed from each Z-stack, and the cell types counted. There were 84.44 ± 15.29 cells total per field (**Figure 3-5 G**). Of these, 17.73 ± 1.400 % of the cells were positive for both GFAP and *IDH-1* R132H. 3.559 ± 1.359 % were positive for GFAP only. 100% of *IDH-1* R132H cells were positive for GFAP. (**Figure 3-5 H**, n=3 from 9 slices total).

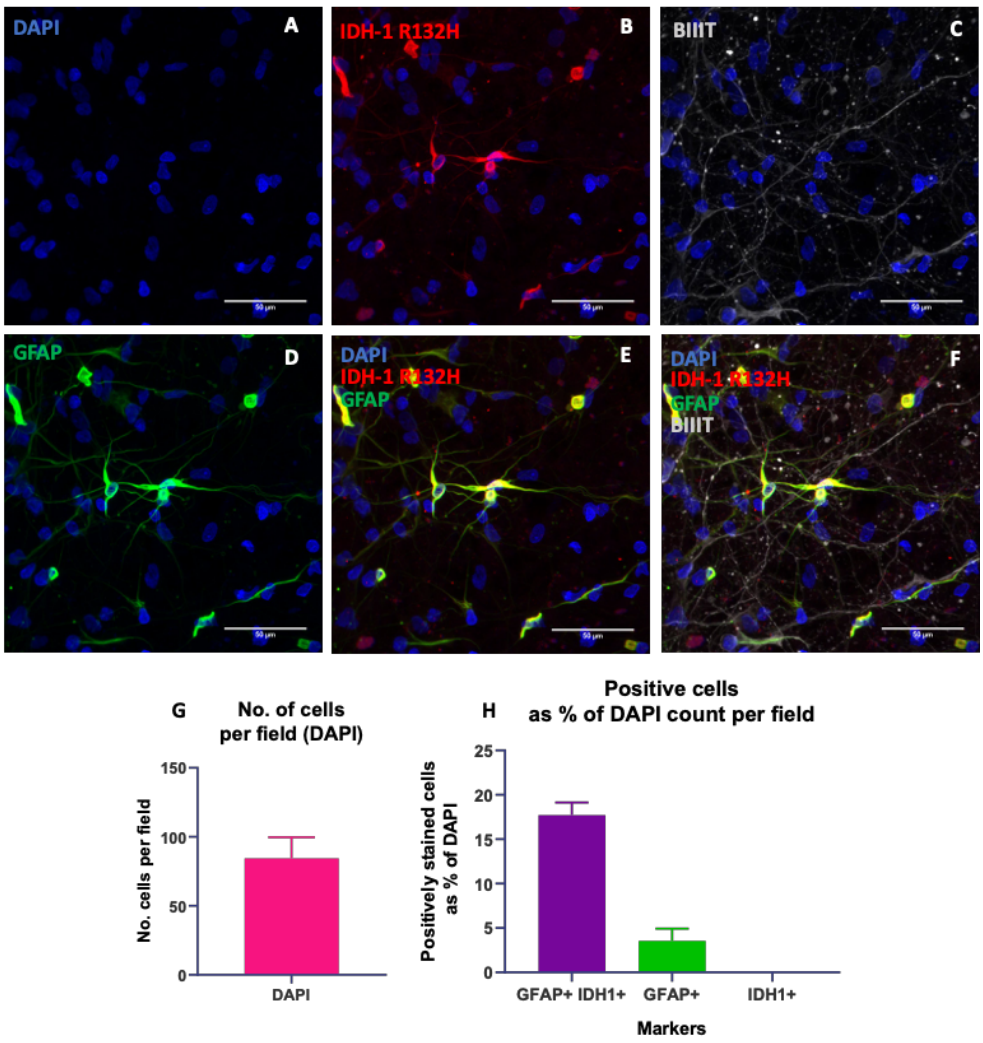

Figure 3-5: IDH-1 R132H, GFAP, B-IIIT immunofluorescence.

A-F: Immunofluorescence images of HiSpots® stained for nuclei (DAPI, blue), IDH-1 R132H (red), ß-IIIT (white) and GFAP (green). Scale bars are shown for reference. Panel A shows the DAPI channel, B shows IDH-1 R132H staining, C shows ß-IIIT staining, D shows GFAP staining. Panel E shows a composite image of panels A, B and D. Panel F shows a composite image of panels A-D.

G: The number of nuclei (DAPI) per field of a Z-stack slice in a confocal image (40x). Data are mean ± SEM, n=3 from 9 slices. H. Cells positive for GFAP, IDH-1 R132H or both as a percentage of total DAPI count per field. Data are mean ± SEM. n=3 from 9 slices.

3.2.3 GFAP+ β-IIIT+ cells are also co-positive for SOX2

HiSpots® were costained for SOX2, GFAP and β-IIIT to determine whether GFAP+β-IIIT+ cells were also positive for SOX2, a marker of stem cells. A significant overlap was clearly visible in the HiSpots®. Example images from GBM45 and 49 are shown below (**Figure 3-6**). DAPI, SOX2, GFAP and β-IIIT channels are shown separately (**Figure 3-6 A-D, F-I**), and a channel overlay is shown for each image to demonstrate overlap (**Figure 3-6 E, J**). All images were taken from $2.5x10^8$ cells/ml HiSpots®.

Confocal images of SOX2, GFAP and β-IIIT staining were used for quantification of the overlap between SOX2 and GFAP/β-IIIT positivity. For thinner Z-stacks, maximum intensity projection images were quantified. For thicker Z-stacks, with multiple separate cell layers, two or three slices (at least 6 µm apart) were quantified, and the mean values taken for analysis. HiSpots® from patients GBM45 and 49 showed 200.4 ± 59.76 cells per field (**Figure 3-6 K**), of which 77.27 ± 0.2672 % were SOX2+ (**Figure 3-6 L**). Of these SOX2+ cells, 98.31 ± 1.007 % were also positive for GFAP and β-IIIT (**Figure 3-6 M**, n=4 from 9 slices, 2 patients).

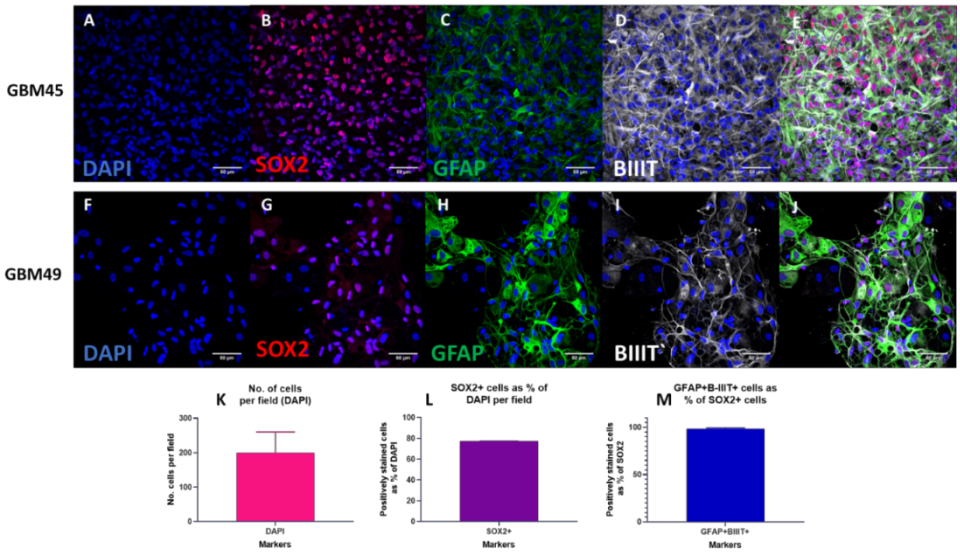

Figure 3-6: SOX2, GFAP and β-IIIT immunofluorescence.

A-J: Immunofluorescence images of HiSpots® stained for nuclei (DAPI, blue), SOX2 (red), GFAP (green) and β-IIIT (white). Individual channels are shown for DAPI (A, F), SOX 2 (B, G), GFAP (C, H) and β-IIIT (D, I). Overlay images of all channels are shown in E and J. Panels A-E show a HiSpot® from sample GBM45, panels F-J GBM49. Scale bars are shown for reference.

Panels K-M show quantification of images including those in panels A-J. Data shown are mean ± SEM. K: The number of cells per field (DAPI). L: The percentage of total cells (DAPI) which are positive for SOX2. M: The percentage of SOX2+ cells which are also positive for GFAP and β-IIIT.

3.2.4 HiSpots® do not contain endothelial cells

HiSpots® were stained with an antibody for the endothelial cell marker CD31. Only one possible positive cell was seen within the stained HiSpots® (**Figure 3-7 A-C**). HiSpots® were almost entirely absent of positive staining for CD31 (**Figure 3-7 D-E**). All images were taken from $2.5x10^8$ cells/ml HiSpots®.

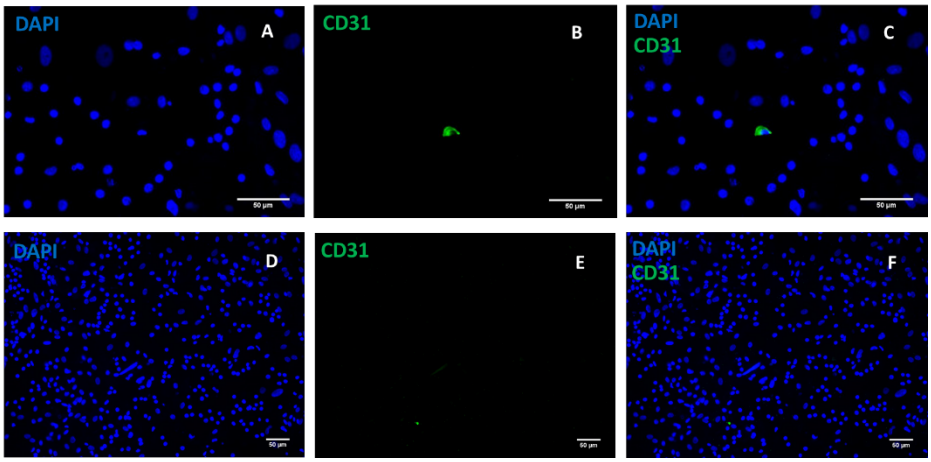

Figure 3-7: Demonstration of CD31 antibody testing.

Immunofluorescence images of HiSpots® stained for nuclei (DAPI, blue) and CD31 (green). A, D: Individual DAPI channel. B, E: Individual CD31 channel. C, F: Overlay images. A-C: High magnification of the one potentially positive cell within a HiSpot®. D-F: A lower magnification showing no positive staining within a large region of HiSpot® cells. Scale bars are shown for reference.

3.2.5 GBM HiSpots® do not survive long term in serum-based media

3.2.5.1 HiSpots® lose cells over time

In order to be a useful model for GBM, it must be possible to maintain HiSpots® in culture for longer than 7 DIV. HiSpots® were fixed at 7 DIV and 21 DIV for analysis after culture in HSM. This media was initially chosen as it was used in previous HiSpot® studies. Data were not normally distributed so non-parametric tests were performed. Between 7 and 21 DIV, the number of cells decreased significantly (183.7 ± 35.43 vs 33.80 ± 7.142, $p<0.0001$, n=24 from 4 patients, Mann Whitney test). The percentage of β-IIIT+ cells was not significantly affected (26.06 ± 2.805 vs 32.28 ± 5.530, p=0.7885, n=20-24 from 4 patients, Mann Whitney test). The percentage of GFAP+ cells was not significantly different between 7 and 21 DIV (7.268 ± 1.449 vs 15.34 ± 3.467, p=0.0790, n=20-24 from 4 patients, Mann Whitney test), although there was a trend towards an increase. These data are visualised in **Figure 3-8** below, panels A-C. Panel D shows an example from the images used to produce these data. The image shows cells positive for β-IIIT and/or GFAP expression. Cell survival is further investigated in **3.2.8.2.**

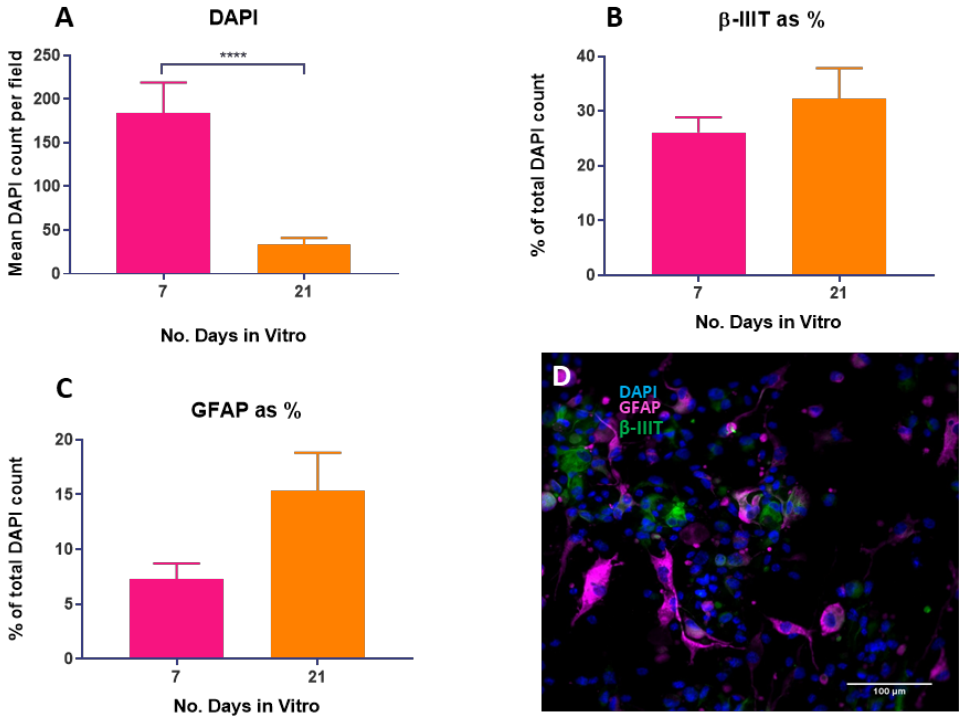

Figure 3-8: Total cell counts and cell types at 7 and 21 DIV.

*A: Total cell counts per field after 7 and 21 DIV. ****p<0.0001. Data shown are mean ± SEM. n=24 from 4 patients. B: β-IIIT positive cells as a percentage of total cell count per field. Data shown are mean ± SEM. n=20-24 from 4 patients. C: GFAP positive cells as a percentage of total cell count per field. Data shown are mean ± SEM. n=20-24 from 4 patients. D: Immunofluorescence image of HiSpot® cells. Cells were stained with DAPI and antibodies for GFAP (pink) and β-IIIT (green). A scale bar is shown for reference.*

3.2.5.2 HiSpots® survive up to 21 DIV but the proportion of cycling cells is reduced

HiSpots® were stained for Ki-67 to identify cycling cells, and EdU to identify cells in the S-phase of the cell cycle (**Figure 3-9**). These factors provide an indication of the proportion of the cells within the HiSpots® which are proliferative (Ki67+/DAPI, known as the growth fraction), and the speed at which this proliferation is occurring (Edu+/Ki67+, known as the labelling index). These factors enable the cell cycle to be compared between different timepoints. An example of Ki-67 and EdU staining is shown in **Figure 3-9 D**, with individual channels of DAPI, Ki-67 and EdU shown in **A-C** respectively.

Data were not normally distributed, so non-parametric tests were performed. Total cell counts initially dropped significantly between 1 and 3 DIV (778.6 ± 103.7 vs 381.0 ± 65.53, p=0.0204, n=15 from 3 patients), according to a Kruskal-Wallis test with Dunn's multiple comparisons, with comparisons limited to consecutive timepoints. There was also a significant drop in cell count between 14 and 21 DIV (175.5±18.34 vs 153.1±12.93, p=0.0441, n=15 from 3 patients, **Figure 3-9B**). The Ki-67+ (cycling) fraction increased significantly between 3 and 7 DIV (0.2813 ± 0.074 vs 1.228 ± 0.276, p=0.0180, n=15 from 3 patients) and then trended downwards from 9 DIV. The percentage of Ki-67+ cells which were EdU+ varied significantly according to a Kruskal-Wallis test (p=0.0035) but Dunn's multiple comparisons did not show any significant changes between consecutive timepoints (n=10-15 from 3 patients, **Figure 3-9C**).

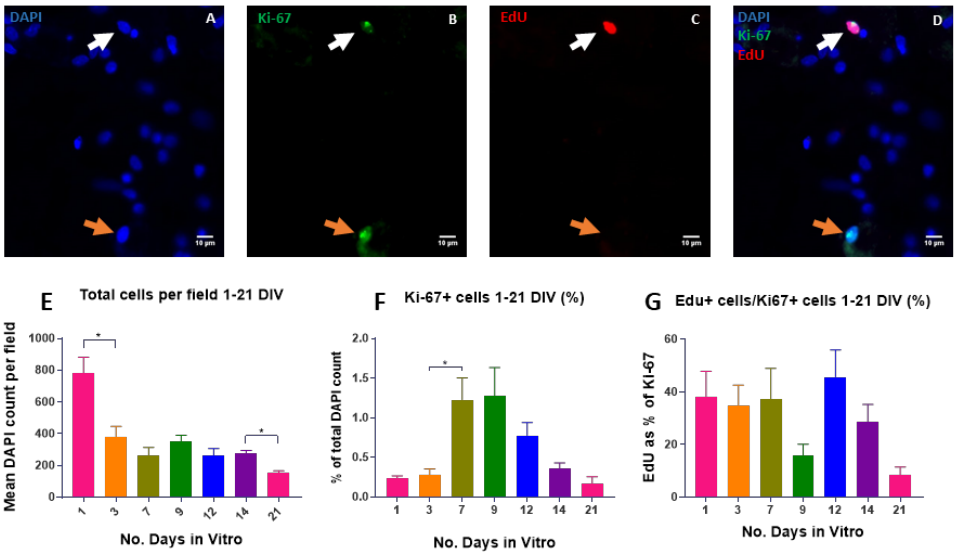

Figure 3-9: Cell counts and proliferation in HiSpots®

*A-D: Immunofluorescence images of HiSpots® stained with DAPI and EdU, and an antibody for Ki-67. The upper white arrow indicates a nucleus positive for Ki-67 and EdU. The lower orange arrow indicates a nucleus positive for Ki-67 but negative for EdU. Panel A shows DAPI staining (blue), B shows Ki-67 staining (green), and C shows EdU staining (red). D shows all four channels as a composite image. Scale bars are shown for reference. E: Graph showing total cells per field over timepoints 1-21 DIV. *p<0.05. Data are shown as mean ± SEM. F: Ki-67+ cells as a percentage of total cell count per field over timepoints 1-21 DIV. *p<0.05. Data are shown as mean ± SEM. G: EdU+ cells as a percentage of Ki-67+ cells per field over timepoints 1-21 DIV. Data are shown as mean ± SEM. n=10-15 from 3 patients.*

3.2.6 Optimisation of serum levels in media

3.2.6.1 Serum containing medium increases cell death and reduces cycling cells

In order to try and improve the HiSpot® survival and proliferation, different media conditions were compared. As described above (3.2.5.2), the percentage of Ki67+ cells peaked at 7 DIV, so media was changed at this timepoint in order to try and prevent the reduction in proliferation. HiSpots® were kept in HSM (25% serum) or transferred to either SFM (0% serum) or a 50:50 mix of the two media types (12.5% serum). A visualisation of this protocol is shown in **Figure 3-10E.**

Data were not normally distributed so non-parametric tests were performed. At 14 DIV, there was no significant difference in the total cell count between the conditions (one way ANOVA, p=0.2861, F (2, 40) = 1.291, n=13-15 from 3 patients, **Figure 3-10A**). At 21 DIV, the number of cells remaining in each condition varied significantly (p=0.0013, n=14-15 from 3 patients, **Figure 3-10B,** Kruskal-Wallis test). There was a significantly larger total cell count in the 0% serum condition than in the 25% serum condition (91.15±15.53 vs 19.90±6.598, p=0.0011, n=14-15 from 3 patients, Dunn's multiple comparisons), and in the 12.5% serum condition compared with the 25% serum condition (63.23±13.66 vs 19.90±6.598, p=0.0489, n=15 from 3 patients, Dunn's multiple comparisons).

The percentage of Ki67+ cells at 14 DIV varied significantly (p=0.0477, n=13-15 from 3 patients, Kruskal-Wallis test). The percentage was significantly higher in the 0% serum condition than the 25% serum condition (1.818 ± 0.5265 vs 0.3983 ± 0.1599, p=0.0414, n=15 from 3 patients, **Figure 3-10C,** Dunn's multiple comparisons). There was no significant difference between the percentages of Ki67+ cells at 21 DIV (p=0.9939, n=12-14 from 3 patients, **Figure 3-10D,** Kruskal-Wallis test).

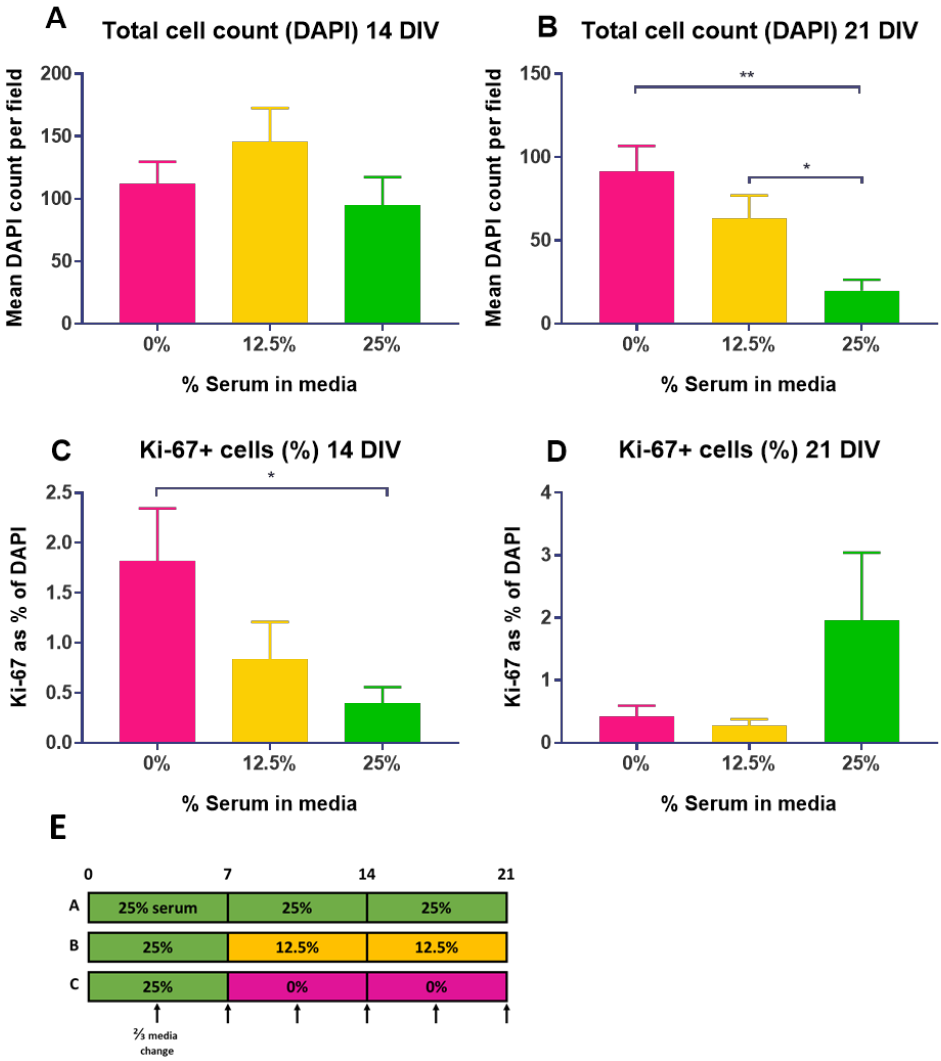

Figure 3-10: The effect of serum on cycling cells

*A-D: HiSpots® cultured in HSM then transferred to 0% (pink), 12.5% (orange) or kept in 25% (green). A: The total number of cells per field in HiSpots® cultured in different conditions at 14 DIV. Data are shown as mean ± SEM. n=13-15 from 3 patients. B: The total number of cells per field in HiSpots® cultured in different conditions at 21 DIV. Data are shown as mean ± SEM. n=14-15 from 3 patients. C: Ki-67+ cells as a percentage of total cells per field at 14 DIV. Data are shown as mean ± SEM. *p<0.05. n=15 from 3 patients. D: Ki-67+ cells as a percentage of total cells per field at 21 DIV. Data are shown as mean ± SEM. n=12-14 from 3 patients. E: Timeline of different conditions for HiSpot® culture.*

3.2.6.2 Transferring HiSpots® to serum free media supports triple-positive tumour cells

As well as overall survival, it is important to support the survival of different cell types within the HiSpot®. In particular, triple-positive tumour cells which are believed to propagate the HiSpot® must be supported for a successful model of GBM. Cells which co-expressed β-IIIT, GFAP and nestin (β-IIIT+GFAP+Nestin+) were clearly visible. These are believed to be triple-positive tumour cells. There were also a number of cells only positive for B-IIIT, and cells positive for GFAP and nestin but not β-IIIT. The majority of cells positive for any of the markers were positive for all three. Examples of these expression patterns are shown in **Figure 3-11B and C**.

After 7 DIV cultured in HSM (25%), some HiSpots® were fixed, and others were transferred to SFM (0%) at 7 DIV, or kept in HSM (25%). These HiSpots® were fixed at 14 DIV for cell type analysis and compared to the HiSpots® fixed at 7 DIV (**Figure 3-11D**). These groups contained significantly different percentages of β-IIIT+GFAP+Nestin+ cells ($p=0.0173$, n=10-15, Kruskal-Wallis test). At 14 DIV, the percentage of cells which were β-IIIT+GFAP+Nestin+ was significantly larger in HiSpots® switched to 0% serum than those kept at 25% serum (16.75 ± 4.905 vs 4.136 ± 1.499, $p=0.0153$, n=10-15, **Figure 3-11A,** Dunn's multiple comparisons).

Figure 3-11: Triple-positive tumour cells and the effect of serum on their survival

*A-E. All images show DAPI. Orange arrows demonstrate cells positive for β-III tubulin, GFAP and nestin. White arrows demonstrate cells only positive for β-III tubulin. Scale bars are shown. B: β-III tubulin staining. C: GFAP staining. D: Nestin staining. E: Overlay of β-III tubulin, GFAP and nestin staining. F: The percentages of cells positive for β-III tubulin, GFAP and nestin at 7 and 14 DIV, with or without serum removal. Serum was removed at 7 DIV, so only one bar is shown for 7 DIV (blue). At 14 DIV, cells with serum removed (0%) are shown in pink, and cells kept in serum (25%) are shown in green. Data analysed by one way ANOVA. *p<0.05. Data are shown as mean ± SEM. n=10-15.*

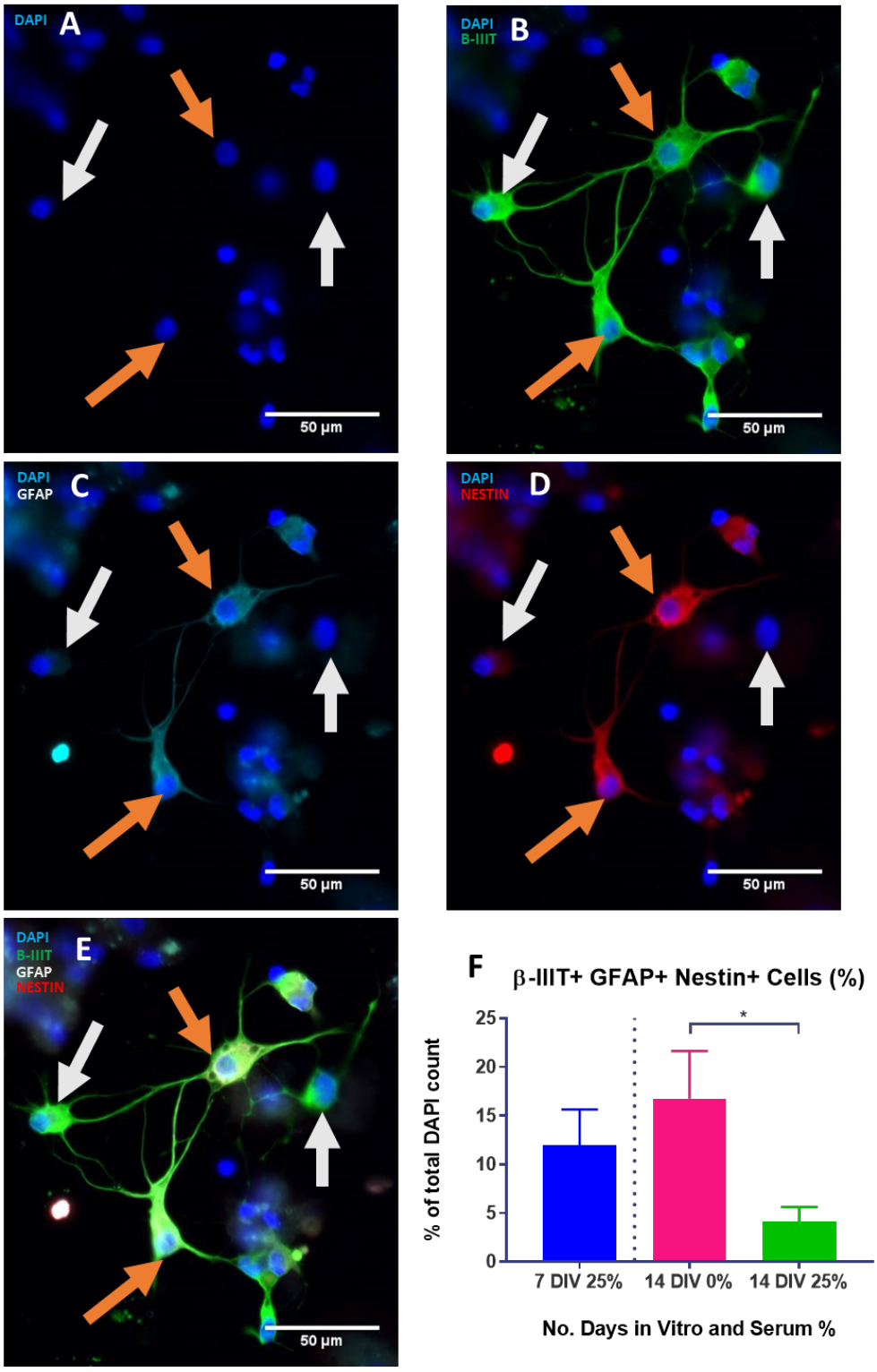
DAPI
A
50 µm
DAPI
B-IIIT
B
50 µm
DAPI
GFAP
C
50 µm
DAPI
NESTIN
D
50 µm
DAPI
B-IIIT
GFAP
NESTIN
E
50 µm
F
β-IIIT+ GFAP+ Nestin+ Cells (%)
% of total DAPI count
25
20
15
10
5
0
*
7 DIV 25%
14 DIV 0%
14 DIV 25%
No. Days in Vitro and Serum %

3.2.6.3 HiSpots® grown entirely without serum do not have a survival advantage

As HiSpots® had been shown to thrive with the removal of serum (3.2.6.2), it was considered that they may be able to survive without serum at all. The most successful culture method of the previous conditions, with HiSpots® grown in HSM (25% serum) for 7 DIV, then transferred to SFM until 14 DIV was compared to others. For the second method, HiSpots® were cultured in SFM (0% serum) for the entire 14 DIV. For the third method, HiSpots® were cultured in SFM (0% serum) with EGF and FGF2 for 14 DIV.

There was no significant difference in total cell count between the three conditions at 14 DIV ($p=0.3391$, n=14-15 from 3 patients, Kruskal-Wallis test, **Figure 3-12A**). There was no significant difference in the percentage of cells which were β-IIIT+GFAP+Nestin+ ($p=0.2646$, n=14-15 from 3 patients, **Figure 3-12B**); cells which were β-IIIT+ only ($p=0.1742$, n=14-15 from 3 patients, **Figure 3-12C**); or cells which were GFAP+Nestin+ ($p=0.6018$, n=14-15 from 3 patients, **Figure 3-12D**) according to the same test.

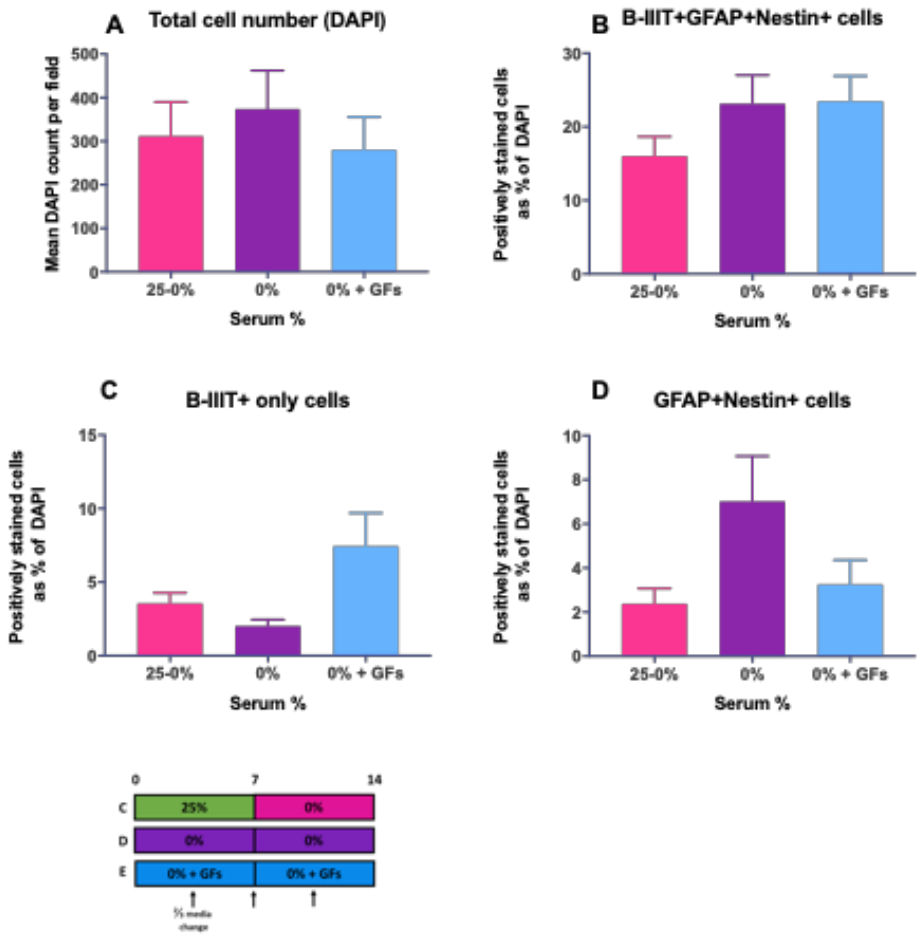

Figure 3-12: HiSpot® cell counts at 14 DIV.

A-D: HiSpots® were cultured in HSM switched to SFM (pink), SFM (purple), or SFM with growth factors (blue) for 14 DIV. A: Total cell count per field. Data shown are mean ± SEM. B: β-IIIT+ GFAP+ Nestin+ cells as a percentage of total DAPI count per field. Data shown are mean ± SEM. C: Cells positive for β-IIIT+ only as a percentage of total cell count per field. Data shown are mean ± SEM. D: GFAP+ Nestin+ cells as a percentage of total DAPI count per field. Data shown are mean ± SEM. E: Timeline of different culture conditions used. N=14-15 from 3 patients.

3.2.7 Increasing density to improve survival

3.2.7.1 Increasing HiSpot® density improves survival

Earlier results (**Figure 3-9E**) show a 50% drop in cell numbers per field within the first few days in culture. It was then hypothesised that creating HiSpots® with a higher initial cell density may compensate for this initial loss, and allow the HiSpots® to survive more reliably. The standard density ($5x10^7$ cells/ml), taken from previous HiSpot® research, was initially compared to a five-fold higher density ($2.5x10^8$ cells/ml). This was then in turn compared to a total of ten-fold higher density ($5x10^8$ cells/ml). All HiSpots® were cultured in HSM (25% serum) for 7 DIV, then transferred to SFM (0% serum) until 14 DIV. HiSpots® were fixed at 14 DIV and total cell numbers per field were counted. It was clear even with the naked eye that the $2.5x10^8$ cells/ml HiSpots® grew to be larger and more three-dimensional than their $5x10^7$ cells/ml counterparts, although it is important to note that there was still a large variability between HiSpots® created from different patients (**Figure 3-13A-D**). Further examples of the three-dimensional structure of these HiSpots® will be discussed later.

Cell count data from HiSpot images (per visual field obtained with a 20x objective lens were normalised to the number of cells present in $5x10^7$ cells/ml HiSpots® from the same patient. This was done by dividing the individual values by the mean value for the lower density repeats. This compensated for the variability in baseline HiSpot® cell numbers between the patients measured. Data were not normally distributed according to a Shapiro Wilk test. A 2.5 fold increase was seen between $5x10^7$ cells/ml and $2.5x10^8$ cells/ml HiSpots® at 14 DIV (1.000±0.04975 vs 2.491±0.3205, $p<0.0001$, n=9-10 from 2 patients, Mann Whitney test, **Figure 3-13E**).

Tile scans were created in the Leica microscope software by stitching multiple images taken using a 5x objective lens together into a single image. These were all taken with identical exposure settings so that DAPI intensity could be directly compared. HiSpots® were outlined in ImageJ, and the mean

intensity for each HiSpot® measured. The values represent the mean pixel intensity within the HiSpot® outline. These values were then multiplied by the size of the HiSpot® area (mm^2) to give a value for total area fluoresence to represent the relative number of cells in the HiSpots® (**2.9.1.3**). These data were then reported as the fold change from the mean of the lower density HiSpots® for each comparison. There were significantly more cells remaining at 14 DIV in the $2.5x10^8$ cells/ml vs $5x10^7$ cells/ml HiSpots® (0.9933 ± 0.08045 vs 14.65 ± 3.276, $p<0.0003$, n=15 from 3 patients, unpaired t-test, **Figure 3-13C**). There was no significant increase in cells remaining in the $5x10^8$ cells/ml HiSpots® compared to the $2.5x10^8$ cells/ml HiSpots® (1.009 ± 0.04951 vs 0.9398 ± 0.2602, p=0.5116, n=10-11 from 2 patients, Mann Whitney test, **Figure 3-13D**).

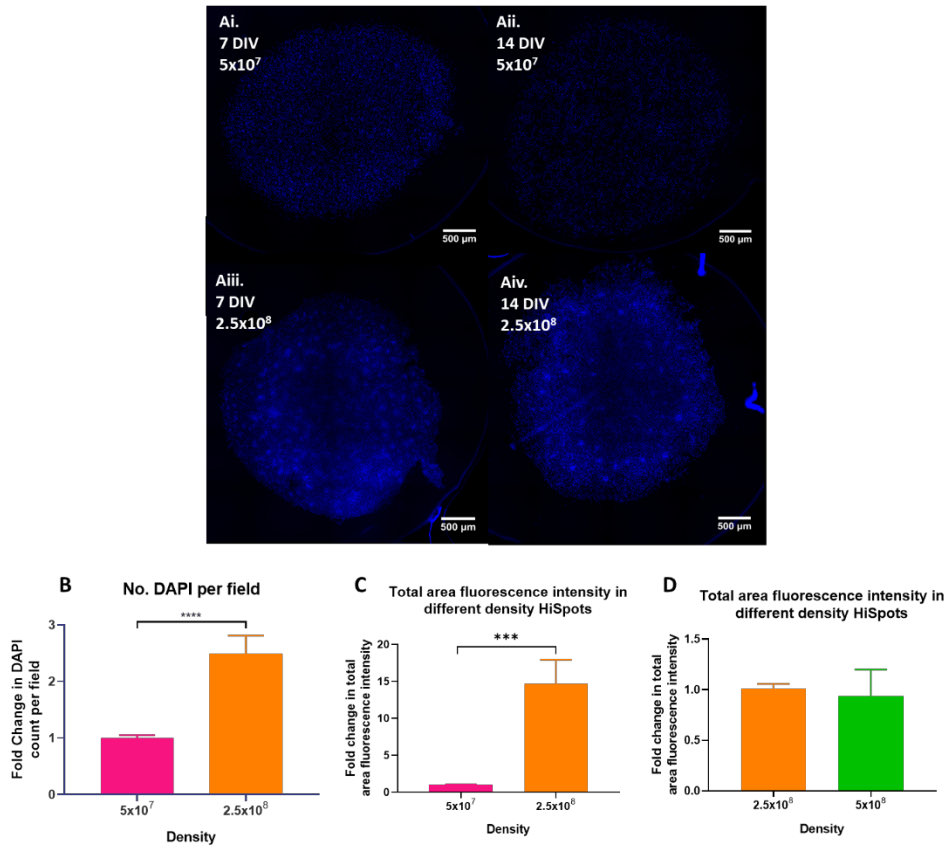

Figure 3-13: Increased density of HiSpots®.

A: Immunofluorescence images of whole HiSpots® stained with DAPI. Scale bars shown for reference. Ai. A 5x10^7 cells/ml HiSpot® cultured for 7 DIV. Aii. A 5x10^7 cells/ml HiSpot® cultured for 14 DIV. Aiii. A 2.5x10^8 cells/ml HiSpot® cultured for 7 DIV. Aiv. A 2.5x10^8 HiSpot® cultured for 14 DIV.

*B: Fold change in total DAPI count per field at 14DIV between 5x10^7 and 2.5x10^8 cells/ml HiSpots®. Data shown are mean ± SEM. n=9-10 from 2 patients. ****p<0.0001. C: Fold change in total area fluorescence intensity per HiSpot® between 5x10^7 and 2.5x10^8 cells/ml HiSpots®. Data shown are mean ± SEM. n=15 from 3 patients. ***p<0.001. D: Fold change in total area fluorescence intensity per HiSpot® between 2.5x10^8 and 5x10^8 cells/ml HiSpots®. Data shown are mean ± SEM. n=10-11 from 2 patients.*

3.2.7.2 Increasing HiSpot® density does not affect the survival of microglia, but does change the survival of B-IIIT+ and triple-positive cells

It is important to characterise the effects of a change in culture condition on the key cell types present. The proportions of cells in HiSpots® were compared between $5x10^7$ cells/ml and $2.5x10^8$ cells/ml HiSpots®. All HiSpots® were cultured in HSM (25% serum) for 7 DIV, then transferred to SFM (0% serum) until 14 DIV. HiSpots® were fixed at 14 DIV and total cell numbers per field taken with a 20x objective lens were counted.

There was no difference between the percentage of IBA1+ cells between the two conditions (17.78 ± 2.419 vs 20.84 ± 1.243, p=0.2770, n=9 from 2 patients, unpaired t-test). The percentage of cells positive for β-IIIT only decreased between $5x10^7$ cells/ml and $2.5x10^8$ cells/ml HiSpots® (5.278 ± 0.5956 vs 2.100 ± 0.3630, p=0.0002, n=9-10 from 2 patients, unpaired t-test) and the percentage of β-IIIT+GFAP+Nestin+ cells increased significantly (3.351 ± 1.097 vs 16.02 ± 3.549, p=0.0076, n=9-10 from 2 patients, Mann-Whitney test).

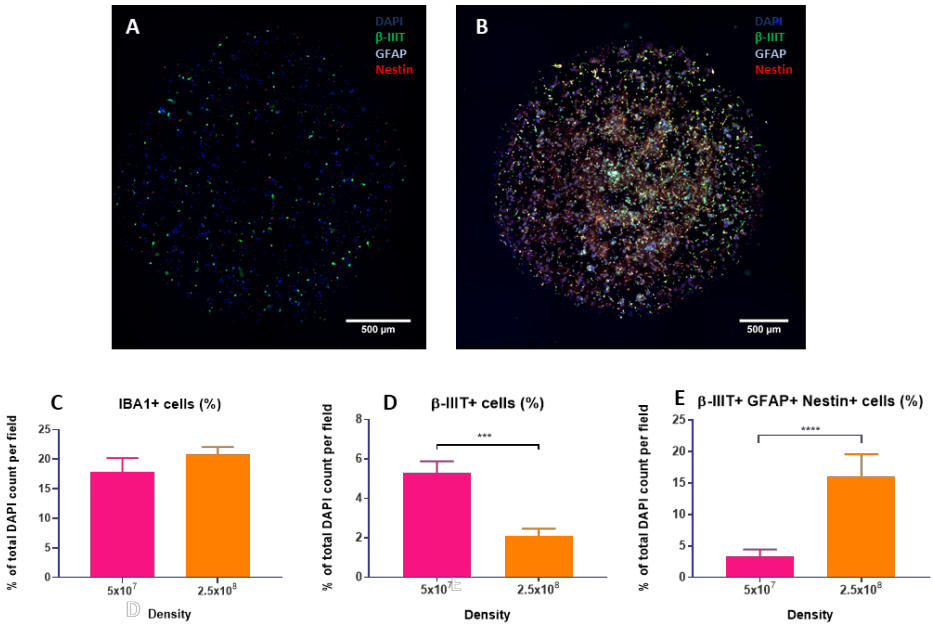

Figure 3-14: Percentages of cell types in 5x10^7 and 2.5x10^8 cells/ml HiSpots®.

A/B: Immunofluorescence images of whole HiSpots® stained with DAPI and antibodies for β-IIIT, GFAP and nestin. Scale bars are shown for reference. A: 5x10^7 cells/ml HiSpot® tile scan image. B: 2.5x10^8 cells/ml HiSpot® tile scan image.

*C: IBA1+ cells as a percentage of total cell count per field. Data shown are mean ± SEM. D: β-IIIT+ cells as a percentage of total cell count per field. Data shown are mean ± SEM. ***p<0.001. E: β-IIIT+ GFAP+ nestin+ cells as a percentage of total DAPI count per field. Data shown are mean ± SEM. ****p<0.0001. n=9-10 from 2 patients.*

3.2.7.3 Increasing HiSpot® density allows the formation of multi-layered structures

Using a confocal microscope, it is possible to visualise multiple distinct layers of cells within a HiSpot®, confirming the 3D structure. Images shown in **Figure 3-15** were taken with a 40x objective lens and show five slices out of a total 19. The interval between z-planes was 2.08µm. The images demonstrate that there are multiple cell layers within the HiSpot®, and that cell types vary in distribution throughout the 3D structure. The images show areas of higher cell density, mostly positive for GFAP and β-IIIT, from which some β-IIIT+GFAP+ cells extend, surrounded by cells positive for IBA1.

Figure 3-15: Confocal image Z-slices.

Immunofluorescence images from a HiSpot® from sample GBM28, cultured in SFM for 14 DIV. Z stack slices taken at an interval of 2.08µm. Slices shown in this figure are 6.24µm apart. Scale bars are shown for reference in the bottom right. Slice distance from the base of the z-stack is shown in the top right. The diagram on the left indicates the total slices taken. Green slices represent the immunofluorescence images shown

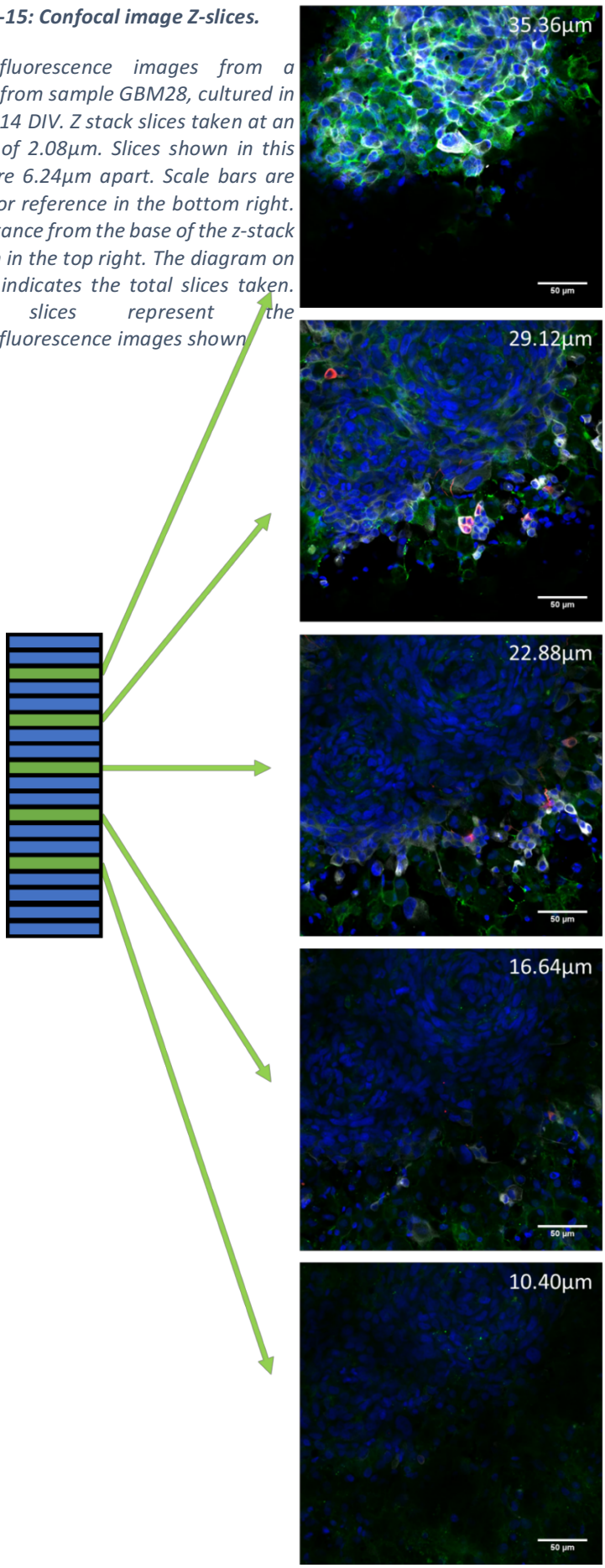

3.2.8 Confirming ideal conditions for high density HiSpots®

3.2.8.1 There is no advantage in returning HiSpots® to serum after removal

After altering the HiSpot® culture density from $5x10^7$ cells/ml to $2.5x10^8$ cells/ml, it was important to re-establish whether serum was disadvantageous for cell survival in the new, higher density HiSpots®. Earlier experiments indicated an advantage to removing serum from the culture media. A further experiment was designed to determine if there was an additional advantage to returning some or all of the serum at a later timepoint. $2.5x10^8$ cells/ml HiSpots® were cultured in HSM for 4 DIV, after which they were moved to SFM for a further 7 DIV. At 10 DIV, HiSpots were kept in SFM (0%), returned to HSM with 5% HS but no FBS (5%), returned to HSM with 20% FBS but no HS (20%), or returned to full HSM (25%).

DAPI count data were normally distributed. There was no difference in total cell count at 14 DIV between the four conditions according to a one-way ANOVA (922.8 ± 49.60 vs 896.5 ± 83.13 vs 850.9 ± 37.62 vs 978.2 ± 65.14, $F(3, 32) = 0.7991$, $p=0.5035$, n=8-10 from 2 patients).

Cell type data were not normally distributed so were compared via Kruskal-Wallis test. The percentage of β-IIIT+GFAP+ cells did not significantly differ between the conditions (13.97 ± 4.412 vs 10.44 ± 3.704 vs 10.81 ± 4.027 vs 9.932 ± 4.191, $p=0.7603$, n=8-10 from 2 patients). The percentage of β-IIIT+ only cells also did not differ between the conditions (8.093 ± 2.590 vs 9.042 ± 2.833 vs 6.599 ± 1.915 vs 10.44 ± 2.796, $p=0.5028$, n=8-10 from 2 patients).

It was noted that there was a large variability between HiSpots® from the two patients used for this and the further experiments in their expression of GFAP. Immunofluorescence images from these HiSpots® can be seen in **Figure 3-16** E and F.

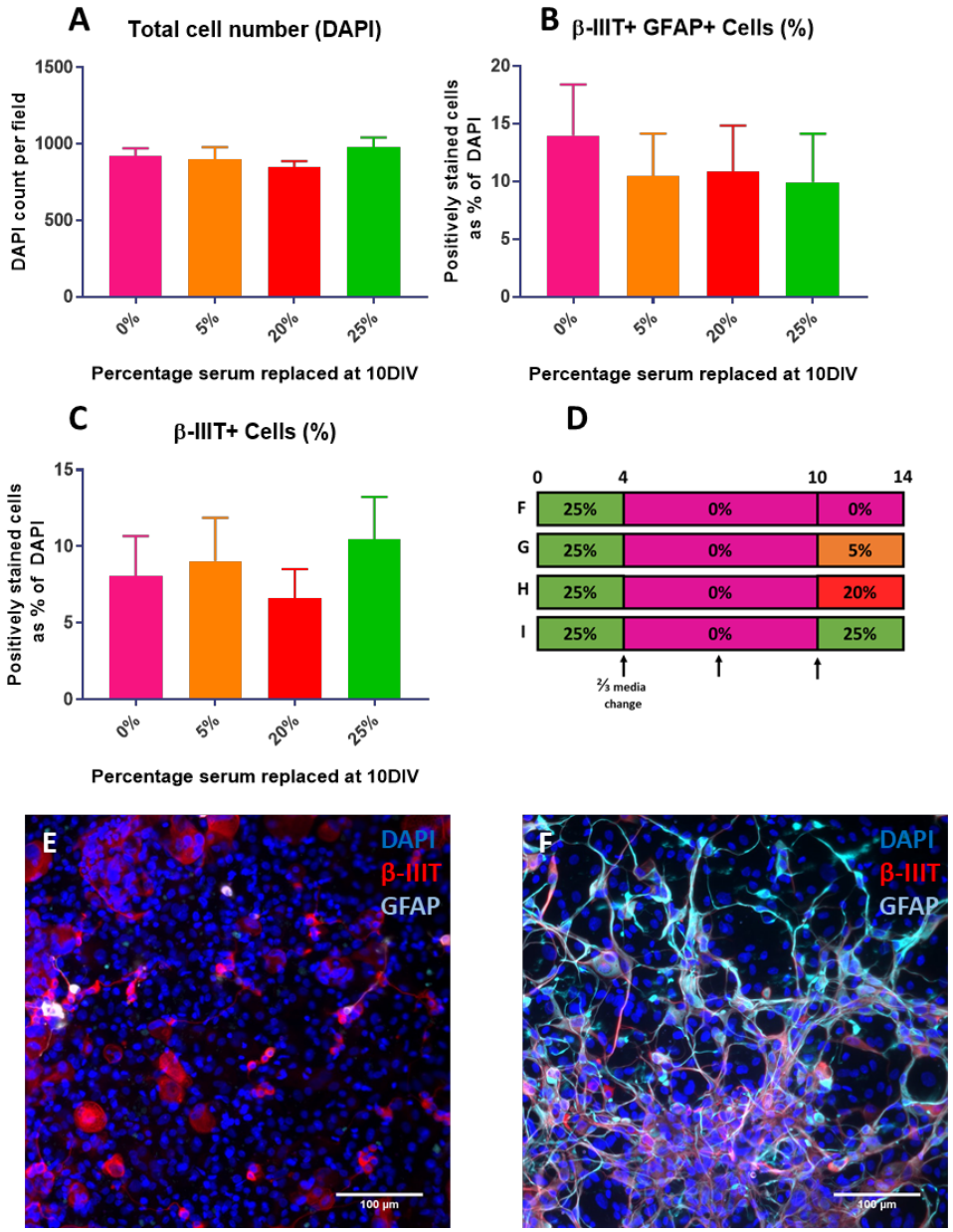

Figure 3-16: HiSpots® returned to different levels of serum in cell culture media after absence.

*A: Total number of cells present per field at 14 DIV in HiSpots®. B: Timeline of different culture conditions for HiSpots®. C: β-IIIT+ only cells as a percentage of DAPI count per field, by GBM sample number. *p<0.05, **p<0.01. D: β-IIIT+ GFAP+ cells as a percentage of total DAPI count per field, by GBM sample.*

E/F: Immunofluorescence images of HiSpots® cultured in HSM (25%) for 4 DIV and SFM (0%) until 14 DIV. Scale bars are shown for reference. HiSpots® were stained for DAPI (blue), β-IIIT (red), and GFAP (turquoise). E: Image from sample GBM28. F: Image from sample GBM34.

3.2.8.2 Total cell count in 2.5x10^8 cells/ml and 5x10^8 cells/ml HiSpots® is unaffected by the presence of serum

Previous experiments established 7 DIV in HSM followed by a switch to SFM until 14 DIV as the best culture condition for the 5x10^7 cells/ml HiSpots®. It was therefore important to establish whether the higher density (2.5x10^8 and 5x10^8 cells/ml) HiSpots® would respond in the same way. The original protocol (25% serum) was compared to the previous optimisation (25-0%) and SFM (0%). No growth factors were used. All HiSpots® were fixed at 14 DIV for analysis. Images were taken using the upright microscope as standard, but in order to clarify the results of culturing 2.5x10^8 cells/ml HiSpots® in SFM, randomly selected HiSpots® from each condition were re-imaged using a confocal microscope. Z-stack images were combined into maximum intensity projections, from which cell count data were calculated.

Total cell count data were not normally distributed so were compared by Kruskal-Wallis tests. DAPI counts were not significantly different in 2.5x10^8 cells/ml HiSpots® in images taken using an upright microscope (899.6 ± 101.5 vs 1024 ± 25.53 vs 854.5 ± 113.4, $p<0.8036$, n=9 from 2 patients, **Figure 3-17A**) or the confocal microscope (1177 ±189.5 vs 1468 ± 67.95 vs 1027 ± 226.6, p=0.4838, n=6 from 2 patients, **Figure 3-17C**). There were also no significant differences between the total cell counts in each group in 5x10^8 cells/ml HiSpots® in images taken using the upright microscope (947.3 ± 105.3 vs 1141 ± 61.52 vs 890.6 ± 159.2, p=0.6335, n=8-10 from 2 patients, **Figure 3-17B**).

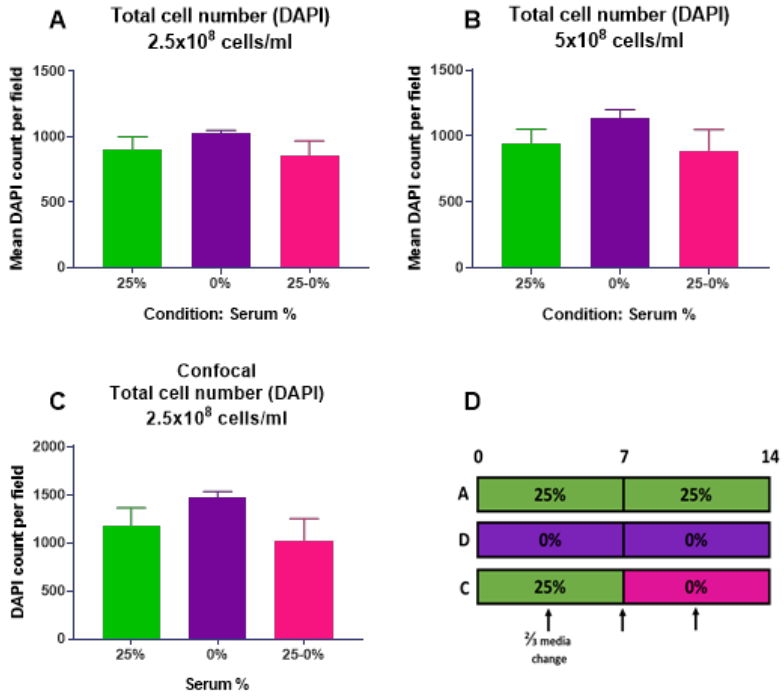

Figure 3-17: Total cell count in HiSpots®

A-C: Total DAPI count per field for each media serum level. A: Total DAPI count per field for 2.5x10^8 cells/ml HiSpots® imaged using the upright microscope. N=9 from 2 patients. B: Total DAPI count per field for 5x10^7 cells/ml HiSpots® imaged using the upright microscope. N=8-10 from 2 patients. C: Total DAPI count per field for 2.5x10^8 cells/ml HiSpots® imaged using the confocal microscope. N=6 from 2 patients. D: Timeline of different media conditions for HiSpots®.

3.2.8.3 β-IIIT+GFAP+ cells and β-IIIT+ cells are not affected by the presence of serum

Previous experiments established 7 DIV in HSM followed by a switch to SFM until 14 DIV as the best culture condition for the $5x10^7$ cells/ml HiSpots®. It was therefore important to establish whether the higher density ($2.5x10^8$ and $5x10^8$ cells/ml) HiSpots® would respond in the same way. The original protocol (25% serum) was compared to the previous optimisation (25-0%) and SFM (0%). All HiSpots® were fixed at 14 DIV for analysis. Images were taken using the upright microscope as standard, but in order to clarify the results of culturing $2.5x10^8$ cells/ml HiSpots® in SFM, randomly selected HiSpots® from each condition were re-imaged using a confocal microscope. Z-stack images were combined into maximum intensity projections, from which cell count data were calculated.

Cell count data were not normally distributed so were compared by Kruskal-Wallis tests. There were no significant differences between the number of β-IIIT+GFAP+ cells in each condition in the $2.5x10^8$ cells/ml HiSpots® when quantified from images taken using:

- An upright microscope (*11.02 ± 4.158 vs 16.48 ± 6.358 vs 14.17 ± 5.483, p=0.8208, n=9 from 2 patients)*
- A confocal microscope *(13.97 ± 6.031 vs 26.86 ± 11.65 vs 12.72 ± 5.723, p=0.6522, n=6 from 2 patients)*

There were also no significant differences between the groups in $5x10^8$ cells/ml HiSpots® (14.90 ± 5.143 vs 16.66 ± 6.242 vs 14.69 ± 4.648, p=0.9881, n=8-10 from 2 patients). The data perhaps show a slight trend towards a higher percentage of β-IIIT+GFAP+ cells being present in the HiSpots® cultured in 0% serum.

There were no significant differences in the number of β-IIIT+ only cells in:

- 2.5x10^8 cells/ml HiSpots® *(9.896 ± 3.108 vs 8.578 ± 2.708 vs 14.65 ± 4.448, p=0.1836, n=9 from 2 patients)*
- 5x10^8 cells/ml HiSpots® (*16.39 ± 5.681 vs 10.74 ± 3.430 vs 11.33 ± 3.568, p=0.2964, n=8-10 from 2 patients)*

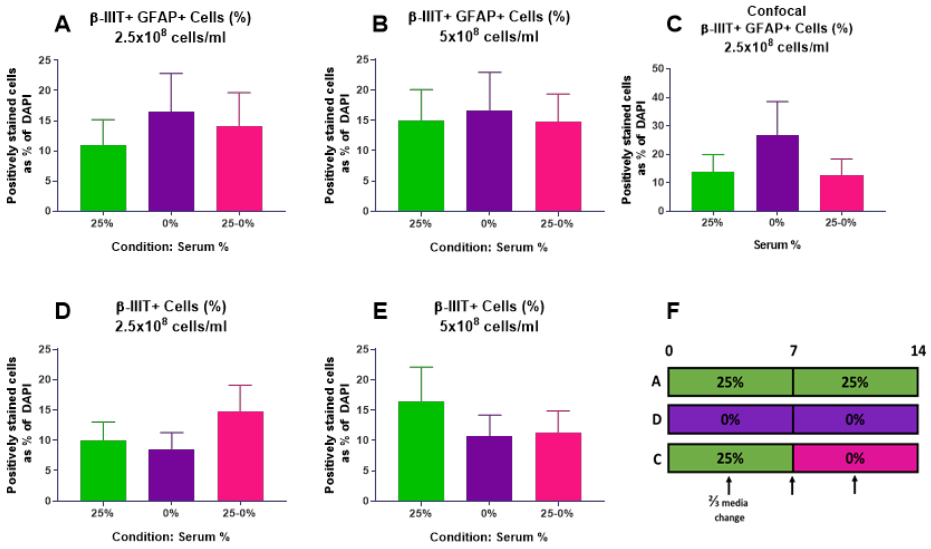

Figure 3-18: Cell type percentages in higher density HiSpots®

A-E: Percentage of positive cells per field. F: Timeline of different media conditions for HiSpots®. A: Percentage of β-IIIT+GFAP+ cells per field for 2.5x10^8 cells/ml HiSpots® imaged using the upright microscope. N=9 from 2 patients. B: Percentage of β-IIIT+GFAP+ cells per field for 5x10^8 cells/ml HiSpots® imaged using the upright microscope. N=8-10 from 2 patients. C: Percentage of β-IIIT+GFAP+ cells per field for 2.5x10^8 cells/ml HiSpots® imaged using the confocal microscope. N=6 from 2 patients. D: Percentage of β-IIIT+ cells per field for 2.5x10^8 cells/ml HiSpots® imaged using the upright microscope. N=9 from 2 patients. E: Percentage of β-IIIT+ cells per field for 5x10^8 cells/ml HiSpots® imaged using the upright microscope. N=8-10 from 2 patients.

3.2.8.4 IBA1+ cells are not affected by the presence of serum

Previous experiments established 7 DIV in HSM followed by a switch to SFM until 14 DIV as the best culture condition for the $5x10^7$ cells/ml HiSpots®. It was therefore important to establish whether the higher density ($2.5x10^8$ and $5x10^8$ cells/ml) HiSpots® would respond in the same way. The original protocol (25% serum) was compared to the previous optimisation (25-0%) and SFM (0%). All HiSpots® were fixed at 14 DIV for analysis. Randomly selected HiSpots® from each condition were imaged using a confocal microscope. Z-stack images were combined into maximum intensity projections, from which cell count data were calculated. It was not possible to get a total DAPI count per field for HiSpots® from patient GBM30, so instead the raw counts of IBA1+ cells per field were used, as the IBA1+ cells were easy to distinguish (**Figure 3-19D/E**).

The percentage data for IBA1+ cells were normally distributed, so were analysed by one-way ANOVA. There was a significant difference between values (11.87 ± 1.219 vs 10.36 ± 2.267 vs 21.71 ± 4.892, $F(2, 15) = 3.372$, $p=0.0484$, n=6 from 2 patients), however this did not result in any significant differences by multiple comparisons (Bonferroni's test). There is a clear trend towards a higher IBA1+ percentage in the 25-0% HiSpots®. A Shapiro-Wilk test could not determine distribution normality for the 25% group for the raw IBA1+ counts due to two identical readings, so a non-parametric test was applied. Again there was a significant difference between the groups (5.333 ± 0.6667 vs 36.00 ± 7.810 vs 7.000 ± 3.215, $p=0.0464$, n=3 from 1 patient) but differences were not significant according to multiple comparisons (Dunn's test). There is a clear trend towards a higher IBA1+ percentage in the 0% HiSpots®.

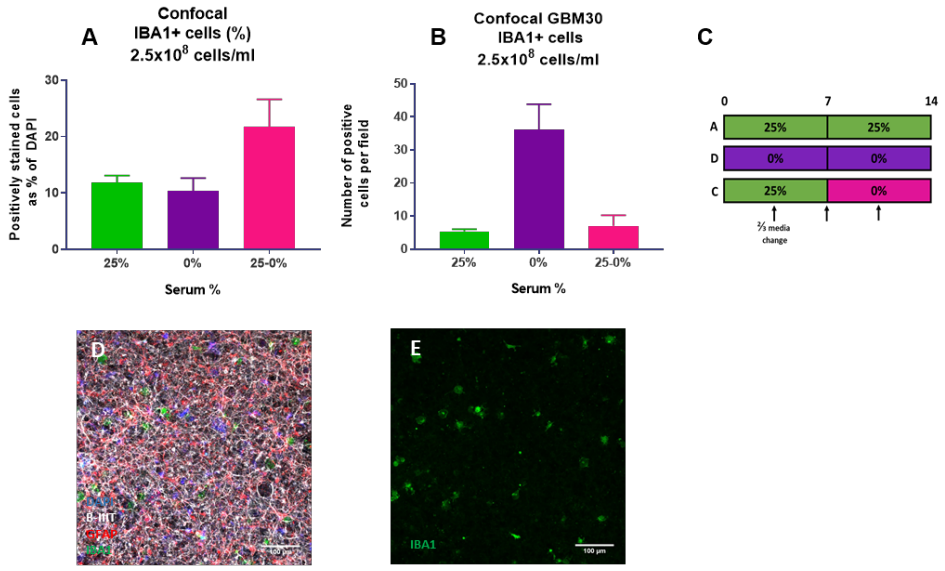

Figure 3-19: IBA1+ cells in 2.5x10^8 cells/ml HiSpots®

A: Percentage of IBA1+ cells per field for 2.5x10^8 cells/ml HiSpots® imaged using the confocal microscope. N=6 from 2 patients. B: Raw counts of IBA1+ cells per field for 2.5x10^8 cells/ml HiSpots® imaged using the confocal microscope. N=3 from 1 patient. C: Timeline of different media conditions for HiSpots®. D/E: Immunofluorescence images of GBM30 HiSpots® cultured in SFM (0%) until 14 DIV. Scale bars are shown for reference. HiSpots® were stained for DAPI (blue), β-IIIT (white), GFAP (red) and IBA1 (green). D: Shows all channels. E: Shows just IBA1 staining.

3.3 Discussion

3.3.1 Primary GBM cells can be grown using the HiSpot® system

3.3.1.1 Need for optimisation

Preliminary experimental work had highlighted the potential of the HiSpot® as a model for GBM (Biggs *et al.* 2011; Rymer 2011). Therefore, the first 10 or so patient samples were intended for establishing technique and expertise for the HiSpots®. Some early patient tissue failed to establish cultures, and the author believes that this may have been explained by insufficient cell density, poor quality tissue (damaged by necrosis or radiotherapy), or human error. The success rate of cultures improved over time with the optimisations discussed below. As previous experiments had relied on serum-based media, the decision was made to begin optimisations with media constituents. However, even with these early optimisations, the HiSpots® were not growing to multi-layered structures. This then triggered the density-based optimisation experiments. After these were complete, it was important to confirm whether serum was still required for the culture of GBM HiSpots® to survive, given the disadvantages of using serum for primary GBM cell culture.

3.3.1.2 Survival and cell death

These initial experiments used HiSpots® created at $5x10^7$ cells/ml. The results shown in **3.2.1.1** showed low levels of staining for cleaved caspase-3 (<5%) in HiSpots® at 7 DIV and 14 DIV, confirming low baseline levels of apoptosis. To more rigorously investigate the health of the HiSpots®, it was also important to look at the levels of necrosis in the HiSpots®. Attempts were made to record this using propidium iodide, a commonly used indicator of necrotic cell death within live cultures. However, the HiSpots® require mounting on microscope slides in order to be imaged, and this made it impractical to apply PI to a large number of HiSpots® for a set time before imaging. The microscope camera available for live imaging could only provide low resolution images, which also made it difficult to image PI

stained HiSpots® accurately. It was therefore decided that this was not a suitable tool for the HiSpots®. Instead, the decision was made to use an LDH assay. LDH is released when cells die via necrosis, and the levels of this enzyme can be measured in the culture media. Despite attempts at optimisation, the results from the LDH assay varied greatly between HiSpots® from different patients, and did not always match with the visible culture survival under the microscope (**Figure 3-2A, B**). A comparative control was created for the LDH assay, using the included lysis buffer from the LDH assay kit. Media taken from HiSpots® treated with lysis buffer were recorded as having less LDH release than untreated HiSpots®. Confusingly, this would indicate that there was somehow less cell death in the lysed HiSpots® (**Figure 3-2C**). A more detailed look at the related literature found that even a 10% level of serum in culture media can interfere with the readout from the LDH assay, which, given the 25% serum in the HiSpot® HSM, could explain the contradictory results seen above (Hiebl *et al.* 2017). The assay was also designed for cells cultured as a monolayer, allowing an ideal density to be established. Due to the three-dimensional nature of the HiSpots® it was not possible to use the assay in this manner. It is therefore possible that the high cell density of the HiSpots® compared to the volume of media created a large amount of noise, which made it difficult for the assay to accurately detect any changes in LDH levels, and therefore necrosis. For these reasons, the LDH assay was considered not appropriate for future HiSpot® analysis, and its use was discontinued. The total DAPI count was used to analyse culture health in the HiSpots® for comparison between conditions and timepoints.

3.3.2 Cell types in HiSpots®

3.3.2.1 Microglia

Microglia are a key cell type in GBM, providing up to 50% of the tumour mass, and are often not represented in 2D *in vitro* models of the disease. Established cell lines will, intentionally or not, select for certain other cell types, meaning that the impact of microglia is excluded. However, microglia

are especially important for screening drugs and cellular responses, as they have been shown to have a protective effect on tumour cells, reducing their sensitivity to treatment. Therefore, it is important to have models which include microglia, in order to help avoid taking falsely positive drug candidates forward into animal and human testing.

The microglia shown in **Figure 3-3** show an amoeboid (activated) morphology, demonstrated by the large, relatively round structure with minimal projections. In comparison, ramified (inactive/resting) microglia have a smaller body, with many long processes extending from it (see **Figure 3-20**). Amoeboid microglia are typically associated with a diseased state, whereas a healthy brain would contain more ramified microglia (Hambardzumyan *et al.* 2016). The interactions between microglia and tumour cells are complex. As discussed in the introduction (**1.1.4.2**) tumour cells have been demonstrated to recruit microglia (along with macrophages from nearby vessels) to the tumour, where they are used to further support tumour growth and invasion. Therefore microglia were considered a key cell type to be represented and supported in GBM HiSpots®. In **3.2.2.1**, HiSpots® were demonstrated to contain 10-30% microglia, which are of the amoeboid (tumour-associated) phenotype (**Figure 3-3**).

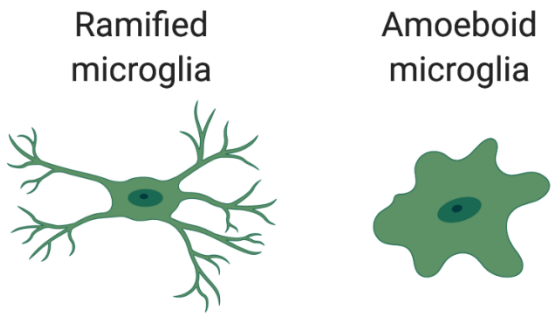

Figure 3-20: Structural differences between ramified and amoeboid microglia.

A simple representation of the differences in structure between ramified and amoeboid microglia. Figure created using biorender.com.

3.3.2.2 Triple-positive tumour cells

Cells co-expressing β-IIIT, GFAP and nestin were demonstrated by Rieske *et al.* (2007), among others. The authors showed that β-IIIT, GFAP and nestin are co-expressed in self-renewing cells which can give rise to either neuronal or glial cells. The cells they used were extracted from foetal human brains. In this study, these β-IIIT+GFAP+Nestin+ tumour cells have been treated as the key cell type along with microglia to be represented within the HiSpots®. It is believed that these cells represent a key population of the tumour cells due to their co-expression of markers which are not co-expressed in healthy brain tissue. For optimisations, these cells are considered representative of the health of the HiSpot®, and maintenance of this cell population is considered the desirable outcome, as long as the HiSpots® do not lose the other key cell type, microglia. Galli *et al.* (2004) have also highlighted these cells and believe them to be the tumour's neural stem cell equivalent, capable of creating tumours as xenografts, and recapitulating general and patient-specific features. This supports the decision to establish and support this cell population within the HiSpots®.

Over the course of the experiments in this chapter, many tumour cells were found to co-express β-IIIT, GFAP and nestin (**Figure 3-4**). These are referred to throughout as triple-positive tumour cells. These cells made up ~ 15% of the lower density ($5x10^7$ cells/ml) HiSpots®, and ~ 35% in the higher density ($2.5x10^8$ cells/ml) HiSpots® (**Figure 3-14E**)**.** In the $5x10^7$ cells/ml HiSpots®, there were a noticeable number of cells only positive for β-IIIT, but co-staining analysis found that the overlap of GFAP and nestin staining was almost 100%, so it was considered wasteful to use both antibodies for further experiments. However, this co-staining of GFAP and nestin was not exhaustively demonstrated. It is possible that there was bleed-through of signal (where a bright signal in one channel is detectable in another). Further confirmatory staining and confocal imaging would be useful to be absolutely certain of GFAP and nestin co-staining. As only three channels (in addition to DAPI) can be used at one time, it was decided that nestin would be

replaced with IBA1 for the standard triple stain going forward to allow investigation of the interactions between microglia and triple-positive tumour cells.

The experiments in this chapter also highlight the enormous heterogeneity between GBM patients. As demonstrated, the expression of various markers can vary greatly between HiSpots® from different patients. For example, GBM28 had minimal GFAP staining (**Figure 3-16E**), with only a few GFAP+ cells per field, whereas in HiSpots® from many other patients (e.g. GBM34 (**Figure 3-16F**), GBM27) there were very few β-IIIT+ cells which weren't also positive for GFAP. The distribution of these cell types within the respective HiSpots® seems to indicate that they are representing the same cellular population, but that in GBM28 the expression of GFAP had been almost entirely lost due to accumulated mutations in the individual tumour.

3.3.2.3 The IDH-1 R132H mutation is detectable in HiSpots® from secondary GBM

The *IDH-1* R132H mutation can provide a useful marker for identifying all tumour-derived cells in order to then investigate other properties of the cells. *IDH-1* R132H staining is predominantly used for histological analysis and confirmed using genetic analysis. It is however very rare for an *IDH-1* R132H antibody to be used for immunofluorescent staining (Abiria *et al.* 2014; Sabit *et al.* 2014). As it is only present in secondary GBMs, it was not possible to use it for all GBM patients. The DIANOVA antibody was selected as it has successfully been used for immunofluorescent staining by Abiria *et al.* (2014) previously at 1:20 and 1:100 dilutions. In secondary GBMs, the *IDH-1* R132H should successfully stain almost all of the tumour cells. All *IDH-1* R132H staining was performed in HiSpots® created at $2.5x10^8$ cells/ml.

Fortunately, one patient (GBM41) was diagnosed as a GBM with the IDH-1 R132H mutation and provided sufficient tissue for antibody optimisation (**Figure 2-6**). This confirmed the presence of *IDH-1* R132H+ cells in the HiSpots® at 14DIV. With comparison to a negative control, it was possible to

confirm the selectivity of the *IDH-1* R132H antibody, and the dilution ratio of 1:100. This positive staining confirms that the HiSpots® have maintained this definitively tumour-derived cell population. Immunofluorescence was considered a simpler solution than attempting to develop a protocol for histological staining for the HiSpots®. Antibody optimisation was also attempted on remaining HiSpots® from other patients with the *IDH-1* R132H mutation (GBM43, 38) but was not successful. This may have been a result of the different diagnoses for these patients (see **Table 4-1**), or merely a failure of the antibody to sufficiently detect mutated cells. GBM38 had a highly calcified appearance, which may also have affected the antibody function (data not shown). This variability demonstrates the importance of *IDH-1* status being confirmed by genetic analysis, which is a more reliable indicator of the tumour status than immunohistochemistry alone.

3.3.2.4 IDH-1 R132H positive cells also express GFAP

The GFAP+β-IIIT+ cell population was used in most experiments as a representation of tumour cells in the HiSpots® as these markers would not be co-expressed on healthy adult brain cells. However, the only definitive marker of GBM cells is for them to contain a mutation limited to tumour cells. Therefore, the decision was made to co-stain remaining GBM41 HiSpots® for *IDH-1* R132H, GFAP and β-IIIT. Unfortunately, the limited availability of patients with the *IDH-1* R132H mutation meant this staining was only performed on HiSpots® from one patient sample. The staining successfully demonstrated the co-expression of *IDH-1* R132H and GFAP on tumour cells (**Figure 3-5A-F**). Strangely, β-IIIT was not co-expressed with either marker, but formed an independent network. This could indicate a different expression pattern of secondary GBMs for β-IIIT, or a particular quirk of the cells from this patient. However, with only one patient it is not possible to confirm either theory. Quantification of the *IDH-1* R132H and GFAP staining confirmed that all *IDH-1* R132H+ cells also expressed GFAP, and there was a small population of GFAP+ cells which were negative for *IDH-1* R132H (**Figure 3-5H**). This may represent a small population of non-

tumour derived astrocytes, which are known to be present within the GBM microenvironment (Charles *et al.* 2012; Henrik Heiland *et al.* 2019). Although it is difficult to draw definite conclusions from only one patient, this staining supports the use of GFAP as a marker for all tumour cells, but indicates that it may also pick up a few non-tumour astrocytes. In most HiSpots® where GFAP is mostly co-expressed with β-IIIT, the β-IIIT positivity should be serving the same role of separating out tumour-derived cells from tumour-associated astrocytes. In further work it would be beneficial to identify and isolate patients with the *IDH-1* R132H mutation for further investigations into the best tumour cell markers. It would be especially advantageous to have an alternative marker available for GSM patients, this would be a rare case as *IDH-1* mutants and GSMs are both relatively rare within GBM (Cachia *et al.* 2015).

3.3.2.5 GFAP+ β-IIIT+ cells also co-express stem cell marker SOX2

SOX2 is a commonly used stem cell marker which has been demonstrated to be highly overexpressed in GBM. It is a key transcription factor for maintaining the invasive and migratory properties of the tumour, and is also being investigated as a potential therapeutic target. SOX2 is also one of the markers used to identify CSCs in GBM (Garros-Regulez *et al.* 2016; Garnier *et al.* 2019). These features demonstrate the importance of identifying SOX2+ cells in the GBM HiSpots®. Immunofluorescent staining confirmed both the presence of SOX2+ cancer stem cells, and that these are the GFAP+β-IIIT+ cells discussed above. In the HiSpots® stained (from patients GBM45, 49), SOX2+ cells provided approximately 77% of the total cell population (**Figure 3-6L**). 98% of GFAP+β-IIIT+ cells were also SOX2+ (**Figure 3-6M**). It is therefore possible to extrapolate that the GFAP+β-IIIT+ cells are representative of the CSC population. Given the rising interest in targeting CSCs for GBM, rather than a differentiated population, this highlights a role for the HiSpot® model in GBM therapeutic research going forward. It is important to note that this and the *IDH-1* R132H staining were both performed in HiSpots® created at $2.5x10^8$ cells/ml.

3.3.2.6 Single-positive tumour cells

In the $5x10^7$ cells/ml HiSpots®, up to 10% of the cells were positive for β-IIIT only. It is possible that these cells were originally present in the tumour tissue and have been recapitulated in the HiSpots®. Alternatively, these cells may be derived from the triple-positive tumour cells discussed above, after HiSpot® creation. Ideally, the numbers of these cells would remain low, and the HiSpots® would instead maintain the triple-positive tumour cell population.

3.3.2.7 Astrocyte-like cells

The $5x10^7$ cells/ml HiSpots® also contained approximately 5% cells positive for GFAP and nestin but not β-IIIT (**Figure 3-4F**). It is possible that, as above, these are derived from triple-positive tumour cells which have lost their β-IIIT expression either in the tumour or since HiSpot® creation. There is also a possibility that these cells represent non-tumour astrocytes which were embedded in the tumour bulk. Given that there were a small number of GFAP+ *IDH-1* R132H- cells, it is likely that these represent a population of non-tumour astrocytes.

3.3.2.8 Endothelial cells

Endothelial cells are an important part of the GBM microenvironment (**1.1.4.3**). An antibody for the endothelial cell marker CD31 was tested on HiSpots® (post-optimisation steps), but no significant positivity was found (**Figure 3-7**). No positive control for endothelial cells was available, so no further staining or characterisation was completed. It is assumed that HiSpots® do not support a population of endothelial cells using the protocol developed in this study.

3.3.2.9 Changes in cell types over time

HiSpots® demonstrated a large drop in cell number between 7 DIV and 21 DIV in $5x10^7$ cells/ml HiSpots®, but with no significant change in β-IIIT or GFAP percentages (**Figure 3-8**). There was a trend upwards in GFAP, which may indicate that the cell death is slightly higher in the other cell types

present, perhaps microglia, than in the GFAP+ cells. This may also indicate that the serum-based media used was inducing progressive differentiation in the cells. The loss of approximately 200 cells per field between 7 and 21 DIV clearly indicates that the culture conditions were not suitable for the long term maintenance of primary GBM cells, and required optimisation. Without a steady population of cells to start with, any use of the model for drug testing would be fundamentally flawed.

3.3.3 Proliferation in HiSpots®

In order to better understand the loss of cells seen earlier, a more detailed look at the cell survival was planned using Ki-67 staining and EdU detection, over more timepoints within the same 21 DIV window (**Figure 3-9**). All HiSpots® were created at $5x10^7$ cells/ml. It was clear from the DAPI counts at 1 and 3 DIV that a large proportion of cells were lost in the first few days in culture (**Figure 3-9E**). This could simply be the result of cells damaged in the surgical or isolation purposes dying, so some initial cell loss is to be expected and is not too much of a concern. The cell numbers were then relatively stable but dropped again after another week in culture, so this pointed towards the time between approximately 7 and 14 DIV as a good timeline for future investigations.

The Ki-67 data allowed this to be condensed down further. The proportion of actively cycling Ki-67+ cells started and ended low, with a peak at 7-9 DIV significantly higher than the levels at 3 DIV (**Figure 3-9F**). These data indicate that if an intervention is required, then this would be the appropriate timepoint, having allowed the cultures to settle, but not deteriorate.

It is important to note, however, that the levels of Ki-67 staining in the HiSpots® are still vastly lower than those *in situ*. The HiSpots® analysed in 3.2.5.2 reached a maximum of 1.5% cells positive for Ki-67. In comparison, (Sabit *et al.* 2014) demonstrated Ki-67 as 13.35± 1.27% of total cell numbers, and (Yoshida *et al.* 2010; Oka *et al.* 2013) showed a range of 15-38% Ki-67+ cells. Some variation is to be expected, partly due to GBM heterogeneity,

and because the percentage of Ki-67 increases with glioma grade (Sabit *et al.* 2014).

EdU+ cells are shown as a percentage of the Ki-67+ cells in the HiSpots®, to indicate the speed of the cell cycle. This did not change significantly over the majority of the timepoints, demonstrating that the cells were cycling at the same speed throughout, until they trended downwards at 21 DIV (**Figure 3-9G**). In the context of the DAPI and Ki-67 data, this would indicate that the cells are mostly dying off at this point and proliferating cells are being lost or becoming quiescent. This supports the decision to change conditions earlier than this timepoint to help support the cycling cells. Unfortunately, it was not possible to repeat these experiments in the higher density HiSpots® due to insufficient cellular material.

3.3.4 Optimisation of culture media

3.3.4.1 Removing serum at 7 DIV confers a short-term advantage

As mentioned above, 7 DIV presented itself as a logical timepoint to change the culture conditions in order to try and maintain and further improve the higher levels of proliferation. The decision was made to remove some or all of the serum at 7 DIV, to see if this allowed the cells to be supported for longer. Serum was either half or fully removed, providing three conditions for comparison. All HiSpots® were created at $5x10^7$ cells/ml.

There was not a significant difference in the total cell numbers remaining at 14 DIV, but by 21 DIV there was a clear survival benefit to removing the serum, with the total serum removal HiSpots® having approximately four times more cells remaining than in the HiSpots® left in full HSM (**Figure 3-10A, B**).

At 14 DIV there were significantly more Ki-67+ cells in the HiSpots® with some or all serum removed, although the levels were not any higher than the previous experiment at 7 DIV. This indicates that the removal of serum did help maintain the proliferating cells, but did not increase the proportions overall. By 21 DIV, this effect was lost, which indicates that there was still a

problem maintaining the population of proliferating cells beyond 14 DIV (**Figure 3-10C, D**). Combined, these data suggest that the removal of serum provided a boost to the proliferating cells, allowing them to increase the total cell numbers, but that this effect was not maintainable beyond a week, leading to a drop in the level of proliferation.

Lee *et al.* (2006) demonstrated that culturing primary GBM cells in serum causes them to differentiate, and this can't be reversed by switching them to serum-free afterwards. This may suggest that the HiSpots® removed from serum may have then maintained any stem-like cells remaining, but would still contain differentiated cells, highlighting the importance of also testing a fully serum-free condition. As will become clear later (**3.3.6**) however, the behaviour of these HiSpots® does not necessarily represent those grown in the final conditions, after other optimisations.

3.3.4.2 Removing serum at 7 DIV supports triple-positive tumour cells

In addition to supporting proliferation, the optimum culture conditions also need to support the key triple-positive tumour cells in the $5x10^7$ cells/ml HiSpots®. HiSpots® with all serum removed at 7 DIV had significantly more triple-positive tumour cells remaining at 14 DIV than those which were kept in HSM (**Figure 3-11F**). As noted in **3.2.6.2**, cells were also noted which were single-positive. This may imply that the triple-positive tumour cells go down neuronal or astrocytic-like pathways once they start to differentiate, losing the triple-positive tumour population and potentially the actively proliferating cells. The percentage of triple-positive tumour cells was not significantly higher in those switched out of serum at 14 DIV than at 7 DIV, although there was a trend towards an increase. This may indicate that removing the serum has allowed the triple-positive tumour cells to proliferate more, producing a slightly larger population of them within the HiSpots®, and that these were the cells to suffer when maintained in HSM for a further week.

3.3.4.3 HiSpots® cultured without serum do not have a survival advantage

The next step was to try removing serum from the culture media entirely, comparing the previously best condition (transferring to SFM after 7 DIV HSM), with SFM for the entire time, with and without growth factor supplementation. All HiSpots® were created at $5x10^7$ cells/ml. The SFM and growth factors used were based on another previously established GBM culture protocol. There were no significant differences between the conditions for total cell count, triple-positive tumour or single-positive cell types (**Figure 3-12**). As there was no significant advantage to removing the serum, at this point the decision was made to continue with the serum switch method (HSM 0-7 DIV, SFM 7-14 DIV). Given the data discussed later, it is possible that a difference in these HiSpots® may have developed significance after longer term culture, or with a larger number of patients, although this was not explored at the time. As the HiSpot® protocol was further optimised, it became unnecessary to perform further repeats, as the conditions required comparison within the new model nonetheless.

3.3.5 HiSpot® density

3.3.5.1 Increasing HiSpot® density improves total cell numbers at 14 DIV

At this point in HiSpot® optimisation, there was still a large amount of variability between HiSpots® from different patients. As discussed earlier (**3.3.3**), a large number of cells were lost in the first few DIV. This led to the hypothesis that increasing the initial density of the HiSpots® might compensate for this loss, allowing better survival and development of the HiSpots®. The density was first increased five fold (to $2.5x10^8$ cells/ml), then ten fold (to $5x10^8$ cells/ml) for further comparison (**Figure 3-13**). The five fold increase in cell density created a vast improvement to the HiSpots®, visible with the naked eye. The data supported this visible change. DAPI was quantified by two different methods: cell count of images taken with a 20x lens, and whole HiSpot® area fluorescence intensity. Both methods showed an increase in DAPI, with over a 2 fold increase in direct cell counting and a 15 fold increase in total area fluorescence intensity. This demonstrates the

reliability of the fluorescence intensity method for detecting large changes in total cell count. This imaging method could therefore be applied to later experiments for looking at DAPI changes in whole HiSpot® images.

There was no further increase in total area fluorescence intensity between the five and ten fold increased density HiSpots®. When weighed up against the total number of HiSpots® able to be created per patient, the $2.5x10^8$ cells/ml HiSpots® were considered the best option for improved growth and potential experimental group size.

3.3.5.2 Increasing HiSpot® density affects survival of certain cell types

It was important to establish that microglia were not negatively impacted by the increased density. It was hypothesised that the main tumour cell population would be able to survive at the higher density, as a result of the mutations accumulated. Microglia are recruited from the surrounding brain and transition to a pro-tumour phenotype, but are not themselves directly derived from tumour cells, therefore may not have the same resilience to changes in culture density as the tumour cells. Fortunately, the proportion of microglia in the HiSpot® cultures was not significantly affected by the increased density, remaining between 17-20% of the total cell population (**Figure 3-14C**).

Within the tumour cell population, the proportion of single-positive cells decreased, and the triple-positive tumour cells increased dramatically (**Figure 3-14D, E**). It is possible that this represents the triple-positive tumour cells being maintained in their multi-expressive state, rather than losing their GFAP+Nestin+ expression. As described above, it is believed that the multi-expressive cells represent the key tumour cell population which continue to repopulate the tumour, and were therefore important to retain over the single-positive cells. Altogether, the $2.5x10^8$ cells/ml HiSpots® were better supportive of the GBM cells than the $5x10^7$ cells/ml HiSpots®, reinforcing the decision to move forward with the $2.5x10^8$ cells/ml HiSpots® as the standard protocol. As the $2.5x10^8$ cells/ml HiSpots® successfully

supported both triple-positive cells and microglia, this density was deemed a desirable optimisation to the original protocol, and implemented for all future GBM HiSpot® experiments.

To confirm the multiple cell layers within the HiSpots®, an example set of images were taken using a confocal microscope. Selected images are shown above with over 4µm between them (**Figure 3-15**), which demonstrate that there are multiple distinct cell layers in the HiSpots®.

3.3.6 Further optimisation of culture media for higher density HiSpots®

The experimental data presented in **3.2.8** were produced from two GBM patients with a large variation in expression patterns, specifically of GFAP. The lack of GFAP expression in the HiSpots® from one patient was also noted in the hospital pathology report for the fresh tissue, so it is not considered an artefact of the HiSpot® method. Although it would have been useful to repeat this experiment more times, with further patient samples, a combination of time limitations and demanding experimental requirements made it necessary to highlight any key differences and move forward. These experiments were all performed using the $2.5x10^8$ cells/ml and $5x10^8$ cells/ml HiSpots®.

3.3.6.1 There is no advantage to returning HiSpots® to serum

This experiment was designed with the serum switch method (HSM 0-7 DIV, SFM 7-14 DIV) in mind as the previously established best method. It was queried that serum removal may have a temporary benefit, but the HiSpots® may survive better if returned to serum. In order to keep the total culture time the same as previous experiments, the methods were designed to have the HiSpots® out of serum for a whole week in between serum conditions, in order to allow the HiSpots® to fully adjust to the serum free condition (**Figure 3-16**). All HiSpots® used were created at a density of $2.5x10^8$ cells/ml.

There was no significant difference between the conditions for total cell counts. This indicates that none of the conditions provided an overall survival advantage between the groups. There were no significant

differences in the percentages of triple-positive tumour cells or β-IIIT+ only cells. There was a downward trend in the percentage of triple-positive tumour cells with increasing serum percentage. This may indicate that a significant difference may have arisen with a longer culture time, and perhaps indicates a negative effect on the triple-positive tumour cells of returning HiSpots® to serum. Overall, these data indicate that there is no survival advantage to total cells or cell types to returning cells to serum once they have been removed.

3.3.6.2 Serum does not confer a survival advantage on total cell count in $2.5x10^8$ cells/ml or $5x10^8$ cells/ml HiSpots®

These experiments compared the original HiSpot® protocol (25% serum for 14 DIV) with the previously most successful condition (25% switched to 0% at 7 DIV) and the serum free condition (0% serum for 14 DIV) for HiSpots® created at $2.5x10^8$ cells/ml and $5x10^8$ cells/ml. The results did not show a survival advantage for any of the conditions in either density (**Figure 3-17A, B**). Some HiSpots® were reimaged using the confocal microscope but also showed no difference (**Figure 3-17C**). There are slightly higher mean values for all HiSpots® cultured in SFM, so it is possible that this condition would have confirmed a survival advantage long term, although longer term studies would be needed to confirm this. Interestingly the total cell numbers were very similar (~1000 per field) for the $2.5x10^8$ cells/ml and $5x10^7$ cells/ml HiSpots®, indicating that perhaps these HiSpots® had reached the maximum cell density that they could support.

3.3.6.3 Serum does not confer a survival advantage on β-IIIT+GFAP+ cells or β-IIIT+ cells in 2.5x10^8 cells/ml or 5x10^8 cells/ml HiSpots®

The percentages of triple-positive cells and β-IIIT+ only cells were measured in 2.5x10^8 cells/ml and 5x10^8 cells/ml HiSpots® cultured in the three conditions mentioned above. There were no significant differences between any of the groups, indicating that none of the media conditions confer a major survival advantage or disadvantage on these cell types (**Figure 3-18**). Especially in the data taken from the confocal images, there is a trend towards a larger percentage of triple-positive cells in SFM. As with the total cell counts, it is possible that with a longer culture time this difference would become more stark, but longer term experiments would be needed to clarify this. Importantly, the key triple-positive cells survive well in any of the three conditions.

As one of the examples discussed in the introduction **(3.1.3.1**), Stockhausen *et al.* (2014) demonstrated that both serum (10% foetal calf serum) and retinoic acid (an inducer of differentiation) cause differentiation of human GBM neurosphere cells in culture, also causing a loss of expression of *EGFR* and *EGFRvIII*. The authors also showed that blocking EGFR and EGFRvIII signalling induced differentiation, reduced cell viability, and decreased tumorigenicity in the neurosphere cultures. This suggests that the use of serum in culture has a negative effect on the tumorigenicity of GBM cells and encourages their differentiation, changing the culture phenotype. Ideally, this would be avoided in the HiSpots®.

3.3.6.4 Serum does not confer a survival advantage on microglia in HiSpots®

The levels of microglia differed between the groups measured, but not enough to present significance in multiple comparison testing. Data from HiSpots® from two patients are presented as percentages, however, an exceptionally high density network and high levels of noise for GBM30 prevented percentages being calculated, so raw count data are shown (**Figure 3-19A**, **B**). However, GBM30 showed a large, but not statistically significant, increase in raw microglia numbers per image in SFM than the

other conditions. This clearly demonstrates a large variability between HiSpots® from different GBM patients for microglia response but indicates that the removal of some or all of the serum is advantageous.

The data in this section showed a large amount of variation between HiSpots® from different patients, but demonstrate that at least some of the serum should be removed from culture for optimum HiSpot® development. Importantly, all conditions successfully supported the cells, so none of the choices would be significantly detrimental to the methodology. When the potential effects of serum on tumour cells (discussed in 3.1.3.1) were taken into account, SFM presented itself as the most favourable option. Various groups have successfully cultured primary human microglia in 5-10% FBS (Biber *et al.* 2011; Melief *et al.* 2016; Rustenhoven *et al.* 2016). However, Parney *et al.* (2009) compared microglia cultured in 10% FBS or serum-free media with those immediately removed from gliomas, and found that, the microglia cultured in serum-free media more closely represented the expression patterns of cells taken directly from the tumour. This supports the conclusion that it is preferable to keep the HiSpot® microglia in SFM, to avoid their expression patterns being altered.

3.3.7 General conclusions

It was important to balance the various advantages of the different conditions tested throughout this chapter, in order to develop an optimum protocol for the culture of GBM HiSpots® for future experiments. The increase in density between the $5x10^7$ cells/ml and $2.5x10^8$ cells/ml HiSpots® was key to growing more three dimensional and well connected HiSpots®. This indicates that GBM cells may require a variable minimum activation density in order to thrive, and that this is reached by the $2.5x10^8$ cells/ml HiSpots® more reliably than the $5x10^7$ cells/ml HiSpots®. Although the highest density HiSpots® ($5x10^8$ cells/ml) formed even more extensive networks than the $2.5x10^8$ cells/ml HiSpots®, this difference was not considered significant enough to counteract the disadvantage of creating 50% fewer HiSpots®, especially given that later experiments (3.3.6) did not see a difference between the number of cells per field between $2.5x10^8$ cells/ml and $5x10^8$ cells/ml HiSpots®. Similarly, a longer culture time (21 DIV vs 14 DIV) did not confer an advantage to the HiSpot® development which was worth extending the overall experimental timeline for another week. Overall, it is possible that high levels of debris or red blood cells lead to overcalculations of cell density, and therefore increasing the required density corrected for this overcalculation.

Once the HiSpot® density had been decided, the media conditions were re-evaluated and showed that SFM was overall the best choice for supporting both overall cell number and key tumour cells and microglia. This is supported by Lee *et al.* (2006) who found that their primary GBM cells grown in their serum-free media (with FGF2 and EGF supplements) retained their stemness and comparability to the parent tumour, whereas the cells cultured in serum, even when switched to serum-free, lost their stemness and became dissimilar from the parent tumour. The authors did include growth factors, which raises the question of whether these are necessary in the HiSpots®. As the $2.5x10^8$ cells/ml HiSpots® were demonstrated to grow successfully without the addition of growth factors, it was considered

unnecessary to add these in. It is possible that the high density and connectivity of the HiSpots® allows them to produce their own endogenous growth factors and support the culture as a whole via paracrine and autocrine signalling, therefore the addition of extra growth factors would only complicate the conditions and perhaps disrupt the natural balance of growth factors that the HiSpots® have created. This also highlights the importance of only changing ~2/3 of the media each time, rather than replacing the entire volume and potentially losing the majority of the endogenous factors created. In summary, the final culture conditions for future experiments are a HiSpot® density of $2.5x10^8$ cells/ml in serum-free media (Neurobasal A, B27, Glutamax, penicillin/streptomycin). Combined, these conditions have been demonstrated to support the growth and development of GBM HiSpots®.

3.3.7.1 Key Conclusions

- GBM HiSpots® contain high numbers of key cell types: triple-positive (β-IIIT+GFAP+Nestin+) cells and microglia (IBA1+).
- All tumour cells confirmed by *IDH-1* R132H positivity in HiSpots® are GFAP+
- β-IIIT+GFAP+ cells are also SOX2+ and make up the majority of the HiSpot® cell population
- GBM HiSpots® at lower densities ($5x10^7$ cells/ml) survive better when removed from serum
- GBM HiSpots® survive better and support key types at higher densities ($2.5x10^8$ cells/ml)
- GBM HiSpots® at higher density no longer require serum

4 Chapter 4 Validation of GBM HiSpots®

4.1 Introduction

For a model such as the HiSpot® to be a useful tool for research, it must recapitulate features of the original tumour. Although there are generally accepted features of GBM used for diagnosis, the heterogeneity of GBM can make it difficult to predict which features the HiSpots® from each patient should be replicating. Patient-matched pathology reports can be used to note general and patient-specific features of GBM for comparison to HiSpots® produced from the same patient. The first section of this chapter will compare qualitative data from HiSpots® and pathology reports.

Drug sensitivity is also an important feature to recapitulate in models of GBM, especially if the model is to be used for validation or prediction of drug response in the future. Approximately 50% of GBMs will have a methylated *MGMT* promoter, which sensitises the tumour to treatment with the alkylating agent TMZ. Tumours without this methylation are able to repair the damage caused by the drug, so are not expected to respond. The second section of this chapter will explore whether GBM HiSpots® can demonstrate the difference between *MGMT* methylated and unmethylated tumours, via their response to treatment with TMZ.

4.1.1 Glioblastoma pathology and genetics

In order to aid diagnosis of a tumour, a tissue biopsy is taken for analysis by a pathologist. If the tumour is thought to be a GBM, a combination of immunohistochemical and genetic features are analysed to provide a diagnosis. Infiltration into healthy tissue and astrocytic features along with nuclear atypia, high levels of mitosis, florid microvascular proliferation and pseudopalisading necrosis are all histological features of GBM (Wesseling *et al.* 2011; Louis *et al.* 2016).

One common feature of GBM is high levels of mitosis, as this increases with glioma grade. Tumour sections are stained with an anti-Ki-67 antibody,

which identifies actively cycling cells. The higher the percentage of Ki-67+ cells, the higher the level of proliferation (growth fraction) within the tumour. There can be high variation within the patients, due to factors such as biopsy area and tumour heterogeneity. Ki-67% is therefore reported as the highest level seen in the stained tumour sections.

The same variation is also true for GFAP staining. Gliomas are known to be highly positive for the astrocytic marker GFAP so this marker is also used to identify GBMs. Most GBMs have a very high percentage of GFAP immunoreactivity, so this has historically provided a useful diagnostic tool. However, it is possible for GBMs to lose their GFAP reactivity as mutations accumulate within the tumour. Gliosarcomas (GSMs) can develop areas of a sarcomatoid phenotype, which do not express GFAP (Romero-Rojas *et al.* 2013).

During analysis, the pathologist will also note features such as giant multinucleated cells and epithelioid-like cells which can indicate variants of GBM (**1.1.3.2**). Once pathological analysis has provided a probable diagnosis, further tissue is sent for genetic analysis to confirm diagnosis and identify diagnostic and prognostic features. The *IDH-1* R132H mutation is now considered key to determine whether a GBM is secondary, and the methylation status of the *MGMT* promoter is used to predict response to the alkylating chemotherapy drug TMZ. Amplifications and mutations in *EGFR* are also analysed, as tumours with these irregularities can be more sensitive to some treatments, and *EGFR* amplifications and rearrangements have been identified as markers of malignancy even in tumours which appear low grade (Wesseling *et al.* 2011).

4.1.2 Pathological validation of the HiSpot® model

If HiSpots® are maintaining patient specific tumour features, then certain pathological features should be visible via immunohistochemical analysis. Notably, proliferation levels should correlate with those seen in pathology, as should GFAP staining patterns. Although more rare, giant cells should be

visible in HiSpots® from giant cell variant tumours. Pathological data are collated in **Table 4-1**. The factors compared between pathological reports and images and HiSpots® are Ki-67 staining, GFAP staining, IDH1 mutations, MGMT promoter methylation status and giant cells. The patient pathological reports were selected for comparison if matched HiSpot® staining was available, from $2.5x10^8$ cells/ml HiSpots®. Labels were assigned to HiSpot® staining before comparison with pathology reports. Additional pathological images were then requested for specific patients which represented the range of the features shown.

4.1.3 Modelling TMZ response

After testing whether HiSpots® replicate pathological features of GBM, the next step is to replicate their response to treatment with the first line GBM chemotherapy TMZ. TMZ is an alkylating agent which kills proliferative cells in GBM and other tumour types. TMZ is a prodrug which is taken up into cells where it is converted into the active drug form 5-(3-methyltriazen-1-yl)-imidazole-4-carboxamide (MTIC). MTIC then reacts with water to form 5-aminoimidazole-4-carboxamide and a methyldiazonium cation, which acts by preferentially methylating guanine bases in DNA. Without repair, this causes cell cycle arrest in the G_2/M phase of the cell cycle, which prevents cells from continuing to the S-phase and proliferating and is followed by death via apoptosis. This results in a reduction in proliferation and overall cell number (Calzolari *et al.* 2010; Zhang *et al.* 2012). However, the MGMT enzyme removes the methylation, restoring the DNA to its previous state (Zhang *et al.* 2012). Methylation of the *MGMT* promoter reduces the levels of MGMT in the cells, sensitising them to DNA damage, and therefore cell death via apoptosis (Hegi *et al.* 2005). This is why tumour tissue samples are tested for *MGMT* methylation, and why patients with this methylation respond better to treatment with TMZ in addition to radiotherapy and surgery.

If the HiSpot® model can be shown to predict patient response to TMZ, it could also be extrapolated to test other treatment options, perhaps second

line therapies for the unfortunately inevitable tumour recurrence or testing other first line options which are currently under research or in trials. Having a patient-specific *in vitro* drug testing platform could help inform treatment decisions at each stage of their clinical care. The second part of this chapter will establish whether GBM HiSpots® respond to TMZ, and whether this is determined by the patient's *MGMT* methylation status. This will be measured by the number of proliferative (EdU+) and apoptotic (Caspase-3+) cells in the HiSpots®. EdU is incorporated into the cell nucleus as the cell enters S-phase, and can therefore be used as a marker of proliferation levels. It will not be incorporated into all cycling cells, unless the exposure time is as long as the cell cycle. However, EdU will be incorporated into any cells which enter the S-phase during the 4 hour exposure time. TMZ prevents cells from successfully proliferating, and should therefore reduce the number of EdU+ cells within a culture (Zhang *et al.* 2012). The DNA damage caused by TMZ eventually causes the affected cells to die via apoptosis, so cleaved caspase-3 expression will be used as a marker of apoptosis levels. In this chapter, an autofluorescent substrate for the caspase-3 enzyme is used rather than an antibody for the activated enzyme.

TMZ was tested at a range of doses in order to plot a dose-response relationship. It is important to test a range of doses in order to identify a dose-dependent effect. The heterogeneity between HiSpots® from different GBM patients may also mean that the TMZ concentration needed to elicit a response differs between patients, and therefore there is unlikely to be a 'one-size fits all' dose. DMSO is used as the vehicle for TMZ. A dose of DMSO vehicle only was applied to the HiSpots® recorded as being treated with 0 µM TMZ. DMSO has been shown to have an effect itself on certain cell types so DMSO-treated HiSpots® were compared with untreated HiSpots® as a separate experiment in order to check for any effect of DMSO rather than TMZ (Verheijen *et al.* 2019).

Together, these pathological and pharmacological factors will be used to validate the HiSpot® model for GBM.

4.2 Results

4.2.1 Patient data table

Key analyses are performed on patient tissue by a pathologist in order to confirm diagnosis. These include immunohistochemical analyses of Ki-67 and GFAP, and genetic analyses of *MGMT* promoter methylation status, and *IDH-1* mutation status. Features such as giant cells, sarcomatoid features or epithelioid features are also noted. The diagnosis and key pathological features are shown in **Table 4-1** below for all patients from whom tissue was collected as part of this study.

42 out of 50 (84%) of patients were confirmed as GBM. Of the 42 confirmed GBMs, 24 were male and 18 female. The median age at diagnosis was 65. 48% of patients had *MGMT* promoter methylation, 36% were unmethylated, and data were unavailable for the remaining patients.

41 of the 42 patients had wildtype *IDH-1*, and one had the *IDH-1* R132H mutation. Tissue was collected from two other *IDH-1* R132H mutant patients, but these patients were reported as having lower grade or unclear high grade glioma.

In the 50 patients from whom tissue was collected, Ki-67% ranged from <1% (LGG) to >70%, with most patients between 20-50%, as measured by the pathologist. GFAP levels were qualitative, and marked as positive, patchy positivity, or positive/negative for certain cell types or areas. Giant, multinucleated or large cells were noted for four patients. Epithelioid and/or squamoid features were noted for three patients.

These factors are later compared to HiSpot® features from the end of the optimisation steps onwards.

Table 4-1: Pathological data and diagnosis of all patients from whom tissue was collected.

Pathological and diagnostic data are shown for all patients from whom tissue was collected during this study. All features are listed as reported by the pathologist. Dashes indicate data unavailable or not applicable. From left to right the columns show patient number, diagnosis, MGMT methylation status (methylated: M, unmethylated: U), IDH-1 status (wildtype: WT, mutant MUT), Ki-67%, GFAP staining pattern, and other key features.

Patient	*Male/Female*	*Age at presentation*	*Diagnosis*	*MGMT (M/U)*	*IDH-1 (MUT/WT)*	*Ki-67%*	*GFAP*	*Key features*
1	M	71	GBM	M	WT	15-20%	Positive	-
2	F	76	GBM	M	WT	-	-	-
3	M	69	GBM	-	WT	20%	Positive	-
4	M	65	GBM	-	WT	High	-	-
5	F	38	GBM	-	WT	High	Positive	-
6	M	65	GBM	M	WT	-	-	-
7	M	59	GBM	U	WT	-	-	-
8	F	65	GBM	M	WT	50%	Fibrillary positivity	-
9	M	68	GBM	M	WT	~50%	-	-
10	M	49	Reactive changes	-	-	-	-	-
11	M	70	GBM	M	WT	50%	Positive in astrocytes, sparse in oligodendroid areas	-
12	F	77	GBM	-	WT	~20%	Small number of stained cells	-
13	M	54	GBM	-	WT	-	-	-

14	F	56	GBM	U	WT	Up to 50%	Subtotal positive	-
15	M	73	Anaplastic astrocytoma (grade III)	U	WT	Up to 25%	Disorganised fibrillary positivity	-
16	F	74	GBM	M	WT	Up to 40%	Positive	Some features of GSM/epithelioid GBM
17	M	70	Metastatic adenocarcinoma	-	-	-	-	-
18	M	48	GBM	M	WT	Up to 40%	Positive	-
19	F	69	GBM	U	WT	>50%	Positive (patchy)	-
20	F	62	GBM	M	WT	50%	Positive and negative cells	-
21	M	60	GBM	U	WT	40%	Positive (focal negative)	-
22	F	60	GBM	M	WT	40%	Positive (variable in giant cells)	-
23	M	69	GBM	-	WT	-	-	-
24	M	54	GBM	M	WT	50%	positive	
25	M	65	GBM: GSM	M	WT	50%	Positive in nests, negative in areas	Multinucleated cells

26	M	73	GBM	U	WT	Up to 40%	Positive	-
27	F	70	GBM	U	WT	Up to 30%	Patchy positivity	Large nuclei, some epithelioid cells
28	M	50	GBM: GSM	-	WT	>70%	Largely negative	
29	M	68	GBM	M	WT	Up to 40%	Positive	-
30	F	66	GBM/Oligodendroglioma	M	WT	Variable, up to 50%	Reactive astrocytes, most tumour cells -ve	-
31	F	50	Low grade glioma	-	-	<1%	Reactive astrocytes	-
32	M	65	No active tumour	-	-	-	-	-
33	F	46	GBM	M	WT	60%	Positive	Giant cells
34	F	60	GBM	U	WT	20%	Positive	-
35	M	65	GBM	M	WT	40%	Positive	-
36	F	70	GBM	U	WT	20%	Positive	Giant cells
37	M	67	GBM	U	WT	20-25%	Positive	-
38	M	54	Gemistocytic astrocytoma (grade II)	-	MUT	5%	Positive	-
39	M	67	GBM	U	WT	40%	Positive	-

40	M	52	GBM	U	WT	30%	Positive	-
41	F	66	GBM	M	MUT	40%	Some positive, many negative	-
42	M	74	GBM	U	WT	30%	Positive	-
43	M	49	Glial tumour (grade III/IV)	-	MUT	Low, but areas of 20-40%	Positive	-
44	F	64	GBM	U	WT	30%	Positive	-
45	F	54	GBM	M	WT	30%	Positive	-
46	M	66	GBM	U	WT	Up to 25%	Patchy positivity	Epithelioid and squamoid features
47	M	66	GBM	U	WT	Up to 30%	Positive	-
48	M	65	GBM	M	WT	40%	Positive	-
49	F	58	GBM	M	WT	25%	Fibrillary positivity	-
50	M	80	Metastasis	-	-	-	-	-

4.2.2 HiSpots® recapitulate patient-specific pathological features of GBM

4.2.2.1 HiSpots® demonstrate a range of Ki-67 levels

One of the pathological features tested for in potential GBM patients is Ki-67%. Tissue slices are stained with an antibody for Ki-67, which is a nuclear protein expressed in actively cycling cells. This is used to determine the growth fraction. The growth fraction is highly variable between slices, so pathologists report the highest level of proliferation within the stained slices, although the exact phrasing used varies slightly between pathologists.

In **Figure 4-1** below examples are shown of low (L), medium (M) and high (H) Ki-67 positivity from pathology reports, alongside EdU stained HiSpots® from the same patients. EdU is incorporated into cycling cells in the S-phase, so shows the cycling cells which were in S-phase during the exposure time. Ki-67 will stain for all cycling cells. Both markers can be used to investigate levels of proliferation. Relative proportions of Ki-67 and EdU can therefore be compared between pathology and HiSpots® to determine whether the HiSpots® are capturing the range of proliferation levels found in GBM, but exact levels will vary as EdU+ cells only represent a subset of the total cycling cells (Ki-67+). It was not possible to use Ki-67% immunoreactivity as a measure of proliferation in the HiSpots® due to poor Ki-67 antibody penetration with the higher density cultures ($2.5x10^8$ cells/ml). HiSpots® were exposed to EdU for 4 hours, so EdU positivity will only represent a subset of the total growth fraction. The comparison of reported Ki-67% and HiSpot® EdU staining is not an ideal approach as direct EdU quantification is not possible in these cases. However, it provides a preliminary insight into the ability of the HiSpot® model to represent the variety of proliferation levels in GBM, and it therefore worth including.

Within the pathology reports from patients used in this study, Ki-67% ranged from <1% to >70%, although patients diagnosed as GBM were usually reported with a Ki-67% of 20% or higher. Patients with <20% are referred to as low staining, 20-35% as medium, and 40%+ as high. Ki-67% values are

shown for 14 patients in **Table 4-2**. HiSpot® staining was also categorised into high, medium, and low. Labels were assigned by eye according to the number of EdU+ cells per field. 'High' was assigned to samples with many EdU+ cells visible throughout the HiSpot®. 'Medium' was assigned to samples with more sparse EdU+ cells, or where EdU+ cells were only present in small areas of the HiSpot®. 'Low' was assigned to samples with very sparse EdU+ cells, where very few cells were positive within the whole HiSpot®. Labels were assigned before comparison with pathology data. 50% of the patients matched between pathology and HiSpots®. Of the remaining patients, only one (GBM48) showed a stark difference in proliferation levels between pathology (high) and HiSpot® (low).

Example images from four patients (shaded orange in **Table 4-2**) were taken by an NHS pathologist and are shown in **Figure 4-1 A-D**. Nuclear staining for all cells is visible as a light blue stain, and Ki-67+ cells in a dark brown. These are shown above images of EdU staining in HiSpots® cultured from the same patients, where nuclei are stained with DAPI (dark blue) and EdU for proliferative cells (red) (**Figure 4-1 E-H**). The relative levels of EdU staining in the HiSpot® images visibly correlate with the levels of Ki-67 staining in the matched pathology images. Patients 30 and 39 show high levels of Ki-67/EdU, as reported, whereas staining levels are visibly lower in patient GBM37, and extremely low in patient GBM38. It was not possible to quantify the percentage of EdU staining for the HiSpots®, so only qualitative comparisons are available.

Table 4-2: Pathological report data: Ki-67 levels.

A summary of relevant data from pathology reports for patients 30 – 34, 37 – 39, 43 – 49, showing a range of Ki-67% levels. Values are shown as reported by a pathologist. These have been allocated into three categories: high, medium, low. HiSpot® EdU positivity levels are also reported as high, medium, or low. Notes show any non-GBM diagnoses. Orange shaded rows show the patients demonstrated in images below.

Patient	Ki-67 pathology	Pathology results	HiSpot® results	Notes
30	Up to 50%	HIGH	HIGH	
31	<1%	LOW	MED	LGG
33	60%	HIGH	HIGH	
34	20%	MED	LOW	
37	20-25%	MED	MED	
38	5%	LOW	LOW	LGG
39	40%	HIGH	HIGH	
43	Low, but areas of 20-40%	LOW	LOW	
44	30%	MED	MED	
45	30%	MED	LOW	
46	Up to 25%	MED	LOW	
47	Up to 30%	MED	HIGH	
48	40%	HIGH	LOW	
49	25%	MED	LOW	

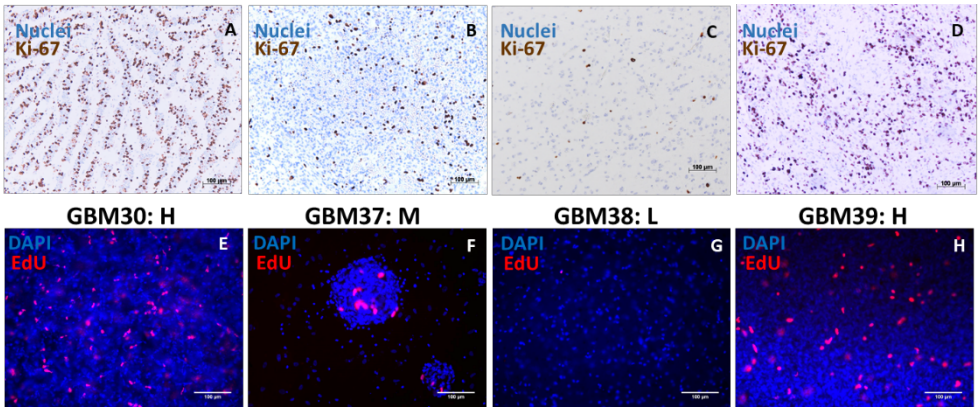

Figure 4-1: Comparative images from four matched patient samples for proliferation.

Panels A-D show histology images stained for nuclei (blue) and Ki-67+ proliferative cells (brown). Panels E-H show immunofluorescence images of HiSpots® cultured from the matched patient samples taken using a 20x lens. DAPI (blue) shows nuclei and EdU (red) shows proliferative cells. Scale bars are shown for reference.

4.2.2.2 HiSpots® demonstrate a range of GFAP positivity levels

Positive staining for GFAP is a key feature of GBM pathology. However, if the tumour is a gliosarcoma (a variant of GBM, **1.1.3.2**) it can present with very limited GFAP positivity as a result of the tumour also containing a GFAP negative sarcomatoid phenotype. GSMs can therefore have far less GFAP staining than in a standard GBM.

Pathological data from a number of GBM patients are shown below, including those with GSM features, which demonstrate the range of how GFAP positivity is reported (**Table 4-3**). Most GBM patients are reported with positive GFAP reactivity as expected from a glial tumour. However four of the thirteen patients shown in **Table 4-3** were reported as having no or limited positivity. Two of these patients (GBM28, GBM46) were reported as GSM or with sarcomatoid features.

Four patients which demonstrate the range of GFAP staining were selected and example images taken by the pathologist from these are shown in **Figure 4-2 A-D,** with nuclear staining in light blue, and GFAP staining in dark brown. Representative images of GFAP staining from HiSpots® from the same patients are shown in **Figure 4-2 E-H,** with nuclear DAPI staining in dark blue and GFAP staining in green. Levels of GFAP staining in HiSpots® correlate with GFAP staining in the patient-matched pathology images. GBM28 was recorded as a GSM, and histology images show no visible GFAP staining. This was the same in the HiSpot® image, which showed only one clearly GFAP+ cell in the image field. In comparison, patients GBM36 and 40 were recorded as positive for GFAP, and histology images show consistent positivity. High levels of GFAP positivity are also seen in the matching HiSpot® images, although there is still notable variation between the two patients. GBM46 showed only patchy positivity for GFAP and was recorded as having epithelioid/squamoid features which may indicate transformation towards a GSM phenotype. The GFAP positivity in the matched HiSpot® is also patchy, showing less extensive staining than either of the 'positive' patients, but visibly more than GBM28.

Table 4-3: Pathological report data: GFAP levels.

A summary of relevant data from pathology reports for patients 28, 34, 36, 37, 39 – 41, 44 - 49, showing a range of GFAP positivity levels. Levels are shown as reported by a pathologist in the second column. The pathologist's diagnosis is shown in the third column and HiSpot® staining results in the final column. Orange shaded patients are shown in the figure below.

Patient	*GFAP pathology*	*Diagnosis*	*HiSpot® results*
28	Largely negative	GSM	Negative
34	Positive	GBM	Positive
36	Positive	GBM	Medium
37	Positive	GBM	Positive
39	Positive	GBM	Positive
40	Positive	GBM	Positive
41	Some positive, many negative	GBM	Medium
44	Positive	GBM	Positive
45	Positive	GBM	Positive
46	Patchy positivity	GBM with epithelioid/squamoid features	Medium
47	Positive	GBM	Positive
48	Positive	GBM	Positive
49	Fibrillary positivity	GBM	Positive

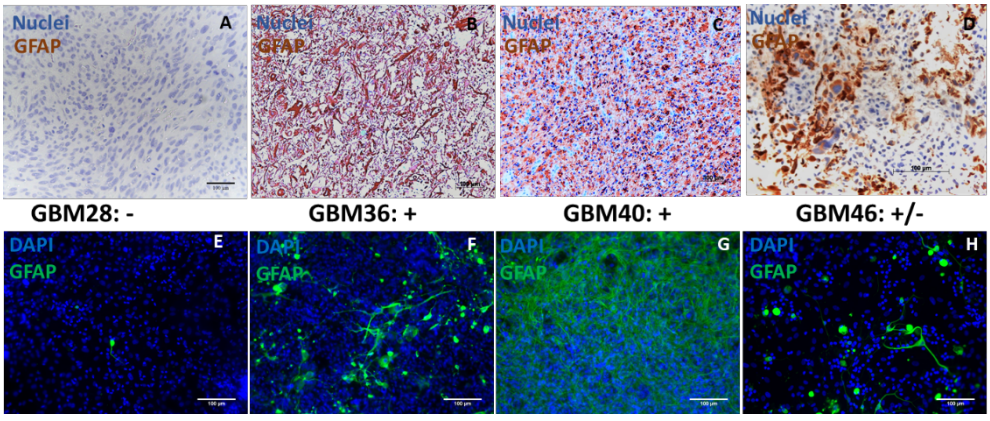

Figure 4-2: Comparative images from four matched patient samples for GFAP positivity.

Panels A-D show histology images stained for nuclei (blue) and GFAP (brown). Panels E-H show immunofluorescence images of HiSpots® cultured from the matched patient samples taken using a 20x lens. DAPI (blue) shows nuclei and GFAP positive cells are shown in green. Scale bars are shown for reference.

4.2.2.3 HiSpots® represent the giant cell variant of GBM

Giant cells are a common pathological feature of GBM and the defining feature of the giant cell GBM subvariant. Therefore, the presence of a high percentage of giant cells is noted in GBM pathology reports. Giant cells are visible as cells with either one very large nucleus, or multiple nuclei condensed within one cell. **Table 4-4** shows data from 15 patients with their diagnosis, whether the pathologist reported giant cells, and whether giant cells were visible in HiSpot® cultures derived from those patients. In all patients where giant cells were reported (GBM28, 33, 36), they were visible in HiSpots®, and no giant cells were seen in HiSpots® where they had not been reported pathologically.

Example patients showing the presence and absence of giant cells are shown in **Figure 4-3**. Histopathological images (**A-C**) are shown above HiSpot® images from the same patients (**D-F**). Patients GBM33 and GBM36 were both recorded as containing many giant cells, whereas patient GBM40 did not have any giant cells identified. Examples of giant cells in each image are demonstrated with yellow arrows.

Table 4-4: Pathological report data: Giant cells.

A summary of relevant data from pathology reports for patients 28, 30, 33, 34, 36, 37, 39 - 41, 44 - 49 showing patients positive and negative for giant cells, as reported by a pathologist (third column). The pathologist's diagnosis is shown in the second column. Whether giant cells were present in the corresponding HiSpots® is shown in the final column. Patients shaded in orange are shown in the figure below.

Patient	*Diagnosis*	*Pathologist noted giant cells?*	*HiSpot® results*
28	GSM	Yes	GCs present
30	GBM	No	No GCs
33	GBM	Yes	GCs present
34	GBM	No	No GCs
36	GBM	Yes	GCs present
37	GBM	No	No GCs
39	GBM	No	No GCs
40	GBM	No	No GCs
41	GBM	No	No GCs
44	GBM	No	No GCs
45	GBM	No	No GCs
46	GBM	No	No GCs
47	GBM	No	No GCs
48	GBM	No	No GCs
49	GBM	No	No GCs

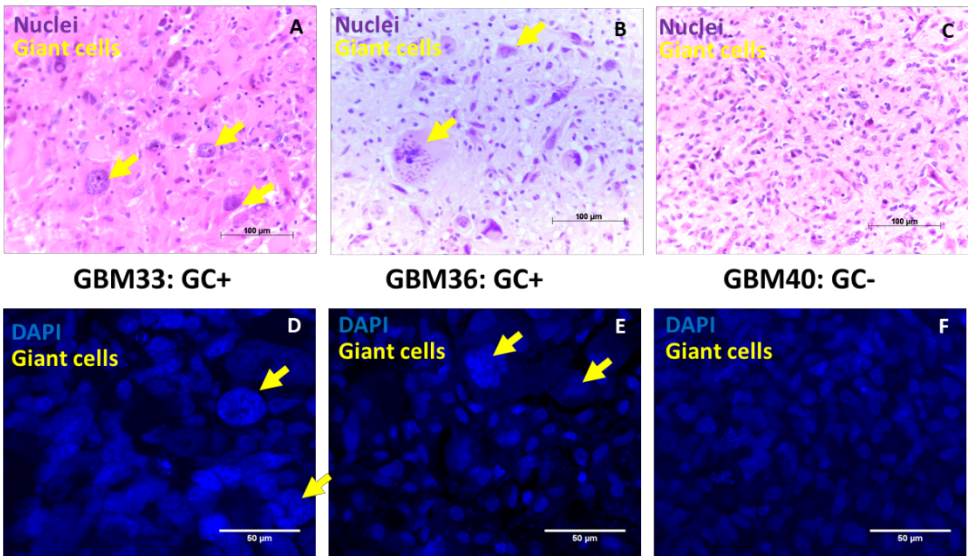

Figure 4-3: Comparative images from three patient matched samples for giant cell GBM.

Panels A-C show histology images stained for nuclei (blue). Giant cells are identified by the yellow arrows. Panels D-F show immunofluorescence images of HiSpots® cultured from the matched patient samples, taken using a 63x lens. DAPI (blue) shows nuclei, and giant cells are identified by the yellow arrows. Scale bars are shown for reference.

4.2.3 HiSpots® respond to TMZ according to *MGMT* methylation status

4.2.3.1 There is no effect of DMSO vehicle on EdU levels in HiSpots®

HiSpots® were treated with DMSO for 5 DIV and compared with untreated HiSpots®. Before fixation, all HiSpots® were treated with EdU for 4 hours. EdU detection was performed and the total number of EdU+ cells was recorded for each HiSpot®. Data from HiSpots® from all patients were grouped together (**Figure 4-4A**). Collated, data were not normally distributed (Shapiro-Wilk). There was no significant difference between the number of EdU+ cells per HiSpot® in DMSO treated and untreated HiSpots® (495.4 ± 130.3 vs 804.5 ± 161.8, p=0.1051, n-17-19, Mann Whitney test). As visible on the graph in **Figure 4-4A**, the data were spread over a large range. It was therefore decided to analyse the differences between HiSpots® from individual patients.

Categorised for each patient, the HiSpot® data were normally distributed (Shapiro-Wilk). Conditions were compared by two-way ANOVA to examine the effects of DMSO treatment on HiSpots® from each patient (**Figure 4-4B**). This showed a significant effect of treatment ($F(3, 28) = 56.16$, $p<0.0001$) and patient ($F(1, 28) = 5.285$, $p=0.0292$) but no interaction effect ($F(3, 28) = 1.026$, $p=0.3962$). However Bonferroni's multiple comparisons test did not show significant differences between DMSO and untreated HiSpots® for the following:

- GBM30 *(936.3 ± 234.2 vs 1299.0 ± 230.1, p=0.2592, n=3-5)*
- GBM33 (*1162 ± 149.2 vs 1506.8 ±100.8, p=0.2273, n=4-5*)
- GBM34 (*17.80 ± 2.059 vs 97.60 ± 13.93, p>0.9999, n=5)*
- GBM37 (*174.6 ± 12.77 vs 192.0 ± 15.38, p>0.9999, n=4-5*)

Data are visualised for HiSpots® from each patient in **Figure 4-4B** below. Error bars for HiSpots® from patients GBM34 and GBM37 are not visible as they are smaller than the symbols used.

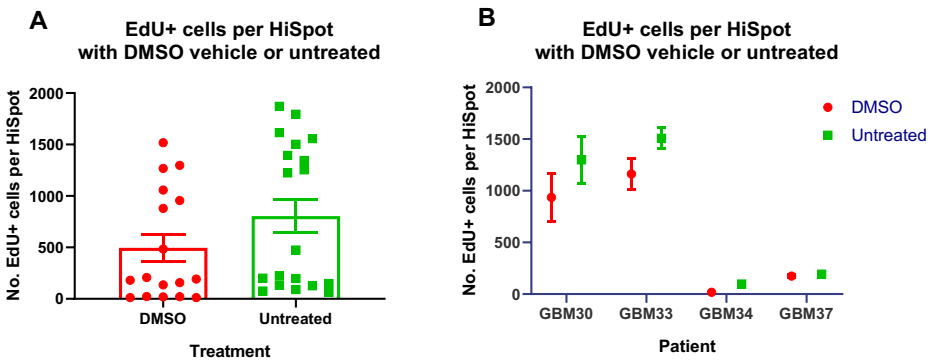

Figure 4-4: The effect of DMSO treatment on EdU+ cells.

For four patient samples (GBM30, 33, 34, 37), the number of EdU+ cells per HiSpot® is shown for DMSO treated HiSpots® (red circle) and untreated HiSpots® (green square). Data are shown grouped (A) and by patient (B). Data shown are mean ± SEM. n=3-5 for each patient and treatment combination. In B, error bars are not visible for patients GBM34 and 37 as they are smaller than the symbols used.

4.2.3.2 Edu levels are a predictive readout for TMZ response

HiSpots® from ten GBM patients (30, 31, 33, 34, 37, 38, 44, 45, 46, 49) were treated with a range of doses of TMZ, and a DMSO control (0 µM = shown as 10^{-10} M on the x-axis in figures). The other doses were 5 µM ($10^{-5.3}$ M), 50 µM ($10^{-4.3}$ M), 100 µM (10^{-4} M) and 500 µM ($10^{-3.3}$ M). TMZ was applied after a media change at 9 DIV. At 14 DIV, HiSpots® were treated with EdU and caspase-3 substrate for 4 hours before fixation. EdU uptake was detected and imaged as previously. When processed by apoptotic cells, the caspase-3 substrate fluoresces at wavelength 488 nm and so was detectable during imaging without further processing. Tile scan images were used for quantification of the levels of EdU+ and caspase-3+ nuclei in entire HiSpots® in the different TMZ treatment conditions (**2.9.1.3**).

Once pathology reports were available, two data sets were removed from analysis as they were diagnosed as LGG rather than GBM. These were patients 31 and 38. Therefore data were available for 8 patients.

Not all data sets were normally distributed according to a Shapiro-Wilk test. However, there is no non-parametric alternative for the two-way ANOVA so this test was still used for analysis. The two-way ANOVA showed a significant effect caused by the dose of TMZ ($F(4, 145) = 44.37$, $p<0.0001$, **Figure 4-5**), and significant variation between the GBM patients ($F(7, 145) = 104.2$, $p<0.0001$), and a significant interaction between the two ($F(28, 145) = 19.14$, $p<0.0001$).

Bonferroni's multiple comparisons test was performed comparing all doses to the DMSO control. The number of EdU+ cells in HiSpots® from patient GBM30 (***Figure 4-5 A)*** did not differ between 0 µM and:

- 5 µM TMZ *(936.3 ± 234.2 vs 1116.5 ± 205.5, p=0.0823, n=3-4)*

but did differ between 0μM and:

- 50 μM *(936.3 ± 234.2 vs 380.3 ± 80.86, p<0.0001, n=3-4)*
- 100 μM (*936.3 ± 234.2 vs 107.8 ± 29.75, p<0.0001, n=3-5)*
- 500 μM (*936.3 ± 234.2 vs 38.0 ± 14.99, p<0.0001, n=3-5)*

The number of EdU+ cells in HiSpots® from patient GBM33 (**Figure 4-5 A**) differed from the DMSO control (0 μM) at:

- 5 μM *(1163 ± 149.2 vs 631.2 ± 51.12, p<0.0001, n-4-5)*
- 50 μM (*1163 ± 149.2 vs 343.4 ± 50.63, p<0.0001, n=4-5)*
- 100 μM *(1163 ± 149.2 vs 292.0 ± 54.85, p<0.0001, n=4-5)*
- 500 μM *(1163 ± 149.2 vs 85.60 ±17.54, p<0.0001, n=4-5)*

EdU counts did not differ significantly for GBM34 (**Figure 4-5 B**) from the DMSO control (0 μM) at:

- 5 μM *(17.80 ± 2.059 vs 118.0 ± 60.34, p=0.4719, n=5)*
- 50 μM *(17.80 ± 2.059 vs 35.80 ± 8.54, p>0.9999, n=5)*
- 100 μM *(17.80 ± 2.059 vs 44.00 ± 13.52, p>0.9999, n=5)*
- 500 μM (*17.80 ± 2.059 vs 11.80 ± 3.813, p>0.9999, n=5)*

There were also no significant differences in EdU count for HiSpots® from patient GBM37 (**Figure 4-5 B**) from the DMSO control (0 μM) at:

- 5μM *(174.6 ± 12.77 vs 151.6 ± 7.396, p>0.9999, n=5)*
- 50 μM *(174.6 ± 12.77 vs 147.0 ± 8.556, p>0.9999, n=5)*
- 100 μM *(174.6 ± 12.77 vs 153.2 ± 8.828, p>0.9999, n=5)*
- 500 μM (*174.6 ± 12.77 vs 21.00 ± 5.840, p=0.0687, n=5)*

It is worth noting that this last comparison at the highest dose of TMZ trends towards a difference.

For HiSpots® from patient GBM44 (**Figure 4-5 B**), there were no significant differences between the DMSO control (0 μM) and:

- 5 μM (*13.67 ± 7.172 vs 4.000 ± 1.155, p>0.9999, n=3)*
- 50 μM (*13.67 ± 7.172 vs 4.750 ± 1.493, p>0.9999, n=3-4)*

- 100 µM *(13.67 ± 7.172 vs 6.250 ± 2.287, p>0.9999, n=3-4)*
- 500 µM (*13.67 ± 7.172 vs 10.40 ± 2.768, p>0.9999, n=3-5)*

There were no significant differences in the number of EdU+ cells for GBM45 between the DMSO control (0 µM) and:

- 5 µM *(38.60 ± 10.75 vs 33.20 ± 7.870, p>0.9999, n=5)*
- 50 µM (*38.60 ± 10.75 vs 20.60 ± 4.523, p>0.9999, n=5)*
- 100 µM (*38.60 ± 10.75 vs 21.80 ± 3.455, p>0.9999, n=5)*
- 500 µM (*38.60 ± 10.75 vs 9.600 ± 4.434, p>0.9999, n=5)*

The data indicate a downward trend with increasing TMZ (**Figure 4-5 A**).

EdU counts did not differ significantly for GBM46 from the DMSO control (0 µM) at:

- 5 µM *(9.667 ± 3.283 vs 17.25 ± 4.785, p>0.9999, n=3-4)*
- 50 µM (*9.667 ± 3.283 vs 18.75 ± 3.521, p>0.9999, n=3-4)*
- 100 µM *(9.667 ± 3.283 vs 36.20 ± 6.367, p>0.9999, n=3-5)*
- 500 µM *(9.667 ± 3.283 vs 117.8 ± 23.30, p=0.5752, n=3-5)*

The data indicate an upwards trend at the higher doses of TMZ (**Figure 4-5 B**).

GBM49 (**Figure 4-5 B**) EdU counts did not differ significantly from the DMSO control (0 µM) at:

- 5 µM (*31.40 ± 12.30 vs 14.00 ± 3.606, p>0.9999, n=5)*
- 50 µM *(31.40 ± 12.30 vs 3.600 ± 1.327, p>0.9999, n=5)*
- 100 µM *(31.40 ± 12.30 vs 13.60 ± 3.010, p>0.9999, n=5)*
- 500 µM *(31.40 ± 12.30 vs 22.00 ± 6.348, p<0.9999, n=5)*

Dose-response relationships for HiSpots® from all patients are shown in **Figure 4-5**. Pathology reports showed GBM30, 33 and 45 to have methylated *MGMT* promoters (**Figure 4-5 A**). Patients GBM34, 37, 44, 46, and 49 had unmethylated *MGMT* promoters (**Figure 4-5 B**). Overall, all patients which showed significant responses (25%) had *MGMT* methylation, but not all patients with *MGMT* methylation (37.5%) showed a significant response. No patients with unmethylated *MGMT* (62.5%) responded significantly to TMZ treatment.

A chi-squared analysis was performed to determine the correlation between patient methylation status and the response of HiSpots® to TMZ according to the number of EdU+ cells. A significant association was found between methylation status and HiSpot® response (Chi-square=4.444, p=0.0350, sensitivity=0.6667, specificity=1.000, z=2.108, n=8, **Table 4-5**).

Figure 4-5: The effect of TMZ treatment on EdU+ cells per HiSpot®.

*The number of EdU+ cells per HiSpot® after treatment with a range of TMZ doses for 8 patients. Data shown are mean ± SEM. **** p<0.0001. Dose-response relationships are shown in both graphs. N=3-5 for each patient per dose. 0 µM TMZ (DMSO vehicle control) is shown as 10^{-10} on the x-axis. Y-axes are consistent between graphs for comparison.*

*A: Data are shown from HiSpots® created from patients **with** MGMT promoter methylation. GBM30 (pink) shows a high initial EdU count which decreases significantly with increasing TMZ dose from 5 µM upwards. GBM33 (orange) also shows a high initial EdU count which decreases significantly with increasing TMZ dose. GBM45 (blue) shows a low initial EdU count which does not change significantly with increasing TMZ dose.*

*B: Data are shown from HiSpots® created from patients **without** MGMT promoter methylation. GBM34 (green) shows a low EdU count with a slight non-significant uptick at 5 µM. GBM37 (blue) shows a relatively low EdU count which remains steady until it drops at 500 µM. GBM44 shows a very low EdU count which does not change with increased TMZ dose. GBM46 shows a very low EdU count which is steady until a slight uptick at 500 µM. GBM49 shows a very low EdU count which does not change with increased TMZ dose.*

A

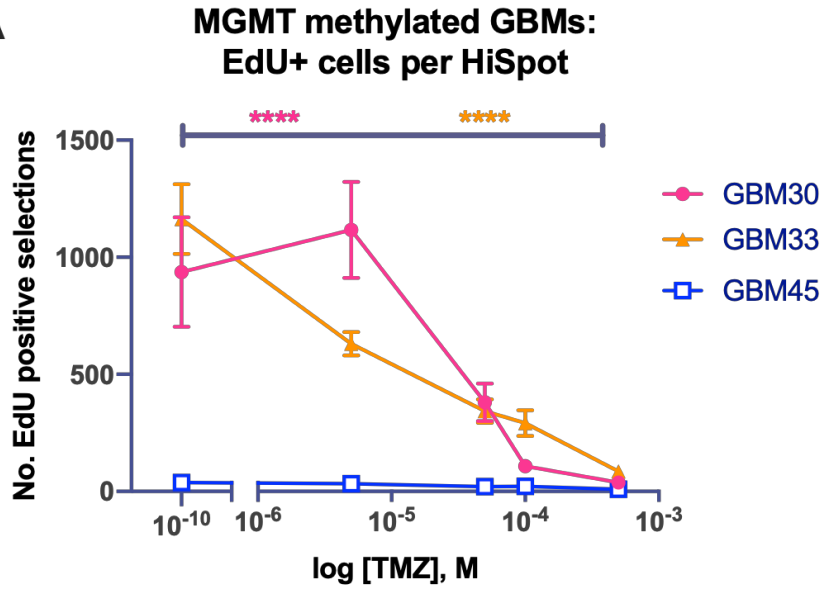
MGMT methylated GBMs:
EdU+ cells per HiSpot
****
****
No. EdU positive selections
1500
1000
500
0
10-10
10-6
10-5
10-4
10-3
log [TMZ], M
GBM30
GBM33
GBM45

B

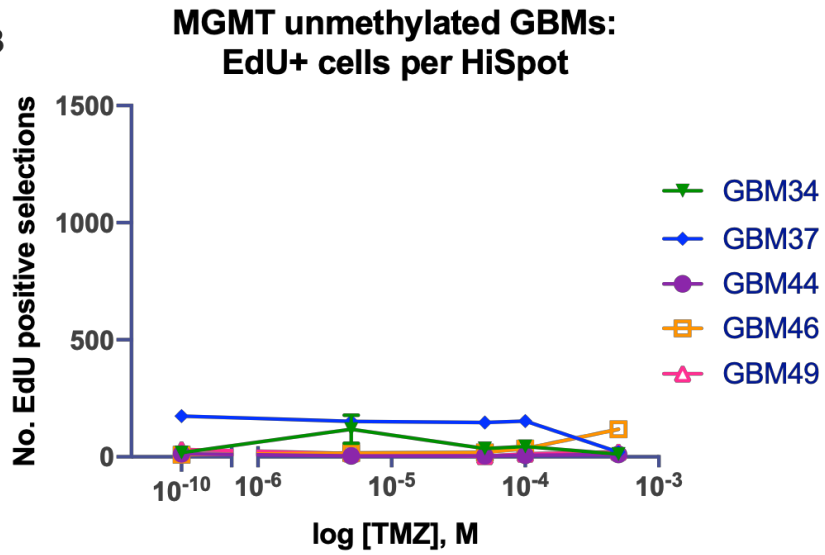
MGMT unmethylated GBMs:
EdU+ cells per HiSpot
No. EdU positive selections
1500
1000
500
0
10-10
10-6
10-5
10-4
10-3
log [TMZ], M
GBM34
GBM37
GBM44
GBM46
GBM49

Table 4-5: Chi-squared analysis of TMZ response (EdU+ cells).

Data used for a chi-squared test are shown. Patients were categorised as responders if they demonstrated a significant decrease in EdU+ cells with increasing TMZ treatment. Pathological data categorised patients as either having a methylated or unmethylated MGMT promoter.

HiSpot® response to TMZ (EdU)	*Methylated*	*Unmethylated*
Responder	2	0
Non-responder	1	5

4.2.3.3 Caspase-3 levels are not predictive of TMZ response

The number of caspase-3 positive cells was measured per HiSpot® for 6 patients. The data set from one patient (GBM38) was removed before analysis, as it was confirmed to be a LGG, not a GBM. These data sets were normally distributed according to a Shapiro-Wilk test. A two-way ANOVA showed no significant effect of the TMZ dose ($F(4, 89) = 0.7990$, $p=0.5290$, **Figure 4-6**) or interaction ($F(16, 89) = 1.385$, $p=0.1676$), but did show that the patients were significantly different from each other ($F(4, 89) = 19.03$, $p<0.0001$). There was an upwards trend in the number of caspase-3+ cells per HiSpot® for patient 33, which had a methylated *MGMT* promoter as mentioned above. Individual dose-response relationships are visible in **Figure 4-6** for HiSpots® from methylated MGMT promoter patients GBM33 and GBM45 (**A**), and unmethylated MGMT promoter patients GBM34, GBM37 and GBM44 (**B**). As no HiSpots® from any patients showed a significant change in caspase-3+ cells with TMZ treatment, it was not possible to perform a chi-squared analysis to determine the correlation between patient methylation status and the response of HiSpots® to TMZ according to the number of Cas3+ cells. The chi-squared test requires at least one responder to determine associations.

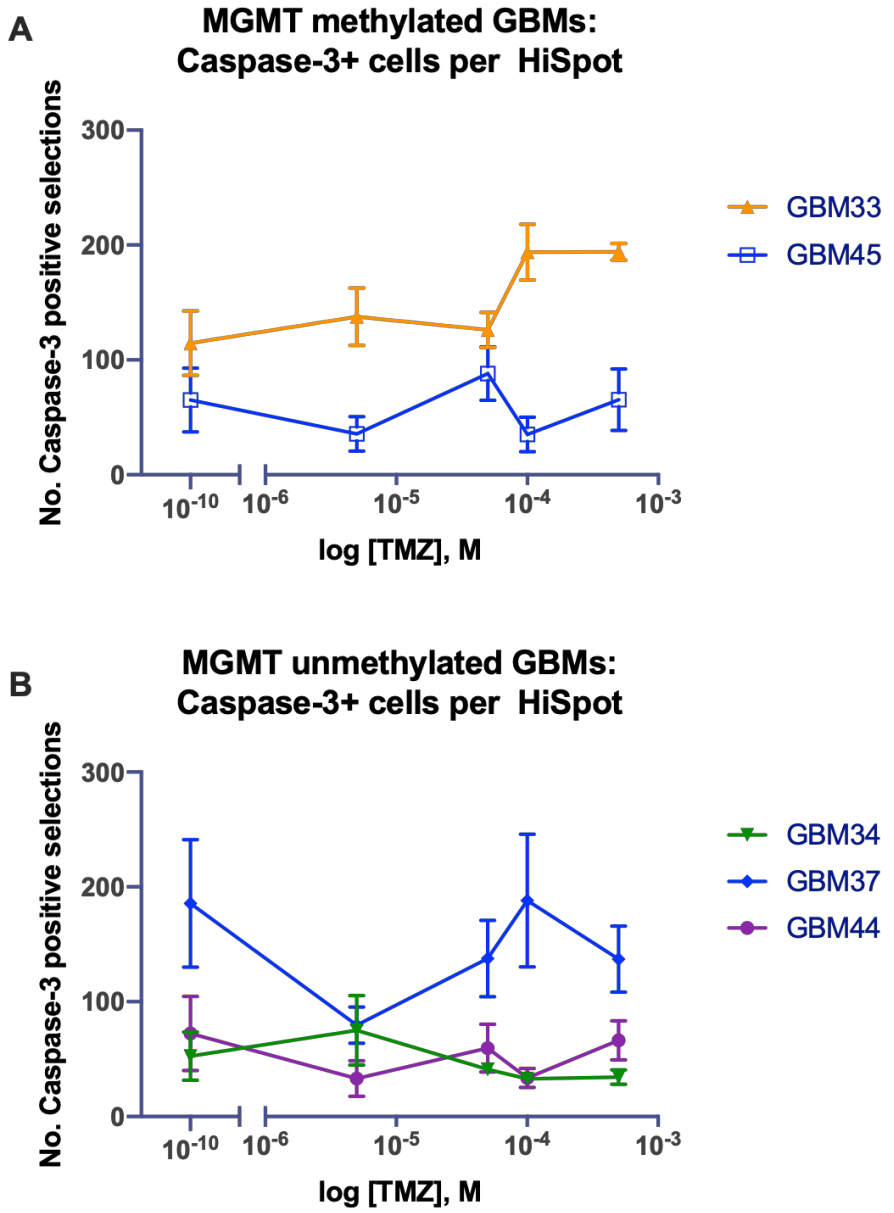

Figure 4-6: The effect of TMZ treatment on caspase-3+ cells per HiSpot®.

The number of caspase-3+ cells per HiSpot® after treatment with a range of TMZ doses for 5 patients. Data shown are mean ± SEM. N=3-5 for each patient at each dose. 0 µM TMZ (DMSO vehicle control) is shown as 10^{-10} on the x-axis. Dose-response relationships are shown in both graphs.

*A: Cas3+ cell count data are shown from HiSpots® created from patients **with** MGMT promoter methylation. GBM33 (orange) shows a steady cas3 count from 0 µM to 50 µM TMZ, then a non-significant increase between 50 and 100 µM. The count is then steady again to 500 µM. GBM45 (blue) shows a non-significant fluctuation in cas3 count with increased TMZ dose.*

*B: Cas3+ cell count data are shown from HiSpots® created from patients **without** MGMT promoter methylation. GBM34 (green) shows a relatively steady cas3 count with increased TMZ dose. GBM37 (blue) shows a high initial cas3 count, and is highly variable over the range of TMZ doses, with a particularly low count at 5 µM. GBM44 (purple) shows a relatively steady cas3 count with increased TMZ dose.*

4.3 Discussion

4.3.1 HiSpots® replicate pathological features of GBM

4.3.1.1 Study patients are representative of the wider population

For any study using primary patient tissue, it is important to know whether the patients from whom tissue is collected are representative of the wider patient population for the disease. Data relevant for comparison to HiSpots® was collated for **Table 4-1**. This includes age, sex, *MGMT* methylation status and *IDH-1* mutation status.

The median age for primary GBM presentation is ~62 years (Reitman *et al.* 2018). The median age of patients with confirmed GBM from whom tissue was collected for this study was ~63. This did include one secondary GBM but this did not affect the median age. The GBM patient population from whom tissue was collected had more males than females, with a ratio of 4:3. A higher incidence has been generally reported in men than women for GBM (Philips *et al.* 2018). Both the age and sex distributions of the study population are very similar to reported averages and hopefully therefore representative of the overall GBM population.

Approximately 48% of the GBMs collected for this study had a methylated *MGMT* promoter, and 36% unmethylated, although data were unavailable for remaining patients (16%). This is comparable to the 45% of 206 patients found to have a methylated *MGMT* promoter by Hegi *et al.* (2005). *IDH-1* R132H mutations are only found in ~10% of GBMs, and in this study only one confirmed GBM patient had the *IDH-1* R132H mutation, although two other patients were categorised as other grades of glioma (Louis *et al.* 2016). This lower percentage may have been a result of the small sample size, or simply chance. For further research, it would be worth aiming to collect more *IDH-1* R132H mutants, allowing for the comparison of various features and behaviours between primary and secondary GBMs.

Ki-67% is used to guide diagnosis, but is not considered definitive enough to be the only diagnostic factor to define GBM (Skjulsvik *et al.* 2014). The median levels of Ki-67 staining have been reported at around 20%, but have a vast range from 2.2% to 80% (Skjulsvik *et al.* 2014; Wong *et al.* 2019). Due to differences in reporting measures, it was not possible to determine a median Ki-67% for this study, but levels ranged from <1% to >70% in all patients, and from ~15% to >70% in those with a confirmed GBM diagnosis, which aligns with other studies. It is important to note that it is usually the highest level of Ki-67 positivity which is reported (e.g. up to 30%).

GFAP immunostaining is an important marker for the diagnosis of brain tumours. Its key role is in distinguishing gliomas (usually GFAP+) from metastases (GFAP-). In combination with CAM5.2 (gliomas negative, metastases positive), the two tumour types can be distinguished, despite their similar appearances on imaging (Goyal *et al.* 2015). However as noted in **1.1.3.2**, GFAP positivity can vary in GSMs due to the biphasic nature of the tumour, which could lead to some biopsies being entirely GFAP negative if they are predominantly the sarcomatoid area of the tumour, despite being a variant of GBM (Romero-Rojas *et al.* 2013).

Approximately 1% of all GBMs are giant cell GBMs, and 2% are GSMs, although some studies have found a higher proportion (Kozak and Moody 2009; Oh *et al.* 2016; Zhang *et al.* 2016). In this study, two patients were clearly recorded as being giant cell GBMs, with a further two noted to have large or multinucleated cells. Two patients were diagnosed with GSM, with a further two patients recorded as having some sarcomatoid features. These indicate a slightly larger percentage of presentation than may be expected, but it is difficult to draw conclusions from such a small sample of GSMs. There is also a chance that now GSMs and giant cell GBMs are recognised variants, they are more likely to be recorded as such, rather than as just a description of the phenotype. Overall, the patients from whom tissue was collected as part of this study seem to be mostly representative of the general GBM population. However, it is important to determine whether

these features are replicated on a patient-specific basis in HiSpot® cultures. A small number of pathological reports and histological images were collated for comparison to HiSpots® cultured from the same patients and are presented alongside comparative data for available post-optimisation HiSpots®.

4.3.1.2 Ki-67 levels show patient-matched correlation with histological data

EdU data is shown for all available HiSpot® patients from GBM28 onwards alongside pathological reports from the same patients. Many of the patients have correlating levels of proliferation (high, medium, low) between the pathological reports and HiSpots®, with 50% directly matching. However, this is a qualitative analysis only. Most of the remaining patients are only one level apart, which highlights that different cut-off points may have yielded different results. Ki-67 data were not available for these HiSpots® due to poor antibody penetration, but future work should aim to independently quantify the growth fraction for each patient and plot the pathological report data against HiSpot® data to better determine the correlation between the two.

Comparative histological images were requested for four patients: 30, 37, 38 and 39 (**Figure 4-1**). Although only qualitative comparisons are shown, there are stark differences between the patients and these varying levels of proliferation are matched in the HiSpot® cultures. The extremely low levels in patient 38 (**Figure 4-1G**) are visible in both images. Although this patient was eventually diagnosed as a gemistocytic astrocytoma, the percentage of Ki-67 reported (5%) is within the reported ranges from other studies for GBM (Skjulsvik *et al.* 2014; Wong *et al.* 2019). This low proliferation did not affect the ability of the tumour cells to reaggregate in the HiSpot® model, demonstrating that the system is capable of supporting other glioma types than GBM.

HiSpots® from patient GBM37 (**Figure 4-1F**) show some focal positivity for EdU, matching the Ki-67% closest to recorded median levels for GBM. The

HiSpot® image from GBM37 also demonstrates the focal growth seen in certain patients. This growth could potentially be caused by the medium level proliferation, if the foci grow as a result of a small group of highly proliferative cells, or if these cells are more likely to survive the cell isolation process. In future experiments, it would be interesting to determine whether the proliferation levels noted by the pathologist affect the growth pattern of the HiSpots®, or whether this is affected by another factor such as tumour subtype. Future work could investigate the HiSpot® growth patterns by fixing HiSpots® at multiple timepoints throughout the culture period and analysing cell number and proliferation levels.

Patients 30 and 39 (**Figure 4-1E, H)** show higher levels of staining in both histology (Ki-67) and HiSpot® (EdU) images. The HiSpot® images for these patients in particular demonstrate why it was difficult to obtain quantitative data for the proliferation percentage, as they have multiple layers of overlapping nuclei, and the magnification required to distinguish individual cells would have limited the detection of EdU+ cells due to very small image fields. These four patients demonstrate that HiSpots® are capable of representing the varying levels of proliferation within GBMs, and that this feature which may affect tumour development or response to treatment is not lost as a result of transferring the tumour cells to the HiSpot® model.

Proliferation levels are regularly investigated for the validation of GBM models. Ki-67 is a commonly used marker as it is used in standard pathological staining, and correlates with tumour grade in gliomas (Skjulsvik *et al.* 2014). Smith *et al.* (2012) found similar levels of Ki-67 staining between patient pathology and their 3D GBM rotary cell culture model. EdU has also been used to analyse proliferation levels in 3D models (Xiao *et al.* 2018). Both Ki-67 and EdU are useful indicators of proliferation levels in GBM models (Welker *et al.* 2017; Linkous *et al.* 2019). Therefore EdU provides a useful method for the analysis of proliferation levels in the HiSpot® model. However it is important to reiterate that EdU+ cells only represent a

subpopulation of the total growth fraction (Ki-67+/DAPI) and will therefore underestimate the total proliferation levels of the patient tumour.

4.3.1.3 GFAP immunoreactivity levels correlate with patient-matched histological data

The levels of GFAP immunoreactivity in GBMs vary but are reported in a qualitative manner noting whether positivity is present, universal, or limited to specific cell types or areas. A complete absence of GFAP is very rare in GBM, but can occur in GSM, in the sarcomatoid area of the bisphasic tumour (Beaumont *et al.* 2007; Oh *et al.* 2016). This is replicated in the HiSpot® model, as demonstrated by patient GBM28, which was diagnosed as a GSM. The HiSpot® image clearly shows that GFAP staining is extremely rare in this patient (**Figure 4-2E**), and is in clear contrast to the otherwise normal GBMs 36 and 40, which show dense GFAP positivity in both the histological images and the HiSpots® (**Figure 4-2B, C, F, G**). There is still some variation between the patients, clearest in the HiSpot® images for these two GBMs, although the histological images perhaps indicate a difference in cellular organisation. In addition to general patient variation, it is possible that these patients are representative of different GBM subtypes or different tumour areas. Future HiSpot® analysis could investigate the range of GFAP immunoreactivity within the HiSpots® to clarify what a standard level of positivity is. GBM46 (**Figure 4-2D, H**) interestingly seems to lie between the mostly negative GSM and the mostly positive GBMs, demonstrating patchy GFAP positivity and noted squamoid features, which could indicate the tumour is developing towards a GSM. These features are also visible in the HiSpot® image, which shows far more GFAP+ cells than the HiSpot® image from patient 28, but less than the other GBMs.

The interwoven cells and high density of GBM40 (**Figure 4-2G**) demonstrate the difficulty of accurately quantifying GFAP positivity in these HiSpots®, and without quantitative histological data to compare to, this would have still required sorting the patients into categories for comparison. However, it is

clear that the variations of GFAP reactivity noted in the pathological reports are being replicated in patient-matched HiSpots®.

Many models use GFAP positivity to confirm tumour development or location as GBM tumours are usually highly positive for this marker. Its use has been demonstrated in zebrafish (Welker *et al.* 2017), mouse (Jun *et al.* 2018) and 3D *in vitro* models (William *et al.* 2017; Akay *et al.* 2018). It is used diagnostically along with CAM5.2 to differentiate between glial tumours and metastases from other sites (Goyal *et al.* 2015).

4.3.1.4 Giant cells are reproduced in HiSpots® from giant cell GBMs

Giant cell GBM is a recognised variant of GBM, which contains *"bizarre, multinucleated giant cells"* (Louis *et al.* 2016). The presence of giant cells was noted in the pathology reports for patients 33 and 36 and were also detectable in the matched HiSpots® (**Figure 4-3D, E**). In the histology image from patient 33, the arrows indicate very large, round nuclear staining. The same shape is visible with DAPI staining in the matched HiSpot® image. In comparison, the histology image for patient 36 shows less uniform nuclear staining, which more clearly indicates multiple nuclei compressed together in one cell. This is also clear in the HiSpot® image, as the large nuclear staining has a rougher edge, more indicative of multiple nuclei than one singular, large nucleus. Patient GBM40 was used as a negative control, as no giant cells were reported present and the HiSpot® image shows uniform nuclei throughout (**Figure 4-3F**). This demonstrates that HiSpot® cultures can support the definitive giant cells from this GBM variant. As giant cell GBM is a rare variant, the HiSpot® model could provide an excellent platform for investigating these giant cells and their interactions with other cell types in the tumour.

4.3.2 HiSpots® can be used as a model for GBM treatment response

4.3.2.1 DMSO vehicle should be used as a baseline comparison for TMZ experiments

In order to be delivered to the cells precisely, TMZ must be dissolved in a solvent such as the commonly used DMSO. Although this is delivered at the same concentration to every well, it is important to establish whether DMSO has any effect on the cells independently of any added TMZ. HiSpots® treated with DMSO at the concentration to be used with TMZ were compared to untreated HiSpots®. EdU+ cells were detected as a readout as this was also used as a readout for the TMZ analysis.

The data did not show a significant difference between DMSO treated and untreated HiSpots® from any patients, either when grouped, or analysed by patient (**Figure 4-4**). To maintain consistency between TMZ doses, the decision was made that a DMSO control should be used for comparison to other TMZ doses. All TMZ doses were made up to the same DMSO concentration, ensuring that any effect of the DMSO vehicle was constant over all TMZ doses, and would not create false positive responses.

4.3.2.2 Proliferation levels in HiSpots® respond to TMZ treatment in patients with MGMT promoter methylation

To avoid any confounding behaviour, patients which were later diagnosed as LGG (31, 38) were eliminated from analysis for TMZ response. The dose range for this experiment was selected to provide a logarithmic dose-response curve, correlating with similar doses used in other 3D *in vitro* experiments (Yang *et al.* 2014; Akay *et al.* 2018; Linkous *et al.* 2019). In hindsight, another higher dose may have been useful to further establish the sensitivity of the HiSpots® to TMZ. Additionally, it is important to keep in mind that the use of EdU incorporation to monitor proliferation levels is not necessarily an ideal readout for drug response. EdU incorporation may increase during DNA repair, which could affect the readout from HiSpots® which are damaged by TMZ but subsequently recover, for instance if they

have unmethylated *MGMT* promoters and can therefore repair DNA damage (Verbruggen *et al.* 2014).

HiSpots® from patient GBM30 (**Figure 4-5A**) showed a small, non-significant increase with the lowest TMZ dose, followed by a significant dose-dependent decrease in EdU+ cells with increasing TMZ. This suggests a response to treatment, as a reduction in cycling cells overall would be represented by a reduction in S-phase entry (and EdU incorporation). This would result in EdU levels being reduced significantly, to almost absent at the highest dose. GBM33 (**Figure 4-5B**) responded similarly, showing a dose-dependent reduction in proliferation to almost zero proliferation at the 500 µM dose. These patients were both recorded as having *MGMT* promoter methylation, which indicates sensitivity to TMZ. Therefore, the HiSpot® responses for these patients align with the expected patient responses. Patient GBM45 (**Figure 4-5F**) was also recorded as having *MGMT* promoter methylation, but did not show a significant response to TMZ at any dose. However, there is a clear downwards trend in the data, which may indicate that a response may have been detectable with a higher number of HiSpots® (better experimental power), or if the patient had a higher baseline proliferation. In comparison to the other methylated patients, with baseline EdU+ cell numbers around 1000 per HiSpot®, patient 46 only had ~40 EdU+ cells per HiSpot®. It is possible that a minimum baseline proliferation level is required to detect a response in HiSpots®, and that perhaps the treatment timeline could be altered slightly in order to start treatment at a similar baseline for each patient. However, low proliferation levels may simply be a feature of the specific tumour. A longer EdU exposure time may allow a larger proportion of cycling cells to be detected, increasing the detectable baseline levels. Interestingly, the pathology reports noted Ki-67 levels of 'up to 50%' and 60% for patients 30 and 33 respectively, but only 30% for patient 45. This could explain why the baseline levels of proliferation were so different between the HiSpots® from the different patients and indicates

that pathological information could be used to guide the optimisation of the HiSpot® for the prediction of treatment response.

Patients 34, 37, 44, 48 and 49 (**Figure 4-5C, D, E, G, H**) were all recorded as having unmethylated *MGMT* promoters, and did not show a significant response to TMZ treatment in HiSpots®. This aligns with the predicted patient response for each. There were however some interesting trends in the response, rather than consistent data sets across each dose. GBM34 (**Figure 4-5C**) showed a very large level of variation at the lowest dose, which may indicate that some HiSpots® compensated for the low-level damage with an increase in proliferation. It is possible that an increasing trend in proliferation with treatment represents a recovery of tumour cells after damage.

In breast cancer, it has been demonstrated that radiation treatment can trigger de-differentiation of tumour cells to CSCs, which then proliferate to repopulate the tumour (Lagadec *et al.* 2012). William *et al.* (2018) discussed a similar phenomenon with temozolomide treatment in GBM cells and demonstrated that two cycles of 72 hour TMZ treatment were sufficient to increase tumorigenicity in patient-derived lines. It is important to note however that these lines were cultured in media containing 10% foetal calf serum, which is known to affect the CSC population. It is possible that the increased trend in HiSpot® proliferation with increasing TMZ dose represents the activation or formation of a CSC population.

GBM37 (**Figure 4-5D**) showed no significant responses, but the highest dose showed a reduction in overall values compared to the other doses. This may indicate that only the 500 µM dose, far higher than would normally reach the tumour, would be damaging, but lower levels would not affect the tumour. Although the difference between control and 500 µM was not significant, it was close to significance (0.0687) so may have been noted as significant with a less stringent post-hoc test than Bonferroni's multiple comparisons. HiSpots® from patient GBM44 showed high variability at the DMSO control, which may have affected the ability to detect any differences

later on. There is some indication of a trend upwards with increasing dose from 5 µM to 500 µM. A more extreme trend upwards with dose is seen in HiSpots® from patient GBM46 (**Figure 4-5G**), show a very low baseline proliferation level, that trends upwards at the 100 µM and 500 µM doses. HiSpots® from patient GBM49 (**Figure 4-5H**) show a large variability and no clear trend in any direction.

Overall, the only patients which showed a clear, dose-dependent response to TMZ both had *MGMT* promoter methylation, and the only other methylated patient shows a non-significant trend downwards, indicating some level of response to the drug. Some unmethylated patients showed a trend towards increasing proliferation with treatment, which may indicate that TMZ is not just ineffective in these patients, but could potentially have pro-tumour effects due to DNA repair in damaged cells, or a hormetic effect. A chi-squared analysis found a significant correlation between patient *MGMT* methylation status and HiSpot® response (EdU levels) to TMZ. Although this was based on a small number of patients (n=8), it supports the HiSpot® as a predictive model for *MGMT* status and expected TMZ response.

Comparisons here have been based on genetic analysis of *MGMT* to predict patient response. It would be of great interest to compare the patients' clinical response to TMZ treatment, to see if this aligns with the response expected by *MGMT* methylation status, and predicted by the HiSpot® model.

4.3.2.3 Treatment-induced levels of apoptosis are not detectable

When TMZ is effective in damaging cancer cells, the cells eventually die via apoptosis (Zhang *et al.* 2012). Although an antibody to cleaved capsase-3 was available, this required two further days of incubation and wash steps after EdU detection. In order to try and reduce signal loss over this time, the Nucview caspase-3 substrate was selected as an alternative. The substrate had been demonstrated to work well in spheroid cultures, so the 3D structure of the HiSpots® was not considered a limitation for the use of this

product (Cheng *et al.* 2009). It was also possible to add the substrate with the EdU for a four hour incubation, which it was hoped would capture a larger percentage of the apoptotic cells within the HiSpot® than possible with an antibody for cleaved caspase-3, as well as reducing the possibility of signal loss. Unfortunately, no significant differences were detected using the caspase-3 substrate (**Figure 4-6**). As HiSpots® from patients 34, 37, 44 and 45 and did not show any significant changes in proliferation, it is possible that there were no changes in apoptosis to be detected. However, it is possible that these HiSpots® instead responded to TMZ treatment with an increase in apoptosis and that this was not detected using this method. However, HiSpots® from the *MGMT* methylated patient 33 (**Figure 4-6 A**) did show a significant decrease in proliferation, so would be predicted to be matched by an increase in apoptosis demonstrated by caspase-3 levels. There is an upwards trend at the higher doses of TMZ (100 µM, 500 µM) but these changes are not significant. It is possible that high levels of variability or noise in the HiSpots® affected the ability of the test to detect statistical significance. This indicates that the caspase-3 readout could potentially be used to detect treatment response but will require some optimisation before it can be used reliably. There is also a possibility that the peak changes in proliferation and apoptosis would not appear at the same time. Potentially, the ideal readout for proliferation levels would be 5 DIV after treatment, as used in this experiment and in accordance with (Zhang *et al.* 2012), but that for apoptosis it would be much earlier. It would be useful to establish this using a time-course experiment in future research. Ideally, HiSpots® would be live-imaged over the treatment course, but at the moment this is not possible with EdU use for the detection of proliferation, as this requires the cells to be fixed. Longer or repeated TMZ exposure may also lead to larger responses, more able to reach significance despite the variability of caspase-3 levels. Repeated TMZ exposure would align more closely with the clinical course of treatment, where patients receive TMZ regularly over many months. However, it would be important to determine

the dose and spacing of these treatments in order to most accurately represent the clinical treatment regime.

Overall, it seems that the HiSpot® proliferation readout using EdU can be used to detect patient response to TMZ, but that false negatives are possible with low-proliferating tumours. For further experiments, the 100 µM dose will be used to detect responders (such as patients 30 and 33), but not patients such as 37 which did not show a dose-dependent response.

4.3.3 Chapter conclusions

The HiSpot® model can recapitulate a range of features from a representative population of GBM patients. It demonstrates a range of Ki-67 levels and differences in GFAP positivity with sarcomatoid patients. Both Ki-67 and GFAP are commonly used in the validation of GBM models, although not always with patient-specific comparison. Interestingly the HiSpot® was also noted to replicate the presence of giant cells where these were reported in pathology reports. This rare subtype of GBM is still poorly understood but provides an increased overall survival to other GBM, so it is important to determine that this subtype can be modelled and its features maintained (Kozak and Moody 2009). The HiSpot® model has also been demonstrated to distinguish between patient-specific responses to TMZ, highlighting its potential for development as a pharmaceutical model for GBM.

5 HiSpot® and Tumour Heterogeneity

5.1 Introduction

5.1.1 Intra-tumour heterogeneity

GBM is well-known for its inter- and intra- tumour heterogeneity (Sottoriva *et al.* 2013). This is one of the biggest challenges in both modelling and treating the disease. Although there are differences in tumour presentation between patients, the variations, particularly in treatment sensitivity, within an individual tumour create a difficult challenge for identifying treatment options, either clinically or in research.

Structural heterogeneity is clearly visible in the presentation of GBM on MRI or CT scans. With the administration of gadolinium as a contrast-enhancing agent, the tumour will usually be visible as a ring of enhancement around a darker mass. The contrast-enhancing area is a result of the leaky vasculature at the tumour edge. The tumour will extend cells beyond this enhancement, into the brain, which contributes to its inevitable recurrence (Claussen *et al.* 1985; Persano *et al.* 2011; Zhou and Lu 2013).

The differences in appearance between these areas also indicates a difference in microenvironment. The core of the tumour often contains necrotic tissue, with poor vascularisation and relative hypoxia. It is also proliferative and highly positive for markers of stemness such as nestin and CD133 (Pistollato *et al.* 2010; Persano *et al.* 2011). The contrast-enhancing area is less hypoxic, with better access to the vasculature. The cells in this area have less expression of stem cell markers, and increased expression of markers of more differentiated cells such as neuronal β-IIIT and astrocytic GFAP (Pistollato *et al.* 2010; Persano *et al.* 2011). Models also describe an intermediate area between the two, which is a transitional area between the contrast-enhancing and necrotic areas on standard MRI imaging (Pistollato *et al.* 2010; Persano *et al.* 2011). A representation of this is shown in **Figure 5-1**.

Given the spectrum of radiological appearance and cellular expression patterns, it is important to characterise the phenotypes and treatment sensitivities of different tumour areas separately. It is possible that the more differentiated cells of the outer edge of the tumour will be sensitive to a treatment to which the less differentiated cells of the core will be resistant, or vice versa (Persano *et al.* 2011). Any variations in treatment sensitivity can lead to surviving populations of cells which develop into a recurrent tumour. As GBMs inevitably recur, there are obviously still great strides to be made in predicting treatment response and developing treatments which are more successful. It is also important to recognise differences in biopsy area when investigating new treatments, especially as the core of the tumour is normally removed, but recurrence still occurs. Although there are many CSCs in the core of the tumour, these are usually removed during surgery, so it is more likely that the fewer CSCs which are closer to the healthy brain, in areas such as the perivascular niche, are the ones which recur (Chen *et al.* 2012; Codrici *et al.* 2016). Therefore it is essential to assess the sensitivity of these CSCs to treatment, especially given that they will be in a very different microenvironment to those in the core (Pistollato *et al.* 2010; Persano *et al.* 2011). A hypoxic gradient has been demonstrated in GBM, with the highest oxygen availability at the edge of the tumour, and the lowest in the core (**Figure 5-1**, Pistollato *et al.* 2010). Hypoxia has been demonstrated to reduce sensitivity to radiation (Sheehan *et al.* 2010), and promote chemotherapy resistant CSCs (Soeda *et al.* 2009; Chen *et al.* 2012). Other features of the microenvironment such as the presence of microglia have also been shown to vary between the core and edge of the tumour, and are known to support tumour growth and invasion, and in some cases drug resistance (Komohara *et al.* 2008; Kaffes *et al.* 2019).

In addition to the differences between the inner (core) and outer (contrast-enhancing) tumour, there are differences between other spatial areas of the tumour. As the tumour develops from an initial population, it accumulates mutations. These mutations can provide treatment resistance or produce

different subtypes and phenotypes. Eventually, this can lead to the tumour containing multiple subclones, each with different characteristics (Sottoriva *et al.* 2013).

For all these reasons, GBM becomes an extremely complex disease to accurately model. Certain aspects such as the effect of microglia or 3D cellular interactions are often absent in published models, and additional factors such as serum exposure can permanently alter the phenotype of the tumour cells *in vitro*. In an attempt to circumvent this regional heterogeneity by sampling different areas of the same tumour, it may be possible to determine how these regions differ in phenotype, cellular activity, and treatment response. This could enable a more biologically strategic approach to developing new treatments, such as those that target the cellular response to hypoxia, to be tested on and targeted to specific tumour areas (Yang *et al.* 2012).

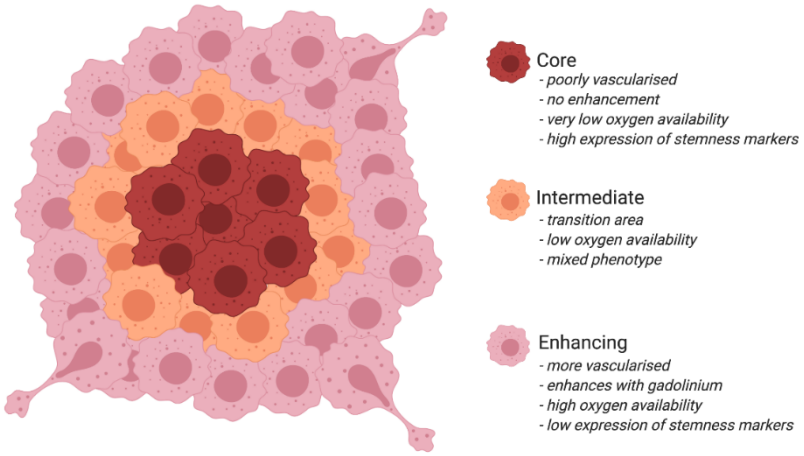

Figure 5-1: Regions of GBM.

A representation of the different depths of a GBM tumour are shown. The core (red) cells are in the centre, surrounded by the intermediate cells (orange), which are in turn surrounded by the contrast-enhancing cells (pink). Key features of the different cell regions are described. Figure adapted from Persano *et al* (2011).

5.1.2 Chapter aims

The experiments in this chapter aim to characterise the differences between HiSpots® produced from different patients and biopsy locations within the same tumour examining cell numbers, types, and distributions, and individual cell morphologies. The response of the HiSpots® to temozolomide treatment will also be measured. Finally, in an attempt to capture the regional heterogeneity of the whole tumour, "pan-tumour" HiSpots® will be generated from a combination of cells from two different biopsy sites, to determine whether these combined HiSpot® cultured recapitulate features from one or both constituent site-specific biopsies. If successful this may present substantial advantages for drug testing over conventional single biopsy site *in vitro* models.

5.2 Results

HiSpots® were created from multiple biopsies from five patients (see **Chapter 2** for details of biopsy identification). Biopsies from the tumour core and contrast-enhancing rim were collected from patients GBM39, 40, 41, and 47. An additional peripheral biopsy (beyond the contrast-enhancing rim) was collected from patient GBM39. Due to the presence of a large cyst, it was not possible to identify the original locations of the biopsies from patient GBM46, but two biopsies (A and B) were collected from distinct and separate areas of the tumour mass. Relevant patient and pathology report data (from **Table 4-1**) are reiterated in **Table 5-1** below.

Table 5-1: Pathological data for patients used for multiple biopsy experiments.

A reiteration of data from Chapter 4, showing only patients relevant to this chapter: 39, 40, 41, 46, 47.

Patient	*Male/ Female*	*Age at presentation*	*Diagnosis*	*MGMT (M/U)*	*IDH-1 (MUT/ WT)*	*Ki-67%*	*GFAP*	*Key features*
39	M	67	GBM	U	WT	40%	Positive	-
40	M	52	GBM	U	WT	30%	Positive	-
41	F	66	GBM	M	MUT	40%	Some positive, many negative	-
46	M	66	GBM	U	WT	Up to 25%	Patchy positivity	Epithelioid and squamoid features
47	M	66	GBM	U	WT	Up to 30%	Positive	-

5.2.1 Inter- and intra- patient variability in HiSpot® cell levels

Whole HiSpot® tile scan images were taken from many different patient and biopsy sources. The total area fluorescence intensity was measured for each image (mean pixel intensity x area (mm^2)). This value gives an indication of the relative number of cells within HiSpots®. This can be used to determine whether the variability seen in HiSpots® stems from a patient, biopsy area, or HiSpot® model source. Total area fluorescence intensity is relatively consistent within HiSpot® repeats, as can be seen as individual HiSpot® scatter points from each patient or biopsy origin (**Figure 5-2**) but varies greatly between patients (mean ± SEM, **Figure 5-2**). There is significant variation between HiSpots® from different patients (7883 ± 256.0 vs 5311 ± 160.3 vs 6718 ± 698.6 vs 3000 ± 359.2 vs 1091 ± 60.28 vs 2323 ± 239.9 vs 2053 ± 77.03 vs 2904 ± 130.0 vs 7035 ± 395.4 vs 7794 ± 343.4 vs 4797 ± 395.2 vs 4313 ± 272.2 vs 5005 ± 167.4 vs 3950 ± 736.8 vs 2212 ± 233.8, 7032 ± 125.9 vs 1466 ± 437.8 vs 1614 ± 455.3 n=84 from 18 patients or biopsies, Kruskal-Wallis test, **Figure 5-2**). Due to this high inter-patient variability, and small patient numbers, further data in this chapter will be examined independently for each patient.

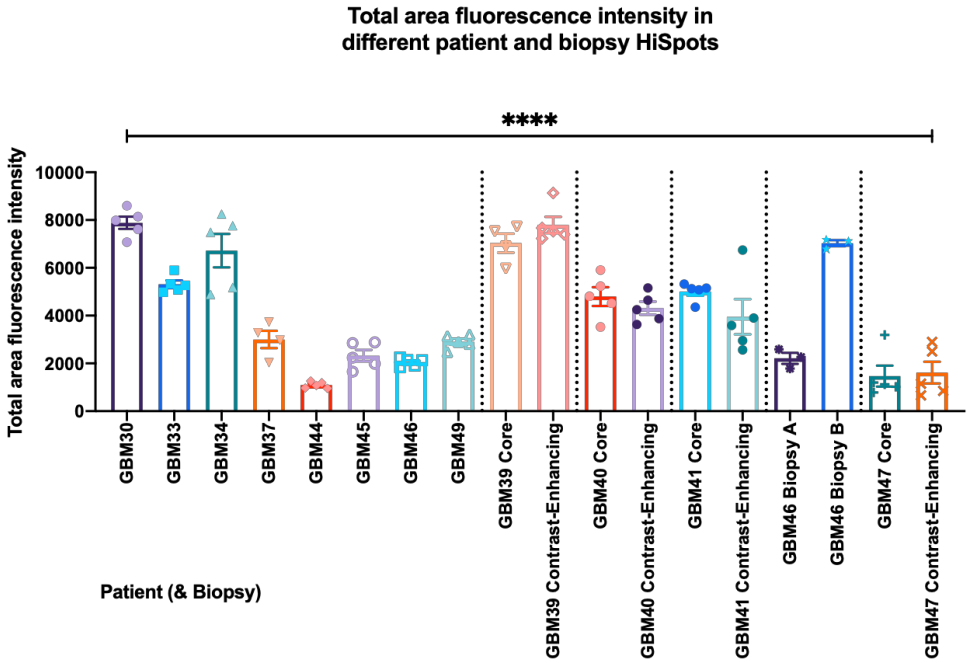

Figure 5-2: Total area fluorescence intensity in different patient and biopsy HiSpots®.

*Total area fluorescence intensity values are shown for different patient and biopsy HiSpots®. Individual HiSpot® values are shown as scatter points, imposed over the mean ± SEM. All patients are shown. Where multiple biopsies were taken from one patient, these are shown separately, with biopsies from the same patient within dashed vertical lines. ****p<0.0001, n=84 from 18 patients or biopsies.*

5.2.2 Structural differences between HiSpots® from different biopsy areas and different patients

5.2.2.1 HiSpots® created from different biopsies have limited variation in cell numbers

HiSpots® were created from biopsies extracted from the core and contrast-enhancing areas of the tumour, separately, and as combined HiSpots®. Differences between these core, contrast-enhancing and combined HiSpots® were analysed. Total area fluorescence intensity was measured for HiSpots® from the core and contrast-enhancing biopsies for four patients (GBM39, 40, 41, 47), and combined HiSpots® were measured for two patients (GBM39, 47). Higher magnification images were also taken of HiSpots® from patients 39, 40 and 47 for further quantification. Images were taken at the centre of the HiSpot® and the edge in order to represent the observable variability between these areas. These areas are therefore analysed separately below.

Total area fluorescence intensity was compared between HiSpots® from different biopsy areas for each patient. GBM39 HiSpots® did not vary significantly between core, contrast-enhancing, and combined biopsies (7933 ± 761.6 vs 6257 ± 625.0 vs 8208 ± 547.5, p=0.1449, n=5 per biopsy, Kruskal-Wallis, **Figure 5-3A**).

Total area fluorescence intensity was not significantly different between core and contrast-enhancing HiSpots® from patient GBM40 (4797 ± 395.2 vs 4313 ± 272.7, p=0.3432, t= 0.1.007, n=5 per biopsy, unpaired t-test, **Figure 5-3B**). There was no significant difference in total area fluorescence intensity in HiSpots® from patient GBM41 between core and contrast-enhancing (5005 ± 167.4 vs 3950 ± 736.8, p=0.1508, n=5 per biopsy, Mann-Whitney test, **Figure 5-3C**).

There were no significant differences in total area fluorescence intensity between HiSpots® from core, contrast-enhancing or combined biopsies for

GBM47 (1466 ± 437.8 vs 1614 ± 455.3 vs 908.7 ± 296.3, p=0.3195, n=4-5 per biopsy, Kruskal-Wallis test, **Figure 5-3D**.

DAPI counts per field were also compared from high powered images of HiSpots® from multiple biopsies. Cell counts from the centre of the HiSpots® show a smaller mean number of cells per field in the contrast-enhancing biopsy HiSpots® than the core or combined biopsies but this difference was not significant (100.4 ± 7.050 vs 174.5 ± 24.28 vs 159.2 ± 41.19, F (2, 20) = 2.944, p=0.0757, n=6-9 from 3 patients, one way ANOVA, **Figure 5-3E**). At the edge of the HiSpots® (within the outer ring, see **Figure 2-14**), the numbers of cells showed a similar distribution, however these data varied significantly (F (2, 21) = 4.215, p=0.0289, n=6-9 from 3 patients, one way ANOVA, **Figure 5-3F**). The number of cells per field in the contrast-enhancing HiSpots® was less than in those from the core (88.44 ± 8.233 vs 172.1 ± 30.07, p=0.0255, Bonferroni's multiple comparisons), but did not differ between the core and combined HiSpots® (172.1 ± 30.07 vs 131.0 ± 16.84, p=0.6476) or the contrast-enhancing and combined HiSpots® (88.44 ± 8.233 vs 131.0 ± 16.84, p=0.6023).

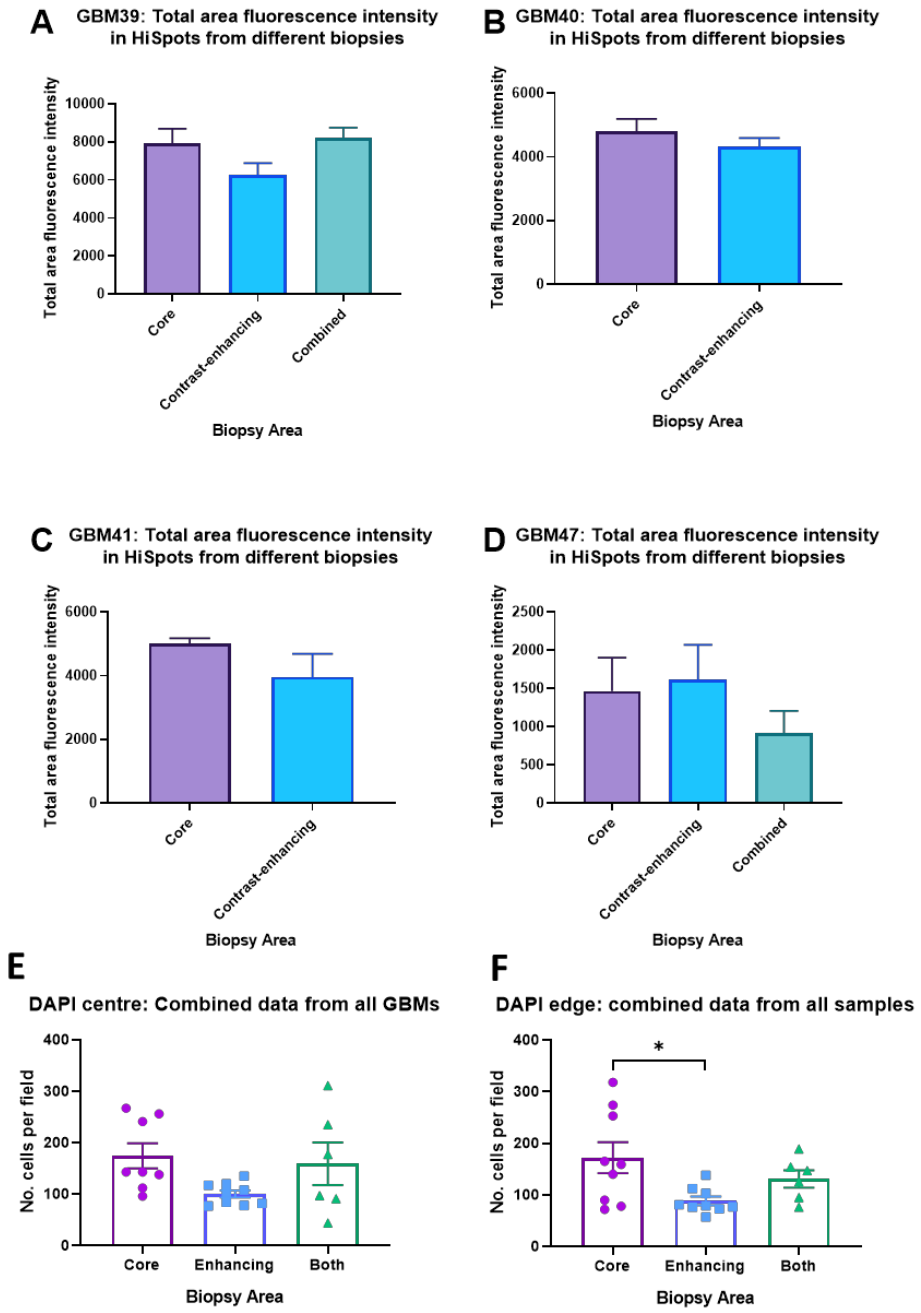

Figure 5-3: Total area fluorescence intensity and count in HiSpots® from multiple biopsies.

A-D: Total area fluorescence intensity was measured for 4-5 HiSpots® per biopsy per patient from tile scan images of HiSpots®. Data shown are mean ± SEM. A: GBM39 total area fluorescence intensity for core, contrast-enhancing, and combined HiSpots®. B: GBM40 total area fluorescence intensity for core and contrast-enhancing HiSpots®. C: GBM41 total area fluorescence intensity for core and contrast-enhancing HiSpots®. D: GBM47 total area fluorescence intensity for core, contrast-enhancing, and combined HiSpots®.

*E: Total cell counts per field from images taken from the centre of the HiSpot® for each biopsy. All data points are shown as scatter points imposed over the mean ± SEM. n=6-9 from 3 patients. F: Total cell counts per field from images taken from the edge of the HiSpot® for each biopsy. Data are mean ± SEM. *p<0.05. n=6-9 from 3 patients.*

5.2.2.2 HiSpots® demonstrate intra- and inter-tumour heterogeneity in overall structure

Here, HiSpots® were created from different tumour biopsies as described above. Tile scan images (multiple images stitched together to provide an overview, **2.9.1.1**) were taken of whole HiSpots® (up to 5 per patient, per biopsy) to identify any major structural differences between HiSpots® from different biopsy areas. Cells isolated from all four patient samples shown in **Figure 5-4** formed HiSpot® cultures but appear vastly different. Patients GBM39, 40, and 47 had unmethylated *MGMT* promoters, and wild type *IDH-1*, along with positive GFAP staining. GBM41 had a methylated *MGMT* promoter and carried the *IDH-1* R132H mutation, characterising it as a secondary GBM. It was also noted as having many GFAP negative cells. All patients had similar reported Ki-67 levels (30-40%).

GBM39 showed a large monolayer of cells identified by DAPI staining surrounding the main HiSpot® mass in both core and contrast-enhancing HiSpots®, but this was greatly reduced in the combined HiSpots® (**Figure 5-4A-C**). This layer showed some positivity for IBA1, but did not stain for the other markers tested (β-IIIT, GFAP) A higher magnification image of this border can be seen in **Figure 5-6 A**. Although this band was not visible in HiSpots® from the other patients, GBM40 showed a similar multi-ringed HiSpot® structure, with a central mass differing in appearance from the outer ring. The overall structure also differed greatly between HiSpots® created from the core and contrast-enhancing biopsies, with the cells appearing more rounded and clearly defined in HiSpots® from the contrast-enhancing biopsy than those created from the core biopsy (**Figure 5-4D-E**). HiSpots® from GBM41 appeared very similar between core and contrast-enhancing biopsies, but the cellular content was more uniformly distributed than in the HiSpots® from the other three patients (**Figure 5-4F-G**). HiSpots® from GBM47 formed a much smaller main cellular mass than the other patients, surrounded by smaller satellite clusters and single cells. This did not seem to vary greatly between HiSpots® from the core, contrast-

enhancing and combined biopsies (**Figure 5-4H-**J). The total area of the HiSpots® remained relatively similar throughout all four patients.

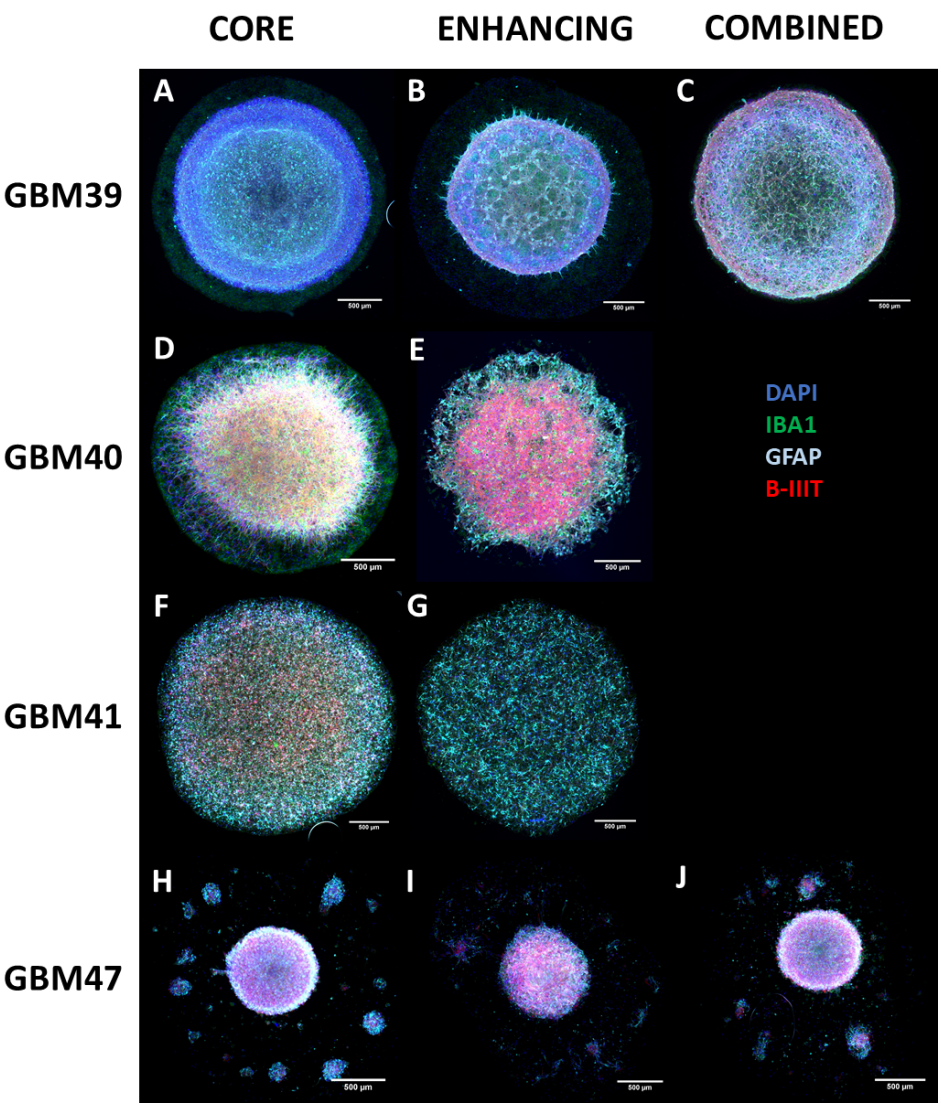

Figure 5-4: Tile scan images of HiSpots® from multiple biopsies.

Example tile scan HiSpot® immunofluorescence images are shown of each patient and biopsy. Scale bars are shown on each image for reference. All HiSpots® had been stained for DAPI (blue), IBA1 (green), GFAP (turquoise) and β-IIIT (red).

A-C: HiSpots® from patient GBM39. D-E: HiSpots® from patient GBM40. F-G: HiSpots® from sample GBM41. H-J: HiSpots® from patient GBM47. A, D, F, H: HiSpots® cultured from core biopsies. B, E, G, I: HiSpots® cultured from contrast-enhancing biopsies. C, J: HiSpots® cultured from combined core and contrast-enhancing biopsies.

5.2.2.3 HiSpot® structural features vary between biopsy areas

Morphological differences between HiSpots® were also quantified using ImageJ analysis. Total HiSpot® area was measured for all available HiSpots® (**Figure 5-5A**). Combined HiSpots® were not available for patients GBM40 or 41, so it was not possible to perform a two-way ANOVA on the entire data set. Differences between HiSpots® from different patients were compared with data from separate biopsies grouped together. HiSpot® area varied significantly between GBM patients ($p<0.0001$, n=10-15 for each patient, Kruskal-Wallis test, **Figure 5-3B**). The area of HiSpots® from GBM39 was significantly larger than:

- GBM40 *(5.971 ± 0.1977 vs 4.570 ± 0.1636, p=0.0021)*
- but not GBM41 *(5.971 ± 0.1977 vs 6.946 ± 0.5683, p>0.9999)*
- or GBM47 *(5.971 ± 0.1977 vs 5.070 ± 0.2236, p=0.0698)*

GBM41 HiSpots® were significantly larger than those from:

- GBM40 *(6.946 ± 0.5683 vs 4.570 ± 0.1636, p<0.0001)*
- GBM47 *(6.946 ± 0.5683 vs 5.070 ± 0.2236, p=0.0041)*

There was no significant difference between the area of HiSpots® from GBM40 and GBM47 (4.570 ± 0.1636 vs 5.070 ± 0.2236, p>0.9999).

Other morphological features were measured for HiSpots® from each individual patient, as most features were limited to a specific patient. For GBM39, the respective areas of the central mass, migratory ring and outer ring were measured (described in methods) and compared between core, contrast-enhancing and combined HiSpots® (**Figure 5-5C).** There were significant differences in area between the different HiSpot® areas ($F(2, 36) = 273.0$, $p<0.0001$, n=5 from 1 patient, two way ANOVA), the different biopsies ($F(2, 36) = 5.480$, $p=0.0084$), and an interaction effect ($F(4, 36) = 64.77$, $p<0.0001$). The outer ring was significantly larger in the HiSpots® from the contrast-enhancing biopsy than those from the core biopsy (3.466 ± 0.120 vs 2.562 ± 0.402, p=0.0010, Bonferroni's multiple comparisons) or combined HiSpots® (3.466 ± 0.120 vs 0.434 ± 0.084,

p<0.0001), and in the HiSpots® from the core compared to the combined HiSpots® (2.562 ± 0.402 vs 0.434 ± 0.084, p<0.0001).

For GBM40, the same morphological features were measured between core and contrast-enhancing HiSpots®. The three areas measured differed significantly in size (F (2, 24) = 70.26, p<0.0001, n=5 from 1 patient, two way ANOVA) but there was no significant difference between the core and contrast-enhancing HiSpots® (F (1, 24) = 2.418, p=0.1330) or any interaction effect (F (2, 24) = 0.5678, p=0.5742).

As visible in **Figure 5-4H-J,** GBM47 HiSpots® from all biopsies showed a central mass surrounded by single cells and satellite masses. In addition to the total HiSpot® size (**Figure 5-5A-B**), the size of the central mass and number and size of the satellite masses were measured. The area of the central mass differed significantly between biopsies (F (2, 10) = 10.85, p=0.0031, one way ANOVA, n=4-5 from 1 patient, **Figure 5-5E**). The central mass was significantly larger in the contrast-enhancing HiSpots® than in HiSpots® from the:

- core biopsy *(0.8302 ± 0.03865 vs 0.6777 ± 0.04317, p=0.0348, Bonferroni's multiple comparisons)*
- combined biopsy *(0.8302 ± 0.03865 vs 0.6076 ± 0.01326, p=0.0034)*

There was no significant difference between the core and combined HiSpots® (0.6777 ± 0.04317 vs 0.6076 ± 0.01326, p=0.6259). However, when calculated as a percentage of the total HiSpot® area, there was no significant difference between the core, contrast-enhancing and combined HiSpots® (15.07 ± 2.036 vs 15.01 ± 1.370 vs 12.83 ± 0.8740, F (2, 10) = 0.7023, p=0.5183, n=4-5 from 1 patient, one way ANOVA, **Figure 5-5F).**

The number of satellites surrounding the central mass did not vary significantly between the core, contrast-enhancing and combined HiSpots® (12.50 ± 1.848 vs 8.400 ± 2.040 vs 11.75 ± 1.931, F (2, 10) = 1.297, p=0.3157, n=4-5 from 1 patient, one way ANOVA, **Figure 5-5G**). The size of the satellites did vary significantly between the core, contrast-enhancing and combined HiSpots® (p=0.0434, n=4-5, Kruskal-Wallis test, **Figure 5-5H**), but no significant differences were seen in multiple comparisons between HiSpots® from the following biopsies:

- core and contrast-enhancing *(0.02191 ± 0.006306 vs 0.06618 ± 0.01820, p=0.0502)*
- core and combined *(0.02191 ± 0.006306 vs 0.03713 ± 0.008733, p=0.9539)*
- contrast-enhancing and combined *(0.06618 ± 0.01820 vs 0.03713 ± 0.008733, p=0.5410)*

There is however a clear trend towards contrast-enhancing HiSpots® having significantly more satellites than core HiSpots®.

Figure 5-5: Quantification of structural differences between HiSpots® from multiple biopsies.

*Data shown are mean ± SEM. All areas are shown as mm^2. A: Total HiSpot® area grouped by patient number and biopsy area. N=5 for each biopsy per patient. B: Total HiSpot® area grouped by patient number only. Biopsies are combined. N=10-15. **p<0.01, ****p<0.0001. C: Area of individual sections of HiSpots® from patient GBM39 only, by biopsy area. N=5 from 1 patient. **p<0.01, ***p<0.001. D: Area of individual sections of HiSpots® from patient GBM40 only, by biopsy area. N=5 from 1 patient.*

*E-H: Quantification of HiSpot® structural features from patient GBM47. N=4-5 from 1 patient for all data sets. E: The area of the central mass in HiSpots® by biopsy area. *p<0.05, **p<0.01. F: The area of the central mass as a percentage of the total HiSpot® area by biopsy area. G: The number of satellite clusters per HiSpot® by biopsy area. H: The mean size of satellites per HiSpot® by biopsy area.*

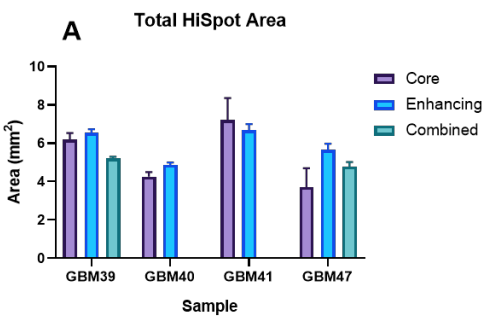
A
Total HiSpot Area
Area (mm²)
Core
Enhancing
Combined
GBM39
GBM40
GBM41
GBM47
Sample

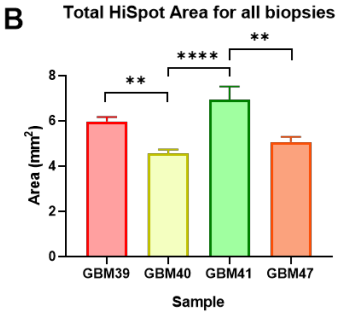
B
Total HiSpot Area for all biopsies
Area (mm²)
**
****
**
GBM39
GBM40
GBM41
GBM47
Sample

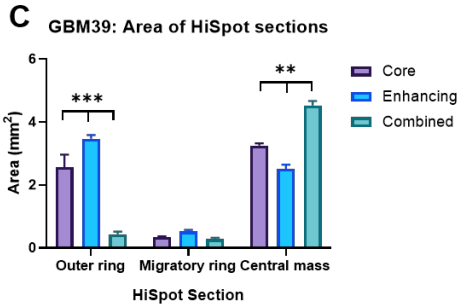
C
GBM39: Area of HiSpot sections
Area (mm²)
***
**
Core
Enhancing
Combined
Outer ring
Migratory ring
Central mass
HiSpot Section

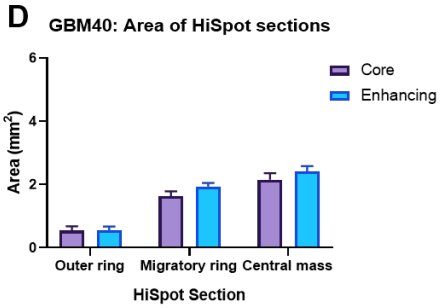
D
GBM40: Area of HiSpot sections
Area (mm²)
Core
Enhancing
Outer ring
Migratory ring
Central mass
HiSpot Section

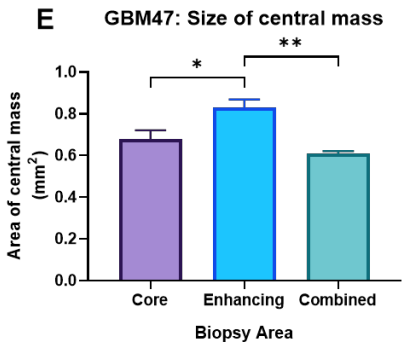
E
GBM47: Size of central mass
Area of central mass (mm²)
*
**
Core
Enhancing
Combined
Biopsy Area

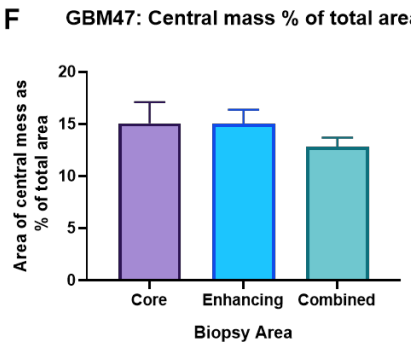
F
GBM47: Central mass % of total area
Area of central mess as % of total area
Core
Enhancing
Combined
Biopsy Area

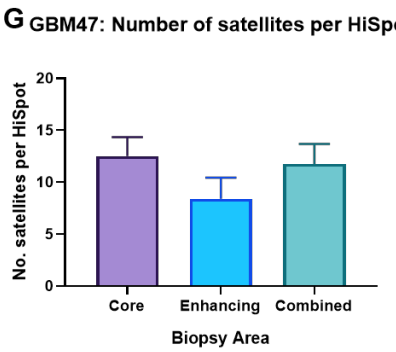
G
GBM47: Number of satellites per HiSpot
No. satellites per HiSpot
Core
Enhancing
Combined
Biopsy Area

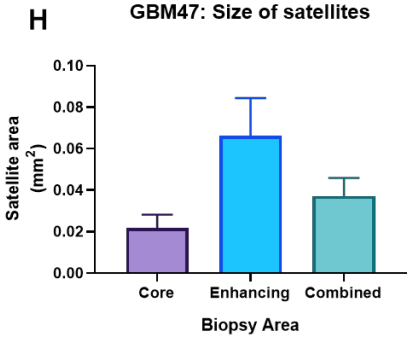
H
GBM47: Size of satellites
Satellite area (mm²)
Core
Enhancing
Combined
Biopsy Area

5.2.3 Tumour cells

5.2.3.1 The number and length of protrusions per HiSpot® vary between biopsy areas

In HiSpots® from certain patients, invasive-like cells were noted at the edge of the central HiSpot® mass, with cellular protrusions spreading into the thinner outer ring of the tumour. These cells were positive for GFAP and β-IIIT, although the expression was not always consistent along the length of the protrusion (**Figure 5-6A**). The length and number of protrusions per HiSpot® were measured using ImageJ and were analysed separately for each patient. Tile scan images were used to capture all protrusions present on each HiSpot® and avoid overlap within fields.

In HiSpots® from GBM39, the number of protrusions per HiSpot® varied significantly ($F(2, 12) = 46.65$, $p<0.0001$, n=5 from 1 patient, one way ANOVA, **Figure 5-6B**). There were far more protrusions in the HiSpots® from the contrast-enhancing biopsy than in either those from the core biopsy (79.00 ± 10.11 vs 6.400 ± 0.9274, $p<0.0001$, Bonferroni's multiple comparisons) or combined (79.00 ± 10.11 vs 12.00 ± 1.378, $p<0.0001$). There was no significant difference between the number of protrusions in the HiSpots® from the core and combined biopsies (6.400 ± 0.9274 vs 12.00 ± 1.378, $p>0.9999$).

The length of the protrusions also showed a similar pattern of significant differences between the different biopsies ($F(2, 12) = 43.74$, $p<0.0001$, n=5 from 1 patient, one way ANOVA, **Figure 5-6C**). The cell protrusions were significantly longer in the HiSpots® from the contrast-enhancing biopsy compared with either those from the core biopsy (72.78 ± 3.020 vs 38.77 ± 3.460, $p<0.0001$, Bonferroni's multiple comparisons) or combined (72.78 ± 2.020 vs 42.65 ± 1.637, $p<0.0001$) HiSpots®. There was no significant difference between the core and combined HiSpots® (38.77 ± 3.460 vs 42.65 ± 1.637, $p>0.9999$).

In GBM40, the pattern of protrusions was reversed, with significantly more protrusions in the core than contrast-enhancing HiSpots® (112.6 ± 5.644 vs 31.20 ± 3.137, $p<0.0001$, $t=12.61$, $n=5$ from 1 patient, unpaired t-test, **Figure 5-6C**). No HiSpots® created from combined biopsies were available for analysis. The protrusions were also longer in the HiSpots® from the core than the contrast-enhancing biopsy (169.1 ± 24.05 vs 80.02 ± 3.612, $p<0.0064$, $t=3.664$, $n=5$ from 1 patient, unpaired t-test, **Figure 5-6D**).

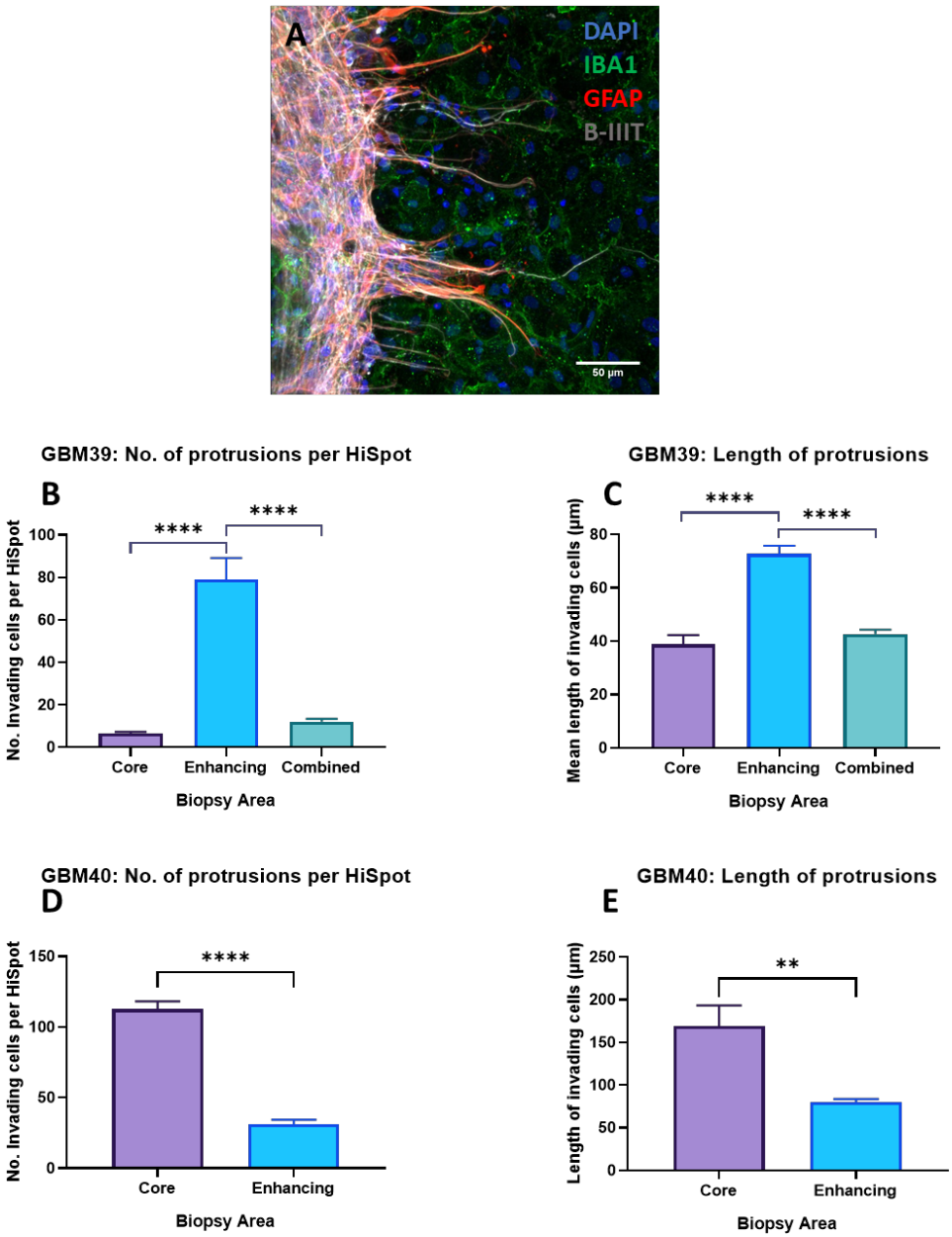

Figure 5-6: Differences in protrusions in HiSpots® from multiple biopsies.

A: An example immunofluorescence image of protrusions at the border of the central HiSpot® mass. HiSpots® were stained for DAPI (blue), IBA1 (green), GFAP (red) and β-IIIT (grey). A scale bar is shown for reference.

*B-E: Data shown are mean ± SEM. **p<0.01, ****p<0.0001. n=5 from 1 patient. B: The number of protrusions per HiSpot® from patient GBM39, by biopsy area. C: The mean length of protrusions in HiSpots® from GBM39, by biopsy area. C: The number of protrusions per HiSpot® from patient GBM40, by biopsy area. E: The mean length of protrusions per HiSpot® from patient GBM40, by biopsy area.*

5.2.3.2 The number of tumour cells in HiSpots® does not vary with biopsy area

Tumour cells identified by co-expression of GFAP and β-IIIT form the bulk of the HiSpots® from these patients. Confocal images from the centre and edge of HiSpots® from patients GBM39, 40 and 47 were used for quantification of these cell types.

In the centre of the HiSpot®, there was no significant difference between the percentage of GFAP+β-IIIT+ cells in the HiSpots® from the core, contrast-enhancing and combined biopsies (78.49 ± 5.231, 77.51 ± 3.509 vs 80.79 ± 2.612, F (2, 20) = 0.1497, p=0.8619, n=6-8 from 3 patients, one way ANOVA, **Figure 5-7A**). There was also no significant difference in the percentage of GFAP+β-IIIT+ cells at the edge of the HiSpot® (65.67 ± 7.167 vs 66.31 ± 4.361 vs 76.29 ± 6.029, p=0.2677, n=6-8 from 3 patients, Kruskal-Wallis, **Figure 5-7B**).

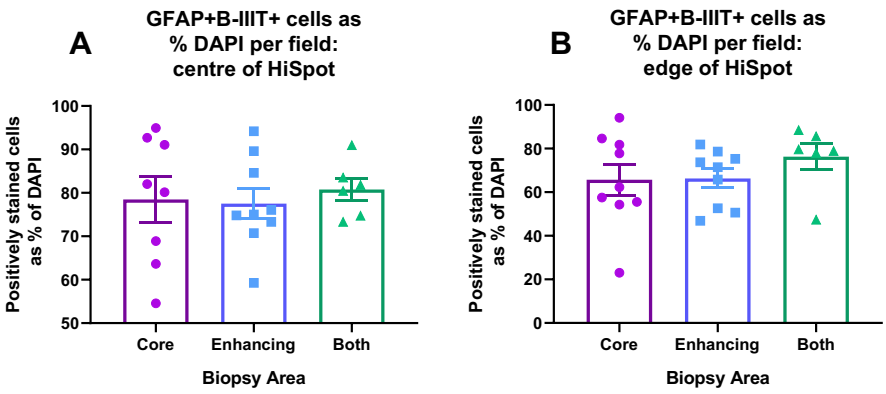

Figure 5-7: Tumour cells in HiSpots® from multiple biopsies.

All data points are shown imposed over mean ± SEM. n=6-8 from 3 patients. A-B: The number of GFAP+β-IIIT+ tumour cells as a percentage of the total cell count per field, by biopsy area. A: Tumour cell percentages at the centre of the HiSpots®. B: Tumour cell percentages at the edge of the HiSpots®.

5.2.3.3 Morphological differences are present between HiSpots® from different biopsy areas

In addition to the macroscopic structural differences highlighted earlier **(5.2.2.2**), differences were also noted in the structure of individual tumour cells in HiSpots® between and within patients. Within HiSpots® from patient GBM39, the tumour cells in the HiSpots® created from the core biopsy appeared randomly arranged, with no overarching structure. Microglia are clearly present beyond the main body of tumour cells, although some positive staining is present within the tumour cells (**Figure 5-8A**). In comparison, the tumour cells in the HiSpots® from the contrast-enhancing biopsy appear more organised, with groups of protrusions running in parallel, and around large areas of microglia (**Figure 5-8B**). The combined HiSpots® seem to contain features of both biopsies, with a somewhat disorganised structure in comparison with the contrast-enhancing HiSpots®, but microglia clearly present in the spaces between tumour cells (**Figure 5-8C**). In GBM40 HiSpots®, a similar comparison is visible. The HiSpots® from the core biopsy show tumour cells growing directly outwards towards the edge of the HiSpot®, interspersed with microglia (**Figure 5-8D**), whereas the HiSpots® from the contrast-enhancing biopsy show clearer cell-cell interactions and a more rounded cytoplasm in the tumour cells, with rounded microglia in the inter-tumour cell spaces (**Figure 5-8E**). No combined HiSpots® were available for this patient. Overall, the tumour cells in core GBM47 HiSpots® appear more rounded and condensed than the other two biopsies, forming an almost cobblestone-like appearance, with microglia visible towards the edge of the tumour cell bulk (**Figure 5-8F**). This is very similar in the combined HiSpots®, with microglia clustered within the edge of the tumour cells (**Figure 5-8H**). However, the contrast-enhancing biopsy HiSpots® seem to show more extended tumour cells, with a less cobblestone-like appearance. Microglia are still found along the border of the tumour cells, but are also clearly visible interspersed with the tumour cells (**Figure 5-8G**).

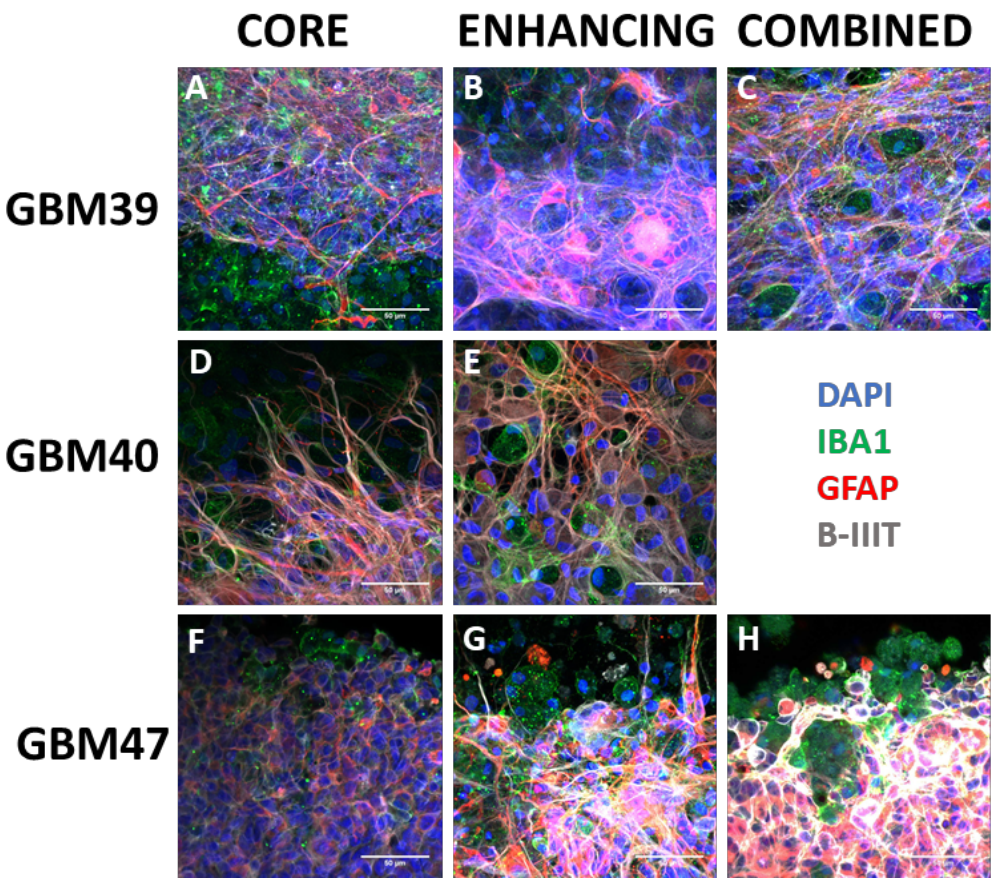

Figure 5-8: Cellular morphological differences in HiSpots® from multiple biopsies.

Example immunofluorescence images of HiSpot® cellular morphology and distribution in HiSpots® from core, contrast-enhancing, and combined biopsies. All HiSpots® were stained for DAPI (blue), IBA1 (green), GFAP (red) and β-IIIT (grey). Images are shown from patients GBM39 (A-C), GBM40 (D-E), and GBM47 (F-H). HiSpots® are from core (A, D, F), contrast-enhancing (B, E, G) or combined (C, H) biopsies.

5.2.4 Microglia

5.2.4.1 Microglia clusters in GBM39

It was noted in HiSpots® from patient GBM39 that microglia appeared to have grouped together in pairs or larger clusters. In the contrast-enhancing biopsy HiSpots®, the microglia were clustered together in large groups, appearing to have around ten microglia per cluster, surrounded by a network of tumour cells (**Figure 5-9B**). In core and combined biopsy HiSpots®, the microglia also clustered together but in smaller groups, which are less clearly visible in a tile scan (**Figure 5-9A, C**). The number and size of these clusters was measured for each of the GBM39 HiSpots® from each biopsy. Clusters were defined by two or more connected microglia which did not have tumour cell protrusions running between them.

The number of microglia clusters varied significantly between biopsies, ($p=0.0084$, n=5 from 1 patient, Kruskal-Wallis, **Figure 5-9D**). There was a significantly higher number of microglia clusters in the combined HiSpots® compared to the core (141.4 ± 29.41 vs 69.80 ± 11.04, $p=0.0173$, Dunn's multiple comparisons) but not to the contrast-enhancing biopsy HiSpots® (141.4 ± 29.41 vs 80.40 ± 6.787, $p=0.1311$). There was no significant difference between the HiSpots® from the core and contrast-enhancing biopsies in numbers of microglia clusters (69.80 ± 11.04 vs 80.40 ± 6.787, $p>0.9999$). The size of the microglia clusters also varied significantly between biopsies ($F(2, 12) = 23.15$, $p<0.0001$, n=5 from 1 patient, one way ANOVA, **Figure 5-9E**). The microglia clusters were far larger in HiSpots® from the contrast-enhancing biopsy than those from the core biopsy (10794 ± 1455 vs 4107 ± 447.1, $p=0.0005$) or combined HiSpots® (10794 ± 1455 vs 2877 ± 190.5, 0=0.0001). There was no significant difference between the size of microglia clusters between the core and combined biopsy HiSpots® (4107 ± 447.1 vs 2877 ± 190.5, $p>0.9999$).

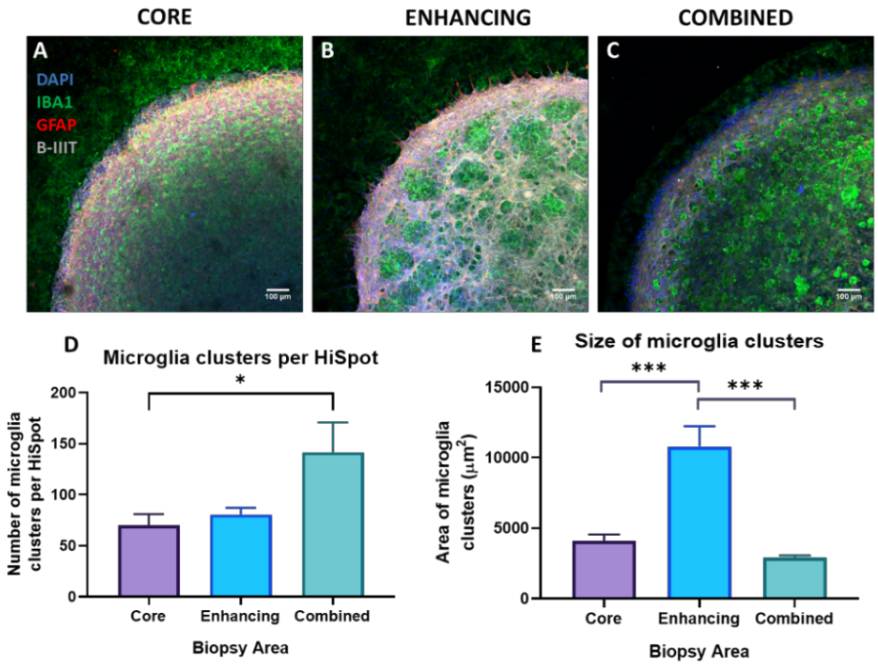

Figure 5-9: Differences in microglial clusters in HiSpots® from multiple biopsies.

*All images and data are from patient GBM39. A-C: Example immunofluorescence images from core (A), contrast-enhancing (B) and combined (C) biopsy HiSpots®. All HiSpots® were stained for DAPI (blue), IBA1 (green), GFAP (red) and β-IIIT (grey). Scale bars are shown for reference. D-E: Quantification of microglia clusters. N=5 from 1 patient. Data shown are mean ± SEM. D: The number of microglia clusters per HiSpot® in core, contrast-enhancing and combined biopsy HiSpots®. *p<0.05. E: The mean size of microglia clusters per HiSpot® from core, contrast-enhancing and combined biopsy HiSpots®. ***p<0.001.*

5.2.4.2 The number of microglia in HiSpots® varies slightly from different biopsy areas

To determine whether the overall percentage of microglia varied between HiSpots® created from different biopsies from patients GBM39, 40 and 47, confocal images were taken of the centre and edge of each HiSpot®. Microglia were quantified and recorded as a percentage of the total DAPI count per image.

The percentage of IBA1+ microglia varied significantly in the centre of the HiSpot® (p=0.0454, n=6-9 from 3 patients, Kruskal-Wallis, **Figure 5-10A**). There were significantly more microglia present in HiSpots® from the contrast-enhancing biopsy compared to the combined HiSpots® (12.86 ± 2.071 vs 5.751 ± 0.8384, p=0.0387, Dunn's multiple comparisons). There was no significant difference between the percentage of microglia in HiSpots® from the core and contrast-enhancing biopsies (12.31 ± 4.296 vs 12.86 ± 2.071, p=0.8419) or core and combined biopsies (12.31 ± 4.296 vs 5.751 ± 0.8384, p=0.4361). The percentages of microglia did not vary significantly at the edge of the HiSpot® between core, contrast-enhancing and combined biopsy HiSpots® (13.80 ± 2.334 vs 16.50 ± 2.684 vs 13.90 ± 4.086, F (2, 21) = 0.2959, p=0.7469, n=6-9, one way ANOVA, **Figure 5-10B**).

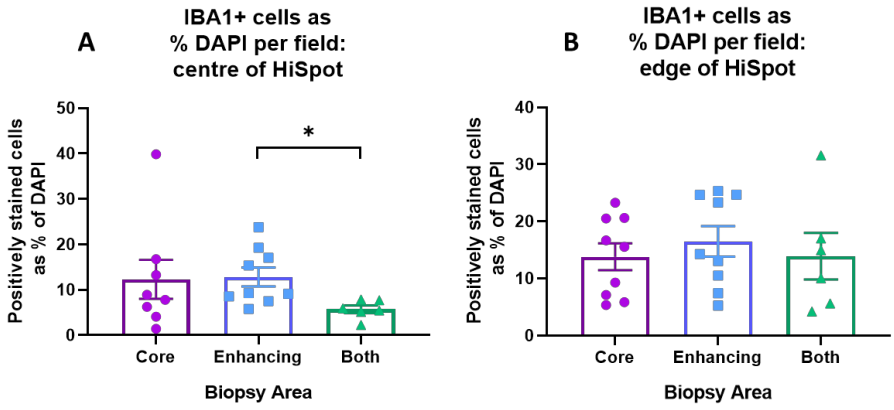

Figure 5-10: Numbers of microglia cells in HiSpots® from multiple biopsies.

*A-B: All data points are shown as scatter points imposed over mean ± SEM. n=6-9 from 3 patients. Number of IBA1+ cells as a percentage of total cell count per field for core, contrast-enhancing and combined biopsy HiSpots®. A: Percentage of cells which are IBA1+ in the centre of the HiSpot®. *p<0.05. B: Percentage of cells which are IBA1+ at the edge of the HiSpot®.*

5.2.5 TMZ response

5.2.5.1 Total area fluorescence intensity varies between HiSpots® produced from different biopsy areas but is not affected by treatment

Total area fluorescence intensity was measured in whole HiSpot® tile scans to provide a representation of the total cell population. The more nuclei present within the HiSpot®, the higher the total area fluorescence intensity should be. Total area fluorescence intensity was measured in untreated (0 µM) and treated (100 µM) HiSpots® from different tumour areas. For patient GBM39, HiSpots® from biopsies from the core, contrast-enhancing and peripheral areas were analysed. For GBM47, the core and contrast-enhancing areas were biopsied and compared to a combined HiSpot® containing the same proportion of cells from each area. Patients are compared independently due to the high levels of inter-patient variability described above (**5.2.1**). All data were analysed by two-way ANOVA.

For GBM39, there was no significant effect of TMZ dose ($F(1, 23) = 0.07897$, $p=0.7812$, n=4-5 per group, **Figure 5-11A**), but there was a significant difference in biopsy areas ($F(2, 23) = 230.4$, $p<0.0001$), and no interaction effect ($F(2, 23) = 1.376$, $p=0.2726$). Untreated HiSpots® did not have different total area fluorescence intensity between the core and contrast-enhancing biopsies (7035 ± 395.5 vs 7793 ± 323.4, $p>0.9999$), but the peripheral HiSpots® had significantly lower total area fluorescence intensity than the core (2039 ± 106.5 vs 7035 ± 395.4, $p<0.0001$) or contrast-enhancing (2039 ± 106.5 vs 7793 ± 343.4, $p<0.0001$) biopsies.

For GBM47, there was a significant overall effect of TMZ dose ($F(1, 22) = 6.142$, $p=0.0213$ **Figure 5-11B**), and biopsy area ($F(2, 22) = 4.579$, $p=0.0217$) but no interaction ($F(2, 22) = 1.517$, $p=0.2415$, n=4-5 for all groups). However, there were no significant differences between untreated HiSpots® from core and contrast-enhancing (1466 ± 437.8 vs 1614 ± 455.3, $p>0.9999$), or combined (1466 ± 437.8 vs 908.7 ± 296.3, $p>0.9999$) biopsies, or between contrast-enhancing and combined biopsies (1614 ± 455.3 vs 908.7 ± 296.3,

p>0.9999, Bonferroni's multiple comparisons). There were also no differences between untreated and treated HiSpots® from the core (1466 ± 437.8 vs 3000 ± 529.4, p=0.8380), contrast-enhancing (1614 ± 455.3 vs 3491 vs 922.0, p=0.3261), or combined biopsies (908.7 ± 296.3 vs 893.1 ± 105.053, p>0.9999).

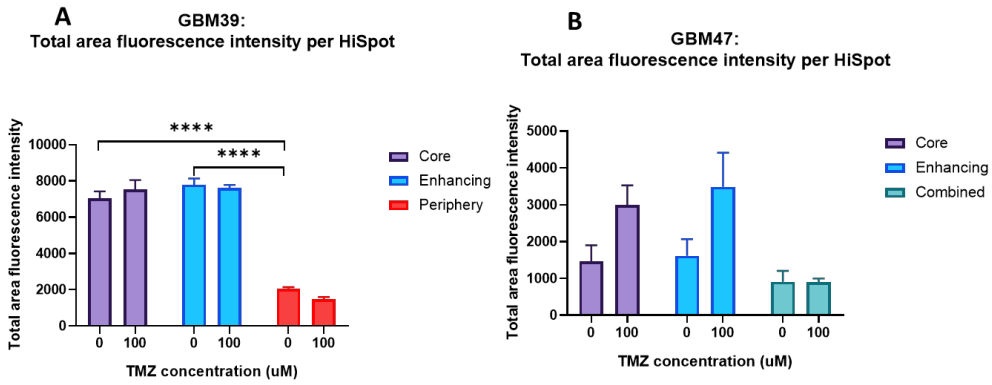

Figure 5-11: Total area fluorescence intensity in TMZ treated and untreated HiSpots® from multiple biopsies.

*A-B: Data shown are mean ± SEM. ****p<0.0001. n=4-5 from 1 patient per graph. Graphs show total area fluorescence intensity per HiSpot® from multiple biopsies, when untreated (0 µM) and treated (100 µM) with TMZ. A: Total area fluorescence intensity per HiSpot® from core, contrast-enhancing and periphery biopsies from GBM39. B: Total area fluorescence intensity per HiSpot® from core, contrast-enhancing and combined biopsies from GBM47.*

5.2.5.2 EdU levels change with TMZ treatment and are affected by biopsy location

EdU is a thymidine analogue taken up by cells as they replicate DNA in the S-phase. It can then be detected post-fixation with a fluorescent azide to give an indication of the number of dividing cells in the culture depending on the length of EdU exposure. EdU exposure for 4 hours gives an index of S-phase entry and will only represent a subset of the total population of cycling cells. Different biopsy areas within a GBM have previously been demonstrated to have different levels of proliferation (**5.1.1**). TMZ targets proliferating cells, so a reduction in the number of these should be seen in HiSpots® that respond to the treatment. The number of EdU+ dividing cells per HiSpot® were measured in untreated (0 μM) and treated (100 μM) HiSpots® from different tumour areas. Biopsies were collected as described above (**2.4.2**). All patients are compared independently due to the high levels of baseline variation, and the necessity of comparing matched biopsy HiSpots® from the same patient. All data were analysed by two-way ANOVA. This experiment determines whether different biopsy areas from each patient have different levels of proliferation (EdU+ cells), and whether they respond differently to TMZ treatment.

The number of EdU+ cells in GBM39 HiSpots® varied significantly between HiSpots® created from different biopsy areas ($F(1, 23) = 19.57$, $p=0.0002$, n=4-5, **Figure 5-12A**). The number of EdU+ cells was also affected by treatment with TMZ ($F(2, 23) = 369.5$, $p<0.0001$) and an interaction effect between these two factors was also present ($F(2, 23) = 14.39$, $p<0.0001$). Untreated HiSpots® had a significantly higher number of EdU+ cells per HiSpot® in HiSpots® created from the following biopsy areas:

- core compared to contrast-enhancing *(1335 ± 38.84 vs 472.8 ± 19.80, p<0.0001)*
- core compared to peripheral *(1335 ± 38.84 vs 3.200 ± 0.374, p<0.0001)*

- contrast-enhancing compared to peripheral *(472.8 ± 19.80 vs 3.200 ± 0.374, p<0.0001)*

There was a significant reduction in EdU incorporation between untreated and treated HiSpots® from the core (1335 ± 927.4 ± 73.87, p<0.0001) but no change from the contrast-enhancing (472.8 ± 19.80 vs 432.2 ± 51.13, p>0.9999) or peripheral (3.200 ± 0.374 ± 5.200 ± 2.131, p>0.9999) areas.

In HiSpots® from patient GBM47, the level of EdU incorporation per HiSpot® also differed by biopsy area (F (2, 22) = 17.16, p<0.0001, n=4-5, **Figure 5-12B**), TMZ dose (F (1, 22) = 13.93, p=0.0012), and due to an interaction between the two factors (F (2, 22) = 4.332, p=0.0259). There were no significant differences between HiSpots® created from the biopsy areas when untreated:

- core vs contrast-enhancing *(461.0 ± 70.55 vs 295.2 ± 31.28, n=5, p=0.7403)*
- core vs combined *(461.0 ± 70.55 vs 332.3 ± 46.57, p>0.9999)*
- contrast-enhancing vs combined *(295.2 ± 31.28 vs 332.3 ± 46.57, p>0.9999).*

Between untreated and treated HiSpots®, there was a significant increase in EdU incorporation in the HiSpots® from the core (461.0 ± 70.55 vs 832.0 ± 74.12, p=0.0018), but not the contrast-enhancing (295.2 ± 31.28 vs 421.2 ± 58.06, p>0.9999) or combined (332.3 ± 46.57 vs 371.5 ± 47.35, p=0.9999) biopsies.

As the increase in EdU incorporation with TMZ treatment was unexpected, confocal images were taken of the same HiSpots® for further analysis. Z-stack images were taken from the centre and edge of three HiSpots® each for quantification of EdU+ cells. Three Z-stack images were analysed per image and the mean values used for analysis. There was a significant increase in EdU numbers between untreated and treated HiSpots® in both areas (F (1, 8) = 273.4, p<0.0001, n=3, **Figure 5-12D**), the centre of the

HiSpot® (149.7 ± 10.04 vs 280.3 ± 3.528, p<0.0001) and the edge (142.0 ± 8.185 vs 246.3 ± 4.667, p<0.0001).

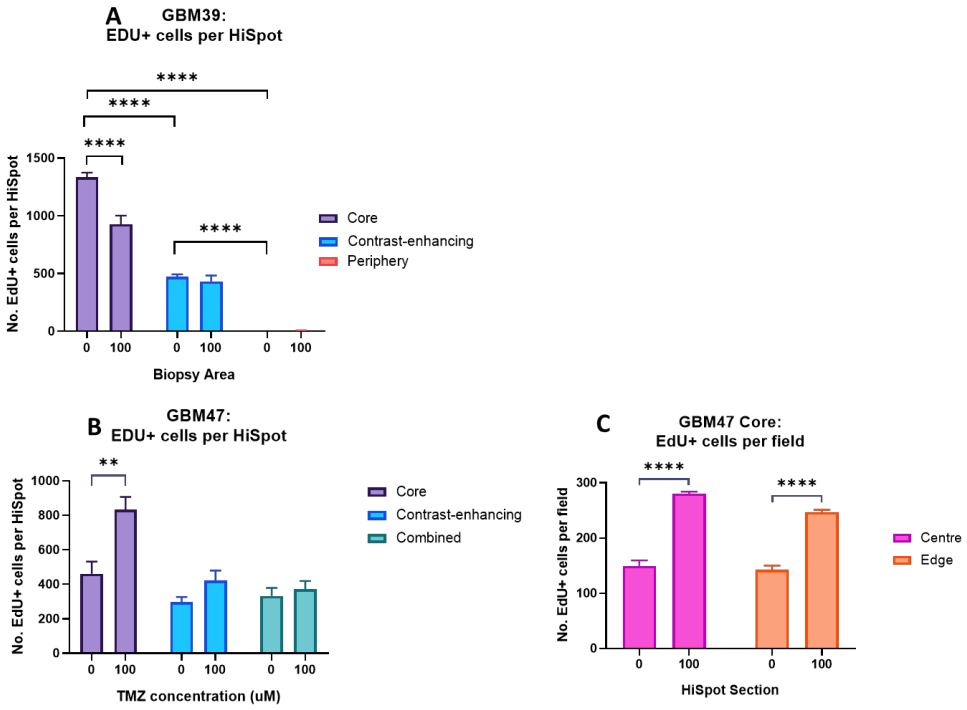

Figure 5-12: EdU+ cells per HiSpot® in response to TMZ in multiple biopsies.

*Data shown are mean ± SEM. **p<0.01, ***p<0.001, ****p<0.0001. Data show results from HiSpots® untreated (0 µM) and treated (100 µM) with TMZ. A: Number of EdU+ selections per HiSpot® from patient GBM39 core, contrast-enhancing and periphery biopsy HiSpots®. N=4-5 from 1 patient. B: Number of EdU+ selections per HiSpot® from patient GBM47 core, contrast-enhancing and combined HiSpots®. N=4-5 from 1 patient. C: Number of EdU+ cells per high powered field in HiSpots® from GBM47 core biopsy HiSpots® at the centre and edge of the HiSpot®. N=3 from 1 patient.*

5.3 Discussion

The complex heterogeneity of GBM is a key factor to represent in models of the disease. Three key heterogeneic factors are: the depth within the tumour, and therefore the availability of oxygen; the genetic subtype or state of the tumour cells, known to vary throughout the tumour; and the variations in microenvironmental cells throughout the tumour. These factors constantly interact, and so wherever possible should be investigated in combination. It is also possible that variations in results could arise from inter-patient heterogeneity, intra-tumour heterogeneity (between biopsy areas) or as a result of the HiSpot® model. It was important to establish which of these factors contributed to the differences seen so far.

The depth of the tumour biopsy in models using primary human tissue is often not taken into account. As demonstrated by Pistollato *et al.* (2010), the depth of the tumour biopsy significantly influences the level of hypoxia, protein expression, and TMZ resistance, and these factors are maintained in culture. The 3D GBM-on-a-chip model developed by Yi *et al.* (2019) recreates an oxygen gradient within their microfluidic system, allowing the hypoxia of a tumour *in situ* to be recreated with a uniform population of GBM cells. The authors also include HUVEC cells in their model, to add the influence of endothelial cells, and track the pro-angiogenic behaviour of the tumour.

Genetic diversity is another key feature of GBM. Tumour cells are highly plastic and form different subpopulations with varied expression patterns within the tumour, reminiscent of a number of different cell types (Sottoriva *et al.* 2013; Akgül *et al.* 2019; Neftel *et al.* 2019). This is a key feature which is often lost in long term culture, as the populations become more uniform (Lee *et al.* 2006; Allen *et al.* 2016). Low passage, patient-derived lines are becoming more popular as a replacement for established lines such as U87. Some of these lines contain multiple subtypes (TCGA classification) and can present with different classifications in culture or xenograft models (Stringer

et al. 2019). Single cell RNA sequencing of GBM has revealed high plasticity of individual tumour cells (Neftel *et al.* 2019). This increases the potential for heterogeneity within GBM models, and highlights the importance of developing methods which can accurately represent the condition *in situ.*

Microenvironmental cells (non-tumour cells present in and around the tumour) also contribute to GBM heterogeneity. Microglia in particular have been demonstrated to vary in number and phenotype between tumour subtypes (TCGA classification) and at different depths within the tumour (Kaffes *et al.* 2019). As microglia have been shown to influence tumour cells, their impact adds another layer of heterogeneity to the tumour environment (Komohara *et al.* 2008). Microglia are often lacking entirely from GBM models, and when they are present they are often mouse derived or cultured in serum, both of which have been demonstrated to be poorly representative of primary human microglia due to differences in expression profiles and interactions with tumour cells (Parney *et al.* 2009; Masuda *et al.* 2019).

Hypoxia, genetic heterogeneity, and microglia have all been demonstrated to affect tumour growth and response to treatment (Komohara *et al.* 2008; Pistollato *et al.* 2010; Coniglio *et al.* 2012; Sottoriva *et al.* 2013; Colwell *et al.* 2017; Hermida *et al.* 2019). If these factors are not represented or investigated in models, the results will be limited in their translatability to humans. Treatments may progress along the drug discovery pipeline which are only effective in one subtype or oxygen level, but ineffective in entire tumours. In order to treat GBM effectively, it is essential to understand the heterogeneity through representative models.

Although heterogeneity is present between patients, and within tumours as different clones, it also exists between different the inner and outer areas of the tumour, which are visible with gadolinium administration on CT/MRI images as the non-contrast enhancing core and the contrast-enhancing border (**Figure 5-1**). This is a useful starting point for investigating tumour

heterogeneity, as biopsy areas can be selected and recorded using CT/MRI images.

The HiSpot® model was used to investigate the differences in overall HiSpot® organisation, cell types, and treatment response between different biopsies (core and contrast-enhancing, where possible), with the theory that this could be extrapolated to investigating the differences between further defined locations within the 3D tumour structure, or the differences between different genetic subtypes. Combined HiSpots® were used to elucidate whether any differences are maintained in a combined biopsy, or if certain features predominate, perhaps leaving one biopsy area unrepresented in a combined model.

5.3.1 HiSpots® demonstrate inter-tumour heterogeneity

GBM is known to be a highly heterogeneic disease, showing variability between and within tumours (Verhaak *et al.* 2010; Sottoriva *et al.* 2013; Neftel *et al.* 2019). It was important to determine whether inter- or intra-tumour heterogeneity contributed the most to the variability seen in HiSpots®, or if any differences seen were a function of the method itself. The total area fluorescence intensity, a representation of the total cellularity of the HiSpot®, was used for comparison. In HiSpots® from a selection of 13 patients, with or without combining the results from multiple biopsy areas (5 patients), a highly significant variability was seen (**Figure 5-2**). As the differences were smaller between HiSpots® created from different biopsies from the same patients, these data imply that the main contributor to heterogeneity in the HiSpot® model is the variability between patients. The graphs in **Figure 5-2** also show small standard error bars, which indicates that the variability between HiSpots® from the same origin (whether this be patient or biopsy specific) is very low. This suggests that variability in GBM HiSpot® cultures is a characteristic of the tumour, and not a characteristic of the HiSpot® model. Therefore, it was decided to analyse further data in this chapter by individual patient, rather than grouping them together.

5.3.2 Cellular differences between multiple biopsy HiSpots®

5.3.2.1 Core and contrast-enhancing HiSpots® do not vary significantly in their cellular density

Whole HiSpot® total area fluorescence intensity and DAPI cell counts (from confocal images) were used to compare cell numbers between biopsies. With higher density HiSpots®, it became difficult to quantify cell numbers using previous methods (**2.9.1.2**). There were no significant differences in HiSpot® total area fluorescence intensity between biopsy locations for any of the patients analysed (39, 40, 41, 47, **Figure 5-3A-D**).

In images taken from the centre of the HiSpot® the difference did not reach significance, but at the edge of the HiSpot® there were significantly fewer cells in HiSpots® created from the contrast-enhancing biopsy than the core biopsy (**Figure 5-3E, F**). Given that no differences were detected using total area fluorescence intensity, this result may be an artefact of the particular HiSpots® sampled. Alternatively, this result could be explained by higher proliferation levels in the core than contrast-enhancing biopsies that may be easier to detect using a higher magnification. There was a higher level of EdU incorporation in GBM39 HiSpots® from the core biopsy compared with those from the contrast-enhancing biopsy. A similar trend was seen in HiSpots® from patient GBM47 but did not reach significance. Alternatively, this trend could be caused by a better cell survival over the 14 DIV culture period of the core biopsy HiSpots®. Further investigations would be required to deduce whether either of these are the reason for the differences in cell count. Further patient repeats and intermediate timepoints would be useful to understand the differences in cell counts between the core and contrast-enhancing HiSpots®. Histological and neurosphere investigations have also found differences in overall growth or tumour cell density between biopsies taken from different layers of the tumour (Pistollato *et al.* 2010; Eidel *et al.* 2017).

In both centre and edge images, although clearer in the edge data, the combined HiSpots® seemed to have a cell count somewhere between the core and contrast-enhancing HiSpots®, although not significantly different from either (**Figure 5-3E, F**). Further repeats could reveal whether this is the case. This would support the theory that combined HiSpots® maintain some features of both the core and contrast-enhancing areas, forming a model which lies somewhere in between the two.

5.3.2.2 HiSpots® demonstrate inter- and intra-tumour heterogeneity in general appearance

The most obvious differences between HiSpots® cultured from different biopsies are visible in their overall structure. Although there are some obvious differences between the different patients, there is almost as much variation between the biopsies from each (**Figure 5-4**). The most obvious difference between core and contrast-enhancing biopsy HiSpots® from the same patient is with GBM40. The core HiSpot® shows spindly, poorly defined cells, in a mostly random arrangement, spreading from a central mass into an outer ring of IBA1+ cells. The GFAP and β-IIIT staining almost entirely overlaps. In comparison, in the contrast-enhancing biopsy HiSpot® the tumour cells are more well defined and rounded, with a clear gradient showing stronger β-IIIT staining in the centre of the HiSpot® and stronger GFAP staining around the edge, although there is much overlap. There appear to be fewer microglia in the surrounding ring in the contrast-enhancing biopsy HiSpot®. Both HiSpots® have microglia visibly dispersed throughout the HiSpot® structure, although not as clustered as in GBM39. GBM40 in particular highlights the possibility that HiSpots® from core and contrast-enhancing biopsies develop different expression patterns. GBM tumour cells can switch between invasive or proliferative phenotypes, and this can be affected by various microenvironmental factors and tumour heterogeneity (Dhruv *et al.* 2013; Oliveira *et al.* 2017). This switch is known as the 'go or grow' hypothesis and is under the regulation of factors such as Wnt family member 5a (Wnt5a), NF-κB, and c-Myc. In the 'go or grow'

hypothesis, the tumour cells are either more proliferative, which is the often the case in the core of the tumour, or more invasive, as they predominantly are at the tumour outer rim (Dhruv *et al.* 2013; Binda *et al.* 2017; Mehta and Lo Cascio 2018; Parker *et al.* 2018). However, hypoxia has been demonstrated to promote cell invasion in GBM (Joseph *et al.* 2015), and a number of common GBM mutations in *EGFR*, *PTEN* and *p53* have been shown to promote hypoxic signalling via HIFs (Monteiro *et al.* 2017). Hypoxia, proliferation, and invasion are related in a complex manner, mediated by a range of signalling molecules including HIFs, zinc finger E-box-binding homeobox 1 (ZEB1), and vascular endothelial growth factor (VEGF) (Soeda *et al.* 2009; Siebzehnrubl *et al.* 2013; Joseph *et al.* 2015).

It is possible that the HiSpots® in this case are demonstrating and maintaining these different tumour phenotypes. Lee *et al.* (2006) demonstrated the importance of avoiding serum-containing media to maintain tumour cell state. The serum-free media used for these HiSpots® may allow for the maintenance of these different tumour cell phenotypes, rather than driving them all towards differentiation.

There are also some clear differences in structure between the core and contrast-enhancing biopsy HiSpots® for GBM39. In addition, this patient also provided sufficient cellular material for combined HiSpots®, so these are also presented. All GBM39 HiSpots® grew in a very uniformly round manner, providing clearly defined rings, although the relative sizes of these rings differed between the groups. In the core and contrast-enhancing HiSpots®, a band of single-thickness cells are visible surrounding the bulk of the HiSpot®. However, in the combined HiSpot®, this ring is almost non-existent. Instead the bulk of the HiSpot® extends to the far edge of the cellular population. As determined in **5.2.2.3**, the central mass in the combined HiSpots® is significantly larger than in either the core or contrast-enhancing biopsies, and the reverse is true for the outer ring of cells. Overall this could suggest that the bulk of the combined biopsy HiSpots® grew faster or more horizontally than its matched biopsies, overwhelming the area in which the

single-thickness cells may have been. Alternatively, this could represent a difference in cellular behaviour, potentially a synergistic effect of the two biopsies being combined, resulting in a change in growth pattern. This is not the only difference between the biopsies for patient GBM39. The arrangement of the tumour cells also varies. In the core biopsy, the tumour cells are well contained within the main bulk of the HiSpot®, and do not seem to have a defined arrangement, overlapping with themselves and microglia. The contrast-enhancing HiSpot® shows a clear pattern of groups of tumour cells forming into structures, leaving clusters of microglia between them. The tumour cells also appear to send protrusions of cell body outwards from the HiSpot® into the outer ring. These appear to be extensions from cells at the edge of the HiSpots®, perhaps indicating the more migratory nature of cells collected from the outer edge of the tumour in comparison to the inner cells which may be more proliferative (Dhruv *et al.* 2013; Binda *et al.* 2017; Mehta and Lo Cascio 2018). Interestingly, the tumour cells in the combined HiSpot® appear somewhere in between the two arrangements, with a more clearly defined structure than those in the core biopsy HiSpot®, but without the clustering that is so clear in the contrast-enhancing biopsy HiSpot®. This further supports the theory that the combined biopsy HiSpots® represent a mixture of the cell types present in the biopsies, and that they are not overwhelmed by the properties of one or the other.

There are many fewer differences visible between HiSpots® from different biopsies in patients 41 and 47. Patient 41, a secondary GBM, would have developed from a LGG. There does appear to be some difference in cell density and β-IIIT reactivity between the biopsies, with both being higher in the core biopsy than contrast-enhancing biopsy HiSpot®. However, the overall cellular structure appears similar between the two, and no obvious differences in arrangement are visible. It is possible that this is a result of sampling error, if the biopsies taken were not accurately sourced and were actually from similar areas of the tumour. The biopsy location method is

considered accurate, but there is a possibility that it is not as precise as would be ideal. This could explain the less pronounced differences between the HiSpots®. The cells also seem to be evenly distributed across the HiSpot® area, in contrast to the multi-ringed structure of patients GBM39 and 40 (**Figure 5-4**). It is possible that the development of this tumour from a lower grade has led to a more uniform structure. Alternatively, if the LGG had been previously noted or treated, this may have led to recurrence of the tumour from a particular subclone, or earlier detection, perhaps reducing the time in which the tumour could develop the stark heterogeneity between biopsies visible in the earlier patients. However, it is also possible that the two biopsies were from overlapping or similar areas, and so do not have the contrasting behaviour seen earlier. Future comparisons to other secondary GBMs and LGGs may be able to determine whether this behaviour is particular to secondary GBMs or merely representative of this particular patient.

GBM47 does also not show clear differences between the HiSpots® from different biopsies, but is itself an interesting representation of GBM heterogeneity. Instead of a singular mass, the cells of GBM47 appear to have formed a much smaller central mass, surrounded by much smaller satellite clusters, within a sparse arrangement of single cells. The pathology report for this patient did not note it as being a multifocal tumour, although this is a phenotype which sometimes arises. It is possible that this is the result of a particular subtype, but analysis and comparison to known common GBM mutations would be required to determine this. Interestingly, Hubert *et al.* (2016) also noted a satellite-like growth of smaller tumour structures surrounding their central organoid in a primary human tumour-derived Matrigel model. This would support the idea that the formation of these satellite cultures is a result of a particular mutation or subtype. The HiSpots® from the four patients shown in **5.2.2.2** clearly demonstrate the heterogeneity present between GBM patients, and the importance of

determining biopsy location wherever possible in order to more precisely characterise GBM populations.

5.3.2.3 Structural patient-specific features of HiSpots® vary between biopsies

In order to provide some clarity to the structural differences between biopsies discussed above, these features were quantified and compared where possible. Firstly, the total HiSpot® area was measured for all patients, to identify whether there were major differences between them. Analysis showed that GBM41 formed the largest HiSpots®, and GBM40 the smallest. This did not indicate a large difference between HiSpots® from different patients, particularly GBM47, which despite having a much smaller central mass, still only extended to approximately the same area as the other HiSpots®. **Figure 5-5A**, which shows the total HiSpot® areas broken down by biopsy demonstrates the variation within patients is relatively limited, which indicates that the differences seen are likely to be a result of inter-patient variability.

The multi-ring structure of HiSpots® from patients GBM39 and 40 was analysed individually for comparison between biopsies. For both patients, the area of the outer ring, migratory ring and central mass were measured in HiSpots® from all available biopsies (**Figure 5-5C, D**). There were no significant differences in these areas between biopsies for patient GBM40. However there were significant differences for patient GBM39. As mentioned above, the most obvious difference is in the size of the outer ring of single-thickness cells. The cells in this ring were mostly positive for IBA1, indicating that they are a population of microglia surrounding the main HiSpot® body. This IBA1+ staining is visible in **Figure 5-6A**. This ring is the largest in the contrast-enhancing biopsy HiSpots®. It is slightly smaller in the core biopsy HiSpots® but reduced to a very small area in the combined biopsy HiSpots®. This difference is somewhat offset by the central mass being much larger in the combined biopsy HiSpots® than others, and in fact the contrast-enhancing biopsy HiSpots® have the smallest central mass overall. The size of the migratory ring is very small in HiSpots® from all

biopsies, and did not vary significantly between them. These interesting results suggest that the behaviour of the combined biopsies may be more complicated than just a 50:50 split of the features of the core and contrast-enhancing biopsies. Potentially, the combination of the two biopsy sites promoted cell growth outwards, eclipsing the majority of the outer ring.

In contrast, there were no significant differences in the areas of the rings in core and contrast-enhancing biopsy HiSpots® from patient GBM40 (**Figure 5-5D**). The outer ring was much smaller in comparison with GBM39, although the migratory ring was larger. The size of the central mass correlated with that of GBM39, although without combined biopsy HiSpots® it is difficult to know whether the same relationship would be seen. It is clear that there are significant structural differences between the HiSpots® from the immunofluorescence images. No further structural analysis was performed for GBM41 as the cell distribution was uniform, without any ring or satellite features to measure.

For GBM47, a number of features were measured (**Figure 5-5E-H**). Firstly, the size of the central mass was recorded. Although this analysis showed that the contrast-enhancing biopsy HiSpots® had larger central masses than either the core or combined biopsies, this difference was not significant when calculated as a percentage of the total HiSpot® area. This could imply that as the central mass grows, the monolayer surrounding the HiSpot expands outwards, or that the size of the central area is merely representative of the overall HiSpot® growth. As the central mass of these HiSpots® was surrounded by satellite clusters of cells, the size and number of these was also analysed. The number of satellites per HiSpot® did not change significantly between the different biopsies. The size of the satellites was not significant, but showed a trend towards a statistically significant difference ($p=0.0502$) between contrast-enhancing and core biopsy HiSpots®, with the former having satellite clusters approximately three times larger than the latter. However, this may not be a result of proliferation, as there was no significant difference between the levels of

EdU incorporation between the core and contrast-enhancing biopsy HiSpots®, and the trend would suggest higher proliferation in the core-derived HiSpots®. The size of the satellites in the combined HiSpots®, although not significantly different, appeared somewhere in between the core and contrast-enhancing biopsy HiSpots®. This further supports the theory that the combined HiSpots® demonstrate features between those of the core and contrast-enhancing biopsy HiSpots®. The level of variation in HiSpots® created from different biopsies for GBM47 was much lower than for patients GBM39 and GBM40, although the patient GBM47 itself does stand out from the others due to its cellular distribution.

Overall, a large amount of both inter- and intra-tumour variability is detectable in these multiple biopsy HiSpots®, which demonstrates the ability of the HiSpot® model to capture and maintain aspects of GBM heterogeneity *in vitro*. Tumour heterogeneity is a key feature for any model which aims to improve understanding of GBM behaviour and biology.

5.3.2.4 HiSpots® extend protrusions which vary between biopsy areas

Tumour cell protrusions were noted in GBM39 and GBM40 HiSpots® which seemed to extend into the ring of mostly microglial cells surrounding the central mass. The length and number of these protrusions were counted in both patients (**Figure 5-6**). In GBM39 there were far more protrusions per HiSpot® in the contrast-enhancing biopsy HiSpots® than either the core or combined HiSpots®. These were also longer than those in HiSpots® from the other biopsies. These data suggest that the contrast-enhancing biopsy cells from GBM39 had a more invasive phenotype than the core, and that the cells favoured this outward growth in comparison to, potentially, a more proliferative phenotype. This is supported by the data in **5.2.5.2** which show a significantly higher incorporation of EdU in HiSpots® created from the core biopsy than those from the contrast-enhancing biopsy for patient GBM39.

This would imply that the cells have maintained their microenvironmental cues from the original tumour. Their behaviour is reminiscent of the ‘go or

grow' hypothesis, with cells from the outer edge of the tumour remaining predominantly invasive, and cells from the core remaining less so (Dhruv *et al.* 2013; Mehta and Lo Cascio 2018). For both the number and length of the protrusions, HiSpots® from the combined biopsy behaved similarly to the core biopsy, which indicates that this particular behaviour may have been overridden by the presence of core cells. However, this is in contrast to HiSpots® from GBM40, where the protrusions present were both longer and more numerous in the core compared to the contrast-enhancing biopsy HiSpots®. This implies that the differences seen may not be determined by whether the biopsies are from the core or contrast-enhancing areas, but represent other types of heterogeneity within the tumour. The phenotypes seen are not universal throughout the GBM cases which highlights once again the importance of representing the heterogeneity present in this tumour type. Taking into account the appearance of the HiSpots® from these two biopsies, it is possible that the number and length of the invasive protrusions is not necessarily representative of the same phenotype as in GBM39. It is possible that these biopsies are from different subtypes, or that the two biopsies represent different subclones within the tumour as well as different biopsy locations. It is also possible that these migratory cell phenotypes seen in HiSpots® are a random artefact of the culture method. Further patient repeats and comparison to subtype data will help determine whether this is the case. Using a patient-derived ECM model, Koh *et al.* (2018) demonstrated how human GBM cells can have both elongated and rounded invasive phenotypes, which they associated with mesenchymal or amoeboid-like behaviours. They pointed out that these have different invasive behaviours, with the elongated (mesenchymal) cells growing consistently in one direction, and the rounded (amoeboid) cells invading in random directions, with less well-defined protrusions. These differences in invasive behaviour could explain the significantly different phenotypes seen in patient GBM40.

5.3.2.5 Tumour cells vary in morphology but not number in HiSpots® from different biopsies

The number of GFAP+ β-IIIT+ tumour cells was recorded at both the centre and edge of HiSpots® from multiple biopsies (**Figure 5-7**). There were no significant differences between percentages of tumour cells in HiSpots® from the core, contrast-enhancing or combined biopsies either at the centre or edge of the HiSpots®. At the centre they were approximately 80% of the cell population, and around 60-70% at the edge. Therefore it is likely that the differences seen between the biopsies for each patient are not a result of the number of GFAP+ β-IIIT+ tumour cells, but of their behaviour.

These behavioural differences are perhaps represented by the differences in cellular morphology visible in **Figure 5-8**. This provides a different viewpoint to the tile scan images, highlighting individual cell structure. Firstly, there are striking differences between the three different patients shown. HiSpots® from GBM41 were not imaged for this analysis due to loss of immunofluorescent signal. The images presented are from the edge of the HiSpots®, within the migratory ring, where the structural differences between biopsies and patients are more clear. At a glance, patients GBM39 and 47 seem more densely packed than GBM40. Patient GBM47 has a uniform, almost cobblestone-like pattern, especially in the core and combined biopsies. This pattern is lost somewhat in the contrast-enhancing biopsy. In comparison, the contrast-enhancing biopsy HiSpots® from GBM39 seem to be the most organised, contrasting with the more erratic arrangement of the cells in the HiSpots® from the core biopsy in particular. A similar case is present in GBM40, where the tumour cells have more clearly defined cytoplasm. The GBM40 core biopsy tumour cells appear thin, with long extensions reaching out from the higher density area. Cellular protrusions are still visible in the contrast-enhancing biopsy but seem to be more organised, connecting to other cells in the immediate area. The microglia in this biopsy particularly appear more rounded, and clearly interspersed within the tumour cells, than in the core HiSpots®.

The image from the core biopsy HiSpot® from GBM39 shows very spindly, long cellular extensions, arranged erratically. In the image from the contrast-enhancing HiSpot®, these seem to be more organised into paths, leaving gaps in between. The combined biopsy lies somewhere in between, with the cellular organisation appearing more structured than the core, but not as complex as the contrast-enhancing image. The microglia seem more integrated within the tumour cells of the contrast-enhancing and combined biopsies, and mostly restricted to the edge of the tumour cell mass in the core HiSpot®.

The HiSpots® from GBM47 all show a dense field of tumour cells, with microglia bordering the mass. In all images, the microglia are somewhat intertwined with the tumour cells near the edge, but this is far more noticeable in the contrast-enhancing and combined biopsy HiSpots®. As noted above, the tumour cells seem smaller in GBM47, and the most extensions are seen in the contrast-enhancing biopsy HiSpots®. The cellular arrangement in the combined HiSpot® does indicate a combination of the core and contrast-enhancing phenotypes, but perhaps more reminiscent of the core in this case.

Throughout the three patients, there seems to be a theme of the contrast-enhancing biopsies having more microglia embedded within the main HiSpot® mass than their matched core or combined biopsies. Further experimentation would be required to see if this is a result of a higher proportion of microglia in the original biopsy. An interesting future experiment could combine the two cell types from different biopsies and see if the number of microglia within the HiSpot® is affected by the origin of either cell type. Microglia have been demonstrated to increase glioma cell invasion, triggered by the release of factors such as metalloprotease-2 from tumour cells, so it is possible that this feedback loop is responsible for the varying behaviours of microglia in the different biopsies presented (Markovic *et al.* 2005; Carvalho da Fonseca *et al.* 2014; Hambardzumyan *et al.* 2016).

5.3.2.6 Microglia demonstrate different behaviours between different biopsy areas

The most stand-out feature of GBM39 contrast-enhancing biopsy HiSpots® is the microglial clustering, surrounded by a network of tumour cells. The size and number of these clusters was quantified for each biopsy (**Figure 5-9D, E**). This showed that the most clusters were present in the combined biopsy, but that the clusters were far larger in the contrast-enhancing biopsy HiSpots® than either of the others (**Figure 5-9E**). This is reasonable, given that as the number of clusters increases, they may eventually overlap or combine to form larger clusters. As the clusters in the combined biopsy HiSpots® are of a similar size to those in the core biopsy HiSpots® but far outnumber them, this may represent a combination of the two phenotypes. This also reinforces the idea that microglial infiltration is increased in the contrast-enhancing biopsy HiSpots® in comparison with the core or combined HiSpots®.

Interestingly however, the percentage of microglial cells was not significantly higher in HiSpots® from the contrast-enhancing area than the core (**Figure 5-10**). However, in images from the centre of the HiSpots®, the percentage of microglia was higher in the contrast-enhancing HiSpots® than in the combined HiSpots® (**Figure 5-10A**). No significant differences were seen in images from the edge of the HiSpots®. It has been recognised that the M1/M2 theory of microglia is over-simplified, and that microglia exist on more of a spectrum between the states (Hambardzumyan *et al.* 2016). In addition, it has been demonstrated that microglia within and around GBMs are often converted to a pro-tumour state which does not fully align with any healthy phenotype (Pyonteck *et al.* 2013; Carvalho da Fonseca *et al.* 2014). Future work could attempt to characterise different microglial states within the HiSpots® from different biopsies, and test the growth of the HiSpots® if microglial communication via M-CSF or other factors is disrupted.

5.3.3 HiSpots® can demonstrate biopsy-specific differences in proliferation and TMZ response

One of the important roles of disease models is to predict the response in humans to potential types of treatment. The heterogeneity of GBM adds an extra layer of complexity to this as the response may not necessarily be consistent throughout an individual tumour, let alone from one patient to the next. Therefore it is important to have a model capable of representing these areas and recapitulating their potentially contrasting behaviour. This chapter has focused on the differences between the core and contrast-enhancing areas of GBM tumours, but with access to sufficient tissue from each tumour, these experiments could be extrapolated to investigate more sub-populations at once.

This set of experiments looking at the response of multiple biopsies to treatment used two patients. GBM39 provided core, contrast-enhancing and peripheral biopsies. GBM47 provided core, contrast-enhancing and combined biopsies. All biopsies collected were treated with 100 μM TMZ and compared to DMSO-treated controls.

5.3.3.1 Total area fluorescence intensity can vary with biopsy area but does not demonstrate significant change with TMZ treatment

Total area fluorescence intensity was used again to provide a representation of the total cell population within the HiSpot®. None of the biopsies from any patient showed a change in total area fluorescence intensity with treatment (**Figure 5-11**). However total area fluorescence intensity did vary between the DMSO control HiSpots® from each biopsy. In GBM39, both core and contrast-enhancing biopsy HiSpots® had significantly higher total area fluorescence intensity than the peripheral biopsy HiSpots®, indicating potentially poor growth with this biopsy (**Figure 5-11A**). There were no significant differences for GBM47 (**Figure 5-11B**). These data indicate that even with the same calculated cell density, there are differences in growth and survival between different biopsy areas. Various factors could cause these differences. It is not possible to exclude that the cell density varied

between the biopsies due to variations in levels of debris or red blood cells. The time between tissue removal and processing will vary between multiple biopsies but should not greatly impact cell survival as all biopsies were kept on ice during surgery. These differences could be caused just by the different biopsy locations, and the heterogeneity they represent. A mixture of factors can affect multiple biopsy sampling, so consistency and communication with surgical staff is key to producing the best model going forward. It is also key to have matched controls from each biopsy for any measurements.

Overall, these data imply that, using this treatment protocol, TMZ does not have a significant effect on the total cell population in the HiSpots®. As all of the patients used for this experiment were confirmed to have unmethylated *MGMT* promoters, they would not be expected to respond to treatment. It is possible that a longer or repeated exposure to TMZ would eventually show a detectable effect on the total cell count and total area fluorescence intensity.

5.3.3.2 Proliferation levels vary between biopsy areas and with TMZ treatment

EdU is used as a marker of proliferation levels in culture. It was used in this experiment to track the HiSpots® response to TMZ, as the drug should prevent tumour cells from being able to proliferate. Cleaved caspase-3 was not used as a marker for apoptosis for this experiment (as it was in the previous chapter) due to high variability in previous work leading to unclear results. EdU levels in the HiSpots® from different biopsies may also give an insight into the underlying levels of proliferation in those biopsies.

As may have been expected from the low total area fluorescence intensity, the peripheral biopsy HiSpots® from patient GBM39 had almost no EdU positivity, and therefore very low levels of proliferation. In comparison, the core and contrast-enhancing biopsy HiSpots® from the same patient had much higher proliferation levels (**Figure 5-12A**). The core biopsy HiSpots® had significantly higher proliferation levels in DMSO-treated controls than

the contrast-enhancing biopsy HiSpots®. This correlates with Pistollato *et al.* (2010), who demonstrated higher levels of proliferation (using Ki-67) in core compared with contrast-enhancing (labelled peripheral in their work) primary human cell cultures. Multiple other groups have also demonstrated higher proliferation levels in the core of the tumour than at the edge, in concordance with the 'go or grow' hypothesis (Dhruv *et al.* 2013; Smith *et al.* 2017; Mehta and Lo Cascio 2018). Given that the GBM contrast-enhancing HiSpots® showed higher migratory capacity than the core HiSpots®, it follows that they would have the opposite relationship for proliferation levels. Patient GBM47 did not show any significant differences in proliferation between the different biopsies, but the trend does indicate a slightly higher baseline proliferation in the core compared with the contrast-enhancing HiSpots®.

Only the core biopsy HiSpots® in GBM39 showed a significant reduction in proliferation following TMZ treatment. The contrast-enhancing biopsy HiSpots® did not respond, and the peripheral biopsy HiSpots® were non-proliferative which did not change with treatment (**Figure 5-12A**). This would suggest that for this patient, the tumour cells of the core were sensitive to TMZ, but the cells of the contrast-enhancing area were not. This is likely to be a result of tumour heterogeneity, and highlights the importance of testing multiple tumour areas for drug sensitivity. Interestingly, this is in contrast with Pistollato *et al.* (2010), who demonstrated responses to TMZ in the contrast-enhancing, but not core, cultures. Given the high inter-patient variability present in GBM, it is likely that these location-specific responses would also vary between patients. However, the authors also described that the levels of MGMT activity also varied between their biopsy locations, and the use of the MGMT inhibitor 6-BG clarified that this was the probable cause of the difference in sensitivity to TMZ that they recorded (Pistollato *et al.* 2010). The levels of MGMT activity in different biopsy locations could be investigated in further work using the HiSpot® model.

In HiSpots® from patient GBM47, the core was shown to respond to TMZ treatment and the contrast-enhancing and combined HiSpots® did not (**Figure 5-12B**). However, the response seen in the core biopsy HiSpots® was a significant, approximately two-fold increase in EdU incorporation, rather than the expected decrease. As this was unexpected, further imaging was performed to check that this was not an artefact of the imaging or quantification techniques. Confocal imaging at the centre and edge of the HiSpots® in question confirmed the increase in EdU+ cells between DMSO control and TMZ-treated HiSpots® (**Figure 5-12D**). As this response was confirmed using further imaging it is unlikely to be a random result. Therefore, other explanations must be explored. One possibility is that the increased incorporation of EdU is a result of DNA repair in the tumour cells. All patients were confirmed to have unmethylated *MGMT* promoters, which results in normal levels of the MGMT enzyme in the cell. Cells with active MGMT (unmethylated) are able to repair the DNA damage caused by the drug, and recover (Hegi *et al.* 2005; Zhang *et al.* 2012). DNA repair may include the synthesis of new DNA, which would cause the cells to incorporate EdU under these conditions, although the ability to detect this using the kit may be limited when compared to the much stronger, whole nucleus signal of S-phase cells (Verbruggen *et al.* 2014). There is a possibility that the increases in proliferation for patient GBM47 represents the recovery of the tumour after initial DNA damage and repair, and that the single dose of TMZ has acted as a trigger to cause increased proliferation in the repaired cells. This could be mitigated by using a repeated dose protocol going forward. It will be key to compare the responses of multiple biopsies in patients with methylated *MGMT* promoters, as these would be expected to respond to TMZ treatment without recovery. It is important to elucidate whether the increase in proliferation is a feature of certain patients using this particular treatment protocol, or a feature of any TMZ treatment in unmethylated HiSpots®.

Another potential cause is the phenomenon of hormesis. Hormesis is defined as the contradictory, biphasic effects of a molecule or treatment. It results in a non-linear dose-response relationship, often described as a U-shaped, inverted U-shaped, or J-shaped curve. For example, a drug which has a pro-proliferative effect at a low dose and an anti-proliferative effect at a higher dose would be described as having a hormetic effect. Hormesis has roles in many cellular pathways, including cancer related pathways such as the NF-κB pathway, known to be involved in the 'go or grow' proliferation/invasion switch (Maynard 2011; Dhruv *et al.* 2013; Bhakta-Guha and Efferth 2015). PARP is also hormetic. Low levels of PARP activation lead to the repair of DNA damage, but excessive levels of PARP activation lead to neuronal injury and excitotoxicity. Some cancer treatments have been demonstrated to have hormetic activity, including treatments for colon, breast and bladder cancers (Calabrese 2005). It is possible for drugs to have completely different uses at different doses. For example, metformin is used at a low dose as an anti-diabetic treatment, but at high doses as an anti-cancer treatment due to its hormetic effect (Bhakta-Guha and Efferth 2015). The prevalence of hormesis in targetable biological pathways has caused the FDA to suggest comprehensive analysis of dose-response relationships in drug development, although this is not currently a requirement (Bhakta-Guha and Efferth 2015).

Hormesis has been demonstrated in the treatment of certain ocular diseases with anti-proliferative drugs which, at a lower dose have a pro-proliferative effect instead. Anti-tumour drugs have been shown to enhance rather than prevent proliferation at lower doses (Calabrese 2005). Hormetic responses have also been demonstrated in a number of GBM cell lines, as well as patient astrocytoma cultures. Inter-individual variation in hormesis is a concern, especially if there is a narrow window between the contradictory effects.

Coupled with the multi-factoral heterogeneity present in GBM, it is possible that any potential hormetic effect of TMZ could be present in TMZ-treated

HiSpots® if the particular dose received by the cells was within the right concentration range. This could potentially explain the marked increase in proliferation seen in TMZ-treated HiSpots® from patient GBM47. As the HiSpots® only received one 100 µM treatment but remained in culture for five days, it is possible that as TMZ degraded, the concentration was reduced to one with a hormetic, proliferative effect, causing the response seen above.

In future experiments, certain factors could be optimised to reduce the possibility of hormesis. Even if this is not the cause of the result in these cases, it is an important feature to take into account in any future drug-testing protocols. In patients, TMZ is administered daily over the course of the treatment, which results in the tumour facing constant onslaught. In comparison, the HiSpots® only received one treatment. With a half-life of 1.8 hours in plasma, this dose of TMZ would quickly degrade, reducing the effective concentration (Brada *et al.* 1999; Zhang *et al.* 2012). A similar half-life has been reported in aqueous solution (Bobola *et al.* 2010; Svec *et al.* 2018).

Future experiments should address the potential of repeated dosing of TMZ, perhaps once daily, until fixation. Ideally, HiSpots® could be fixed at multiple timepoints within the treatment regime, in order to identify the peak response time for analysis. This will however require a vast number of cells, and therefore a large volume of tumour tissue. This is a limiting factor for how expansive HiSpot® experiments can be. Alternatively, live imaging systems or daily media analysis could be implemented to track the response of the HiSpots® to TMZ over time.

Another key question is whether combined HiSpots® from multiple biopsies represent one or all of the constituent populations. Although combined HiSpots® have been shown to contain phenotypic features of the original biopsies (**5.3.1**), their sensitivity to treatment may be determined by only one of the constituent biopsies. For example, if one biopsy is resistant to treatment, this may allow the combined HiSpots® to survive, even if the

other biopsy is sensitive to treatment. The HiSpots® from GBM47 indicate that the combined HiSpots® respond like those from the contrast-enhancing area. Further experiments should expand on this format, with further separate and combined biopsies, and potentially multiple doses of TMZ for comparison. It is important to clarify whether a combined HiSpot® would respond to treatment if created from one responsive and one non-responsive biopsy, in order to determine the potential for combined HiSpots® in treatment response analysis going forward. Unfortunately it was not possible to collect the same biopsy areas from each patient for these experiments, which limits generalised conclusions. Nevertheless it is clear that the treatment protocol requires some optimisation, and further experiments should stress the collection of biopsies from the same radiological areas from each patient.

5.3.4 Chapter conclusions

Structural and cell type analyses of HiSpots® from multiple biopsies have demonstrated clear inter- and intra-tumour heterogeneity, particularly between the core and contrast-enhancing biopsies. These differences dramatically affect the overall structure, tumour cell behaviour, microglial morphology, and tumour cell: microglial interactions. It is therefore extremely important to have these differences represented in the HiSpot® model. Although further characterisation is required, it seems that combined HiSpots® retain features of each biopsy, and may be able to act as a bridge between different biopsy areas. However, at this point it is still important to determine the features of each biopsy area, especially which differences are patient- or subtype- specific, and which are specific to the biopsy area. Overall, the HiSpot® method is capable of representing differences in treatment response between biopsies from the same tumour via proliferation levels. However, further experiments are required in order to determine the optimum dosing regimen, further readouts, and the possible impact of hormesis in this model.

The HiSpot® is an excellent tool for identifying and characterising differences in cell organisation, structure, and behaviour between different areas of a GBM tumour. It is also useful for investigating differences in cell proliferation levels under drug treatment, but requires further optimisation to fulfil its potential for this purpose.

6 General Discussion

6.1 Reiteration of aims and background

A plethora of models are available for GBM, and all have their advantages and limitations. Many models are limited by the use of established cell lines, serum-containing media, or a lack of appropriate microenvironmental conditions. Animal models in particular are expensive, raise ethical concerns, and their contributions to significant pharmacological developments have been limited. The HiSpot® model provides a more complex cellular environment than 2D models, without the use of the artificial scaffolds or gels often used in 3D modelling. The aim of this project was to develop the HiSpot® model for use in GBM research for examining cellular interaction and pharmaceutical development, through optimisation, validation, and utilisation stages. This chapter will discuss whether and how these aims have been met.

The aims as stated in the introduction were:

1. Optimise the pre-existing HiSpot® protocol to stably culture primary human GBM cells, prioritising tumour cells and microglia
2. Confirm that the optimised protocol produces a culture model which represents key pathological features and pharmacological response of GBM in human patients
3. Determine whether the HiSpot® model can recapitulate the variation of cellular and structural features, and pharmacological responses, between biopsy locations

6.2 Overview of results

The first set of experiments (**Chapter 3**) were designed to optimise the previous HiSpot® protocol for primary GBM cells. The existing protocol was used for the culture of primary human brain tissue from patients with epilepsy. Given the different aetiology between this disease and glioblastoma, it was considered likely that primary cells from glioblastoma

may require different culture conditions. Initial characterisation of GBM HiSpots® showed poor long-term survival, which improved with the removal of serum from the culture media. However, the HiSpots® did not form cultures noticeably thicker than one cell layer until the initial cell density was increased. It is likely that large amounts of debris or red blood cells confounded the initial counting step, but by increasing the calculated density, this problem was overcome, producing multi-layered HiSpots®. Further optimisation of the culture media demonstrated that these higher density HiSpots® were capable of surviving in serum-free media without requiring supplemental growth factors, and that both triple-positive tumour cells and microglia were supported in this system. Triple-positive tumour cells were confirmed as tumour-derived by *IDH-1* R132H positivity in a secondary GBM patient, and tumour cells were confirmed to express SOX2, making it probable that these cells represent the CSC population, and that the stemness is supported by the optimised HiSpot® protocol. Therefore the first aim was achieved, as the HiSpots® were successfully optimised to stably culture primary human GBM cells, specifically tumour cells and microglia.

The second set of experiments (**Chapter 4**) focused on validating the HiSpot® as a disease model for GBM. Firstly, the patients used for this study were compared against the wider population. A similar distribution of sex, age, MGMT methylation status and *IDH-1* mutation status were found between the patients used for this study and the general patient population. Specific pathological features were then compared. It was demonstrated that GBM HiSpots® recapitulate a range of proliferation levels and GFAP positivity, and also capture specific pathological features such as giant cells. These features validate that GBM HiSpots® represent pathological features of GBM from a representative patient population.

Dose-dependent reductions in proliferation in response to TMZ treatment were seen in HiSpots® from patients with MGMT promoter methylation and not in those without, which demonstrated the potential validity of the HiSpot® as a potential model for pharmaceutical testing. Therefore, the

second aim was achieved, as the HiSpots® were demonstrated to represent pathological features and recapitulate MGMT methylation status-specific response to TMZ treatment.

However, some unexpected responses were seen in HiSpots® from unmethylated patients. Further investigation with multiple biopsies from each patient was performed. A decrease in EdU+ cells was seen in the core biopsy HiSpots® only from patient GBM39, which may indicate an increased sensitivity of the core compared with contrast-enhancing biopsy area, and an unexpected increase in proliferation with TMZ treatment was seen in the core biopsy HiSpots® from patient GBM47. Given that all biopsies were from patients with unmethylated MGMT promoters, this aligns somewhat with the previous data. It is possible that this increase in proliferation was a result of damage-induced DNA repair, or a hormetic effect (altered response at a different dose, see **5.3.2.2**). Cells with unmethylated MGMT promoters are damaged by TMZ but are able to repair the damage (Zhang *et al.* 2012). It is possible that the damaged tumour cells then increase their proliferation rate as a result of this attack, causing the increases seen. These results demonstrate that the HiSpot® model demonstrates significant utility for drug testing and for identifying and investigating unexpected or off target effects of pharmaceutical interventions. Some optimisation may be required before the HiSpot® model can be implemented for large scale investigations.

In addition to showing some intra-tumour differences in HiSpot® response to TMZ from unmethylated patients, GBM HiSpots® were also demonstrated to recapitulate structural and cellular differences between tumour locations (**Chapter 5**). HiSpots® showed that many features of the tumour cells and microglia can vary between HiSpots® from core and contrast-enhancing areas of the tumour, and that combining multiple biopsies often results in an intermediate representation. In particular, there were differences in the interactions between microglia and tumour cells, which indicates the importance of the former being included by the model. Therefore, the final aim was mostly met as the HiSpots® could recapitulate variations in cellular

features such as microglia numbers, and organisational features such as multi-ringed structures, as well as TMZ response, between different biopsy locations. However, histology was not available for individual biopsies, so it was not possible to confirm that the differences seen were representative of differences within each patient. The features seen may be a result of the re-aggregation culture method which allows the tissue to reorganise, and not necessarily visible in histology.

6.2.1 The HiSpot® model does not detect a response to TMZ treatment in unmethylated patients

In both experiments where HiSpots® were treated with TMZ, there were a number of unmethylated *MGMT* patients (**4.2.3.2** and **5.2.5.2**). Although there were clear reductions in EdU+ cells per HiSpot® in patients with methylated *MGMT*, the HiSpots® from patients with unmethylated *MGMT* showed less clear results. As no *MGMT* methylated patients were available for the later experiment using multiple biopsies, all samples shown for this experiment are from unmethylated patients. It is possible that the differences seen in **Figure 5-12** would have been insignificant when compared to the response of methylated samples, or that the non-responsive patient HiSpots® in **Figure 4-5** would be significant if not compared to methylated samples. The decision was made to group all unmethylated samples together for a null analysis. Core and contrast-enhancing biopsy data from **5.2.5.2** were grouped with the same dose-point data from **4.2.3.2** to produce an overall comparison of untreated (0 µM) and TMZ treated (100 µM) HiSpots® from unmethylated patients. These data can be seen in **Figure 6-1** below. There was no significant difference between the untreated (0 µM) and treated (100 µM) doses overall (190.0±105.3 vs 197.7 ±100.8, p=0.9453, n=3-10 for each patient and dose combination, paired Wilcoxon test). Overall it can be concluded that the HiSpot® model does not detect a response to TMZ treatment in unmethylated patient HiSpots®.

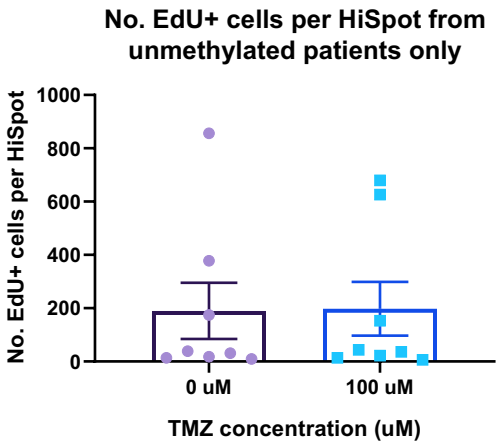

Figure 6-1: Number of EdU+ cells per HiSpot® after TMZ treatment in unmethylated patients.

Previous data from chapters 4 and 5 were grouped together to compare the difference in EdU+ cells per HiSpot® between untreated and treated unmethylated patient HiSpots®. Mean data per patient are shown imposed over mean ± SEM. n=3-10 for each patient and dose combination.

6.3 The utility of the HiSpot® model for GBM

6.3.1 Comparison to other models of GBM with a focus on the most similar (complex 3D)

The HiSpot® model has clear advantages over 2D culture systems. As the cells reaggregate in a 3D structure, they are able to form more complex networks. This allows greater cell-cell communication, an increased tissue density, and trophic support within the culture. The use of primary cells is also an advantage over standard 2D models which often rely on established cell lines which are phenotypically dissimilar from the original tumours. In simple 3D models such as spheroids it is difficult to maintain uniform sizes or track individual spheroids long term. The HiSpot® model also has certain advantages over *in vivo* models in general, as these have species differences, are usually immuno-incompetent when using patient-derived xenografts, and more expensive than *in vitro* models.

The point at which more specific advantages come into question is with other, similarly complex 3D models. These include scaffolds, gels,

microfluidic chips and organ slices. Below is a table summarising key models used in other GBM research, key advantages and disadvantages, and examples of where this model has been used (**Table 6-1**). This list is not exhaustive but covers the most commonly used model types.

Table 6-1: Models of GBM.

The main complex 3D models used for GBM research are described with their key advantages, limitations, and examples of their use in research.

Model	*Description*	*Advantages*	*Limitations*	*Examples*
Scaffold	Cells are seeded into and bind to a solid network of fibres, allowing them to form 3D interactions	Cells are maintained in 3D environment allowing them to grow and connect	Scaffolds are formed of artificial substances	(Gomez-Roman *et al.* 2017; Saleh *et al.* 2019)
Hydrogel	Cells are seeded or resuspended into a gel which holds them in a 3D structure	Cells are maintained in 3D and physical properties of the gel can be altered to match the brain environment	Hydrogels vary batch to batch and often contain high levels of non-brain ECM components	(Wang *et al.* 2016; Xiao *et al.* 2018; Hermida *et al.* 2019; Yi *et al.* 2019)
Microfluidic chip	Structures are formed in a microfluidic chip	Chip structures can be customised for each experiment and many factors and cell types can be included	Chips are often formed of unusual substrates for cell growth. Fluid volumes are very small.	(Akay *et al.* 2018; Yi *et al.* 2019)
Organ-slice	Whole slices of tissue are placed on a semi-permeable membrane	Original tissue connections are maintained	Slices are not uniform between sections, preparation of slices is labour intensive	(Stoppini *et al.* 1991; Marques-Torrejon *et al.* 2018; Henrik Heiland *et al.* 2019)
HiSpots®	Primary cellular material is reaggregated at an air-liquid interface	GBM tumour stem cells and microglia are both supported in a 3D network and serum-free media	Endothelial cells are not supported by the current system	

Scaffold and gel models both depend on an additional, artificial substance to provide 3D support for the cells. Hydrogels in particular can vary in constitution between batches and often include high levels of collagen, which is only a small part of the ECM of the brain when compared with other organs (Barros *et al.* 2011; Schiffer *et al.* 2019). Factors such as hyaluronic acid are further upregulated in GBM, meaning that the tumour ECM is different to that of healthy brain (Ferrer *et al.* 2018; Wolf *et al.* 2019).

The 3D bioprinted model developed by Hermida *et al.* (2019) is one of the few GBM models to co-culture tumour cells with human microglia and their modification of the cell lines to express fluorescent proteins allowed for easy cell-type identification without reliance on immunofluorescent staining. However, the microglia used were purchased from an independent supplier, isolated from healthy brain, and cultured in serum-containing media. Although their model necessitates separate populations of cancer stem cells and microglia, these factors may have had unintended effects on the microglia, potentially affecting their interactions with the tumour cells. In addition, all the cell lines used for their project were initially cultured in 2D.

An interesting model by Coniglio *et al.* (2012), with further adaptations described in their 2016 follow-up, uses the co-culture of microglia and GBM cells to investigate the influence of microglia on GBM cell invasion (Coniglio *et al.* 2016). However, this model does use microglia isolated from mice alongside established mouse and human GBM cell lines, which limits the translatability of the model to humans. In later work, the cells are also embedded in Matrigel which adds an additional confounding factor to the protocol, as Matrigel is not well defined (Wolf *et al.* 2019). Henrik Heiland *et al.* (2019) demonstrated that tumour cells and microglia can both be supported in a slice model from human patients. However, the slices were prepared from healthy patient brain tissue, and tumour cells were injected in from a different source, although still a human line, and so both the tumour and brain microenvironments were not typical of human GBMs in their model.

Overall, the current models do not satisfactorily represent the behaviour of the microglia within the tumour, and often rely on additional, artificial substances to allow the tumour cells to form a 3D structure. The HiSpot® model addresses these limitations through co-culture of primary tumour and microglial cells, and the reaggregation of cells producing their own self-generating 3D structure.

6.3.2 Key advantages and limitations of the HiSpot® model

The most important advantage of the HiSpot® model over other complex 3D *in vitro* models is the inclusion of the patient's microglia along with their CSCs. Very few of the models of GBM discussed above include microglia, and where they do the microglia are often not derived from the same origin as the tumour. Melief *et al.* (2016) demonstrated that, much like GBM cell lines, human microglia are subject to significant genetic drift in long term culture, making established cell lines such as CHME-5 a poor representation of microglial behaviour *in situ*. In addition, Szulzewsky *et al.* (2016) used RNA sequencing to demonstrate that GBM associated microglia/macrophages had many upregulated genes related to the mitotic cell cycle, migration, adhesion, and ECM organisation in comparison to non-tumour human control cells. Importantly, they did not demonstrate upregulated genes related to immune activation, whereas these are upregulated in mouse comparisons between tumour and non-tumour GAMs. This highlights the potential benefits of the HiSpot® model using human microglia, and specifically those isolated directly from a GBM.

This research has demonstrated the capability of the HiSpot® model to support both primary human microglia and GBM CSCs in the same structure, with the two cell types clearly interacting rather than growing in isolated populations. This provides potential for monitoring the effects of various factors or therapeutic options on the ability of the two cell types to communicate and interact. In addition to this advantage, the HiSpot® model is also able to support both microglia and GBM CSCs in serum-free media. It is now established that GBM CSCs lose their stemness if cultured in serum,

and become unrepresentative of the original tumour (Lee *et al.* 2006). Primary human microglia have also been demonstrated to lose their immune profile if not cultured in serum-free media (Parney *et al.* 2009). The HiSpot® model provides an avenue to culture these two cell types together in the same serum-free media, potentially maintaining their expression profiles as close to the patient's tumour as possible. This also has the advantage of being a more well-defined media, without the batch variability of serum products. This should make the HiSpot® model much more translatable into a high throughput or pharmaceutical screening platform.

GBM HiSpots® represent a number of pathological features found in GBM. They produce proliferation levels which correlate well with their patient-matched origins. This is a key feature to recapitulate as Ki-67 is a prognostic indicator for GBM (Wong *et al.* 2019). GFAP expression levels are maintained from patient to HiSpot®, including in GSM patients with significantly reduced expression. When present in the original tumour, giant cells are also seen in the HiSpots®. These features demonstrate that the HiSpot® can recapitulate important variants of GBM.

The culture of HiSpots® from multiple tumour biopsies identified key differences between the core and contrast-enhancing areas of the tumour. Being able to collect and produce cultures from multiple areas individually and in combination provides a key advantage over organ-slice models, as the HiSpots® can represent one or multiple areas, rather than being reliant specifically on the original location of the slice within the tumour. This could be expanded to investigate different subpopulations within tumours, which are a key contribution to tumour heterogeneity (Sottoriva *et al.* 2013). Differences between subtypes of tumour could also be investigated, whether through bulk or single cell RNA sequencing (Wang *et al.* 2017; Neftel *et al.* 2019). The combined 'pan-tumour' HiSpots® provide a relatively simple method for overcoming the regional heterogeneity of GBM in an *in vitro* model.

GBM HiSpots® can also be used to model proliferation in tumours, and how this changes with TMZ treatment. This can be used to detect inter- and intra-patient differences in treatment sensitivity. This has potential to be used to support clinical decision making as HiSpots® create responsive 3D cultures within 14 DIV. The HiSpots® can be used for personalised therapy testing and provide a result within a few weeks of surgery. This is a clinically relevant timeline as radiotherapy and chemotherapy are delayed for around four weeks to allow the surgical wound to heal adequately (Davis 2016). Factors such as patient recovery time and testing requirements for clinical trails can sometimes delay therapy, but various studies have demonstrated that a delay of up to 48 days between surgery and radiotherapy is not disadvantageous (Seidlitz *et al.* 2015; Katsigiannis *et al.* 2019). This provides sufficient time for the growth, treatment, and analysis of HiSpot® cultures from surgical tissue before the initiation of therapy.

However, one limitation of the current protocol is that it relies on proliferation levels as a readout for treatment response. TMZ acts by preventing proliferation and triggering apoptosis. Although caspase-3 activity would provide an appropriate indicator as an apoptotic marker, it requires further optimisation for the HiSpot® system to improve the signal to noise ratio. Although used in early HiSpot® optimisation, the LDH media assay was not considered appropriate for TMZ response modelling as it detects necrotic rather than apoptotic cell death. The potential increases in proliferation seen with the multiple biopsy experiments also highlight the need for further optimisation.

The drug treatment protocol as a single dose is not necessarily representative of the human treatment regime. Patients undergo multiple cycles of treatment with both radiotherapy and chemotherapy (Davis 2016). It may be possible to add an aspect of this through repeated TMZ dosing or the introduction of radiotherapy treatment to the HiSpot® protocol, while still producing results within a clinically relevant timeline.

A significant limitation of the HiSpot® model is the lack of endothelial cells. Although all the cells of the microenvironment are important and would ideally be included in the model, endothelial cells have been demonstrated to be of particular interest in drug development for GBM, especially as limiting angiogenesis could severely limit tumour growth. Endothelial cells behave differently in GBMs compared with healthy brain (Charalambous *et al.* 2006). Endothelial and tumour cells support each other through the release of multiple factors such as TGF-β, VEGF, and FGF2, and are therefore an important target for drug development (**1.1.4.3,** Wang *et al.* 2010; Brandao *et al.* 2019; Schiffer *et al.* 2019).

6.3.3 Limitations of the study

One of the key benefits of this study is also a key limitation. The use of primary human tissue makes the HiSpot® model far more representative than if established cell lines or animal cells were used. However, this does mean that the size, complexity, and number of experiments are limited by patient and tissue availability. Ideally, each experiment would have had more HiSpots® per condition from more patients, and initial experiments would have been repeated in detail post-optimisation. However, this study was limited by difficulties in optimising the HiSpot® production and culture conditions for GBM, so it was not possible to repeat all experiments in the higher density optimised cultures. In addition, pathology reports were only available after experiments were completed, which meant that some patients had to be retroactively removed from the data sets if not diagnosed as GBM. Although some studies include genetic characterisation of tumours, such as TCGA subtype, it was not possible to do so for this study. This extensive characterisation is not regularly performed by the local health board, and tissue biopsies were not large enough to perform this characterisation in addition to the creation of HiSpots®. This genetic data analysis will become available at the University Hospital of Wales shortly and will open up exciting avenues for further experiments.

6.4 Future work

Many of the current limitations of the HiSpot® technology can be addressed in future work. Firstly, the lack of endothelial cells is important to address given their importance in the tumour microenvironment (Mccoy *et al.* 2019). Attempting to isolate and culture endothelial cells directly from patient tissue would be limited by tissue availability, and isolation techniques may damage the other cell types present. However, the insert aspect of the model would allow the primary HiSpots® to be cultured with or without an epithelial cell line in the main well. In a similar but reversed fashion to Yan *et al.* (2014), the HiSpots® could be created as per the standard protocol, but some inserts could be transferred to a plate in which HUVECs were in culture. This could provide insight into the contributory effects of the vasculature on the tumour HiSpots® and vice versa, and would also provide the opportunity to detect various factors within the culture media, and investigate their roles using conditioned media or similar protocols (Fessler *et al.* 2015). Alternatively, a small volume of endothelial cells could be placed next to the HiSpot® cells on the confetti, allowing the attraction of the cells to the tumour environment to be modelled. This would allow the advantage of being able to perform immunofluorescence staining on the cells after fixation. Live movement of the endothelial cells could potentially be tracked using an immunofluorescent tag such as GFP, as has been demonstrated in other systems (Hermida *et al.* 2019).

Another important topic to tackle in future research is that of pharmacological testing using the HiSpots®. Although effects were seen in HiSpot® dose-response data for MGMT methylated (TMZ-sensitive) patients, a potentially hormetic or reactive DNA repair response was seen in HiSpots® from some MGMT unmethylated patients, in both the dose-response and multiple sampling experiments. This type of contradictory, biphasic response has been previously demonstrated in other cancers and with chemotherapeutic drugs (Calabrese 2005; Bhakta-Guha and Efferth 2015). Future work should establish the effect of a repeated dosing protocol

on treatment response in HiSpots®. It will also be key to implement a further readout for the HiSpot® response, ideally using a system that could be repeatedly monitored in live cultures, rather than requiring fixation as the EdU detection process does. A media-based assay for apoptosis could be used, or a viability stain such as calcein AM. Further work could also investigate the addition of radiotherapy to the treatment protocol, as this is part of the standard of care received for GBM. The effects of radiotherapy on GBM have been previously investigated in other 3D models, both alone and as part of combination therapy (Kaaijk *et al.* 1997; Narayan *et al.* 2017).

The HiSpot® could also potentially provide an avenue to investigate the four states of GBM cells newly determined using single cell RNA sequencing (Neftel *et al.* 2019). The authors described that the tumour cell population is driven towards the mesenchymal state by hypoxia. Given the more hypoxic state of the tumour core compared with the contrast-enhancing area, it would be interesting to test whether the cellular population states are maintained both in the HiSpots® under normoxic and hypoxic culture conditions and if so, if there are quantifiable differences between biopsies from the different areas. This would require cells to be removed from the confetti for single cell RNA sequencing before and after culture as HiSpots® and would provide great insight into the representativeness of the HiSpot® model. It would also be beneficial to compare freshly isolated tissue with newly generated HiSpots® and HiSpots® after 7 or 14 DIV, to compare whether the cellular states are maintained initially and longer term. Although the β-IIIT+GFAP+ cells in the HiSpot® were demonstrated to express SOX2, it would be interesting to use the multiple biopsy technique to detect whether the levels of SOX2 expression vary between biopsy areas, and how the stem cell population is affected by the combination of core and contrast-enhancing cells.

As a key advantage of the HiSpot® model is the presence of primary human microglia, it is an ideal model to investigate the interaction between these and the tumour cells. Future experiments should investigate whether

blockade of the communication cycle between these cell types affects the growth, survival, and interaction of microglia and tumour cells. EGF and the EGFR could be a particularly interesting system to investigate given the importance of EGF as a communicative factor, and the growing interest in EGFR targeted treatments.

6.5 Final conclusions

The HiSpot® is a useful, novel tool for the investigation, understanding and modelling of GBM cellular behaviour and heterogeneity using primary tissue. It fills a research niche between autogenerated primary/stem cell organoid and neurosphere models and PDX animal models, without relying on artificial gels or scaffolds, so is highly translatable to the human disease. It is well suited to the investigation of cellular interactions, particularly between tumour cells and microglia, both of which can be supported in the same cell preparation from each patient or biopsy. It represents a variety of pathological features of GBM, specific to individual patients and subcategories of GBM. It can also be used for detecting cellular responses to treatment and has a potentially key role in personalising treatments prior to radiotherapy, chemotherapy and immunotherapy in patients within a clinically relevant timeline. The HiSpot® model has been successfully adapted for primary human GBM cells and has great potential for use in GBM research.

7 References

Abdel Hadi, L., Anelli, V., Guarnaccia, L., Navone, S., Beretta, M., Moccia, F., … Riboni, L. (2018). A bidirectional crosstalk between glioblastoma and brain endothelial cells potentiates the angiogenic and proliferative signaling of sphingosine-1-phosphate in the glioblastoma microenvironment. *Biochimica et Biophysica Acta - Molecular and Cell Biology of Lipids*. doi: https://doi.org/10.1016/j.bbalip.2018.07.009.

Abiria, S.A., Williams, T. V, Munden, A.L., Grover, V.K., Wallace, A., Lundberg, C.J., … Cooper, M.K. (2014). Expression of Hedgehog ligand and signal transduction components in mutually distinct isocitrate dehydrogenase mutant glioma cells supports a role for paracrine signaling. *Journal of Neuro-Oncology* **119**(2):243–51. doi: https://doi.org/10.1007/s11060-014-1481-7.

Akay, M., Hite, J., Avci, N.G., Fan, Y., Akay, Y., Lu, G. and Zhu, J.-J. (2018). Drug Screening of Human GBM Spheroids in Brain Cancer Chip. **8**:15423. doi: https://doi.org/10.1038/s41598-018-33641-2.

Akgül, S., Patch, A.M., D'souza, R.C.J., Mukhopadhyay, P., Nones, K., Kempe, S., … Day, B.W. (2019). Intratumoural heterogeneity underlies distinct therapy responses and treatment resistance in glioblastoma. *Cancers* **11**(2). doi: https://doi.org/10.3390/cancers11020190.

Akhavan, D., Alizadeh, D., Wang, D., Weist, M.R., Shepphird, J.K. and Brown, C.E. (2019). CAR T cells for brain tumors: Lessons learned and road ahead. *Immunological Reviews* **290**(1):60–84. doi: https://doi.org/10.1111/imr.12773.

Akkerman, N. and Defize, L.H.K.K. (2017). Dawn of the organoid era. *BioEssays* **39**(4):1600244. doi: https://doi.org/10.1002/bies.201600244.

Alcantara Llaguno, S., Sun, D., Pedraza, A.M., Vera, E., Wang, Z., Burns, D.K. and Parada, L.F. (2019). Cell-of-origin susceptibility to glioblastoma formation declines with neural lineage restriction. *Nature Neuroscience* **22**(4):545–555. doi: https://doi.org/10.1038/s41593-018-0333-8.

Alcantara Llaguno, S., Wang, Z., Sun, D., Chen, J., Xu, J., Kim, E., … Parada, L.F. (2015). Adult Lineage Restricted CNS Progenitors Specify Distinct Glioblastoma Subtypes. *Cancer Cell* **28**(4):429–440. doi: https://doi.org/10.1016/j.ccell.2015.09.007.Adult.

Allen, M., Bjerke, M., Edlund, H., Nelander, S. and Westermark, B. (2016). Origin of the U87MG glioma cell line: Good news and bad news. *Science Translational Medicine* **8**(354):354re3. doi: https://doi.org/10.1126/scitranslmed.aaf6853.

Arvanitis, C.D., Ferraro, G.B. and Jain, R.K. (2019). The blood–brain barrier and blood–tumour barrier in brain tumours and metastases. *Nature Reviews Cancer*:1–16. doi: https://doi.org/10.1038/s41568-019-0205-x.

Azzalin, A., Moretti, E., Arbustini, E. and Magrassi, L. (2014). Cell density modulates SHC3 expression and survival of human glioblastoma cells through Fak activation. *Journal of Neuro-Oncology* **120**(2):245–256. doi: https://doi.org/10.1007/s11060-014-1551-x.

Bady, P., Diserens, A.C., Castella, V., Kalt, S., Heinimann, K., Hamou, M.F., … Hegi, M.E. (2012). DNA fingerprinting of glioma cell lines and considerations on similarity measurements. *Neuro-Oncology* **14**(6):701–711. doi: https://doi.org/10.1093/neuonc/nos072.

Bailey, J.L., O'Connor, V., Hannah, M., Hewlett, L., Biggs, T.E., Sundstrom, L.E., … Chad, J.E. (2011). In vitro CNS tissue analogues formed by self-organisation of reaggregated post-natal brain tissue. *Journal of Neurochemistry* **117**(6):1020–1032. doi: https://doi.org/10.1111/j.1471-4159.2011.07276.x.

Bao, S., Wu, Q., McLendon, R.E., Hao, Y., Shi, Q., Hjelmeland, A.B., … Rich, J.N. (2006). Glioma stem cells promote radioresistance by preferential activation of the DNA damage response. *Nature* **444**(7120):756–760. doi: https://doi.org/10.1038/nature05236.

Barros, C.S., Franco, S.J. and Müller, U. (2011). Extracellular Matrix: Functions in the nervous system. *Cold Spring Harbor Perspectives in Biology* **3**(1):1–24. doi: https://doi.org/10.1101/cshperspect.a005108.

Beaumont, T.L., Kupsky, W.J., Barger, G.R. and Sloan, A.E. (2007). Gliosarcoma with multiple extracranial metastases: case report and review of the literature. *Journal of Neuro-Oncology* **83**(1):39–46. doi: https://doi.org/10.1007/s11060-006-9295-x.

Behling, F., Barrantes-Freer, A., Skardelly, M., Nieser, M., Christians, A., Stockhammer, F., … Schittenhelm, J. (2016). Frequency of BRAF V600E mutations in 969 central nervous system neoplasms. *Diagnostic Pathology* **11**(1):55. doi: https://doi.org/10.1186/s13000-016-0506-2.

Beier, D., Hau, P., Proescholdt, M., Lohmeier, A., Wischhusen, J., Oefner, P.J., … Beier, C.P. (2007). CD133+ and CD133- glioblastoma-derived cancer stem cells show differential growth characteristics and molecular profiles. *Cancer Research* **67**(9):4010–4015. doi: https://doi.org/10.1158/0008-5472.CAN-06-4180.

Beliën, A.T.J., Paganetti, P.A. and Schwab, M.E. (1999). Membrane-type 1 matrix metalloprotease (MT1-MMP) enables invasive migration of glioma cells in central nervous system white matter. *Journal of Cell Biology* **144**(2):373–384. doi: https://doi.org/10.1083/jcb.144.2.373.

Bellail, A.C., Hunter, S.B., Brat, D.J., Tan, C. and Van Meir, E.G. (2004). Microregional extracellular matrix heterogeneity in brain modulates glioma cell invasion. *International Journal of Biochemistry and Cell Biology*.

Ben-David, U., Ha, G., Tseng, Y.Y., Greenwald, N.F., Oh, C., Shih, J., … Golub, T.R. (2017). Patient-derived xenografts undergo mouse-specific tumor evolution. *Nature Genetics* **49**(11):1567–1575. doi: https://doi.org/10.1038/ng.3967.

Bhakta-Guha, D. and Efferth, T. (2015). Hormesis: Decoding two sides of the same coin. *Pharmaceuticals* **8**(4):865–883.

Bhat, K.P.L., Balasubramaniyan, V., Vaillant, B., Ezhilarasan, R., Hummelink, K., Hollingsworth, F., … Aldape, K. (2013). Mesenchymal Differentiation Mediated by NF-κB Promotes Radiation Resistance in Glioblastoma. *Cancer Cell* **24**(3):331–346. doi: https://doi.org/10.1016/j.ccr.2013.08.001.

Bian, S., Repic, M., Guo, Z., Kavirayani, A., Burkard, T., Bagley, J.A., … Knoblich, J.A. (2018). Genetically engineered cerebral organoids model brain tumor formation. *Nature Methods* **15**(8):631–639. doi: https://doi.org/10.1038/s41592-018-0070-7.

Biber, K.P.H., Raj, D., Boddeke, H.W.G.M., Olah, M., Den Dunnen, W.F.A., Brouwer, N., … De Haas, A.H. (2011). An optimized protocol for the acute isolation of human microglia from autopsy brain samples. *Glia* **60**(1):96–111. doi: https://doi.org/10.1002/glia.21251.

Biggs, T., Foreman, J., Sundstrom, L., Regenass, U. and Lehembre, F. (2011). Antitumor compound testing in glioblastoma organotypic brain cultures. *Journal of Biomolecular Screening* **16**(8):805–17. doi: https://doi.org/10.1177/1087057111414895.

Billerbeck, E., Barry, W.T., Mu, K., Dorner, M., Rice, C.M. and Ploss, A. (2011). Development of human CD4+FoxP3+ regulatory T cells in human stem cell factor-, granulocyte-macrophage colony-stimulating factor-, and interleukin-3-expressing NOD-SCID IL2Rγnull humanized mice. *Blood* **117**(11):3076–3086. doi: https://doi.org/10.1182/blood-2010-08-301507.

Binda, E., Visioli, A., Giani, F., Trivieri, N., Palumbo, O., Restelli, S., … Vescovi, A.L. (2017). Wnt5a Drives an Invasive Phenotype in Human Glioblastoma Stem-like Cells. *Cancer Research* **77**(4):996–1007. doi: https://doi.org/10.1158/0008-5472.CAN-16-1693.

Bobola, M.S., Kolstoe, D.D., Blank, A. and Silber, J.R. (2010). Minimally cytotoxic doses of temozolomide produce radiosensitization in human glioblastoma cells regardless of MGMT expression. *Molecular Cancer Therapeutics* **9**(5):1208–1218. doi: https://doi.org/10.1158/1535-7163.MCT-10-0010.

Bonneh-Barkay, D. and Wiley, C.A. (2009). Brain extracellular matrix in neurodegeneration. *Brain Pathology* **19**(4):573–585.

Bousquet, G., El Bouchtaoui, M., Sophie, T., Leboeuf, C., De Bazelaire, C., Ratajczak, P., … Janin, A. (2017). Targeting autophagic cancer stem-cells to reverse chemoresistance in human triple negative breast cancer. *Oncotarget* **8**(21):35205–35221. doi: https://doi.org/10.18632/oncotarget.16925.

Brada, M., Judson, I., Beale, P., Moore, S., Reidenberg, P., Statkevich, P., … Cutler, D. (1999). Phase I dose-escalation and pharmacokinetic study of temozolomide (SCH 52365) for refractory or relapsing malignancies. *British Journal of Cancer* **81**(6):1022–1030. doi: https://doi.org/10.1038/sj.bjc.6690802.

Brandao, M., Simon, T., Critchley, G. and Giamas, G. (2019). Astrocytes, the rising stars of the glioblastoma microenvironment. *Glia* **67**(5):779–790. doi: https://doi.org/10.1002/glia.23520.

Brandenburg, S., Müller, A., Turkowski, K., Radev, Y.T., Rot, S., Schmidt, C., … Vajkoczy, P. (2016). Resident microglia rather than peripheral macrophages promote vascularization in brain tumors and are source of alternative pro-angiogenic factors. *Acta Neuropathologica* **131**(3):365–378. doi: https://doi.org/10.1007/s00401-015-1529-6.

Bristol-Myers Squibb Company (2019). *Bristol-Myers Squibb Announces Phase 3 CheckMate -498 Study Did Not Meet Primary Endpoint of Overall Survival with Opdivo (Nivolumab) Plus Radiation in Patients with Newly Diagnosed MGMT-Unmethylated Glioblastoma Multiforme*. Available at: https://news.bms.com/press-release/corporatefinancial-news/bristol-myers-squibb-announces-phase-3-checkmate-498-study-did [Accessed: 29 August 2019].

Cachia, D., Kamiya-Matsuoka, C., Mandel, J.J., Olar, A., Cykowski, M.D., Armstrong, T.S., … De Groot, J.F. (2015). Primary and secondary gliosarcomas: clinical, molecular and survival characteristics. *Journal of Neuro-Oncology* **125**(2):401–410. doi: https://doi.org/10.1007/s11060-015-1930-y.

Calabrese, E. (2005). Cancer biology and hormesis: Human tumor cell lines commonly display hormetic (biphasic) dose responses. *Critical Reviews in Toxicology* **35**(6):463–582. doi: https://doi.org/10.1080/10408440591034502.

Calzolari, A., Larocca, L.M., Deaglio, S., Finisguerra, V., Boe, A., Raggi, C., … Pallini, R. (2010). Transferrin Receptor 2 Is Frequently and Highly Expressed in Glioblastomas. *Translational Oncology* **3**(2):123–134. doi: https://doi.org/10.1593/tlo.09274.

Capper, D., Jones, D.T.W., Sill, M., Hovestadt, V., Schrimpf, D., Sturm, D., … Pfister, S.M. (2018). DNA methylation-based classification of central nervous system tumours. *Nature* **555**(7697):469–474. doi: https://doi.org/10.1038/nature26000.

Carter, T., Shaw, H., Cohn-Brown, D., Chester, K. and Mulholland, P. (2016). Ipilimumab and Bevacizumab in Glioblastoma. *Clinical Oncology* **28**(10):622–626. doi: https://doi.org/10.1016/j.clon.2016.04.042.

Carvalho da Fonseca, A.C., Wang, H., Fan, H., Chen, X., Zhang, I., Zhang, L., … Badie, B. (2014). Increased expression of stress inducible protein 1 in glioma-associated

microglia/macrophages. *Journal of Neuroimmunology* **274**(1–2):71–7. doi: https://doi.org/10.1016/j.jneuroim.2014.06.021.

Ceccarelli, M., Barthel, F.P., Malta, T.M., Sabedot, T.S., Salama, S.R., Murray, B.A., … Silva, T.C. (2016). Molecular Profiling Reveals Biologically Discrete Subsets and Pathways of Progression in Diffuse Glioma. *Cell* **164**(3):550–563. doi: https://doi.org/10.1016/j.cell.2015.12.028.

Charalambous, C., Chen, T.C. and Hofman, F.M. (2006). Characteristics of tumor-associated endothelial cells derived from glioblastoma multiforme. *Neurosurgical Focus* **20**(4):1–5. doi: https://doi.org/10.3171/foc.2006.20.4.e22.

Charles, N.A., Holland, E.C., Gilbertson, R., Glass, R. and Kettenmann, H. (2012). The brain tumor microenvironment. *Glia* **60**(3):502–514. doi: https://doi.org/10.1002/glia.21264.

Chen, J., Li, Y., Yu, T.S., McKay, R.M., Burns, D.K., Kernie, S.G. and Parada, L.F. (2012). A restricted cell population propagates glioblastoma growth after chemotherapy. *Nature* **488**(7412):522–526. doi: https://doi.org/10.1038/nature11287.

Chen, L., Zhang, Y., Yang, J., Hagan, J.P. and Li, M. (2013). Vertebrate Animal Models of Glioma: Understanding the Mechanisms and Developing New Therapies. doi: https://doi.org/10.1016/j.bbcan.2013.04.003.

Chen, X., Zhang, L., Zhang, I.Y., Liang, J., Wang, H., Ouyang, M., … Badie, B. (2014). RAGE Expression in Tumor-Associated Macrophages Promotes Angiogenesis in Glioma. *Cancer Research* **74**(24):7285–7297. doi: https://doi.org/10.1158/0008-5472.CAN-14-1240.

Chen, Z., Htay, A., Santos, W. Dos, Gillies, G.T., Fillmore, H.L., Sholley, M.M. and Broaddus, W.C. (2009). In vitro angiogenesis by human umbilical vein endothelial cells (HUVEC) induced by three-dimensional co-culture with glioblastoma cells. *Journal of Neuro-Oncology* **92**(2):121–128. doi: https://doi.org/10.1007/s11060-008-9742-y.

Cheng, G., Tse, J., Jain, R.K. and Munn, L.L. (2009). Micro-environmental mechanical stress controls tumor spheroid size and morphology by suppressing proliferation and inducing apoptosis in cancer cells. *PLOS ONE* **4**(2):e4632. doi: https://doi.org/10.1371/journal.pone.0004632.

Cheng, L., Huang, Z., Zhou, W., Wu, Q., Donnola, S., Liu, J.K., … Bao, S. (2013). Glioblastoma stem cells generate vascular pericytes to support vessel function and tumor growth. *Cell* **153**(1):139–152. doi: https://doi.org/10.1016/j.cell.2013.02.021.

Chowdhary, S.A., Ryken, T. and Newton, H.B. (2015). Survival outcomes and safety of carmustine wafers in the treatment of high-grade gliomas: a meta-analysis. *Journal of Neuro-Oncology* **122**(2):367–382. doi: https://doi.org/10.1007/s11060-015-1724-2.

Chuang, D.F. and Lin, X. (2019). Targeted Therapies for the Treatment of Glioblastoma in Adults. *Current Oncology Reports* **21**(7):61. doi: https://doi.org/10.1007/s11912-019-0807-1.

Claussen, C., Laniado, M., Schörner, W., Niendorf, H.P., Weinmann, H.J., Fiegler, W. and Felix, R. (1985). Gadolinium-DTPA in MR imaging of glioblastomas and intracranial metastases. *American Journal of Neuroradiology* **6**(5):669–74.

Codrici, E., Enciu, A.M., Popescu, I.D., Mihai, S. and Tanase, C. (2016). Glioma Stem Cells and Their Microenvironments: Providers of Challenging Therapeutic Targets. *Stem Cells International* **2016**. doi: https://doi.org/10.1155/2016/5728438.

Colwell, N., Larion, M., Giles, A.J., Seldomridge, A.N., Sizdahkhani, S., Gilbert, M.R. and Park, D.M. (2017). Hypoxia in the glioblastoma microenvironment: Shaping the phenotype of cancer stem-like cells. *Neuro-Oncology* **19**(7):887–896. doi: https://doi.org/10.1093/neuonc/now258.

Coniglio, S., Miller, I., Symons, M. and Segall, J.E. (2016). Coculture Assays to Study Macrophage and Microglia Stimulation of Glioblastoma Invasion. (116):53990. doi: https://doi.org/10.3791/53990.

Coniglio, S.J., Eugenin, E., Dobrenis, K., Stanley, E.R., West, B.L., Symons, M.H. and Segall, J.E. (2012). Microglial Stimulation of Glioblastoma Invasion Involves Epidermal Growth Factor Receptor (EGFR) and Colony Stimulating Factor 1 Receptor (CSF-1R) Signaling. *Molecular Medicine* **18**(3):519–527. doi: https://doi.org/10.2119/molmed.2011.00217.

Cooper, G.M. (2000). Intermediate Filaments. *The Cell: A Molecular Approach. 2nd Edition.* Sunderland (MA): Sinauer Associates.

Cosset, E., Locatelli, M., Marteyn, A., Lescuyer, P., Dall Antonia, F., Mor, F.M., … Tieng, V. (2019). Human Neural Organoids for Studying Brain Cancer and Neurodegenerative Diseases. *Journal of Visualized Experiments*(148):1–8. doi: https://doi.org/10.3791/59682.

Davis, M.E. (2016). Glioblastoma: Overview of Disease and Treatment. *Clinical Journal of Oncology Nursing* **20**(5):S2-8. doi: https://doi.org/10.1188/16.CJON.S1.2-8.

deCarvalho, A.C., Kim, H., Poisson, L.M., Winn, M.E., Mueller, C., Cherba, D., … Verhaak, R.G.W. (2018). Discordant inheritance of chromosomal and extrachromosomal DNA elements contributes to dynamic disease evolution in glioblastoma. *Nature Genetics* **50**(5):708–717. doi: https://doi.org/10.1038/s41588-018-0105-0.

Desjardins, A., Gromeier, M., Herndon, J.E., Beaubier, N., Bolognesi, D.P., Friedman, A.H., … Bigner, D.D. (2018). Recurrent Glioblastoma Treated with Recombinant Poliovirus. *New England Journal of Medicine* **379**(2):150–161. doi: https://doi.org/10.1056/NEJMoa1716435.

Dhruv, H.D., McDonough Winslow, W.S., Armstrong, B., Tuncali, S., Eschbacher, J., Kislin, K., … Berens, M.E. (2013). Reciprocal activation of transcription factors underlies the dichotomy between proliferation and invasion of glioma cells. *PLOS ONE* **8**(8):e72134. doi: https://doi.org/10.1371/journal.pone.0072134.

Dick, J.E. and Bonnet, D. (1997). Human Acute Myeloid Leukaemia is organised as a heirarchy that originates from the primitive haematopoetic cell. *Nature Medicine* **3**(7):730–737.

Dráberová, E., Del Valle, L., Gordon, J., Marková, V., Smejkalová, B., Bertrand, L., … Katsetos, C.D. (2008). Class III beta-tubulin is constitutively coexpressed with glial fibrillary acidic protein and nestin in midgestational human fetal astrocytes: implications for phenotypic identity. *Journal of Neuropathology and Experimental Neurology* **67**(4):341–54. doi: https://doi.org/10.1097/NEN.0b013e31816a686d.

Eidel, O., Burth, S., Neumann, J.-O., Kieslich, P.J., Sahm, F., Jungk, C., … Radbruch, A. (2017). Tumor Infiltration in Enhancing and Non-Enhancing Parts of Glioblastoma: A Correlation with Histopathology Kleinschnitz, C. (ed.). *PLOS ONE* **12**(1):e0169292. doi: https://doi.org/10.1371/journal.pone.0169292.

Ernst, A., Hofmann, S., Ahmadi, R., Becker, N., Korshunov, A., Engel, F., … Radlwimmer, B. (2009). Genomic and Expression Profiling of Glioblastoma Stem Cell-Like Spheroid Cultures Identifies Novel Tumor-Relevant Genes Associated with Survival. *Clinical Cancer Research* **15**(21):6541–6550. doi: https://doi.org/10.1158/1078-0432.CCR-09-0695.

Fan, X., Xiong, Y. and Wang, Y. (2019). A reignited debate over the cell(s) of origin for glioblastoma and its clinical implications. *Frontiers of Medicine*:1–9. doi: https://doi.org/10.1007/s11684-019-0700-1.

Feitsma, H., Kuiper, R. V, Korving, J., Nijman, I.J. and Cuppen, E. (2008). Zebrafish with Mutations in Mismatch Repair Genes Develop Neurofibromas and Other Tumors. *Cancer Research* **68**(13):5059–66. doi: https://doi.org/10.1158/0008-5472.CAN-08-0019.

Feng, X., Szulzewsky, F., Yerevanian, A., Chen, Z., Heinzmann, D., Rasmussen, R.D., … Hambardzumyan, D. (2015). Loss of CX3CR1 increases accumulation of inflammatory monocytes and promotes gliomagenesis. *Oncotarget* **6**(17):15077–94. doi: https://doi.org/10.18632/oncotarget.3730.

Ferrer, V.P., Moura Neto, V. and Mentlein, R. (2018). Glioma infiltration and extracellular matrix: key players and modulators. *Glia* **66**(8):1542–1565. doi: https://doi.org/10.1002/glia.23309.

Fessler, E., Borovski, T. and Medema, J.P. (2015). Endothelial cells induce cancer stem cell features in differentiated glioblastoma cells via bFGF. *Molecular Cancer* **14**(1):1–12. doi: https://doi.org/10.1186/s12943-015-0420-3.

Fulton, B., Short, S.C., James, A., Nowicki, S., McBain, C., Jefferies, S., … Chalmers, A.J. (2018). PARADIGM-2: Two parallel phase I studies of olaparib and radiotherapy or olaparib and radiotherapy plus temozolomide in patients with newly diagnosed glioblastoma, with treatment stratified by MGMT status. *Clinical and Translational Radiation Oncology* **8**:12–16. doi: https://doi.org/10.1016/j.ctro.2017.11.003.

Gallagher, P.G., Bao, Y., Prorock, A., Zigrino, P., Nischt, R., Politi, V., … Fox, J.W. (2005). Gene expression profiling reveals cross-talk between melanoma and fibroblasts: Implications for host-tumor interactions in metastasis. *Cancer Research* **65**(10):4134–4146. doi: https://doi.org/10.1158/0008-5472.CAN-04-0415.

Galli, R., Binda, E., Orfanelli, U., Cipelletti, B., Gritti, A., Vitis, S. De, … Vescovi, A. (2004). Isolation and Characterization of Tumorigenic , Stem-like Neural Precursors from Human Glioblastoma. *Cancer Research* **64**(19):7011–7021. doi: https://doi.org/10.1158/0008-5472.CAN-04-1364.

Gan, H.K., Reardon, D.A., Lassman, A.B., Merrell, R., van den Bent, M., Butowski, N., … Kumthekar, P. (2018). Safety, pharmacokinetics, and antitumor response of depatuxizumab mafodotin as monotherapy or in combination with temozolomide in patients with glioblastoma. *Neuro-Oncology* **20**(6):838–847. doi: https://doi.org/10.1093/neuonc/nox202.

Garnier, D., Renoult, O., Paris, F. and Corbet, C. (2019). Glioblastoma Stem- Like Cells , Metabolic Strategy to Kill a Challenging Target. **9**(March):1–18. doi: https://doi.org/10.3389/fonc.2019.00118.

Garros-Regulez, L., Garcia, I., Carrasco-Garcia, E., Lantero, A., Aldaz, P., Moreno-Cugnon, L., … Matheu, A. (2016). Targeting SOX2 as a Therapeutic Strategy in Glioblastoma. *Frontiers in Oncology* **6**:222. doi: https://doi.org/10.3389/fonc.2016.00222.

Giakoumettis, D., Kritis, A. and Foroglou, N. (2018). C6 cell line: the gold standard in glioma research. *Hippokratia* **22**(3):105–112.

Gilbert, M.R., Dignam, J.J., Armstrong, T.S., Wefel, J.S., Blumenthal, D.T., Vogelbaum, M.A., … Mehta, M.P. (2014). A Randomized Trial of Bevacizumab for Newly Diagnosed Glioblastoma. *New England Journal of Medicine* **370**(8):699–708. doi: https://doi.org/10.1056/NEJMoa1308573.

Ginhoux, F., Greter, M., Leboeuf, M., Nandi, S., See, P., Gokhan, S., … Merad, M. (2010). Fate mapping analysis reveals that adult microglia derive from primitive macrophages. *Science* **330**(6005):841–845. doi: https://doi.org/10.1126/science.1194637.

Glass, R. and Synowitz, M. (2014). CNS macrophages and peripheral myeloid cells in brain tumours. *Acta Neuropathologica* **128**(3):347–362. doi: https://doi.org/10.1007/s00401-014-1274-2.

Gomez-Roman, N., Stevenson, K., Gilmour, L., Hamilton, G. and Chalmers, A.J. (2017). A novel 3D human glioblastoma cell culture system for modeling drug and radiation

responses. *Neuro-Oncology* **19**(2):229–241. doi: https://doi.org/10.1093/neuonc/now164.

Goyal, Rama, Mathur, S.K., Gupta, S., Goyal, Rahul, Kumar, S., Batra, A., … Sen, R. (2015). Immunohistochemical expression of glial fibrillary acidic protein and CAM5.2 in glial tumors and their role in differentiating glial tumors from metastatic tumors of central nervous system. *Journal of Neurosciences in Rural Practice* **6**(4):499. doi: https://doi.org/10.4103/0976-3147.168426.

Graeber, M.B., Streit, W.J. and Kreutzberg, G.W. (1988). The microglial cytoskeleton: vimentin is localized within activated cellsin situ. *Journal of Neurocytology* **17**(4):573–580. doi: https://doi.org/10.1007/BF01189811.

Gramatzki, D., Roth, P., Rushing, E.J., Weller, J., Andratschke, N., Hofer, S., … Weller, M. (2018). Bevacizumab may improve quality of life, but not overall survival in glioblastoma: an epidemiological study. *Annals of Oncology* **29**(6):1431–1436. doi: https://doi.org/10.1093/annonc/mdy106.

De Groot, C.J., Montagne, L., Janssen, I., Ravid, R., Van Der Valk, P. and Veerhuis, R. (2000). Isolation and characterization of adult microglial cells and oligodendrocytes derived from postmortem human brain tissue. *Brain Research* **5**(1):85–94.

Guzauskas, G.F., Pollom, E.L., Stieber, V.W., Wang, B.C.M. and Garrison, L.P. (2019). Tumor treating fields and maintenance temozolomide for newly-diagnosed glioblastoma: a cost-effectiveness study. *Journal of Medical Economics*. doi: https://doi.org/10.1080/13696998.2019.1614933.

Haage, V., Semtner, M., Vidal, R.O., Hernandez, D.P., Pong, W.W., Chen, Z., … Gutmann, D.H. (2019). Comprehensive gene expression meta-analysis identifies signature genes that distinguish microglia from peripheral monocytes/macrophages in health and glioma. *Acta Neuropathologica Communications* **7**(1):20. doi: https://doi.org/10.1186/s40478-019-0665-y.

Hadjiloucas, I., Gilmore, A.P., Bundred, N.J. and Streuli, C.H. (2001). Assessment of apoptosis in human breast tissue using an antibody against the active form of caspase 3 : relation to tumour histopathological characteristics. *British Journal of Cancer* **85**(10):1522–1526. doi: https://doi.org/10.1054/bjoc.2001.2115.

Hambardzumyan, D., Gutmann, D.H. and Kettenmann, H. (2016). The role of microglia and macrophages in glioma maintenance and progression. **19**(1). doi: https://doi.org/10.1038/nn.4185.

Hegi, M.E., Diserens, A.-C., Gorlia, T., Hamou, M.-F., de Tribolet, N., Weller, M., … Stupp, R. (2005). MGMT Gene Silencing and Benefit from Temozolomide in Glioblastoma. *New England Journal of Medicine* **352**(10):997–1003. doi: https://doi.org/10.1056/nejmoa043331.

Hemmati, H.D., Nakano, I., Lazareff, J.A., Masterman-Smith, M., Geschwind, D.H., Bronner-Fraser, M. and Kornblum, H.I. (2003). Cancerous stem cells can arise from pediatric brain tumors. *Proceedings of the National Academy of Sciences of the United States of America* **100**(25):15178–83. doi: https://doi.org/10.1073/pnas.2036535100.

Hendrickx, D.A.E., van Eden, C.G., Schuurman, K.G., Hamann, J. and Huitinga, I. (2017). Staining of HLA-DR, Iba1 and CD68 in human microglia reveals partially overlapping expression depending on cellular morphology and pathology. *Journal of Neuroimmunology* **309**:12–22. doi: https://doi.org/10.1016/j.jneuroim.2017.04.007.

Henrik Heiland, D., Ravi, V.M., Behringer, S.P., Frenking, J.H., Wurm, J., Joseph, K., … Schnell, O. (2019). Tumor-associated reactive astrocytes aid the evolution of immunosuppressive environment in glioblastoma. *Nature Communications* **10**(1). doi: https://doi.org/10.1038/s41467-019-10493-6.

Hermida, M.A., Kumar, J.D., Laverty, K.G., Bartolo, A. Di, Bogomolnijs, M., Clavreul, A., … Leslie, N.R. (2019). Three dimensional in vitro models of cancer: bioprinting multilineage glioblastoma models. *Advances in Biological Regulation*:100658. doi: https://doi.org/10.1016/j.jbior.2019.100658.

Hiebl, B., Peters, S., Gemeinhardt, O., Niehues, S.M. and Jung, F. (2017). Impact of serum in cell culture media on in vitro lactate dehydrogenase (LDH) release determination. *Journal of Cellular Biotechnology* **3**(1):9–13. doi: https://doi.org/10.3233/JCB-179002.

Hoang-Minh, L.B., Deleyrolle, L.P., Siebzehnrubl, D., Ugartemendia, G., Futch, H., Griffith, B., … Sarkisian, M.R. (2016). Disruption of KIF3A in patient-derived glioblastoma cells: Effects on ciliogenesis, hedgehog sensitivity, and tumorigenesis. *Oncotarget* **7**(6):7029–7043. doi: https://doi.org/10.18632/oncotarget.6854.

Hoang-Minh, L.B., Siebzehnrubl, F.A., Yang, C., Suzuki-Hatano, S., Dajac, K., Loche, T., … Deleyrolle, L.P. (2018). Infiltrative and drug-resistant slow-cycling cells support metabolic heterogeneity in glioblastoma. *The EMBO Journal*:e98772. doi: https://doi.org/10.15252/embj.201798772.

Hodge, R.D., Bakken, T.E., Miller, J.A., Smith, K.A., Barkan, E.R., Graybuck, L.T., … Lein, E.S. (2019). Conserved cell types with divergent features in human versus mouse cortex. *Nature*:1–8. doi: https://doi.org/10.1038/s41586-019-1506-7.

Hottinger, A.F., Pacheco, P. and Stupp, R. (2016). Tumor treating fields: a novel treatment modality and its use in brain tumors. *Neuro-Oncology* **18**(10):1338–49. doi: https://doi.org/10.1093/neuonc/now182.

Huang, J.-Y., Cheng, Y.-J., Lin, Y.-P., Lin, H.-C., Su, C.-C., Juliano, R. and Yang, B.-C. (2010). Extracellular Matrix of Glioblastoma Inhibits Polarization and Transmigration of T Cells: The Role of Tenascin-C in Immune Suppression. *The Journal of Immunology* **185**(3):1450–1459. doi: https://doi.org/10.4049/jimmunol.0901352.

Huang, J., Yu, J., Tu, L., Huang, N., Li, H. and Luo, Y. (2019). Isocitrate dehydrogenase mutations in glioma: From basic discovery to therapeutics development. *Frontiers in Oncology* **9**(JUN):1–7. doi: https://doi.org/10.3389/fonc.2019.00506.

Huang, R. and Rofstad, E.K. (2017). Cancer stem cells (CSCs), cervical CSCs and targeted therapies. *Oncotarget* **8**(21):35351–35367.

Hubbard, M.E., Arnold, S., Bin Zahid, A., McPheeters, M., Gerard O'Sullivan, M., Tabaran, A.-F., … Pluhar, G.E. (2018). Naturally Occurring Canine Glioma as a Model for Novel Therapeutics. *Cancer Investigation* **36**(8):415–423. doi: https://doi.org/10.1080/07357907.2018.1514622.

Hubert, C.G., Rivera, M., Spangler, L.C., Wu, Q., Mack, S.C., Prager, B.C., … Rich, J.N. (2016). A Three-Dimensional Organoid Culture System Derived from Human Glioblastomas Recapitulates the Hypoxic Gradients and Cancer Stem Cell Heterogeneity of Tumors Found In Vivo. *Cancer Research* **76**(8):2465–77. doi: https://doi.org/10.1158/0008-5472.CAN-15-2402.

Huynh, E. and Zheng, G. (2015). Cancer nanomedicine: addressing the dark side of the enhanced permeability and retention effect. *Nanomedicine* **10**(13):1993–1995. doi: https://doi.org/10.2217/nnm.15.86.

Ignatova, T.N., Kukekov, V.G., Laywell, E.D., Suslov, O.N., Vrionis, F.D. and Steindler, D.A. (2002). Human cortical glial tumors contain neural stem-like cells expressing astroglial and neuronal markers in vitro. *Glia* **39**(3):193–206. doi: https://doi.org/10.1002/glia.10094.

Janeczko, K. (1993). Co-expression of GFAP and vimentin in astrocytes proliferating in response to injury in the mouse cerebral hemisphere. A combined autoradiographic and double immunocytochemical study. *International Journal of Developmental Neuroscience*

11(2):139–147. doi: https://doi.org/10.1016/0736-5748(93)90074-N.

Jawhari, S., Ratinaud, M.H. and Verdier, M. (2016). Glioblastoma, hypoxia and autophagy: A survival-prone 'ménage-à-trois'. *Cell Death and Disease* **7**(10):e2434.

Jin, P., Shin, S.H., Chun, Y.S., Shin, H.W., Shin, Y.J., Lee, Y., … Park, J.W. (2018). Astrocyte-derived CCL20 reinforces HIF-1-mediated hypoxic responses in glioblastoma by stimulating the CCR6-NF-κB signaling pathway. *Oncogene* **37**(23):3070–3087. doi: https://doi.org/10.1038/s41388-018-0182-7.

Jones, C., Perryman, L. and Hargrave, D. (2012). Paediatric and adult malignant glioma: Close relatives or distant cousins? *Nature Reviews Clinical Oncology* **9**(7):400–413. doi: https://doi.org/10.1038/nrclinonc.2012.87.

Joseph, J. V., Conroy, S., Pavlov, K., Sontakke, P., Tomar, T., Eggens-Meijer, E., … Kruyt, F.A.E. (2015). Hypoxia enhances migration and invasion in glioblastoma by promoting a mesenchymal shift mediated by the HIF1α-ZEB1 axis. *Cancer Letters* **359**(1):107–116. doi: https://doi.org/10.1016/j.canlet.2015.01.010.

Jun, H.J., Appleman, V.A., Wu, H.J., Rose, C.M., Pineda, J.J., Yeo, A.T., … Charest, A. (2018). A PDGFRα-driven mouse model of glioblastoma reveals a stathmin1-mediated mechanism of sensitivity to vinblastine. *Nature Communications* **9**(1). doi: https://doi.org/10.1038/s41467-018-05036-4.

Kaaijk, P., Troost, D., Sminia, P., Hulshof, M.C.C.M., Van Der Kracht, A.H.W., Leenstra, S. and Bosch, D.A. (1997). Hypofractionated radiation induces a decrease in cell proliferation but no histological damage to organotypic multicellular spheroids of human glioblastomas. *European Journal of Cancer Part A* **33**(4):645–651. doi: https://doi.org/10.1016/S0959-8049(96)00503-5.

Kaffes, I., Szulzewsky, F., Chen, Z., Herting, C.J., Gabanic, B., Velázquez Vega, J.E., … Hambardzumyan, D. (2019). Human Mesenchymal glioblastomas are characterized by an increased immune cell presence compared to Proneural and Classical tumors. *OncoImmunology* **8**(11):e1655360. doi: https://doi.org/10.1080/2162402x.2019.1655360.

Kalluri, R. and Zeisberg, M. (2006). Fibroblasts in cancer. *Nature Reviews Cancer* **6**(5):392–401.

Kanzawa, T., Germano, I.M., Komata, T., Ito, H., Kondo, Y. and Kondo, S. (2004). Role of autophagy in temozolomide-induced cytotoxicity for malignant glioma cells. *Cell Death and Differentiation* **11**(4):448–457. doi: https://doi.org/10.1038/sj.cdd.4401359.

Katsetos, C.D., Del Valle, L., Geddes, J.F., Assimakopoulou, M., Legido, A., Boyd, J.C., … Khalili, K. (2001). Aberrant localization of the neuronal class III beta-tubulin in astrocytomas. *Archives of Pathology & Laboratory Medicine* **125**(5):613–24. doi: https://doi.org/10.1043/0003-9985(2001)125<0613:ALOTNC>2.0.CO;2.

Katsigiannis, S., Krischek, B., Barleanu, S., Grau, S., Galldiks, N., Timmer, M., … Stavrinou, P. (2019). Impact of time to initiation of radiotherapy on survival after resection of newly diagnosed glioblastoma. *Radiation Oncology* **14**(1). doi: https://doi.org/10.1186/s13014-019-1272-6.

Khoshnevis, M., Carozzo, C., Bonnefont-Rebeix, C., Belluco, S., Leveneur, O., Chuzel, T., … Ponce, F. (2017). Development of induced glioblastoma by implantation of a human xenograft in Yucatan minipig as a large animal model. *Journal of Neuroscience Methods* **282**:61–68. doi: https://doi.org/10.1016/j.jneumeth.2017.03.007.

Kim, H.K., Lin, C.C., Parker, D., Veals, J., Lim, J., Likhari, P., … Nomeir, A.A. (1997). High-performance liquid chromatographic determination and stability of 5-(3-methyltriazen-1-yl)-imidazo-4-carboximide, the biologically active product of the antitumor agent temozolomide, in human plasma. *Journal of Chromatography* **703**(1–2):225–33.

Kim, J.E., Patel, M., Ruzevick, J., Jackson, C.M. and Lim, M. (2014). STAT3 Activation in Glioblastoma: Biochemical and Therapeutic Implications. *Cancers* **6**:376–395. doi: https://doi.org/10.3390/cancers6010376.

Kleinschmidt-DeMasters, B.K., Aisner, D.L., Birks, D.K. and Foreman, N.K. (2013). Epithelioid GBMs show a high percentage of BRAF V600E mutation. *The American Journal of Surgical Pathology* **37**(5):685–98. doi: https://doi.org/10.1097/PAS.0b013e31827f9c5e.

Koh, I., Cha, J., Park, J., Choi, J., Kang, S.-G. and Kim, P. (2018). The mode and dynamics of glioblastoma cell invasion into a decellularized tissue-derived extracellular matrix-based three-dimensional tumor model. *Scientific Reports* **8**(1):4608. doi: https://doi.org/10.1038/s41598-018-22681-3.

Komohara, Y., Ohnishi, K., Kuratsu, J. and Takeya, M. (2008). Possible involvement of the M2 anti-inflammatory macrophage phenotype in growth of human gliomas. *The Journal of Pathology* **216**(1):15–24. doi: https://doi.org/10.1002/path.

Kozak, K.R. and Moody, J.S. (2009). Giant cell glioblastoma: a glioblastoma subtype with distinct epidemiology and superior prognosis. *Neuro-Oncology* **11**(6):833–41. doi: https://doi.org/10.1215/15228517-2008-123.

Ku, M.-C., Wolf, S.A., Respondek, D., Matyash, V., Pohlmann, A., Waiczies, S., … Kettenmann, H. (2013). GDNF mediates glioblastoma-induced microglia attraction but not astrogliosis. *Acta Neuropathologica* **125**(4):609–620. doi: https://doi.org/10.1007/s00401-013-1079-8.

Lagadec, C., Vlashi, E., Della Donna, L., Dekmezian, C. and Pajonk, F. (2012). Radiation-induced reprogramming of breast cancer cells. *Stem Cells* **30**(5):833–844. doi: https://doi.org/10.1002/stem.1058.

Lan, X., Jörg, D.J., Cavalli, F.M.G., Richards, L.M., Nguyen, L. V., Vanner, R.J., … Dirks, P.B. (2017). Fate mapping of human glioblastoma reveals an invariant stem cell hierarchy. *Nature* **549**(7671):227–232. doi: https://doi.org/10.1038/nature23666.

Lathia, J.D., Mack, S.C., Mulkearns-Hubert, E.E., Valentim, C.L.L. and Rich, J.N. (2015). Cancer stem cells in glioblastoma. *Genes & Development* **29**(12):1203–17. doi: https://doi.org/10.1101/gad.261982.115.

Lee, J., Jo, D.H., Kim, Jin Hyoung, Cho, C.S., Han, J.E., Kim, Y., … Paek, S.H. (2019). Development of a patient-derived xenograft model of glioblastoma via intravitreal injection in mice. *Experimental and Molecular Medicine* **51**(4). doi: https://doi.org/10.1038/s12276-019-0241-3.

Lee, J., Kotliarova, S., Kotliarov, Y., Li, A., Su, Q., Donin, N.M., … Fine, H.A. (2006). Tumor stem cells derived from glioblastomas cultured in bFGF and EGF more closely mirror the phenotype and genotype of primary tumors than do serum-cultured cell lines. *Cancer Cell* **9**(5):391–403. doi: https://doi.org/10.1016/j.ccr.2006.03.030.

Lee, Joo Ho, Lee, J.E., Kahng, J.Y., Kim, S.H., Park, J.S., Yoon, S.J., … Lee, J.H. (2018). Human glioblastoma arises from subventricular zone cells with low-level driver mutations. *Nature* **560**(7717):243–247. doi: https://doi.org/10.1038/s41586-018-0389-3.

Lenting, K., Verhaak, R., Ter Laan, M., Wesseling, P. and Leenders, W. (2017). Glioma: experimental models and reality. *Acta Neuropathologica* **133**(2):263–282. doi: https://doi.org/10.1007/s00401-017-1671-4.

Lenz, K.M. and Nelson, L.H. (2018). Microglia and beyond: Innate immune cells as regulators of brain development and behavioral function. *Frontiers in Immunology* **9**(APR). doi: https://doi.org/10.3389/fimmu.2018.00698.

Liau, L.M., Ashkan, K., Tran, D.D., Campian, J.L., Trusheim, J.E., Cobbs, C.S., … Bosch, M.L.

(2018). First results on survival from a large Phase 3 clinical trial of an autologous dendritic cell vaccine in newly diagnosed glioblastoma. *Journal of Translational Medicine* **16**. doi: https://doi.org/10.1186/s12967-018-1507-6.

Liau, L.M., Prins, R.M., Kiertscher, S.M., Odesa, S.K., Kremen, T.J., Giovannone, A.J., … Roth, M.D. (2005). Dendritic cell vaccination in glioblastoma patients induces systemic and intracranial T-cell responses modulated by the local central nervous system tumor microenvironment. *Clinical Cancer Research* **11**(15):5515–5525. doi: https://doi.org/10.1158/1078-0432.CCR-05-0464.

Lim, M., Xia, Y., Bettegowda, C. and Weller, M. (2018). Current state of immunotherapy for glioblastoma. *Nature Reviews Clinical Oncology* **15**(7):422–442. doi: https://doi.org/10.1038/s41571-018-0003-5.

Linkous, A., Balamatsias, D., Snuderl, M., Edwards, L., Miyaguchi, K., Milner, T., … Fine, H.A. (2019). Modeling Patient-Derived Glioblastoma with Cerebral Organoids. *Cell Reports* **26**(12):3203-3211.e5. doi: https://doi.org/10.1016/j.celrep.2019.02.063.

Liu, C., Sage, J.C., Miller, M.R., Verhaak, R.G.W., Hippenmeyer, S., Vogel, H., … Zong, H. (2011). Mosaic Analysis with Double Markers Reveals Tumor Cell of Origin in Glioma. *Cell* **146**(2):209–221. doi: https://doi.org/10.1016/j.cell.2011.06.014.

Louis, D.N., Ohgaki, H., Wiestler, O.D., Cavenee, W.K., Burger, P.C., Jouvet, A., … Kleihues, P. (2007). The 2007 WHO Classification of Tumours of the Central Nervous System. *Acta Neuropathologica* **114**(2):97. doi: https://doi.org/10.1007/S00401-007-0243-4.

Louis, D.N., Perry, A., Reifenberger, G., von Deimling, A., Figarella-Branger, D., Cavenee, W.K., … Ellison, D.W. (2016). The 2016 World Health Organization Classification of Tumors of the Central Nervous System: a summary. *Acta Neuropathologica* **131**(6):803–820. doi: https://doi.org/10.1007/s00401-016-1545-1.

Luca, A.C., Mersch, S., Deenen, R., Schmidt, S., Messner, I., Schäfer, K.L., … Stoecklein, N.H. (2013). Impact of the 3D Microenvironment on Phenotype, Gene Expression, and EGFR Inhibition of Colorectal Cancer Cell Lines. *PLOS ONE* **8**(3). doi: https://doi.org/10.1371/journal.pone.0059689.

Ma, L., Zhang, B., Zhou, C., Li, Y., Li, B., Yu, M., … Yang, H. (2018). The comparison genomics analysis with glioblastoma multiforme (GBM) cells under 3D and 2D cell culture conditions. *Colloids and Surfaces* **172**:665–673. doi: https://doi.org/10.1016/j.colsurfb.2018.09.034.

Magrassi, L., Conti, L., Lanterna, A., Zuccato, C., Marchionni, M., Cassini, P., … Cattaneo, E. (2005). Shc3 affects human high-grade astrocytomas survival. *Oncogene* **24**(33):5198–5206. doi: https://doi.org/10.1038/sj.onc.1208708.

Mahne, A.E., Mauze, S., Joyce-Shaikh, B., Xia, J., Bowman, E.P., Beebe, A.M., … Jain, R. (2017). Dual roles for regulatory T-cell depletion and costimulatory signaling in agonistic GITR targeting for tumor immunotherapy. *Cancer Research* **77**(5):1108–1118. doi: https://doi.org/10.1158/0008-5472.CAN-16-0797.

Markovic, D.S., Glass, R., Synowitz, M., Rooijen, N. van and Kettenmann, H. (2005). Microglia stimulate the invasiveness of glioma cells by increasing the activity of metalloprotease-2. *Journal of Neuropathology and Experimental Neurology* **64**(9):754–62. doi: https://doi.org/10.1097/01.jnen.0000178445.33972.a9.

Marques-Torrejon, M.A., Gangoso, E. and Pollard, S.M. (2018). Modelling glioblastoma tumour-host cell interactions using adult brain organotypic slice co-culture. *Disease Models & Mechanisms* **11**(2). doi: https://doi.org/10.1242/dmm.031435.

Mason, R., Dearden, H.C., Nguyen, B., Oon, J.S., Smith, J.L., Randhawa, M., … Menzies, A.M. (2019). Combined ipilimumab and nivolumab first-line and after BRAF targeted therapy in advanced melanoma. *Pigment Cell & Melanoma Research*. doi:

https://doi.org/10.1111/pcmr.12831.

Masuda, T., Sankowski, R., Staszewski, O., Böttcher, C., Amann, L., Scheiwe, C., … Prinz, M. (2019). Spatial and temporal heterogeneity of mouse and human microglia at single-cell resolution. *Nature* **566**(7744):388–392. doi: https://doi.org/10.1038/s41586-019-0924-x.

Maynard, K.I. (2011). Hormesis pervasiveness and its potential implications for pharmaceutical research and development. *Dose-Response* **9**(3):377–386. doi: https://doi.org/10.2203/dose-response.11-026.Maynard.

Mccoy, M.G., Nyanyo, D., Hung, C.K., Goerger, J.P., Zipfel, W.R., Williams, R.M., … Fischbach, C. (2019). Endothelial cells promote 3D invasion of GBM by IL-8-dependent induction of cancer stem cell properties. *Scientific Reports* **9**:9069. doi: https://doi.org/10.1038/s41598-019-45535-y.

McLendon, R., Friedman, A., Bigner, D., Van Meir, E.G., Brat, D.J., Mastrogianakis, G.M., … Thomson, E. (2008). Comprehensive genomic characterization defines human glioblastoma genes and core pathways. *Nature* **455**(7216):1061–1068. doi: https://doi.org/10.1038/nature07385.

Mega, A., Hartmark Nilsen, M., Leiss, L.W., Tobin, N.P., Miletic, H., Sleire, L., … Östman, A. (2019). Astrocytes enhance glioblastoma growth. *Glia*(September):1–12. doi: https://doi.org/10.1002/glia.23718.

Mehta, S. and Lo Cascio, C. (2018). Developmentally regulated signaling pathways in glioma invasion. *Cellular and Molecular Life Sciences* **75**(3):385–402. doi: https://doi.org/10.1007/s00018-017-2608-8.

Melief, J., Sneeboer, M.A.M., Litjens, M., Ormel, P.R., Palmen, S.J.M.C., Huitinga, I., … de Witte, L.D. (2016). Characterizing primary human microglia: A comparative study with myeloid subsets and culture models. *Glia* **64**(11):1857–1868. doi: https://doi.org/10.1002/glia.23023.

Merz, F., Gaunitz, F., Dehghani, F., Renner, C., Meixensberger, J., Gutenberg, A., … Bechmann, I. (2013). Organotypic slice cultures of human glioblastoma reveal different susceptibilities to treatments. *Neuro-Oncology* **15**(6):670–681. doi: https://doi.org/10.1093/neuonc/not003.

De Meulenaere, V., Bonte, E., Verhoeven, J., Kalala Okito, J.-P., Pieters, L., Vral, A., … Deblaere, K. (2019). Adjuvant therapeutic potential of tonabersat in the standard treatment of glioblastoma: A preclinical F98 glioblastoma rat model study. *PLOS ONE* **14**(10):e0224130. doi: https://doi.org/10.1371/journal.pone.0224130.

Michael, J.S., Lee, B.-S., Zhang, M. and Yu, D.J.S. (2018). Nanotechnology for Treatment of Glioblastoma Multiforme. *Journal of Translational Internal Medicine* **6**(3):128. doi: https://doi.org/10.2478/JTIM-2018-0025.

Middeldorp, J. and Hol, E.M. (2011). GFAP in health and disease. *Progress in Neurobiology* **93**(3):421–443.

Miyai, M., Tomita, H., Soeda, A., Yano, H., Iwama, T. and Hara, A. (2017). Current trends in mouse models of glioblastoma. *Journal of Neuro-Oncology* **135**(3):423–432.

Monteiro, A., Hill, R., Pilkington, G. and Madureira, P. (2017). The Role of Hypoxia in Glioblastoma Invasion. *Cells* **6**(4):45. doi: https://doi.org/10.3390/cells6040045.

Morantz, R.A., Wood, G.W., Foster, M., Clark, M. and Gollahon, K. (1979). Macrophages in experimental and human brain tumors. *Journal of Neurosurgery* **50**(3):305–311. doi: https://doi.org/10.3171/jns.1979.50.3.0305.

Mulholland, P. (2018). *A Phase II, Open Label, Randomised Study of Ipilimumab with Temozolomide versus Temozolomide Alone after Surgery and Chemoradiotherapy in*

Patients with Recently Diagnosed Glioblastoma. Available at: https://www.oncology.ox.ac.uk/about-us/overview/clinical-trials/clinical-trial-portfolio/ipi-glio [Accessed: 6 November 2019].

Müller, A., Brandenburg, S., Turkowski, K., Müller, S. and Vajkoczy, P. (2015). Resident microglia, and not peripheral macrophages, are the main source of brain tumor mononuclear cells. *International Journal of Cancer* **137**(2):278–288. doi: https://doi.org/10.1002/ijc.29379.

Munroe, M. and Kolesar, J. (2016). Olaparib for the treatment of BRCA-mutated advanced ovarian cancer. *American Journal of Health-System Pharmacy* **73**(14):1037–1041.

Narayan, R.S., Fedrigo, C.A., Brands, E., Dik, R., Stalpers, L.J.A., Baumert, B.G., … Sminia, P. (2017). The allosteric AKT inhibitor MK2206 shows a synergistic interaction with chemotherapy and radiotherapy in glioblastoma spheroid cultures. *BMC Cancer* **17**(1). doi: https://doi.org/10.1186/s12885-017-3193-9.

Neftel, C., Laffy, J., Filbin, M.G., Hara, T., Shore, M.E., Rahme, G.J., … Suvà, M.L. (2019). An Integrative Model of Cellular States, Plasticity, and Genetics for Glioblastoma. *Cell* **178**(4):835-849.e21. doi: https://doi.org/10.1016/j.cell.2019.06.024.

Neradil, J. and Veselska, R. (2015). Nestin as a marker of cancer stem cells. *Cancer Science* **106**(7):803–811.

Nguyen, D.T., Fan, Y., Akay, Y.M. and Akay, M. (2016). Investigating Glioblastoma Angiogenesis Using A 3D in Vitro GelMA Microwell Platform. *IEEE Transactions on Nanobioscience* **15**(3):289–293. doi: https://doi.org/10.1109/TNB.2016.2528170.

NICE (2018). *Brain Tumours (Primary) and Brain Metastases in Adults (NICE Guideline 99)*. Available at: https://www.nice.org.uk/guidance/ng99/resources/brain-tumours-primary-and-brain-metastases-in-adults-pdf-1837763558341 [Accessed: 17 July 2018].

Noh, H., Yan, J., Hong, S., Kong, L.-Y., Gabrusiewicz, K., Xia, X., … Li, S. (2016). Discovery of cell surface vimentin targeting mAb for direct disruption of GBM tumor initiating cells. *Oncotarget* **7**(44):72021–72032. doi: https://doi.org/10.18632/oncotarget.12458.

Norden, A.D., Young, G.S., Setayesh, K., Muzikansky, A., Ciampa, A.S., Ebbeling, L.G., … Wen, P.Y. (2008). Bevacizumab for recurrent malignant gliomas: Efficacy, toxicity, and patterns of recurrence. *Neurology* **70**(10):779–787. doi: https://doi.org/10.1212/01.wnl.0000304121.57857.38.

O'Brien, E., Howarth, C. and Sibson, N.R. (2013). The role of astrocytes in CNS tumours: Pre-clinical models and novel imaging approaches. *Frontiers in Cellular Neuroscience* **7**(MAR):1–13. doi: https://doi.org/10.3389/fncel.2013.00040.

Ogawa, J., Pao, G.M., Shokhirev, M.N. and Verma, I.M. (2018). Glioblastoma Model Using Human Cerebral Organoids. *Cell Reports* **23**(4):1220–1229. doi: https://doi.org/10.1016/j.celrep.2018.03.105.

Oh, J.E., Ohta, T., Nonoguchi, N., Satomi, K., Capper, D., Pierscianek, D., … Ohgaki, H. (2016). Genetic Alterations in Gliosarcoma and Giant Cell Glioblastoma. *Brain Pathology* **26**(4):517–522. doi: https://doi.org/10.1111/bpa.12328.

Oka, H., Utsuki, S., Tanizaki, Y., Hagiwara, H., Miyajima, Y., Sato, K., … Fujii, K. (2013). Clinicopathological features of human brainstem gliomas. *Brain Tumor Pathology* **30**(1):1–7. doi: https://doi.org/10.1007/s10014-012-0099-8.

Oliveira, A.I., Anjo, S.I., Vieira de Castro, J., Serra, S.C., Salgado, A.J., Manadas, B. and Costa, B.M. (2017). Crosstalk between glial and glioblastoma cells triggers the "go-or-grow" phenotype of tumor cells. *Cell Communication and Signaling* **15**(1):37. doi: https://doi.org/10.1186/s12964-017-0194-x.

Omuro, A. and DeAngelis, L.M. (2013). Glioblastoma and other malignant gliomas: a clinical review. *Journal of the American Medical Association* **310**(17):1842–50. doi: https://doi.org/10.1001/jama.2013.280319.

Oppermann, H., Dietterle, J., Purcz, K., Morawski, M., Eisenlöffel, C., Müller, W., … Gaunitz, F. (2018). Carnosine selectively inhibits migration of IDH-wildtype glioblastoma cells in a co-culture model with fibroblasts. *Cancer Cell International* **18**(1):1–10. doi: https://doi.org/10.1186/s12935-018-0611-2.

Ovcharenko, D., Chitjian, C., Kashkin, A., Fanelli, A. and Ovcharenko, V. (2019). Two dichloric compounds inhibit in vivo U87 xenograft tumor growth. *Cancer Biology and Therapy*. doi: https://doi.org/10.1080/15384047.2019.1632131.

Pandita, A., Aldape, K.D., Zadeh, G., Guha, A. and James, C.D. (2004). Contrasting in vivo and in vitro fates of glioblastoma cell subpopulations with amplified EGFR. *Genes, Chromosomes and Cancer* **39**(1):29–36. doi: https://doi.org/10.1002/gcc.10300.

Parker, J.J., Canoll, P., Niswander, L., Kleinschmidt-DeMasters, B.K., Foshay, K. and Waziri, A. (2018). Intratumoral heterogeneity of endogenous tumor cell invasive behavior in human glioblastoma. *Scientific Reports* **8**(1):1–10. doi: https://doi.org/10.1038/s41598-018-36280-9.

Parney, I.F., Waldron, J.S. and Parsa, A.T. (2009). Flow cytometry and in vitro analysis of human glioma–associated macrophages. *Journal of Neurosurgery* **110**(3):572–582. doi: https://doi.org/10.3171/2008.7.JNS08475.

Pastrana, E., Silva-Vargas, V. and Doetsch, F. (2011). Eyes wide open: A critical review of sphere-formation as an assay for stem cells. *Cell Stem Cell* **8**(5):486–498.

Perrin, S.L., Samuel, M.S., Koszyca, B., Brown, M.P., Ebert, L.M., Oksdath, M. and Gomez, G.A. (2019). Glioblastoma heterogeneity and the tumour microenvironment: implications for preclinical research and development of new treatments. *Biochemical Society Transactions*(March):BST20180444. doi: https://doi.org/10.1042/BST20180444.

Persano, L., Rampazzo, E., Della Puppa, A., Pistollato, F. and Basso, G. (2011). The Three-Layer Concentric Model of Glioblastoma: Cancer Stem Cells, Microenvironmental Regulation, and Therapeutic Implications. *The Scientific World Journal* **11**:1829–1841. doi: https://doi.org/10.1100/2011/736480.

Philips, A., Henshaw, D.L., Lamburn, G. and O'Carroll, M.J. (2018). Brain tumours: Rise in glioblastoma multiforme incidence in England 1995-2015 Suggests an Adverse Environmental or Lifestyle Factor. *Journal of Environmental and Public Health* **2018**. doi: https://doi.org/10.1155/2018/7910754.

Phillips, H.S.H.S., Kharbanda, S., Chen, R., Forrest, W.F., Soriano, R.H., Wu, T.D., … Parada, L.F. (2006). Molecular subclasses of high-grade glioma predict prognosis, delineate a pattern of disease progression, and resemble stages in neurogenesis. *Cancer Cell* **9**(3):157–173. doi: https://doi.org/10.1016/j.ccr.2006.02.019.

Pistollato, F., Abbadi, S., Rampazzo, E., Persano, L., Della Puppa, A., Frasson, C., … Basso, G. (2010). Intratumoral hypoxic gradient drives stem cells distribution and MGMT expression in glioblastoma. *Stem Cells* **28**(5):851–862. doi: https://doi.org/10.1002/stem.415.

Platten, M., Kretz, A., Naumann, U., Aulwurm, S., Egashira, K., Isenmann, S. and Weller, M. (2003). Monocyte chemoattractant protein-1 increases microglial infiltration and aggressiveness of gliomas. *Annals of Neurology* **54**(3):388–392. doi: https://doi.org/10.1002/ana.10679.

Pollard, S.M., Yoshikawa, K., Clarke, I.D., Danovi, D., Stricker, S., Russell, R., … Dirks, P. (2009). Glioma Stem Cell Lines Expanded in Adherent Culture Have Tumor-Specific Phenotypes and Are Suitable for Chemical and Genetic Screens. *Cell Stem Cell* **4**(6):568–

580. doi: https://doi.org/10.1016/j.stem.2009.03.014.

Preynat-Seauve, O., Suter, D.M., Tirefort, D., Turchi, L., Virolle, T., Chneiweiss, H., … Krause, K.H. (2009). Development of Human Nervous Tissue upon Differentiation of Embryonic Stem Cells in Three-Dimensional Culture. *Stem Cells* **27**(3):509–520. doi: https://doi.org/10.1634/stemcells.2008-0600.

Priceman, S.J., Forman, S.J. and Brown, C.E. (2015). Smart CARs engineered for cancer immunotherapy. *Current Opinion in Oncology* **27**(6):466–474.

Pyonteck, S.M., Akkari, L., Schuhmacher, A.J., Bowman, R.L., Sevenich, L., Quail, D.F., … Author, N.M. (2013). CSF-1R inhibition alters macrophage polarization and blocks glioma progression. *Nature Medicine* **19**(10):1264–1272. doi: https://doi.org/10.1038/nm.3337.

Qian, X., Jacob, F., Song, M.M., Nguyen, H.N., Song, H. and Ming, G.-L. (2018). Generation of human brain region-specific organoids using a miniaturized spinning bioreactor. *Nature Protocols* **13**(3):565–580. doi: https://doi.org/10.1038/nprot.2017.152.

Rahman, M., Deleyrolle, L., Vedam-Mai, V., Azari, H., Abd-El-Barr, M. and Reynolds, B.A. (2011). The cancer stem cell hypothesis: Failures and pitfalls. *Neurosurgery* **68**(2):531–545. doi: https://doi.org/10.1227/NEU.0b013e3181ff9eb5.

Rascher, G., Fischmann, A., Kröger, S., Duffner, F., Grote, E.-H. and Wolburg, H. (2002). Extracellular matrix and the blood-brain barrier in glioblastoma multiforme: spatial segregation of tenascin and agrin. *Acta Neuropathologica* **104**(1):85–91. doi: https://doi.org/10.1007/s00401-002-0524-x.

Ready, N.E., Ott, P.A., Hellmann, M.D., Zugazagoitia, J., Hann, C.L., de Braud, F., … Spigel, D.R. (2019). Nivolumab Monotherapy and Nivolumab Plus Ipilimumab in Recurrent Small Cell Lung Cancer: Results From the CheckMate 032 Randomized Cohort. *Journal of Thoracic Oncology*. doi: https://doi.org/10.1016/j.jtho.2019.10.004.

Reardon, D.A., Lassman, A.B., van den Bent, M., Kumthekar, P., Merrell, R., Scott, A.M., … Gan, H.K. (2016). Efficacy and safety results of ABT-414 in combination with radiation and temozolomide in newly diagnosed glioblastoma. *Neuro-Oncology* **19**(7):now257. doi: https://doi.org/10.1093/neuonc/now257.

Reitman, Z., Winkler, F. and Elia, A. (2018). New Directions in the Treatment of Glioblastoma. *Seminars in Neurology* **38**(01):050–061. doi: https://doi.org/10.1055/s-0038-1623534.

Renfrow, J.J., Soike, M.H., Debinski, W., Ramkissoon, S.H., Mott, R.T., Frenkel, M.B., … Strowd, R.E. (2018). Hypoxia-inducible factor 2α: A novel target in gliomas. *Future Medicinal Chemistry* **10**(18):2227–2236. doi: https://doi.org/10.4155/fmc-2018-0163.

Rieske, P., Azizi, S.A., Augelli, B., Gaughan, J. and Krynska, B. (2007). A population of human brain parenchymal cells express markers of glial, neuronal and early neural cells and differentiate into cells of neuronal and glial lineages. *European Journal of Neuroscience* **25**(1):31–37. doi: https://doi.org/10.1111/j.1460-9568.2006.05254.x.

Robertson, F.L., Marqués-Torrejón, M.-A., Morrison, G.M. and Pollard, S.M. (2019). Experimental models and tools to tackle glioblastoma. *Disease Models & Mechanisms* **12**(9). doi: https://doi.org/10.1242/dmm.040386.

Robson, M., Im, S.A., Senkus, E., Xu, B., Domchek, S.M., Masuda, N., … Conte, P. (2017). Olaparib for metastatic breast cancer in patients with a germline BRCA mutation. *New England Journal of Medicine* **377**(6):523–533. doi: https://doi.org/10.1056/NEJMoa1706450.

Roesch, S., Rapp, C., Dettling, S. and Herold-Mende, C. (2018). When Immune Cells Turn Bad-Tumor-Associated Microglia/Macrophages in Glioma. *International Journal of*

Molecular Sciences **19**(2). doi: https://doi.org/10.3390/ijms19020436.

Romero-Rojas, A.E., Diaz-Perez, J.A., Ariza-Serrano, L.M., Amaro, D. and Lozano-Castillo, A. (2013). Primary gliosarcoma of the brain: Radiologic and histopathologic features. *Neuroradiology Journal* **26**(6):639–648. doi: https://doi.org/10.1177/197140091302600606.

Rustenhoven, J., Park, T.I.H., Schweder, P., Scotter, J., Correia, J., Smith, A.M., … Dragunow, M. (2016). Isolation of highly enriched primary human microglia for functional studies. *Scientific Reports* **6**:1–11. doi: https://doi.org/10.1038/srep19371.

Rymer, B. (2011). *Characterisation of Adult Tumour Hi-Spots*. University of Southampton.

Sabit, H., Nakada, M., Furuta, T., Watanabe, T., Hayashi, Y., Sato, H., … Hamada, J. (2014). Characterizing invading glioma cells based on IDH1-R132H and Ki-67 immunofluorescence. *Brain Tumor Pathology* **31**(4):242–246. doi: https://doi.org/10.1007/s10014-013-0172-y.

Saleh, A., Marhuenda, E., Fabre, C., Hassani, Z., Weille, J. de, Boukhaddaoui, H., … Bakalara, N. (2019). A novel 3D nanofibre scaffold conserves the plasticity of glioblastoma stem cell invasion by regulating galectin-3 and integrin-β1 expression. *Scientific Reports* **9**(1):14612. doi: https://doi.org/10.1038/s41598-019-51108-w.

Sancho-Martinez, I., Nivet, E., Xia, Y., Hishida, T., Aguirre, A., Ocampo, A., … Izpisua Belmonte, J.C. (2016). Establishment of human iPSC-based models for the study and targeting of glioma initiating cells. *Nature Communications* **7**. doi: https://doi.org/10.1038/ncomms10743.

Sandmann, T., Bourgon, R., Garcia, J., Li, C., Cloughesy, T., Chinot, O.L., … Bais, C. (2015). Patients with proneural glioblastoma may derive overall survival benefit from the addition of bevacizumab to first-line radiotherapy and temozolomide: Retrospective analysis of the AVAglio trial. *Journal of Clinical Oncology* **33**(25):2735–2744. doi: https://doi.org/10.1200/JCO.2015.61.5005.

Sarkisian, M.R., Siebzehnrubl, D., Hoang-Minh, L., Deleyrolle, L., Silver, D.J., Siebzehnrubl, F.A., … Reynolds, B.A. (2014). Detection of primary cilia in human glioblastoma. *Journal of Neuro-Oncology* **117**(1):15–24. doi: https://doi.org/10.1007/s11060-013-1340-y.

Schiffer, D., Annovazzi, L., Casalone, C., Corona, C. and Mellai, M. (2019). Glioblastoma: Microenvironment and niche concept. *Cancers* **11**(1):1–17. doi: https://doi.org/10.3390/cancers11010005.

Schiffer, D., Giordana, M.T., Pezzotta, S., Lechner, C. and Paoletti, P. (1978). Cerebral tumors induced by transplacental ENU: study of the different tumoral stages, particularly of early proliferations. *Acta Neuropathologica* **41**(1):27–31. doi: https://doi.org/10.1007/bf00689553.

Scholz, A., Harter, P.N., Cremer, S., Yalcin, B.H., Gurnik, S., Yamaji, M., … Reiss, Y. (2016). Endothelial cell-derived angiopoietin-2 is a therapeutic target in treatment-naive and bevacizumab-resistant glioblastoma. *EMBO Molecular Medicine* **8**(1):39–57. doi: https://doi.org/10.15252/emmm.201505505.

Seidlitz, A., Siepmann, T., Löck, S., Juratli, T., Baumann, M. and Krause, M. (2015). Impact of waiting time after surgery and overall time of postoperative radiochemotherapy on treatment outcome in glioblastoma multiforme. *Radiation Oncology* **10**(1). doi: https://doi.org/10.1186/s13014-015-0478-5.

Selek, L., Seigneuret, E., Nugue, G., Wion, D., Nissou, M.F., Salon, C., … Berger, F. (2014). Imaging and histological characterization of a human brain xenograft in pig: the first induced glioma model in a large animal. *Journal of Neuroscience Methods* **221**:159–65. doi: https://doi.org/10.1016/j.jneumeth.2013.10.002.

Shabtay-Orbach, A., Amit, M., Binenbaum, Y., Na'Ara, S. and Gil, Z. (2015). Paracrine regulation of glioma cells invasion by astrocytes is mediated by glial-derived neurotrophic factor. *International Journal of Cancer* **137**(5):1012–1020. doi: https://doi.org/10.1002/ijc.29380.

Shackleton, M., Quintana, E., Fearon, E.R. and Morrison, S.J. (2009). Heterogeneity in Cancer: Cancer Stem Cells versus Clonal Evolution. *Cell* **138**(5):822–829. doi: https://doi.org/10.1016/j.cell.2009.08.017.

Sheehan, J.P., Shaffrey, M.E., Gupta, B., Larner, J., Rich, J.N. and Park, D.M. (2010). Improving the radiosensitivity of radioresistant and hypoxic glioblastoma. *Future Oncology* **6**(10):1591–1601.

Shete, S., Hosking, F.J., Robertson, L.B., Dobbins, S.E., Sanson, M., Malmer, B., … Houlston, R.S. (2009). Genome-wide association study identifies five susceptibility loci for glioma. *Nature Genetics* **41**(8):899–904. doi: https://doi.org/10.1038/ng.407.

Siebzehnrubl, F.A., Silver, D.J., Tugertimur, B., Deleyrolle, L.P., Siebzehnrubl, D., Sarkisian, M.R., … Steindler, D.A. (2013). The ZEB1 pathway links glioblastoma initiation, invasion and chemoresistance. *EMBO Molecular Medicine* **5**(8):1196–1212. doi: https://doi.org/10.1002/emmm.201302827.

Siebzehnrubl, F.A. and Steindler, D.A. (2013). Isolating and Culturing of Precursor Cells from the Adult Human Brain. Humana Press, Totowa, NJ, pp. 79–86.

Singh, S.K., Clarke, I.D., Terasaki, M., Bonn, V.E., Hawkins, C., Squire, J. and Dirks, P.B. (2003). Identification of a cancer stem cell in human brain tumors. *Cancer Research* **63**(18):5821–5828.

Skjulsvik, A.J., Mørk, J.N., Torp, M.O. and Torp, S.H. (2014). Ki-67/MIB-1 immunostaining in a cohort of human gliomas. *International Journal of Clinical and Experimental Pathology* **7**(12):8905–10.

Smith, S.J., Diksin, M., Chhaya, S., Sairam, S., Estevez-Cebrero, M.A. and Rahman, R. (2017). The invasive region of glioblastoma defined by 5ALA guided surgery has an altered cancer stem cell marker profile compared to central Tumour. *International Journal of Molecular Sciences* **18**(11):1–13. doi: https://doi.org/10.3390/ijms18112452.

Smith, S.J., Wilson, M., Ward, J.H., Rahman, C. V., Peet, A.C., Macarthur, D.C., … Rahman, R. (2012). Recapitulation of Tumor Heterogeneity and Molecular Signatures in a 3D Brain Cancer Model with Decreased Sensitivity to Histone Deacetylase Inhibition Monleon, D. (ed.). *PLOS ONE* **7**(12):e52335. doi: https://doi.org/10.1371/journal.pone.0052335.

Soeda, A., Hara, A., Kunisada, T., Yoshimura, S.I., Iwama, T. and Park, D.M. (2015). The evidence of glioblastoma heterogeneity. *Scientific Reports* **5**:7979. doi: https://doi.org/10.1038/srep07979.

Soeda, A., Park, M., Lee, D., Mintz, A., Androutsellis-Theotokis, A., McKay, R.D., … Park, D.M. (2009). Hypoxia promotes expansion of the CD133-positive glioma stem cells through activation of HIF-1α. *Oncogene* **28**(45):3949–3959. doi: https://doi.org/10.1038/onc.2009.252.

Sottoriva, A., Spiteri, I., Piccirillo, S.G.M., Touloumis, A., Collins, V.P., Marioni, J.C., … Tavaré, S. (2013). Intratumor heterogeneity in human glioblastoma reflects cancer evolutionary dynamics. *Proceedings of the National Academy of Sciences of the United States of America* **110**(10):4009–14. doi: https://doi.org/10.1073/pnas.1219747110.

Stockhausen, M.-T., Kristoffersen, K., Stobbe, L. and Poulsen, H.S. (2014). Differentiation of glioblastoma multiforme stem-like cells leads to downregulation of EGFR and EGFRvIII and decreased tumorigenic and stem-like cell potential. *Cancer Biology and Therapy* **15**(2):216–24. doi: https://doi.org/10.4161/cbt.26736.

Stoppini, L., Buchs, P.-A. and Muller, D. (1991). A simple method for organotypic cultures of nervous tissue. *Journal of Neuroscience Methods* **37**(2):173–182. doi: https://doi.org/10.1016/0165-0270(91)90128-M.

Stringer, B.W., Day, B.W., D'Souza, R.C.J., Jamieson, P.R., Ensbey, K.S., Bruce, Z.C., … Boyd, A.W. (2019). A reference collection of patient-derived cell line and xenograft models of proneural, classical and mesenchymal glioblastoma. *Scientific Reports* **9**(1):1–14. doi: https://doi.org/10.1038/s41598-019-41277-z.

Stummer, W., Pichlmeier, U., Meinel, T., Wiestler, O.D., Zanella, F., Reulen, H.-J. and ALA-Glioma Study Group (2006). Fluorescence-guided surgery with 5-aminolevulinic acid for resection of malignant glioma: a randomised controlled multicentre phase III trial. *The Lancet. Oncology* **7**(5):392–401. doi: https://doi.org/10.1016/S1470-2045(06)70665-9.

Stupp, R., Hegi, M.E., Mason, W.P., van den Bent, M.J., Taphoorn, M.J., Janzer, R.C., … Mirimanoff, R.-O. (2009). Effects of radiotherapy with concomitant and adjuvant temozolomide versus radiotherapy alone on survival in glioblastoma in a randomised phase III study: 5-year analysis of the EORTC-NCIC trial. *The Lancet Oncology* **10**(5):459–466. doi: https://doi.org/10.1016/S1470-2045(09)70025-7.

Stupp, R., Mason, W.P., van den Bent, M.J., Weller, M., Fisher, B., Taphoorn, M.J.B., … Mirimanoff, R.O. (2005). Radiotherapy plus Concomitant and Adjuvant Temozolomide for Glioblastoma. *New England Journal of Medicine* **352**(10):987–996. doi: https://doi.org/10.1056/NEJMoa043330.

Sturm, D., Bender, S., Jones, D.T.W., Lichter, P., Grill, J., Becher, O., … Pfister, S.M. (2014). Paediatric and adult glioblastoma: Multiform (epi)genomic culprits emerge. *Nature Reviews Cancer* **14**(2):92–107. doi: https://doi.org/10.1038/nrc3655.

Sundstrom, L., Biggs, T., Laskowski, A., Stoppini, L., Stroppini, L., Stoppini, L. and Stroppini, L. (2012). OrganDots - an organotypic 3D tissue culture platform for drug development. *Expert Opinion on Drug Discovery* **7**(6):525–534. doi: https://doi.org/10.1517/17460441.2012.686488.

Svec, R.L., Furiassi, L., Skibinski, C.G., Fan, T.M., Riggins, G.J. and Hergenrother, P.J. (2018). Tunable Stability of Imidazotetrazines Leads to a Potent Compound for Glioblastoma. *ACS Chemical Biology* **13**(11):3206–3216. doi: https://doi.org/10.1021/acschembio.8b00864.

Szulzewsky, F., Arora, S., de Witte, L., Ulas, T., Markovic, D., Schultze, J.L., … Kettenmann, H. (2016). Human glioblastoma-associated microglia/monocytes express a distinct RNA profile compared to human control and murine samples. *Glia* **64**(8):1416–1436. doi: https://doi.org/10.1002/glia.23014.

Tosuner, Z., Geçer, M.Ö., Hatiboğlu, M.A., Abdallah, A. and Turna, S. (2018). BRAF V600E mutation and BRAF VE1 immunoexpression profiles in different types of glioblastoma. *Oncology Letters* **16**(2):2402–2408. doi: https://doi.org/10.3892/ol.2018.8919.

Tung, Y.-C., Hsiao, A.Y., Allen, S.G., Torisawa, Y., Ho, M. and Takayama, S. (2011). High-throughput 3D spheroid culture and drug testing using a 384 hanging drop array. *The Analyst* **136**(3):473–8. doi: https://doi.org/10.1039/c0an00609b.

Tunici, P., Bissola, L., Lualdi, E., Pollo, B., Cajola, L., Broggi, G., … Finocchiaro, G. (2004). Genetic alterations and in vivo tumorigenicity of neurospheres derived from an adult glioblastoma. *Molecular Cancer* **3**:1–5. doi: https://doi.org/10.1186/1476-4598-3-25.

Vanderbeek, A.M., Rahman, R., Fell, G., Ventz, S., Chen, T., Redd, R., … Alexander, B.M. (2018). The clinical trials landscape for glioblastoma: Is it adequate to develop new treatments? *Neuro-Oncology* **20**(8):1034–1043. doi: https://doi.org/10.1093/neuonc/noy027.

Vellimana, A.K., Recinos, V.R., Hwang, L., Fowers, K.D., Li, K.W., Zhang, Y., … Tyler, B.M.

(2013). Combination of paclitaxel thermal gel depot with temozolomide and radiotherapy significantly prolongs survival in an experimental rodent glioma model. *Journal of Neuro-Oncology* **111**(3):229–236. doi: https://doi.org/10.1007/s11060-012-1014-1.

Venere, M., Hamerlik, P., Wu, Q., Rasmussen, R.D., Song, L.A., Vasanji, A., … Rich, J.N. (2014). Therapeutic targeting of constitutive PARP activation compromises stem cell phenotype and survival of glioblastoma-initiating cells. *Cell Death and Differentiation* **21**(2):258–269. doi: https://doi.org/10.1038/cdd.2013.136.

Verbruggen, P., Heinemann, T., Manders, E., von Bornstaedt, G., van Driel, R. and Höfer, T. (2014). Robustness of DNA Repair through Collective Rate Control Stelling, J. (ed.). *PLoS Computational Biology* **10**(1):e1003438. doi: https://doi.org/10.1371/journal.pcbi.1003438.

Verhaak, R.G.W. (2016). Moving the needle: Optimizing classification for glioma. *Science Translational Medicine* **8**(350):350fs14. doi: https://doi.org/10.1126/scitranslmed.aah4740.

Verhaak, R.G.W., Hoadley, K.A., Purdom, E., Wang, V., Qi, Y., Wilkerson, M.D., … Cancer Genome Atlas Research Network (2010). Integrated genomic analysis identifies clinically relevant subtypes of glioblastoma characterized by abnormalities in PDGFRA, IDH1, EGFR, and NF1. *Cancer Cell* **17**(1):98–110. doi: https://doi.org/10.1016/j.ccr.2009.12.020.

Verheijen, M., Lienhard, M., Schrooders, Y., Clayton, O., Nudischer, R., Boerno, S., … Caiment, F. (2019). DMSO induces drastic changes in human cellular processes and epigenetic landscape in vitro. *Scientific Reports* **9**(1). doi: https://doi.org/10.1038/s41598-019-40660-0.

Wakimoto, H., Mohapatra, G., Kanai, R., Curry, W.T., Yip, S., Nitta, M., … Rabkin, S.D. (2012). Maintenance of primary tumor phenotype and genotype in glioblastoma stem cells. *Neuro-Oncology* **14**(2):132–144. doi: https://doi.org/10.1093/neuonc/nor195.

Wang, K., Kievit, F.M., Erickson, A.E., Silber, J.R., Ellenbogen, R.G. and Zhang, M. (2016). Culture on 3D Chitosan-Hyaluronic Acid Scaffolds Enhances Stem Cell Marker Expression and Drug Resistance in Human Glioblastoma Cancer Stem Cells. *Advanced Healthcare Materials* **5**(24):3173–3181. doi: https://doi.org/10.1002/adhm.201600684.

Wang, Q., Hu, B., Hu, X., Kim, H., Squatrito, M., Scarpace, L., … Verhaak, R.G.W. (2017). Tumor Evolution of Glioma-Intrinsic Gene Expression Subtypes Associates with Immunological Changes in the Microenvironment. *Cancer Cell* **32**(1):42-56.e6. doi: https://doi.org/10.1016/j.ccell.2017.06.003.

Wang, R., Chadalavada, K., Wilshire, J., Kowalik, U., Hovinga, K.E., Geber, A., … Tabar, V. (2010). Glioblastoma stem-like cells give rise to tumour endothelium. *Nature* **468**(7325):829–835. doi: https://doi.org/10.1038/nature09624.

Wei, J., Marisetty, A., Schrand, B., Gabrusiewicz, K., Hashimoto, Y., Ott, M., … Heimberger, A.B. (2019). Osteopontin mediates glioblastoma-associated macrophage infiltration and is a potential therapeutic target. *Journal of Clinical Investigation* **129**(1). doi: https://doi.org/10.1172/JCI121266.

Weil, R.J., Toms, S.A., Johnson, M.D. and Mealer, A. (2001). Detection of proliferating S-phase brain tumor cells by in situ DNA replication. *Journal of Neurosurgery* **95**(5):833–838. doi: https://doi.org/10.3171/jns.2001.95.5.0833.

Welker, A.M., Jaros, B.D., An, M. and Beattie, C.E. (2017). Changes in tumor cell heterogeneity after chemotherapy treatment in a xenograft model of glioblastoma. *Neuroscience* **356**:35–43. doi: https://doi.org/10.1016/J.NEUROSCIENCE.2017.05.010.

Weller, M., Vlahovic, G., Khasraw, M., Brandes, A.A., Zwirtes, R., Tatsuoka, K., … Bent, M. van den (2016). A randomized phase 2, single-blind study of temozolomide (TMZ) and

radiotherapy (RT) combined with nivolumab or placebo (PBO) in newly diagnosed adult patients (pts) with tumor O6-methylguanine DNA methyltransferase (MGMT)-methylated glioblastoma (GBM)—CheckMate-548. *Annals of Oncology* **27**(suppl_6). doi: https://doi.org/10.1093/annonc/mdw367.34.

Wesolowska, A., Kwiatkowska, A., Slomnicki, L., Dembinski, M., Master, A., Sliwa, M., … Kaminska, B. (2008). Microglia-derived TGF-beta as an important regulator of glioblastoma invasion--an inhibition of TGF-beta-dependent effects by shRNA against human TGF-beta type II receptor. *Oncogene* **27**(7):918–30. doi: https://doi.org/10.1038/sj.onc.1210683.

Wesseling, P., Kros, J.M. and Jeuken, J.W.M. (2011). The pathological diagnosis of diffuse gliomas: Towards a smart synthesis of microscopic and molecular information in a multidisciplinary context. *Diagnostic Histopathology*. doi: https://doi.org/10.1016/j.mpdhp.2011.08.005.

De Wever, O., Westbroek, W., Verloes, A., Bloemen, N., Bracke, M., Gespach, C., … Mareel, M. (2004). Critical role of N-cadherin in myofibroblast invasion and migration in vitro stimulated by colon-cancer-cell-derived TGF-β or wounding. *Journal of Cell Science* **117**(20):4691–4703. doi: https://doi.org/10.1242/jcs.01322.

William, D., Mullins, C.S., Schneider, B., Orthmann, A., Lamp, N., Krohn, M., … Linnebacher, M. (2017). Optimized creation of glioblastoma patient derived xenografts for use in preclinical studies. *Journal of Translational Medicine* **15**(1):27. doi: https://doi.org/10.1186/s12967-017-1128-5.

William, D., Walther, M., Schneider, B., Linnebacher, M. and Classen, C.F. (2018). Temozolomide-induced increase of tumorigenicity can be diminished by targeting of mitochondria in in vitro models of patient individual glioblastoma. *PLOS ONE* **13**(1):1–14. doi: https://doi.org/10.1371/journal.pone.0191511.

Witte, H.T., Jeibmann, A., Klämbt, C. and Paulus, W. (2009). Modeling glioma growth and invasion in Drosophila melanogaster. *Neoplasia* **11**(9):882–8. doi: https://doi.org/10.1593/neo.09576.

Wolf, K.J., Chen, J., Coombes, J.D., Aghi, M.K. and Kumar, S. (2019). Dissecting and rebuilding the glioblastoma microenvironment with engineered materials. *Nature Reviews Materials* **4**(10):651–668. doi: https://doi.org/10.1038/s41578-019-0135-y.

Wong, E., Nahar, N., Hau, E., Varikatt, W., Gebski, V., Ng, T., … Sundaresan, P. (2019). Cut-point for Ki-67 proliferation index as a prognostic marker for glioblastoma. *Asia-Pacific Journal of Clinical Oncology* **15**(1):5–9. doi: https://doi.org/10.1111/ajco.12826.

Xiao, W., Zhang, R., Sohrabi, A., Ehsanipour, A., Sun, S., Liang, J., … Seidlits, S.K. (2018). Brain-Mimetic 3D Culture Platforms Allow Investigation of Cooperative Effects of Extracellular Matrix Features on Therapeutic Resistance in Glioblastoma. *Cancer Research* **78**(5):1358. doi: https://doi.org/10.1158/0008-5472.CAN-17-2429.

Xie, Y., Bergström, T., Jiang, Y., Johansson, P., Marinescu, V.D., Lindberg, N., … Uhrbom, L. (2015). The Human Glioblastoma Cell Culture Resource: Validated Cell Models Representing All Molecular Subtypes. *EBioMedicine* **2**(10):1351–1363. doi: https://doi.org/10.1016/j.ebiom.2015.08.026.

Yan, G.N., Yang, L., Lv, Y.F., Shi, Y., Shen, L.L., Yao, X.H., … Guo, D.Y. (2014). Endothelial cells promote stem-like phenotype of glioma cells through activating the Hedgehog pathway. *Journal of Pathology* **234**(1):11–22. doi: https://doi.org/10.1002/path.4349.

Yang, L., Lin, C., Wang, L., Guo, H. and Wang, X. (2012). Hypoxia and hypoxia-inducible factors in glioblastoma multiforme progression and therapeutic implications. *Experimental Cell Research* **318**(19):2417–2426.

Yang, N., Yan, T., Zhu, H., Liang, X., Leiss, L., Sakariassen, P.Ø., … Wang, J. (2014). A co-

culture model with brain tumor-specific bioluminescence demonstrates astrocyte-induced drug resistance in glioblastoma. *Journal of Translational Medicine* **12**(1):1–9. doi: https://doi.org/10.1186/s12967-014-0278-y.

Yi, H.-G., Jeong, Y.H., Kim, Y., Choi, Y.-J., Moon, H.E., Park, S.H., … Cho, D.-W. (2019). A bioprinted human-glioblastoma-on-a-chip for the identification of patient-specific responses to chemoradiotherapy. *Nature Biomedical Engineering* **3**:509–519. doi: https://doi.org/10.1038/s41551-019-0363-x.

Yoshida, Y., Nakada, M., Harada, T., Tanaka, S., Furuta, T., Hayashi, Yasuhiko, … Hamada, J. (2010). The expression level of sphingosine-1-phosphate receptor type 1 is related to MIB-1 labeling index and predicts survival of glioblastoma patients. *Journal of Neuro-Oncology* **98**(1):41–47. doi: https://doi.org/10.1007/s11060-009-0064-5.

Yu, K.K.H., Taylor, J.T., Pathmanaban, O.N., Youshani, A.S., Beyit, D., Dutko-Gwozdz, J., … Bigger, B.W. (2018). High content screening of patient-derived cell lines highlights the potential of non-standard chemotherapeutic agents for the treatment of glioblastoma. *PLOS ONE* **13**(3). doi: https://doi.org/10.1371/journal.pone.0193694.

Zhang, G., Huang, S., Zhang, J., Wu, Z., Lin, S. and Wang, Y. (2016). Clinical outcome of gliosarcoma compared with glioblastoma multiforme: a clinical study in Chinese patients. *Journal of Neuro-Oncology* **127**(2):355–362. doi: https://doi.org/10.1007/s11060-015-2046-0.

Zhang, I., Beus, M., Stochaj, U., Le, P.U., Zorc, B., Rajić, Z., … Maysinger, D. (2018). Inhibition of glioblastoma cell proliferation, invasion, and mechanism of action of a novel hydroxamic acid hybrid molecule. *Cell Death Discovery* **4**:41. doi: https://doi.org/10.1038/s41420-018-0103-0.

Zhang, J., F.G. Stevens, M. and D. Bradshaw, T. (2012). Temozolomide: Mechanisms of Action, Repair and Resistance. *Current Molecular Pharmacology* **5**(1):102–114. doi: https://doi.org/10.2174/1874467211205010102.

Zhang, J. and Jiao, J. (2015). Molecular Biomarkers for Embryonic and Adult Neural Stem Cell and Neurogenesis. *BioMed Research International* **2015**.

Zhao, S.G., Yu, M., Spratt, D.E., Chang, S.L., Feng, F.Y., Kim, M.M., … Wahl, D.R. (2019). Xenograft-based, platform-independent gene signatures to predict response to alkylating chemotherapy, radiation, and combination therapy for glioblastoma. *Neuro-Oncology* **21**(9):1141–1149. doi: https://doi.org/10.1093/neuonc/noz090.

Zhao, Y., Korolj, A., Feric, N. and Radisic, M. (2016). Human pluripotent stem cell-derived cardiomyocyte based models for cardiotoxicity and drug discovery. *Expert Opinion on Drug Safety* **15**(11):1455–1458. doi: https://doi.org/10.1080/14740338.2016.1223624.

Zhou, Z. and Lu, Z.R. (2013). Gadolinium-based contrast agents for magnetic resonance cancer imaging. *Wiley Interdisciplinary Reviews: Nanomedicine and Nanobiotechnology* **5**(1):1–18.

Zhu, Y. (2018). An examination of the effects of the environment on transplanted human interneuron progenitors in temporal lobal epilepsy.

Zschenker, O., Streichert, T., Hehlgans, S. and Cordes, N. (2012). Genome-wide gene expression analysis in cancer cells reveals 3D growth to affect ECM and processes associated with cell adhesion but not DNA repair. *PLOS ONE* **7**(4). doi: https://doi.org/10.1371/journal.pone.0034279.

8 Appendices

8.1 Patient information sheet

Patient Information Sheet

We would like to invite you to take part in our research tissue bank. Before you decide, we would like you to understand the purpose of the tissue bank, and what being part of it would mean for you. Our team will go through the information sheet with you and answer any questions you may have. If English is not your preferred language and you would like this information in another language, please ask and it will be provided, or an interpreter called. Take as much time as you need to decide whether or not you wish to take part. If you wish to take part, you will be asked to sign the Welsh Neuroscience Research Tissue Bank Consent Form. By signing this form, you indicate that you understand this information, and that you give consent to donate samples (such as, but not restricted to, blood, urine, saliva, cerebrospinal fluid (CSF), brain biopsy, peripheral nerve tissue) to the Welsh Neuroscience Research Tissue Bank. Please take time to read the following information carefully and discuss it with others if you wish.

Thank you for reading this.

What is the purpose of the tissue bank?
The aim of the tissue bank is to help research into the causes, diagnosis, and treatment of neurological diseases. Research with tissue can help find out more about what causes neurological disease, how to prevent it, and how to treat it.

What is the tissue bank?
The tissue bank is a collection of samples of human tissue and body fluids such as blood and urine. The samples are stored in a special freezer in a laboratory within Cardiff University at the University Hospital of Wales. The tissue bank is used to collect tissue for medical research.

Why have I been invited?
You have been invited to take part because you have attended the Neurology/Neurosurgery Department at your local hospital and are over 16 years of age. During your normal treatment, it is usual that samples are collected from you. We are asking your permission to take an extra sample to help study neurological diseases. There are several types of samples that might be collected, not all of which will apply to you.

Do I have to take part?
No, it is up to you to decide to join the research tissue bank. We will describe the research and go through this information sheet. If you agree to take part, we will then ask you to sign a consent form. If you decide not to take part, you do not have to explain your reasons and it will not affect any future medical treatment or legal rights.
You are free to withdraw at any time, without giving a reason, even after signing the consent form. If requested, any unused samples will be disposed of according to locally approved procedures. Any samples used or results generated prior to the withdrawal of consent will continue to be utilised.

What will happen to me if I take part?
We will seek your consent to take, store and analyse a blood sample or other biological sample such as CSF, urine, saliva, hair or nails for research purposes into neurological diseases.
The samples that we are able to store in the tissue bank are listed below:

1) Blood. If you agree to give a blood sample, a trained phlebotomist or clinician will take no more than 50mls (or 10 teaspoons) from a vein in your arm using a standard procedure which

takes place in hospital every day. Blood samples will then be processed so that serum, plasma and DNA are extracted and stored.

2) Cerebrospinal fluid (CSF). If you are having a sample of CSF collected as part of your clinical care we may ask to take surplus CSF, which will be no more than 10mls (or 2 teaspoons), for chemical analysis for research purposes if you are agreeable.

3) If you agree to provide a saliva sample, you will be asked to spit into a collection tube, containing a stabilising agent, at a time that is convenient to you. We will then use this sample to extract DNA for analysis.

4) If you agree to provide samples of urine, nails and hair, these can be collected using non-invasive procedures, over seen by a trained team member or clinician involved with the tissue bank.

5) Brain tissue. If you are having a brain biopsy as part of your clinical care, we may ask to keep any surplus brain tissue not used for diagnostic or clinical purposes for research if you are agreeable.

6) Peripheral nerve tissue. If you are having a peripheral nerve biopsy as part of your clinical care, we may ask to keep any surplus nerve tissue not used for diagnostic or clinical purposes for research if you are agreeable.

If you agree to future contact, further samples may be requested, but not more than twice per year and at a convenient time agreed by you. Your consent is enduring for the duration of the tissue bank approval, however, you are free to withdraw your consent at any time, or opt out on any occasion, without giving a reason and without affecting your medical treatment or legal rights.

We hope that by collecting these samples we can improve the care we provide for patients with neurological conditions in the future.

Will I be paid anything for taking part?
No, you should understand that any samples you give will be as a gift and you will not benefit financially in the future should this research lead to the development of a new treatment or medical test.

How long will my tissue be stored?
Tissue placed in tissue banks are usually kept at very low temperatures, and can be stored this way for a very long time.

What type of research will be done with my tissue?
Many different types of research rely on the use of human tissues. They can be used to help understand what causes diseases, to help diagnose diseases, and can even be used to help develop new tests and new ways to treat or even cure diseases. Some of the research may lead to new medical products, such as diagnostic tests or new procedures. Research that uses the tissue in this bank includes genetic research. This can include looking at the way that diseases might be inherited in families, or how certain genes might cause disease, or how a person's genes influence the way that they respond to treatment.

Will you analyse my DNA?
On the consent form it asks that you give consent for your sample to be used in research that identifies genes or diseases that run in families, for example, disease that can be passed on (through DNA) to blood relatives. If, however you are not happy for your samples to be used for research into genes, then unfortunately we will not be able to recruit you into the tissue bank.
As part of the research we intend to carry out analysis of DNA and other non-diagnostic tests. The type of analyses we will perform are for research purposes and therefore we will not be able to provide clinical feedback.

What are the possible benefits of taking part?
There will be no direct benefits to you for taking part, but your contribution will help us understand more about the symptoms, progression and causes of neurological disorders and possibly other medical conditions.

What are the possible disadvantages and risks of taking part?
If you agree to donate tissue to the tissue bank, we will perform this at the same time as one of your routine clinical samples if possible. If it is not possible to take blood during your routine clinical appointment, a trained phlebotomist or clinician will collect a sample at a time that is convenient to you. You may experience some minor discomfort from having the extra blood sample taken, sometimes there is mild bruising afterwards. The amount of blood we propose to take (no more than 50mls per bleed) should not cause anaemia. We will keep records of donation dates and amounts donated in order to minimise risks. We ask you to inform us if you have given blood for any reason anywhere else over the last month. Collection of cerebrospinal fluid, brain or nerve tissue is strictly controlled and will only be taken as surplus products during your routine clinical intervention. There are no foreseeable risks of over donation and no other obvious disadvantages to taking part in this study.

Will anyone look at my medical records?
The Welsh Neuroscience Research Tissue Bank would like to collect information from your medical record, such as your age and sex, and record the details of your condition such as the diagnosis and results of various tests including results of any imaging. The tissue bank team would also like to follow your progress by looking at information that your doctor has collected from you during your routine follow up visits. You will not have to make a special trip or appointment for this. Your doctor may also record information such as what medications you take.
Under data protection law, we have to specify the legal basis that we are relying on to process your personal data. In providing your personal data for this research we will process it on the basis that doing so is necessary for our public task for scientific and historical research purposes in accordance with the necessary safeguards and is in the public interest. Cardiff University, specifically The Welsh Neuroscience Research Tissue Bank staff will collect information about you for the biobank records from your NHS medical records. The information will include your name, age, gender, race, diagnoses, medication, disease progress for example. We will use your personal information (name, address, NHS number, date of birth) to make sure we are matching the correct medical record to the correct donated samples. All information related to your diagnosis and treatment will be treated in strictest confidence.

Why do you need information from my health records?
In order to do research with your tissue, researchers may need to know some things about you. For example: Are you male or female? What is your race or ethnic group? How old are you? Have you ever smoked? What medications are you taking? Do you have other medical problems? Is there a family history of diseases? This helps the researcher answer questions about diseases.

Who gets to use tissue in the tissue bank?
Access to your tissue and any personal data that may be associated with your tissue is strictly controlled. Various researchers from the University Hospital of Wales/Cardiff University and elsewhere may use your tissue in research studies, including researchers from outside the UK. However, they must make a formal request to use these samples and their research must be approved by the people who are responsible for administering the tissue bank. Samples in the Welsh Neuroscience Research Tissue Bank can only be used for research to advance the understanding of neurological diseases. Samples will not be sold for profit or used for animal research or the commercial sector. Once the study is approved, the researcher receives your tissue and when appropriate, non-identifiable information about you from your hospital record. The information that may be given to the researcher includes but is not restricted to: your age, sex, race, medical history, diagnosis, treatments, and possibly some family history. This information will be collected from your health records by the tissue bank staff. The researcher will not receive your name, address,

phone number, or any other personal identifying information. All samples will be supplied anonymously to researchers. Only the research tissue bank staff will be able to identify which samples you donated. The recipients of your samples will not be able to identify you from your samples. This is done to protect your confidential information.

Will my GP be told I am taking part in the research tissue bank?
We will not inform your GP that you are taking part.

Will my taking part in this tissue bank be kept confidential and can outside bodies like insurance companies access the research tests?
Yes, all information that is collected about you during the course of the research will be kept strictly confidential. We will code your sample, so that a number rather than a name is used in further analysis. The link between the code and your name will not leave the hospital. Coded samples (i.e. without your name) for these tests may be shared with other research groups for analyses. We will store the information on a secure, confidential database, this will enable us to analyse the information gathered for research. You may ask for your personal information to be removed from this database at any time, in accordance with the General Data Protection Regulation 2018.
Cardiff University is the sponsor for this study based in the United Kingdom. We will be using information from you and your medical records in order to undertake this study and will act as the data controller for this study. This means that we are responsible for looking after your information and using it properly. Cardiff University will keep identifiable information about you for 15 years after the study has finished.
Your rights to access, change or move your information are limited, as we need to manage your information in specific ways in order for the research to be reliable and accurate. If you withdraw from the study, we will keep the information about you that we have already obtained. To safeguard your rights, we will use the minimum personally-identifiable information possible. You can find out more about how we use your information at www.cardiff.ac.uk.

What happens to my samples at the end of the study?
With your consent, your samples may be retained at the end of this project for use in future research within the UK and abroad, according to ethically approved procedures. At this stage, we do not know what the research will involve but some of it may include DNA analysis. Your samples will not be sold for profit and will not be used in animal research or the commercial sector.
All samples will be supplied anonymously to researchers. Only the tissue bank team will be able to identify which samples you donated. The recipients of your samples will not be able to identify you from your samples.
You may withdraw your consent for the storage and future use of your samples at any point. If you do withdraw your consent, your samples will not be used in any subsequent studies and will be destroyed according to locally approved practices. Any samples already distributed will continue to be used in that study and will be destroyed at the end of the study.

What will happen to the results of research using samples from this tissue bank?
Our aim is to publish the results from these studies in academic journals and present findings at conferences. You will not be identified in any report, presentation or publication.

What if something goes wrong?
If you are harmed by taking part in this research project, there are no special compensation arrangements. If you are harmed due to someone's negligence, then you may have grounds for legal action, but you may have to pay for it. Regardless of this, if you wish to complain, or have grounds for concerns about any aspect of the way you have been approached or treated during the course of this research, the normal National Health complaints procedure is available to you. The Complaints Officer can be contacted on (029) 20746 296 or by emailing concerns@wales.nhs.uk.

Who is organising and funding the tissue bank?
The tissue bank is organised and administered by Cardiff University, Division of Psychological Medicine & Clinical Neurosciences, together with the University Hospital of Wales, Cardiff. The tissue bank is supported by the Neurosciences Directorate as part of its core activity.

Who has reviewed the study?
All research in the NHS is assessed by an independent group of people, called a Research Ethics Committee, to protect your interests. This study has been reviewed and given a favourable opinion by Wales REC 3.

The Welsh Neuroscience Research Tissue Bank is licensed by the Human Tissue Authority (licence 12422) under the UK Human Tissue Act (2004) to store human samples for research purposes.

Contact for further information:
Director: Professor Neil Robertson
Telephone: (029) 20745403
Email: robertsonnp@cardiff.ac.uk
Address: Division of Psychological Medicine & Clinical Neurosciences, Cardiff University, Heath Park, Cardiff, CF14 4XW

If you decide to take part, you will be given a copy of this information sheet and a signed consent form to keep. We would like to thank you for participating in the Welsh Neuroscience Research Tissue Bank.

8.2 Patient consent form

Welsh Neuroscience Research Tissue Bank

Hospital sticker

Code Number: _____

Telephone number: ._____

Consultant Name: _____

Patient Consent Form

To confirm agreement with each of the statements below, please initial in the box	
1. I confirm that I have read the attached Patient Information Sheet (version 5.0, March 2019) and have been given a copy to keep. I have had the opportunity to ask questions and have had these answered satisfactorily. I understand why the research is being done and any foreseeable risks involved.	☐
2. I understand that my participation is voluntary. I am free to withdraw at any time or decline on any occasion, without giving any reason, and without my medical care or legal rights being affected.	☐
3. I agree to provide biological samples (for example, but not restricted to, blood, saliva, urine, nails, hair) to the tissue bank according to the conditions in the patient information sheet. I understand that any samples will be given as a 'gift' and that there will be no financial reward for taking part.	☐
4. If I have cerebrospinal fluid (CSF) sampled as part of my routine clinical care I agree that surplus cerebrospinal fluid can be collected for the research tissue bank according to the conditions in the patient information sheet.	☐
5. If I have a brain biopsy as part of my routine clinical care, I agree that surplus brain tissue can be collected for the research tissue bank according to the conditions in the patient information sheet.	☐
6. If I have a peripheral nerve biopsy as part of my routine clinical care, I agree that surplus peripheral nerve tissue can be collected for the research tissue bank according to the conditions in the patient information sheet.	☐
7. I give permission for my samples to be used for studies on DNA, that might identify genes or diseases that run in families and can be passed on to the blood relatives. I understand that the samples will be anonymised, and I will not be given any clinical feedback regarding the results of DNA analysis or other non-diagnostic tests.	☐
8. I understand that relevant sections of my medical notes and data collected during the study, may be looked at by individuals from the Welsh Neuroscience Research Tissue Bank (Cardiff University), from regulatory authorities or from the NHS Trust, where it is relevant to taking part in this research. I give permission for these individuals to have access to my records.	☐

Patient Consent Form, Version 4.1, March 2019

9. I agree that my clinical details can be stored in a clinical research database on the NHS hospital computer network. The anonymised data can be shared with other international researchers. I may ask for your personal information to be removed from this database at any time, in accordance with the General Data Protection Regulation 2018. ☐

10. I understand that researchers from other institutions within the UK and abroad may access my samples, that research may take many years, and that the information gained will not benefit me or my family directly. ☐

11. I agree that my samples may be retained for future use by researchers in the UK and abroad, I understand the research may involve DNA analysis and that researchers will not be able to identify me from my samples. ☐

12. I am happy to be contacted by letter for future research projects. **YES** / **NO** (please circle). ☐

13. I agree to take part in this study ☐

Participant's Name (print): _____ Date: _____ Signature: _____

Name of Witness (print): _____ Date: _____ Signature: _____

Person taking consent (print:) _____ Date: _____ Signature: _____

(1 for patient, 1 for researcher, 1 to be kept in the medical notes)

Contact for further information:
Professor Neil Robertson
Tel: (029) 20745403
Email: robertsonnp@cardiff.ac.uk
Address: Division of Psychological Medicine & Clinical Neurosciences, Cardiff University, Heath Park, Cardiff CF14 4XW

8.3 Personal/nominal information sheet

Welsh Neuroscience Research **Tissue Bank**

Personal/Nominal Consultee Patient Information Sheet

(e.g. Next of Kin/Relative/Friend)

You and your next of kin/relative/friend are being invited to take part in our research tissue bank. Before you decide, we would like you to understand the purpose of the tissue bank, and what being part of it would mean for your next of kin/relative/friend. Our team will go through the information sheet with you and answer any questions you may have. If English is not your preferred language and you would like this information in another language, please ask and it will be provided, or an interpreter called. Take as much time as you need to decide whether or not you feel your next of kin/relative/friend would like to take part. If you believe your next of kin/relative/friend wishes to take part, you will be asked to sign the Welsh Neuroscience Research Tissue Bank Consent Form on their behalf. By signing this form, you indicate that you understand this information, and in your opinion your next of kin/relative/friend agrees to donate their samples (such as, but not restricted to, blood, urine, saliva, cerebrospinal fluid (CSF), brain biopsy, peripheral nerve tissue) to the Welsh Neuroscience Research Tissue Bank.

What is the purpose of the tissue bank?
The aim of the tissue bank is to help research into the causes, diagnosis, and treatment of neurological diseases. Research with tissue can help find out more about what causes neurological disease, how to prevent it, and how to treat it.

What is the tissue bank?
The tissue bank is a collection of samples of human tissue and body fluids such as blood and urine. The samples are stored in a special freezer in a laboratory within Cardiff University at the University Hospital of Wales. The tissue bank is used to collect tissue for medical research.

Why has my next of kin/relative/friend been invited?
Your next of kin/relative/friend has been invited to take part because they have attended the Neurology/Neurosurgery Department at their local hospital and are over 16 years of age. During their normal treatment, it is usual that samples are collected. We are asking for permission to take an extra sample to help study neurological diseases. There are several types of samples that might be collected, not all of which will apply to your next of kin/relative/friend.

Do they have to take part?
No, together with your help, we would like to determine whether your next of kin/relative/friend would like to join the research tissue bank. We will describe the research and go through this information sheet. If you feel that your next of kin/relative/friend would agree to take part, we will then ask you to sign a consent form. If you feel they would not like to take part, you do not have to explain your reasons and it will not affect any medical treatment or legal rights.
You or your next of kin/relative/friend are free to withdraw at any time, without giving a reason, even after signing the consent form. If requested, any unused samples will be disposed of according to locally approved procedures. Any samples used or results generated prior to the withdrawal of consent will continue to be utilised.

What will happen to my next of kin/relative/friend if they take part?
If you feel your next of kin/relative/friend would agree to take part we will seek consent, on their behalf, to take, store and analyse a blood sample or other biological sample such as CSF, urine, saliva, hair or nails for research purposes into neurological diseases.
The samples that we are able to store in the tissue bank are listed below:

1) Blood. If able, and you feel your next of kin/relative/friend would agree to give a blood sample, a trained phlebotomist or clinician will take no more than 50mls (or 10 teaspoons) from a vein in their arm using a standard procedure which takes place in hospital every day. Blood samples will then be processed so that serum, plasma and DNA are extracted and stored.

2) Cerebrospinal fluid (CSF). If they are having a sample of CSF collected as part of their clinical care we may ask to take surplus CSF, which will be no more than 10mls (or 2 teaspoons), for chemical analysis for research purposes if you feel they would be agreeable.

3) Saliva. If able, and you feel your next of kin/relative/friend would agree to provide a saliva sample, they will be asked to spit into a collection tube, containing a stabilising agent, at a time that is convenient to you. We will then use this sample to extract DNA for analysis.

4) If able, and you agree for your next of kin/relative/friend to do so, urine, nails and hair can be collected using non-invasive procedures, over seen by a trained team member or clinician involved with the tissue bank.

5) Brain tissue. If they are having a brain biopsy as part of their clinical care, we may ask to keep any surplus brain tissue not used for diagnostic or clinical purposes for research if you are agreeable.

6) Peripheral nerve tissue. If they are having a peripheral nerve tissue biopsy as part of their clinical care, we may ask to keep any surplus nerve tissue not used for diagnostic or clinical purposes for research if you are agreeable.

If you feel your next of kin/relative/friend would agree to future contact, further samples may be requested, but no more than twice per year and at a convenient time agreed by you. The consent is enduring for the duration of the tissue bank approval, however, you or your next of kin/relative/friend are free to withdraw consent at any time, or opt out on any occasion, without giving a reason and without affecting their medical treatment or legal rights.

We hope that by collecting these samples we can improve the care we provide for patients with neurological conditions in the future.

Will my next of kin/relative/friend be paid anything for taking part?
No, you should understand that any samples given will be as a gift and there will be no financial benefit in the future should this research lead to the development of a new treatment or medical test.

How long will the tissue be stored?
Tissue placed in tissue banks are usually kept at very low temperatures and can be stored this way for a very long time.

What type of research will be done on the tissue?
Many different types of research rely on the use of human tissues. They can be used to help understand what causes diseases, to help diagnose diseases, and can even be used to help develop new tests and new ways to treat or even cure diseases. Some of the research may lead to new medical products, such as diagnostic tests or new procedures. Research that uses the tissue in this bank includes genetic research. This can include looking at the way that diseases might be

inherited in families, or how certain genes might cause disease, or how a person's genes influence the way that they respond to treatment.

Will you analyse my next of kin/relative/friend's DNA?
On the consent form it asks that you agree for your next of kin/relative/friend's sample to be used in research that identifies genes or diseases that run in families, for example, disease that can be passed on (through DNA) to blood relatives. If however, you feel your next of kin/relative/friend would not be happy for the samples to be used for research into genes, then unfortunately we will not be able to recruit them into the tissue bank.
As part of the research we intend to carry out analysis of DNA and other non-diagnostic tests. The type of analyses we will perform are for research purposes and therefore we will not be able to provide clinical feedback.

What are the possible benefits of taking part?
There will be no direct benefits to your next of kin/relative/friend for taking part, but the contribution will help us understand more about the symptoms, progression and causes of neurological disorders and possibly other medical conditions.

What are the possible disadvantages and risks of taking part?
If you believe your next of kin/relative/friend would like to donate tissue to the tissue bank, we will perform this at the same time as one of their routine clinical samples if possible. If it is not possible to take blood during their routine clinical appointment, a trained phlebotomist or clinician will collect a sample at a time that is convenient. They may experience some minor discomfort from having the extra blood sample taken, sometimes there is mild bruising afterwards. The amount of blood we propose to take (no more than 50mls per bleed) should not cause anaemia. We will keep records of donation dates and amounts donated in order to minimise risks. We ask you to inform us if your next of kin/relative/friend has given blood for any reason anywhere else over the last month. Collection of cerebrospinal fluid, brain or nerve tissue is strictly controlled and will only be taken as surplus products during your kin/relative/friend's routine clinical intervention. There are no foreseeable risks of over donation and no other obvious disadvantages to taking part in this study.

Will anyone look at my next of kin/relative/friend's medical records?
The Welsh Neuroscience Research Tissue Bank would like to collect information from their medical record, such as their age and sex, and record the details about their condition such as the diagnosis and results of various tests including results of any imaging. The tissue bank team would also like to follow their progress by looking at information that their doctor has collected from them during their routine follow up visits. Your next of kin/relative/friend will not have to make a special trip or appointment for this. Their doctor may also record information such as what medications they take.
Under data protection law, we have to specify the legal basis that we are relying on to process your next of kin/relative/friend's personal data. In providing their personal data for this research we will process it on the basis that doing so is necessary for our public task for scientific and historical research purposes in accordance with the necessary safeguards and is in the public interest. Cardiff University, specifically The Welsh Neuroscience Research Tissue Bank staff will collect information about your next of kin/relative/friend for the biobank records from their NHS medical records. The information will include their name, age, gender, race, diagnoses, medication, disease progress for example. We will use their personal information (name, address, NHS number, date of birth) to make sure we are matching the correct medical record to the correct donated samples. All information related to your next of kin/relative/friend's diagnosis and treatment will be treated in strictest confidence.

Why do you need information from their health records?

In order to do research with their tissue, researchers may need to know some things about them. For example: Are they male or female? What is their race or ethnic group? How old are they? Have they ever smoked? What medications are they taking? Do they have other medical problems? Is there a family history of diseases? This helps the researcher answer questions about diseases.

Who gets to use tissue in the tissue bank?
Access to your next of kin/relative/friend's tissue and any personal data that may be associated with their tissue is strictly controlled. Various researchers from the University Hospital of Wales/Cardiff University and elsewhere may use their tissue in research studies. However, they must make a formal request to use these samples and their research must be approved by the people who are responsible for administering the tissue bank. Samples in the Welsh Neuroscience Research Tissue Bank can only be used for research to advance the understanding of neurological diseases. Samples will not be sold for profit or used in animal research or the commercial sector. Once the study is approved, the researcher receives the tissue and when appropriate, non-identifiable information about them from their hospital record. The information that may be given to the researcher includes but is not restricted to: age, sex, race, medical history, diagnosis, treatments and possible some family history. This information will be collected from your next of kin/relative/friend's health records by the tissue bank staff. The researcher will not receive their name, address, phone number, or any other personal identifying information. All samples will be supplied anonymously to researchers. Only the research tissue bank staff will be able to identify which samples they donated. The recipients of the samples will not be able to identify your next of kin/relative/friend from the samples they receive. This is done to protect their confidential information.

Will my next of kin/relative/friend's GP be told they are taking part in the research tissue bank?
We will not inform their GP that they are taking part.

Will my next of kin/relative/friend participation in this tissue bank be kept confidential and can outside bodies like insurance companies access the research tests?
Yes, all information that is collected about your next of kin/relative/friend during the course of the research will be kept strictly confidential. We will code their sample, so that a number rather than a name is used in further analysis. The link between the code and their name will not leave the hospital. Coded samples (i.e. without their name) for these tests may be shared with other research groups for analyses. We will store the information on a secure, confidential database, this will enable us to analyse the information gathered for research. You may ask for their personal information to be removed from this database at any time, in accordance with the General Data Protection Regulation 2018.
Cardiff University is the sponsor for this study based in the United Kingdom. We will be using information from your next of kin/relative/friend and their medical records in order to undertake this study and will act as the data controller for this study. This means that we are responsible for looking after their information and using it properly. Cardiff University will keep identifiable information about your next of kin/relative/friend for 15 years after the study has finished.
Your next of kin/relative/friend's rights to access, change or move their information are limited, as we need to manage the information in specific ways in order for the research to be reliable and accurate. If you or your next of kin/relative/friend withdraw from the study, we will keep the information about your next of kin/relative/friend that we have already obtained. To safeguard your next of kin/relative/friend's rights, we will use the minimum personally-identifiable information possible. You can find out more about how we use your information at www.cardiff.ac.uk.

What happens to my next of kin/relative/friend's samples at the end of the study?

If you feel your next of kin/relative/friend would agree, their samples may be retained at the end of this project for use in future research within the UK and abroad, according to ethically approved procedures. At this stage, we do not know what the research will involve but some of it may include DNA analysis. The samples will not be sold for profit and will not be used in animal research or the commercial sector.
All samples will be supplied anonymously to researchers. Only the tissue bank team will be able to identify which samples your next of kin/relative/friend donated. The recipients of their samples will not be able to identify them from the samples.
You or your next of kin/relative/friend may withdraw consent for the storage and future use of the samples at any point. If you do withdraw consent, their samples will not be used in any subsequent studies and will be destroyed according to locally approved practices. Any samples already distributed will continue to be used in that study and will be destroyed at the end of the study.

What will happen to the results of research using samples from this tissue bank?
Our aim is to publish the results from these studies in academic journals and present findings at conferences. Your next of kin/relative/friend will not be identified in any report, presentation or publication.

What if something goes wrong?
If your next of kin/relative/friend is harmed by taking part in this research project, there are no special compensation arrangements. If they are harmed due to someone's negligence, then you may have grounds for legal action, but you may have to pay for it. Regardless of this, if you wish to complain, or have grounds for concerns about any aspect of the way you or your next of kin/relative/friend has been approached or treated during the course of this research; the normal National Health complaints procedure is available to you. The Complaints Officer can be contacted on (029) 20746 296 or by emailing concerns@wales.nhs.uk.

Who is organising and funding the tissue bank?
The tissue bank is organised and administered by Cardiff University, Division of Psychological Medicine & Clinical Neurosciences, together with the University Hospital of Wales, Cardiff. The tissue bank is supported by the Neurosciences Directorate as part of its core activity.

Who has reviewed the study?
All research in the NHS is assessed by an independent group of people, called a Research Ethics Committee, to protect your interests. This study has been reviewed and given a favourable opinion by Wales REC 3.
The Welsh Neuroscience Research Tissue Bank is licensed by the Human Tissue Authority (licence 12422) under the UK Human Tissue Act (2004) to store human samples for research purposes.

Contact for further information:
Director: Professor Neil Robertson
Telephone: (029) 20745403.
Email: robertsonnp@cardiff.ac.uk
Address: Division of Psychological Medicine & Clinical Neurosciences, Cardiff University, Heath Park, Cardiff, CF14 4XW

Should you decide your next of kin/relative/friend would like to take part in this research, you will be given a copy of this information sheet and a signed consent form to keep. We would like to thank you and your next of kin/relative/friend for participating in the Welsh Neuroscience Research Tissue Bank.

8.4 Personal/nominal consent form

Welsh Neuroscience Research **Tissue Bank**

Patient Sticker

Code Number: _____

Telephone number: _____

Consultant: _____

Personal/Nominal Consent Form

Personal/Nominal Consultee (e.g Next of Kin/Relative/friend)

To confirm agreement with each of the statements below, please initial in the box

1. I have read the attached Information Sheet (for Personal/Nominal Consultee, Version 5.0, March 2019) and have been given a copy to keep. I have had the opportunity to ask questions about the project and have these answered satisfactorily. I understand why the research is being done and any foreseeable risks involved. ☐
2. I understand that my next of kin/relative/friend's participation is voluntary. We are free to withdraw at any time or decline on any occasion, without giving any reason, and without their medical care or legal rights being affected. ☐
3. In my opinion, my next of kin/relative/friend agrees to give biological samples (for example, but not restricted to, blood, saliva, urine, nails, hair) to the tissue bank according to the conditions in the patient information sheet. I understand that any samples will be given as a 'gift' and that there will be no financial reward for taking part. ☐
4. If my next of kin/relative/friend has cerebrospinal fluid (CSF) sampled as part of their routine clinical care, in my opinion, they agree that surplus cerebrospinal fluid can be collected for the research tissue bank according to the conditions in the information sheet. ☐
5. If my next of kin/relative/friend has a brain biopsy as part of their routine clinical care, in my opinion, they agree that surplus brain tissue can be collected for the research tissue bank according to the conditions in the information sheet. ☐
6. If my next of kin/relative/friend has a peripheral nerve biopsy as part of their routine clinical care, in my opinion, they agree that surplus peripheral nerve tissue can be collected for the research tissue bank according to the conditions in the information sheet. ☐
7. In my opinion my next of kin/relative/friend agrees that samples can to be used for studies on DNA, that might identify genes or diseases that run in families and can be passed on to the blood relatives. I understand that the samples will be anonymised, and that we will not be given any clinical feedback regarding the results of DNA analysis or other non-diagnostic tests. ☐
8. I understand that relevant sections of my next of kin/relative/friend's medical notes and data collected during the study, may be looked at by individuals from the Welsh Neuroscience Research Tissue Bank (Cardiff University), from regulatory authorities or from the NHS Trust, where it is relevant to taking part in this research. I believe my next of kin/relative/friend gives permission for these individuals to have access to these records. ☐

Personal/Nominee Consultee Consent Form, Version 4.1, March 2019

9. In my opinion, my next of kin/relative/friend gives permission for their clinical details to be stored in a clinical research database on the NHS hospital computer network. The anonymised data can be shared with other international researchers. We may ask for their personal information to be removed from this database at any time, in accordance with the General Data Protection Regulation 2018. ☐

10. I understand that researchers from other institutions within the UK and abroad may access my next of kin/relative/friend's samples, that research may take many years, and that the information gained will not benefit my next of kin/relative/friend or their family directly. ☐

11. In my opinion, my next of kin/relative/friend agrees that their samples may be retained for future use by researchers in the UK and abroad. I understand that the research may involve DNA analysis and that researchers will not be able to identify my next of kin/relative/friend from their samples. ☐

12. I am satisfied that the welfare and interests of my next of kin/relative/friend have been properly safeguarded in asking them to participate in this study. ☐

13. I confirm I was present when the above study was explained to my next of kin/relative/friend. In my opinion, he/she does not object or appear to object in either words or action to participating in the research or giving a sample for the above research tissue bank. ☐

14. In my opinion, my next of kin/relative/friend is happy to be contacted by letter for future research projects. **YES / NO (please circle)** ☐

15. I agree to _____ taking part in the above tissue bank for research into neurological diseases. ☐

_____	_____	_____
Name of Next of kin/relative/ friend Representative	**Date**	**Signature**

NOMINEE CONTACT DETAILS:

Relationship to Participant: _____

Address: _____

Telephone Number: _____

Email: _____

_____	_____	_____
Name of person taking consent/researcher	**Date**	**Signature**

(1 for patient, 1 for researcher, 1 to be kept in the medical notes)

Thank you for helping with our research
You will be given a copy of this consent form to keep

Contact for further information:
Professor Neil Robertson
Tel: (029) 20745403
Email: robertsonnp@cardiff.ac.uk
Address: Division of Psychological Medicine & Clinical Neurosciences,
Cardiff University, Heath Park, Cardiff, CF14 4XW